UNIVERSITÉ DE SHERBROOKE
Faculté de génie
Département de génie civil

FLEXURAL BEHAVIOUR OF REINFORCED CONCRETE BEAMS STRENGTHENED WITH NEAR SURFACE MOUNTED FRP BARS

COMPORTEMENT EN FLEXION DE POUTRES EN BÉTON ARMÉ RENFORCÉES PAR DES ARMATURES EN PRF ENCASTRÉES PRÈS DE LA SURFACE

Thèse de doctorat ès sciences appliquées
Spécialité : génie civil

Jury:

Claude Lupien	Président
Kenneth Neale	Rapporteur
Brahim Benmokrane	Directeur de recherche
Ehab El-Salakawy	Codirecteur
Omar Chaallal	Examinateur
Renata Kotynia	Examinateur

Shehab Monir SOLIMAN

Sherbrooke, Québec, Canada **October 2008**

Your file Votre référence
ISBN: 978-0-494-48582-8
Our file Notre référence
ISBN: 978-0-494-48582-8

To my FAMILY

Abstract

As we move into the twenty-first century, the renewal of our lifelines or deterioration of infrastructure becomes a topic of critical importance. The structures may have to carry larger loads, require change in building use, suffer steel corrosion problems, or errors made during the design or construction phases so that the structure may need to be repaired or strengthened before it can be used. The use of fiber reinforced polymers (FRP) in the last few years in various engineering application, forums and configuration offers an alternative design approach for the construction of new concrete structures and the rehabilitation of existing ones. The use of FRP materials for external strengthening of reinforced concrete (RC) structures has emerged as one of the most exciting and promising technologies in material and structural engineering. Externally bonded FRP reinforcement is relatively unprotected against impact, vandalism or severe environmental conditions. Their structural performance can be greatly affected by these drawbacks. But if the composite material is placed in slots inside the concrete cover some of these drawbacks can be overcome. This method is designated by Near Surface Mounted (NSM) method. Therefore, the presented work is carried out using this advantageous strengthening technique utilizing the non-corrodible FRP materials.

My research involved both experimental and analytical investigations on the use of FRP systems for strengthening concrete structures using NSM techniques. The main objectives of my research were to (1) develop/utilize an NSM system composed of FRP bars and adhesives, (2) investigate the bond performance for the proposed NSM system, (3) investigate the effect of freeze and thaw cycles on the of the new proposed system, (4) study the flexural behaviour of RC beams strengthened with NSM FRP bars, (5) develop an analytical model using non-linear finite element analysis (ADINA) taking into consideration the interfacial behaviour between the concrete and FRP bars and (6) establish design recommendations for the use of FRP bars for the NSM method. To achieve these objectives, the research program was divided into two parts. The first part included the experimental work while the second part included the analytical work. The first part consisted of two phases. The first phase included the pullout testing of 76 C-shape

concrete blocks including 16 conditioned blocks. The second phase included testing 20 flexural strengthened concrete beams using the NSM method. The second part included developing an analytical model to be used in a non-linear finite element program and to analyze and predict the behaviour of concrete beams strengthened for flexure using NSM FRP bars. The efficiency and accuracy of the model was verified by comparing its results to the experimental results. The developed analytical model was used to study the effect of different parameters. Test results are presented in terms of deflection, strain in the concrete, steel and FRP and modes of failure. Test results showed the superior performance of the proposed NSM FRP/adhesive system. The NSM system is able to increase both the stiffness and flexural capacity of concrete beams by approximately 100% over the unstrengthened one. The FEM was able to predict of the behaviour of the strengthened beams in flexure with NSM. Based on the experimental and analytical study, useful conclusions and recommendations for flexural strengthening with NSM FRP were provided.

Résumé

Alors que nous entrons dans le XXIème siècle, la dégradation des infrastructures devient un sujet d'une importance cruciale. Les structures doivent supporter des charges plus grandes et subir des changements d'utilisation. En plus de cela s'ajoute les problèmes de corrosion de l'acier, des erreurs de conception et de construction, ce qui souvent nécessitent que la structure soit réparée ou renforcée, des fois même avant sa mise en service. L'utilisation de polymères renforcés de fibres (PRF) dans les dernières années dans divers domaines d'ingénierie a permis une avancée technologique, et leur utilisation dans la construction de nouvelles structures en béton ainsi que la réhabilitation des anciennes. L'utilisation de matériaux en PRF pour le renforcement externe des structures en béton armé est une technologie des plus prometteuses dans l'ingénierie structurale ou de matériaux. Cependant le renforcement par collage externe de PRF n'offre pas une bonne protection contre les chocs, le vandalisme ou les conditions environnementales sévères, ce qui pourraaient affecter les performances structurales des éléments réhabilités. Ces inconvénients peuvent être surmontés si le PRF est inséré dans des rainures réalisées dans le recouvrement de béton. Cette méthode est appelée « mise en place d'Armatures Encastrées Près de la surface (AEPS)». Le présent travail s'articule autours de cette technique de renforcement utilisant des matériaux non corrodables.

Mes travaux de recherches se focalisent sur l'utilisation des AEPS en PRF pour le renforcement des structures, et cela d'un point de vue expérimental et analytique. Les principaux objectifs de mes recherches sont: (1) développer/utiliser un système d'AEPS composé de barres en PRF et d'adhésif, (2) étudier les performance d'adhérence du système proposé, (3) étudier l'effet des cycles gel-dégel sur le système proposé, (4) l'étude du comportement en flexion de poutres en béton armé, renforcées avec des barres d'AEPS en PRF, (5) développer un modèle analytique utilisant des méthodes non-linéaires d'analyse par éléments finis (logiciel ADINA) en tenant compte du comportement de l'interface béton-barres en PRF, et (6) mettre en place des recommandations de calcul pour l'utilisation des barres en PRF comme AEPS.

Pour atteindre ces objectifs, le programme de recherche a été divisé en deux parties. La première partie comprenait les travaux expérimentaux tandis que la deuxième comprenait des travaux d'analyse. La première partie elle même était constituée de deux phases. La première phase comprenait des essais d'arrachement direct de blocs de béton en forme de « C », dont 16 blocs conditionnés dans une chambre environnementale. Alors que la deuxième phase comportait des essais de flexion 20 poutres en béton armé, renforcées par des AEPS en PRF.

La deuxième partie à consisté au développement d'un modèle analytique non-linéaire par éléments finis de façon à pouvoir analyser et prédire le comportement en flexion de poutres en béton armé, renforcées par des AEPS en PRF. L'efficacité et la précision du modèle ont été vérifiées en comparant ses résultats analytiques aux résultats expérimentaux. Le modèle analytique développé a été utilisé pour étudier l'effet de différents paramètres. Les résultats des tests sont présentés en termes de déflexion, de contraintes dans le béton, l'acier et le PRF et les modes de rupture.

Les résultats des essais ont démontré les bonnes performances du système armatures PRF/adhésif proposé, ce dernier a permit d'augmenter à la fois la rigidité en flexion et la résistance des poutres en béton d'environ 100% par rapport à la poutre non renforcée. L'analyse par éléments finis a été en mesure de prédire le comportement en flexion des poutres renforcées avec des AEPS en PRF. Basé sur ces travaux, des conclusions et des recommandations utiles concernant le renforcement en flexion avec des AEPS en PRF ont été fournis.

Mots clés: polymères de fibres, PRFC, PRFV, armé, armatures encastrées près de la surface, AEPS, éléments finis, comportement en flexion

Acknowledgements

Praise be to Allah Almighty and Peace be upon His Prophet Muhammad

I wish to take the opportunity to express my acknowledgements to those whom without their assistance this thesis work could not have been done.

I would like to express my deepest appreciation to my supervisor Professor Brahim Benmokrane who introduced me to the area of research of fibre composites. Without exaggeration, this work could not have been done without his guidance, invaluable advice, helpful discussions and constant encouragement.

I am deeply grateful to my co-supervisor Prof. Ehab El-Salakawy for his constant support and continuous encouragement and guidance, not only on the academic side but also on the personal level. I am also most grateful to him for his help in making my settling in Canada a reality. He helped me in overcoming obstacles that I encountered during my first year in Canada.

The financial support provided by the Natural Sciences and Engineering Research Council of Canada (NSERC), and the Network of Centres of Excellence on Intelligent Sensing of Innovative Structures (ISIS Canada) Pultrall and Hilti Canada are gratefully acknowledged.

Many thanks to Mr. Francois Ntacorigira, Simon Sindayigaya, Nicolas Simard and other technical staff at the Structures Laboratory, Department of Civil Engineering, Université de Sherbrooke, for their technical assistance during the fabrication, construction and testing of the specimens.

Many thanks also go to all my colleagues and friends in the Department of Civil Engineering at the Université de Sherbrooke, in particular Dr. Hussein Abd El-Baky for his great help in the analytical part of my study.

I cannot end my acknowledgements without expressing my profound and eternal gratitude to: my father, my mother, my sister. I owe my loving thanks to my wife Nermine and my lovely son Hussein who continuously encouraged me to strive for success in my life.

This thesis is dedicated to my dad, Prof. Monir Hussein Soliman

TABLE OF CONTENTS

Chapter 3 EXPERIMENTAL PROGRAM

LIST OF FIGURES

LIST OF TABLES

Chapter 1 - Introduction

1.1. General

Since the first structures were formed, whether by nature or early human beings, they have been plagued by deterioration and destruction. Deterioration and destruction could happen due to environmental effects and improper use or maintenance of these structures. These are laws of nature that affect even the most modern structures. Therefore, it is important to have durable structures with long sustained life and low maintenance effort and costs. Maintenance is not only about costs but also a necessity to keep the structure at a specific high performance level, which includes load carrying capacity, serviceability, durability, function and aesthetic appearance. A structure that fulfill all demands of load carrying capacities must, at the same time, satisfy the durability demands or satisfy the society's demands for aesthetic appearance. Absence or incorrect maintenance will, in most cases, increase the speed of the degradation process and, therefore, lower the performance of the structure. The regular maintenance and repair of the different elements of any structure is always needed to restore the original performance of that structure. A reinforced concrete (RC) structure must have a long life. During this time duration, its carrying capacity, use, performance and aesthetic appearance could be changed. This change could be from the owners, users or surrounding society. To meet the changed demands, the RC structure needs to be upgraded or strengthened to increase its life time, durability and reliability. A structure with satisfactory load capacity, aesthetic appearance, and durability might not fulfill the function demands. To meet changed demands, a structure may be upgraded, which furthermore can be a way to increase life, durability and reliability of the structure.

As we moved into the twenty-first century, the renewal of our lifelines or deterioration of infrastructure becomes a topic of critical importance. The structures may have to carry larger loads, require change in building use, suffer steel corrosion problems, or errors made during the design or construction phases so that the structure may need to be repaired or strengthened before it can be used.

The requirement to repair and strengthen old concrete structures is increasing in the last decade. If one considers the capital that has been invested in existing infrastructures, then it is not always economical to replace an existing structure with a new one. The challenge must be taken to develop relatively simple measures to keep or increase a structure performance level through its life. It is important to analyze the problem to be able to select the most suitable method. The improper choice of an inappropriate repair or strengthening method can even worsen the structure's function. In comparison to building a new structure, strengthening an existing one is often more complicated since the structural conditions are already set. In addition, it is not always easy to reach the areas that need to be strengthened. Traditional methods have been used as strengthening techniques for concrete structure, such as: different kinds of reinforced overlays, shotcrete or post-tensioned cables placed on the outside of the structure; normally need much space, (Carolin 2003; Nordin 2003) bonding external steel plates and now using fibre reinforced polymer (FRP).

The use of FRP in the last few years in various engineering applications, forums and configurations offers an alternative design approach for the construction of new concrete structures (Benmokrane et al. 2006a and 2006b) and the rehabilitation of exciting ones (Almusallam 2006).

The use of FRP materials for external strengthening of reinforced concrete (RC) and masonry structures has emerged as one of the most exciting and promising technologies in materials and structural engineering. The key properties that make these materials suitable for structural strengthening are their non-corrodible nature and high strength-to-weight ratio. As a result, their use in rehabilitation and strengthening can present many significant advantages with respect to the conventional methods, (ACI 440.2R-08, ISIS CANADA 2001b and CSA-S806-06).

Externally bonded FRP laminates have been successfully used to increase the flexural or shear capacity and stiffness of RC beams. A considerable amount of experimental research has been carried out and is currently ongoing towards the characterization of RC structures strengthened with externally bonded FRP laminates (Ashour et al. 2004, Wenwei and Guo 2006, Almusallam 2006, El-Maaddawy and Soudki 2008). At the same

time, many successful applications have been conducted through the industrial, commercial, and public markets all over the world (Hag-Elsafi et al. 2001). Externally bonded FRP reinforcement is relatively unprotected against impact, vandalism or severe environmental conditions. Its structural performance can be greatly affected by these drawbacks. But if the composite material is placed in slots inside the concrete cover some of these drawbacks can be overcome. This method is designated by Near Surface Mounted (NSM) method. Therefore, the present work is carried out using this advantageous strengthening technique utilizing the non-corrodible FRP materials.

Extensive research programs are being conducted at the Université de Sherbrooke through the Natural Sciences and Engineering Research Council (NSERC) Industrial Research Chair in Innovative Fibre Reinforced Polymer (FRP) Composite Materials for Infrastructures. A joint effort with the chair partners was established to develop and implement the FRP technologies in concrete structures.

Many researches have been conducted for the use of FRP as internal reinforcement in concrete structures through the NSERC chair (Wang et al. 2002, El-Gamal et al. 2007, El-Sayed et al. 2006 and El-Ragaby et al. 2007). This extensive research has been implemented in many field applications (El-Salakawy, et al. 2005, Benmokrane et al. 2005 and 2006).

The use of FRP bars for strengthening of existing structures has not been yet investigated through the NSERC chair. This research project focuses on the use of the newly developed V–ROD bars manufactured by Pultrall Inc. (Thetford Mines, Quebec) and adhesives manufactured by Hilti Inc. (Montreal, Quebec) for strengthening using near surface mounted techniques.

1.2. Research Objectives

There are significant data available on the flexural and shear strengthening of concrete structures using NSM steel bars, including mechanical and theoretical models. However, these data and models cannot be directly applied to NSM using FRP bars due to the fundamental differences in mechanical and bond properties between FRP and steel bars.

Therefore, changes in the design philosophy of concrete structure strengthened with FRP-NSM bars are required. FRP materials are anisotropic and are characterized by high tensile strength only in direction of the reinforcing fibres. The FRP materials do not exhibit yielding; rather they are elastic until failure. In the recent literature, few data is available regarding the flexural and shear strengthening of concrete structures using NSM-FRP (Cruz et al. 2004; El-Hacha et al. 2004; Hassan and Rizkalla 2003; Lorenzis and Nanni 2001a, b and c; Lorenzis and Nanni 2002; Lorenzis et al. 2002; Taljsten et al. 2003).

However, rehabilitation techniques are usually introduced to the end-users as a strengthening system with specific materials and installation procedures. Therefore, the main objectives of this research project conducted at the University of Sherbrooke through the NSERC research Chair in Innovative Structural FRP Composite Materials for Infrastructure are:

1. To develop/utilize an NSM system composed of FRP V-ROD bars manufactured by Pultrall Inc. (2006) and adhesives manufactured by Hilti Inc. (2006);
2. To investigate the effect of different parameters on the bond performance of the proposed NSM system.
3. To investigate the effect of freeze/thaw cycles on the bond performance of the proposed NSM system.
4. To study the flexural behaviour of RC beams strengthened with the proposed NSM-FRP system.
5. To conduct an analytical model using non-linear finite element analysis taking into consideration the interfacial behaviour between the concrete and FRP bars.
6. To establish design recommendations for the use of FRP bars in the NSM strengthening technique.

1.3. Methodology

To achieve the above objectives, two different approaches have been used. One includes the experimental work, while the second includes the analytical work as shown in Fig. 1.1.

The experimental work consists of two phases. The first phase includes pullout testing of 76 specimens of NSM-FRP bars embedded in C-shaped concrete blocks.

The pullout tests included the following test parameters:

1. Type of FRP bar,
2. Diameter of FRP bar,
3. Groove size,
4. Bonded length,
5. Type of adhesive,
6. Effect of 200 freeze-thaw cycles.

The second phase includes testing of 20 full-scale RC beams strengthened in flexure with NSM-FRP bars having the following test parameters:

1. Internal steel reinforcement ratio,
2. Bonded length,
3. Groove size,
4. Type of FRP bars,
5. Diameter of FRP bars.

The analytical work includes conducting an analytical model to be used in a commercially available non-linear finite element program (ADINA 2004a) to analyze and predict the behaviour of RC beams strengthened in flexural using NSM-FRP bars. The efficiency and accuracy of the model is calibrated against the experimental results. The developed analytical model is also used to study the effect of different parameters.

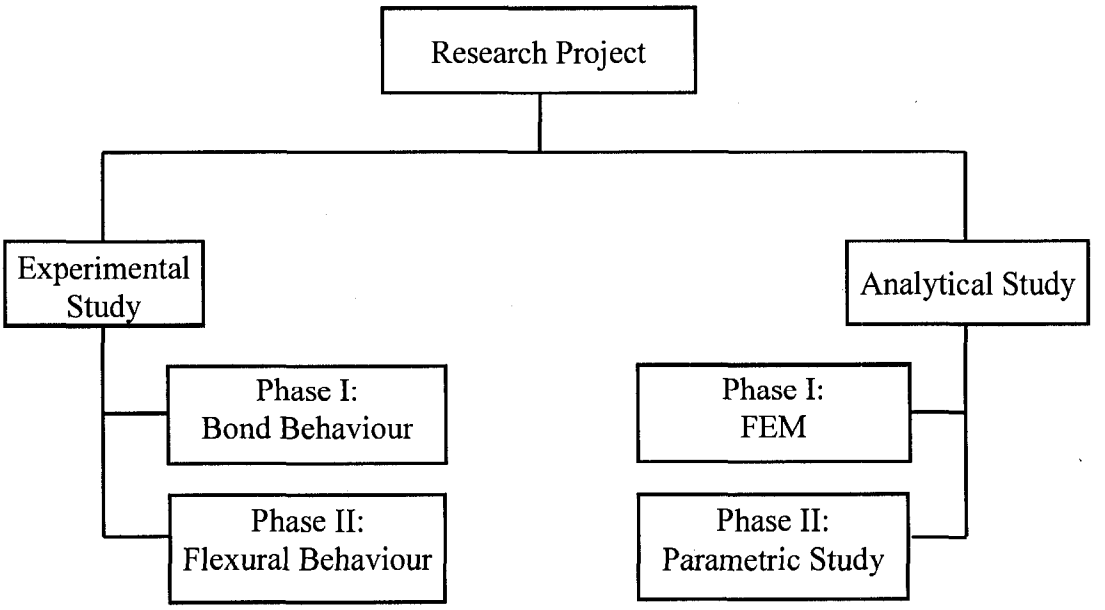

Fig. 1.1. Research program

1.4. Thesis Structure

This thesis is divided into six chapters as shown in Fig. 1.2.

Chapter 1 provides the introduction to FRP and NSM strengthening technique, research objectives, and methodology to achieve these research objectives and the organization of the thesis.

Chapter 2 provides a literature review and a background on FRP, strengthening of concrete structure using either externally bonded or NSM-FRP bars and strips. Also, the durability and effects of the environmental conditions on strengthened structures are reviewed.

Chapter 3 describes the experimental program, fabrication of test specimens, strengthening procedures, instrumentation and test-setup.

Chapter 4 describes the pullout test results and the effect of the studied parameters on the bond performance. Also, a discussion of the bond-slip relationships for the sand-coated V-ROD FRP bars (carbon and glass) is discussed in this chapter.

Chapter 5 discusses the beam test results and the effect of the different studied parameters on the flexural performance of the NSM-FRP strengthened beams.

Chapter 6 discusses the analytical investigation that was carried out using the finite element software, ADINA, (ADINA, 2004a).

Chapter 7 presents the conclusions and recommendations for future work.

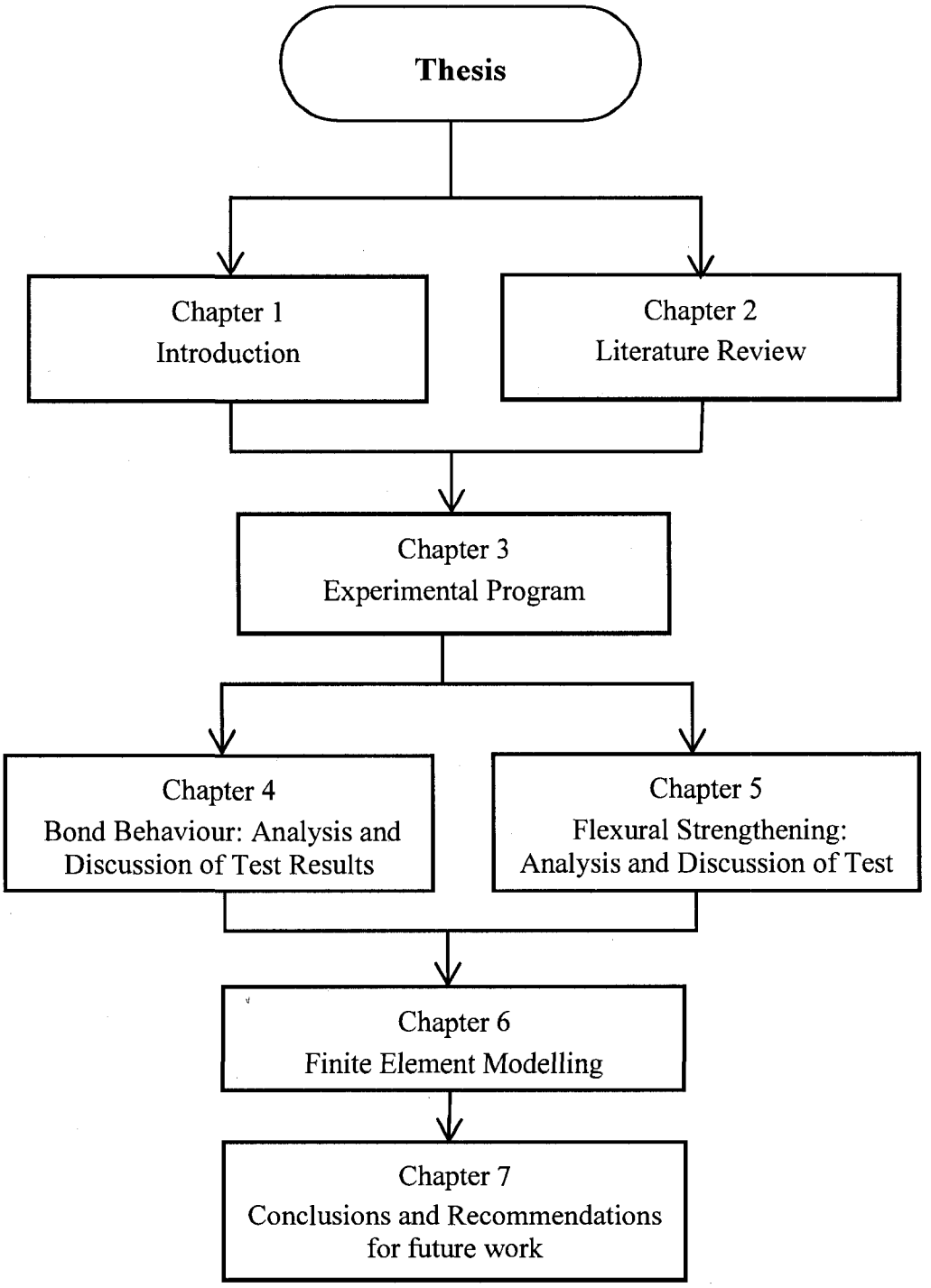

Fig. 1.2. Thesis layout

Chapter 2 - Literature Review

2.1. General

As mentioned earlier, structures often need to be repaired or strengthened. There are a variety of methods to perform these rehabilitation tasks, for example, adding a new structural material, post-tensioned cables, or changing the structural system. In recent years, the development of the plate bonding repair technique showed to be applicable to many existing strengthening problems in the construction industry. The idea of plate bonding is mainly based on the fact that concrete is a building material with high compressive strength and poor tensile strength. A concrete structure without any form of reinforcement subjected to tension or bending will crack and fail at a relatively small load. This means that the concrete structure's load carrying capacity is often limited by the amount of reinforcement. Adding reinforcement, through bonding it to the surface, may result, in many cases, to increase the load carrying capacity. Steel plate-bonding is one of the plate-bonding techniques, even if this method performs quite well it has some drawbacks. First, is that the steel plates are difficult to mount at the work site. If the bonding is required on an overhead application (bottom side of a slab or a beam) it is necessary to apply external pressure during the curing of the adhesive. Second, is the risk of corrosion of the steel plates. Third, is that the steel plates might need splicing due to limited transportation length. Furthermore, steel plates may be difficult to apply to curved surfaces. All these have led to the search for an innovative reinforcing material, which is the FRP composite material.

FRP plate-bonding can be applied by laminate plate bonding or the hand lay-up method. This technique may be defined as one in which composite sheets or plates of relatively small thickness are bonded with an epoxy adhesive to a concrete structure to improve its structural behaviour and strength. The FRP sheets/plates do not require much space and give a composite action between the adherents. The adhesive that is used to bond the FRP fabric/laminate to the concrete surface is a two component epoxy adhesive. The old structure and the new bonded-on material create a new structural element that has a

higher strength and stiffness than the original one. A bonded-surface material is relatively sensitive to fire, accidents or vandalism. But if the composite material is placed in slots in the concrete cover some of these drawbacks can be overcome. This method can be designated as Near Surface Mounted Reinforcement (NSMR).

2.2. Fibre Reinforced Polymer (FRP)

Fibre Reinforced Polymer (FRP) products are composite materials consisting of reinforcing fibres embedded in a polymer resin matrix. The fibres are ideally elastic, brittle and stronger than the matrix. The mechanical performance of the composite depends on the fibre quality, fibre orientation, length, shape, volumetric ratio, adhesion to matrix, and on the manufacturing process. Typical FRP reinforcement products are sheets, grids, bars, fabrics, tendons and ropes. The bars have various types of cross-sectional shapes (square, round, solid, and hollow) and surface deformations (exterior wound fibres, sand coating, and separately formed deformations).

2.2.1. Reinforcing fibres

The fibres are the main load resisting component of the composite. They must have high strength, high modulus of elasticity, sufficient elongation at failure, and sufficient resistance to the environment to which the structure will be implemented. The performance of the fibres is affected by their length, cross-sectional shape, and chemical composition. Fibres are available in different cross-sectional shapes and sizes. Depending on the type of the fibre, the diameter of the fibres is in the range of 5 to 25 microns (Rostasy 1993). The most commonly used fibres for FRPs are Carbon, Glass, and Aramid, where the corresponding composite products would be known CFRP, GFRP, and AFRP, respectively.

2.2.1.1. Carbon fibres

Carbon fibres have a high modulus of elasticity (200 - 800 GPa), high strength and stiffness to weight ratios, low sensitivity to fatigue loads, and excellent moisture and chemical resistance. However, carbon fibres have low impact resistance due to their low ultimate strain. Carbon fibres can also be highly conductive to heat and electricity, which may be an advantage or disadvantage, depending on the designer's viewpoint. As shown in Table 2.1, carbon fibres can be classified into four types based on modulus of elasticity. The four types include low modulus (230 - 250 GPa), intermediate modulus (290 - 300 GPa), high modulus (350 - 380 GPa), and ultrahigh modulus (480 - 760 GPa) (Mallic 1988). In general, the low-modulus carbon fibres have lower density, lower cost, higher tensile and compressive strength, and higher tensile strain to failure than the high-modulus fibres.

2.2.1.2. Glass fibres

Glass fibres are the most common type of all reinforcing fibres for FRPs. The glass fibres are low cost and possess high tensile strength and excellent insulating properties. However glass fibres have a low tensile modulus, high density, sensitivity to abrasion and alkaline environments, and relatively low resistance to moisture, sustained loads, and cyclic loads. The fibres are categorized in three different types: C-glass, S-glass, and E-glass. C-glass provides excellent chemical stability and is used in a variety of environments. E-glass is a low-cost general purpose fibre, which provides strength, electrical resistance, and acid resistance. S-glass fibres have higher strength, stiffness, and ultimate strain than E-glass, but they are more expensive and more susceptible to environmental degradation.

2.2.1.3. Aramid fibres

Aramid, an abbreviated term for aromatic polyamide, is made from para-type fibres with straight-chain benzen nuclei. Aramid fibres are almost fully crystalline, strong in the longitudinal direction but have weaker bonds in the transverse direction (Mallic 1988). Three types of Kevlar aramid fibres are available for fabricating FRP. There are Kevlar 149, Kevlar 49, and Kevlar 29 with a modulus of elasticity of 179, 131, and 82 GPa,

respectively as given in Table 2.1 (ISIS CANADA 2007a). Aramid fibres have excellent impact resistance, high stiffness, high thermal stability, and low density compared with other fibres. However, ultraviolet light causes degradation of the aramids and exposure to moisture facilitates creep. The cost of aramids is higher than glass, but less than carbon (Nanni 1994).

Table 2.1. Mechanical Properties of Fibres, (ISIS CANADA 2007a):

Fibre type		Tensile Strength (MPa)	Modulus of Elasticity (GPa)	Elongation (%)	Coefficient of thermal expansion ($x10^{-4}$)	Poisson's Ratio
Carbon						
Pan	High strength	3500	200-240	1.3-1.8	-1.2 to -0.1	-0.20
	High modulus	2500 - 4000	350 - 650	0.4-0.8		
Pitch	Ordinary	780 - 1000	38 - 40	2.1-2.5	-1.6 to -0.9	N/A
	High modulus	3000 - 3500	400 - 800	0.4-1.5		
Aramid						
Kevlar 29		3620	82.7	4.4	N/A	0.35
Kevlar 49		2800	130	2.3	-2.0 - 59	
Kevlar 129		4210	110	-	N/A	
Kevlar 149		3450	172 - 179	1.9	N/A	
Technora		3500	74	4.6	N/A	
Glass						
E-Glass		3500 - 3600	74 - 75	4.8	5.0	0.2
S-Glass		4900	87	5.6	2.9	0.22
Alkali resistance glass		1800-3500	70-76	2.0-3.0	N/A	N/A
Steel		483-690	200-210	1.4-2.5	11.7	0.30

2.2.2. Resins

Resins are polymeric materials that are rigid or semi rigid at room temperature. The resin not only coats the fibres and protects them from mechanical abrasion, but also transfers inter-laminar and in-plane shear in the composite material, and provides lateral support to fibres against buckling when subjected to compressive loads. In addition, the physical and thermal properties of the resin significantly affect the final mechanical properties of

the composite product. There are two common types of polymeric materials used for FRP composites; namely, thermosetting and thermoplastic (ISIS CANADA 2007a).

2.2.2.1. Thermosetting resin

Thermosetting polymers are used more often than thermoplastic. They are low molecular-weight liquids with very low viscosity. Their molecules are jointed together by chemical cross-links so they form a rigid three-dimensional structure that once set, cannot be reshaped by heat or pressure. Some commonly used thermosetting polymers are polyesters, vinyl esters and epoxies. They all have good thermal stability and chemical resistance and have low creep and stress relaxation. The main disadvantages of these resins are their relatively low strain to failure, short shelf life, and long manufacturing time. Table 2.2 gives the typical properties of these resins.

2.2.2.2. Thermoplastic resin

Thermoplastic matrix polymers are made from molecules in a linear structural form. These are held in place by weak secondary bonds, which can be destroyed by heat or pressure. After cooling, these matrices gain a solid shape. Although it can degrade their mechanical properties, thermoplastic polymers can be reshaped by heating as many times as necessary.

Table 2.2. Typical Properties of Thermosetting Resins, (ISIS CANADA 2007a):

Resin	Specific Gravity	Tensile Strength (MPa)	Tensile Modulus (GPa)	Cure Shrinkage (%)
Epoxy	1.20-1.30	55.00-130.00	2.75-4.10	1.00-5.00
Polyester	1.10-1.40	34.50-103.50	2.10-3.45	5.00-12.00
Vinyl Ester	1.12-1.32	73.00-81.00	3.00-3.35	5.40-10.30

2.2.3. FRP reinforcement products

FRP reinforcing bars are manufactured from continuous fibres (such as carbon, glass, and aramid) embedded in matrices (thermosetting or thermoplastic). Similar to steel reinforcement, FRP bars are produced in different diameters, depending on the manufacturing process. The surface of the bars can be spiral, straight, sanded-straight, sanded-braided, and deformed. The bond of these bars to concrete is usually equal to, or

better than, the bond of steel bars. Table 2.1 gives the mechanical properties of some commercially available FRP reinforcing bars.

There are many methods used for producing FRP materials. Some of these methods are used for the manufacturing of low-cost non structural FRPs, while others are used for higher performance FRP. There are three common manufacturing processes for FRP materials, pultrusion, braiding, and filament winding (Nanni 1994).

2.3. Near Surface Mounted Techniques (NSM)

The use of Near Surface Mounted Reinforcement for concrete structures is not a new invention. The first application was used in Lapland, Finland in 1940s, where a concrete bridge deck slab was strengthened in the negative moment zone, Fig. 2.1, (Asplund 1949). In this application, steel bars were placed in slots in the top concrete cover and then bonded with cement grout. It has also been quite common to use steel bars, fastened to the outside of the structure, covered with shotcrete. However, in these applications, it was often difficult to get a good bond to the original structure, and in some cases, it was not always easy to adequately cast the concrete around the steel reinforcing bars. From the 1960s, the development of strong adhesives, such as epoxies, for the construction industry moved the method further ahead by bonding the steel bars inside sawed-slots in the concrete cover. However, due to the corrosion sensitivity of steel bars an additional concrete cover is still needed. For these applications, epoxy-coated steel bars have also been used. However, it has been shown that over time, epoxy-coated steel bars are not always corrosion-resistant for various reasons that will not be discussed here. It cannot be said that the use of steel NSMR has shown great success. Nevertheless, by using FRP-NSMR some of these drawbacks can be overcome. FRP bars do not corrode, so thick concrete covers are not needed; the lightweight of the FRP makes them easy to mount especially in overhead applications.

The NSM-FRP method has many advantages over the externally-bonded (EB) FRP system rather than it is protected in the concrete cover from the environmental condition. It can be even used in combination with EB, providing enough concrete cover for a desired groove size. No surface preparation is needed for NSM rather than cutting the groove in the concrete cover. Debonding of NSM is not likely to happen due to the

double-bonded area of this method, or it can be efficiently anchored to the adjacent member to prevent debonding. Prestressing the NSM can be more easily than the EB. In addition, in NSM system, the aesthetic appearance of the strengthened structure is unchanged. Due to the above advantages, the NSM-FRP method is in many cases superior to the EB-FRP method.

However, before proceeding, a short description of how to undertake a strengthening work with NSMR is introduced. In real practice, the following steps should be performed during strengthening as shown in Fig. 2.3.

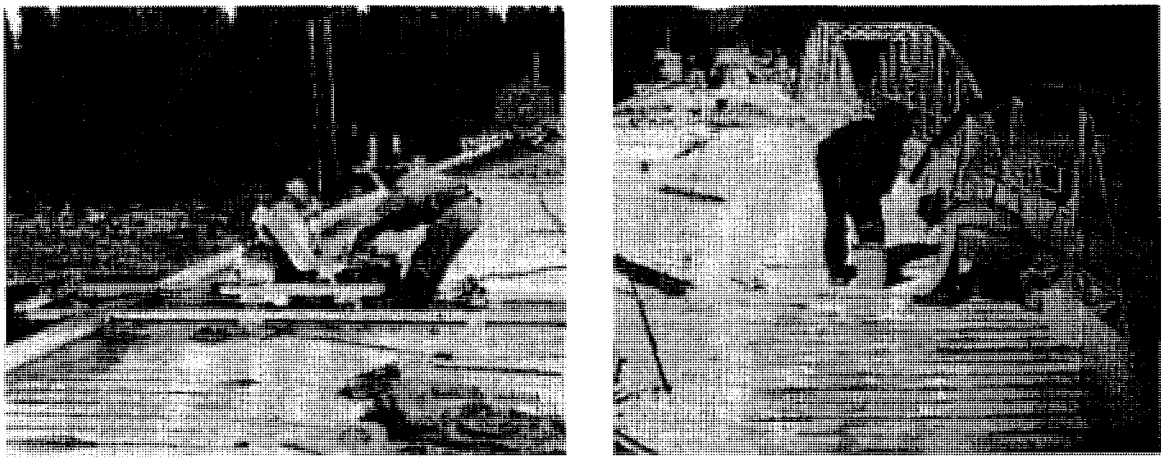

Fig. 2.1. Grouting of steel bars in bridge deck slab, Finland (Asplund 1949)

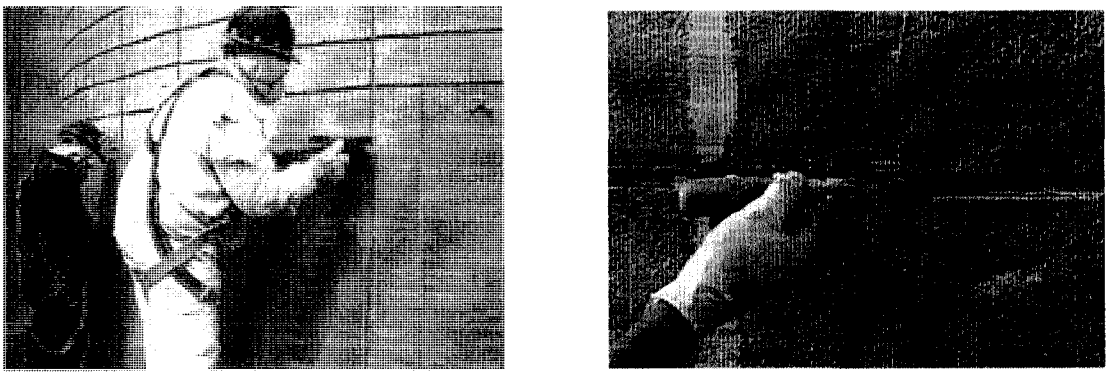

a) cutting the groove with a concrete saw. b) adding the adhesive material to the groove.

Fig. 2.2. Steps of installation of NSM FRP (Sika Canada 2006) (cont. next page)

c) putting the FRP rod in the groove.

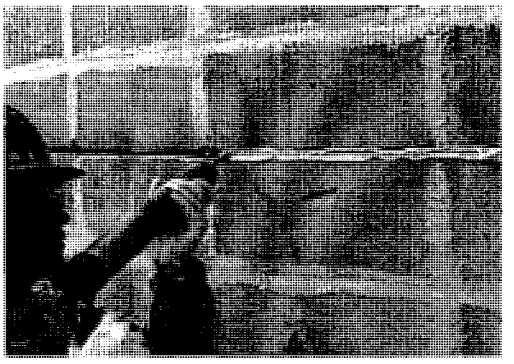

d) additional adhesive is applied to fill the groove

Fig. 2.3. Steps of installation of NSM FRP (Sika Canada 2006)

The process starts with sawing slots in the concrete cover, with a depth depending on the product used and the thickness of concrete cover, Fig. (2.2a).

Following the sawing process, careful cleaning of the slots is performed using high-pressurized air. Then the adhesive is applied in the slot, Fig. (2.2b). The NSMR laminates or bars are mounted in the slot Fig. (2.2c) and additional adhesive is added to fill the groove after mounting the FRP bar, Fig. (2.2d). Extra adhesive is then removed and the surface is levelled.

2.3.1. Bond behaviour

Bond is of primary importance, since it is the means for the transfer of stresses between the concrete and the FRP reinforcement developing the composite action. The bond behaviour influences the ultimate capacity of the reinforced element as well as serviceability aspects such as crack width and crack spacing. The performance of bond of NSM depends on many parameters such as groove and bar dimensions, tensile strength of concrete, type of FRP bar, type of adhesive, the FRP cross sectional shape and surface finishing, and degree of roughness of the groove surface. Few researches were made to investigate the bond performance of NSM-FRP in concrete and the factors affecting it. The most common types of bond test that can be used to investigate the bond behaviour of NSM are direct and beam pullout tests.

De Lorenzis et al. (2002) performed a direct pull-out test to investigate the mechanics of bond between NSM FRP bars and concrete using 36 C-shaped concrete specimens. The

specimen has a pre-formed square groove in the middle to have a smooth groove surface for embedment of the NSM-FRP bar as shown in Fig. 2.4. The test variables were: groove-filling material (epoxy and cement adhesives), bonded length (equal to 4, 12 and 24 times the FRP bar diameter), square groove size (equal to 1.25, 1.50, 2.00 and 2.50 times the FRP bar diameter), and surface texture of the FRP bar (spirally wound sand-coated and ribbed-deformed).

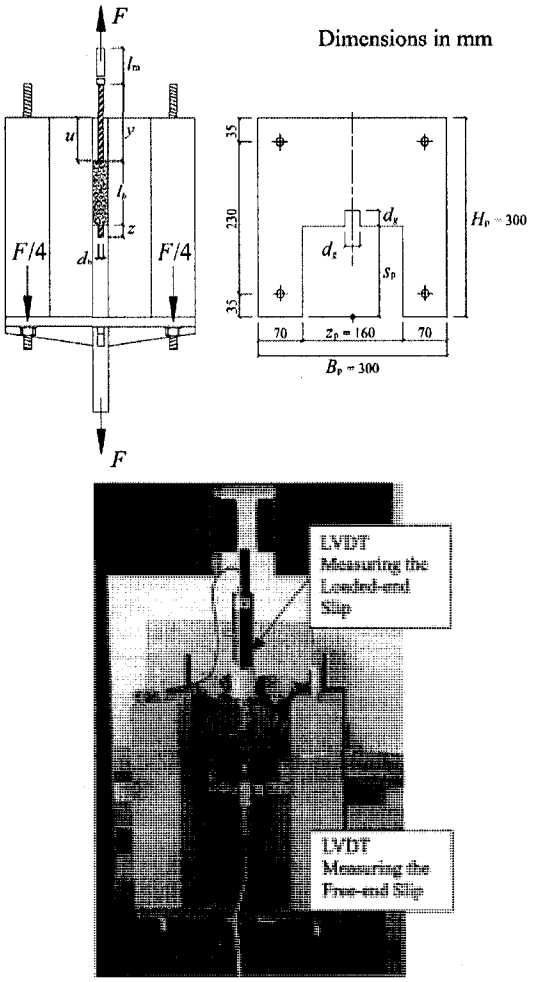

Fig. 2.4. Test specimen, (De Lorenzis et al. 2002)

The specimens had an average concrete compressive strength of 22 MPa, the epoxy had a tensile strength of 28 MPa and the cement mortar had a tensile strength of 6.3 MPa. The ribbed-deformed GFRP bars had 873 MPa tensile strength and 37.17 GPa Young's modulus, the ribbed CFRP bars had 2014 MPa tensile strength and 109.27 GPa Young's

modulus, and the spirally wound CFRP bars had 2214 MPa tensile strength and 174 GPa Young's modulus.

Different failure modes were observed depending on the test variables: slipping at the interface between concrete and groove-filling material, splitting of the cover with no concrete cracking, slipping at the bar-cement interface, and cracking of the concrete surrounding the groove accompanied by formation of splitting cracks in the epoxy cover. For specimens with epoxy resin as groove-filling material, failure at the epoxy–concrete interface was the critical mode of failure in all cases. This was due to the smooth surface of the pre-formed grooves. While for specimens with cement-filled grooves, splitting of the cover was more frequent. The ultimate load of the specimens with cement-filled grooves was much lower than that of epoxy-filled specimens based on an average and considering the same variables, the difference was approximately 70%. This was due to the lower strength of the cement compared to epoxy (the cement mortar had a tensile strength of 6.3 MPa vs. 28 MPa tensile strength of the epoxy),which control the splitting and slip loads, respectively, as well as the adhesion between mortar and concrete. Another factor that might have influenced results is the expansion of the cement mortar. After hardening, it was noted that equally spaced transverse cracks had developed in the mortar along the bonded length of the FRP bar. These cracks were wider and more numerous for specimens with bigger grooves. The presence of such cracks might have been of negative influence on the test results, and could explain why, in some cases, mortar-filled specimens with bigger groove sizes had lower ultimate loads than those with smaller grooves.

For a given depth of the groove, the ultimate load increases as the bonded length increases. However, the average bond strength decreases, due to the non-uniform distribution of the bond stresses along the bonded length where the average bond strength depends on the failure mode. When failure is at the epoxy–concrete interface, the average bond strength, τ_{avlu} is significance at the failed interface which is computed as

$$\tau_{avlu} = \frac{P_{max}}{3d_g l_b} \tag{2.1}$$

where P_{max} is the ultimate load, d_g is the square groove size and l_b is the bonded length. In this case, the average bond strength decreases as the groove size increases, due to the non-uniform distribution of the bond stresses along the perimeter of the groove.

For the other failure mechanisms, the average bond strength, τ_{av2u} is that at the interface between the bar and groove-filling material, which is computed as,

$$\tau_{av2u} = \frac{P_{max}}{\pi d_b l_b} \tag{2.2}$$

where d_b is the bar diameter. This average bond strength increases for increased groove size, as the bigger cover depth delays the occurrence of splitting.

De Lorenzis and Nanni (2002) performed other beam pull-out tests on NSM-CFRP and GFRP ribbed bars, to study the effect of varying the bonded length and the groove size on bond strength. The specimens were 22 unreinforced inverted T-shaped cross section concrete beams with spans of 1067 mm, depth of 254 mm and width of 254/152 mm. The beams were loaded under four point bending with a shear span of 483 mm as shown in Fig. 2.5. The specimen had a steel hinge at the top and a saw cut at the bottom, both at midspan to control the internal force distribution.

The concrete had a compressive strength of 28.2 MPa and the used epoxy had a tensile strength of 13.8 MPa. Tensile strength and modulus of elasticity of the used CFRP deformed bars, No. 3, were 1875 MPa and 104.8 GPa, respectively. For the GFRP No. 4 bars, a tensile strength of 799 MPa and a Young's modulus of 41.3 GPa were obtained. Properties of the CFRP No. 3 sandblasted bars were 1550 MPa tensile strength and 164.7 GPa Young's modulus.

Four different bonded lengths were selected; equal to 6, 12, 18 and 24 times the diameter of the FRP bar. Four different square groove sizes equal to 1.25, 1.5, 2.0 and 2.5 times the diameter of the FRP bar were tested.

Two FRP bar diameters, 9.5 mm and 12.7 mm, were examined. Both CFRP and GFRP bars were used. For the CFRP bars, two different surface conditions, deformed and sandblasted, were examined.

Three different modes of failure were observed in this investigation depending on the testing parameters used. For specimens with the smallest groove size (1.25 times the bar diameter) splitting of the epoxy cover was observed for all the bonded length used. While by increasing the groove size, the mode of failure was changed to cracking of concrete surrounding the groove. For specimens with sandblasted CFRP bar the main mode of failure was pullout of the FRP bar.

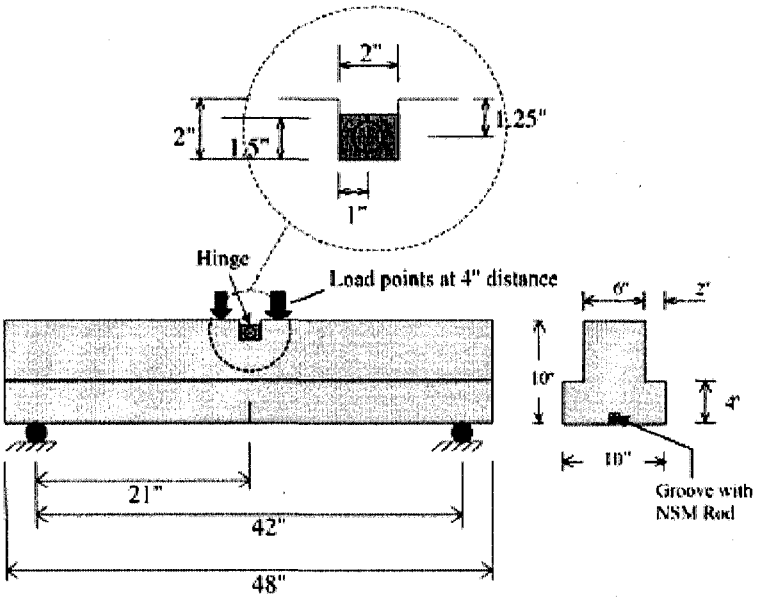

Fig. 2.5. Tested specimens, (De Lorenzis and Nanni 2002)

The strain in the rod was monitored by using strain gauges to plot strain distribution versus location along the bonded length for different values of load as shown in Fig. 2.6. It was found that the strain distribution along the bonded length, highly non-linear at moderate load levels, tends to linear as the applied load increases as shown in Fig. 2.6. This means as the applied load increases, the bond stresses become more evenly distributed along the bonded length.

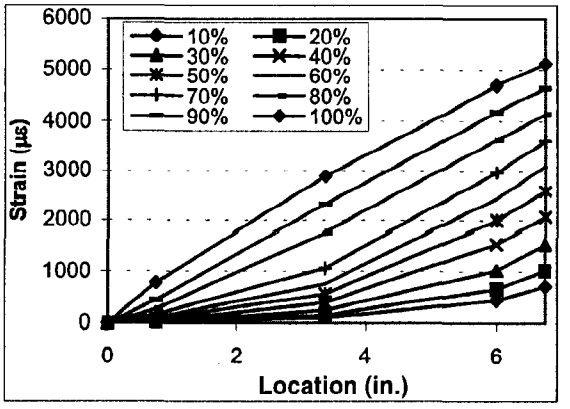

Fig. 2.6. Strain distribution along the CFRP bonded length, (De Lorenzis and Nanni 2002)

Lorenzis and Nanni (2002) used the data obtained from the strain gauges to obtain the local bond stress-slip relationship of NSM-CFRP deformed bar. It is important to define the local bond-slip that completely characterizes the bond behaviour of the system and can be used to evaluate the development length of a given type of FRP bar for each different groove size. The bond stress, τ versus location diagram at a given load level is shown in Fig. 2.8. This diagram can be obtained using equation (2.3) from the first derivative of the strain versus location diagram at that load level multiplied by the elastic modulus E_b and the diameter of the FRP bar

$$\tau(\mathrm{x}) = \frac{d_b}{4}.E_b \frac{d\varepsilon_b(x)}{dx} \tag{2.3}$$

Where x is the coordinate along the longitudinal axis of the FRP bar within the bonded length. The definition of slip is given by:

$$s_l(\mathrm{x}) = s_l(0) + \int_0^x \varepsilon_b(x)dx \tag{2.4}$$

Where $s_l(0)$ is the free-end slip of the FRP bar.

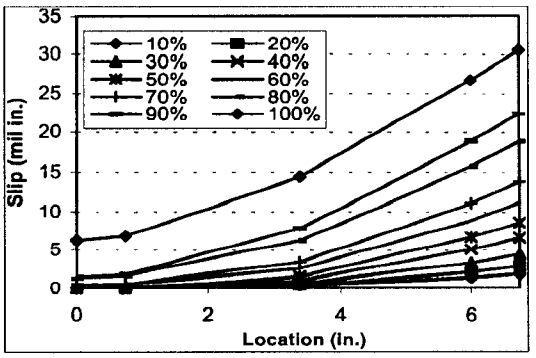

Fig. 2.7. Slip distribution along the CFRP bonded length, (De Lorenzis and Nanni 2002)

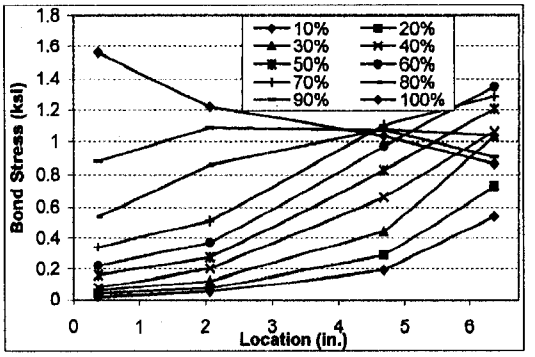

Fig. 2.8. Bond stress distribution along the CFRP bonded length, (De Lorenzis and Nanni 2002)

The local bond-slip relationship can be obtained by combining the two curves $\tau(x)$ and $s_l(x)$, (Fig. 2.7 and Fig. 2.8 given from equation (2.3) and (2.4)). τ versus x curve and s_l versus x curve can be obtained for each value of the applied load. Therefore, τ versus slip diagram corresponding to each value of applied load can be drawn at a given load level as shown in Fig. 2.9.

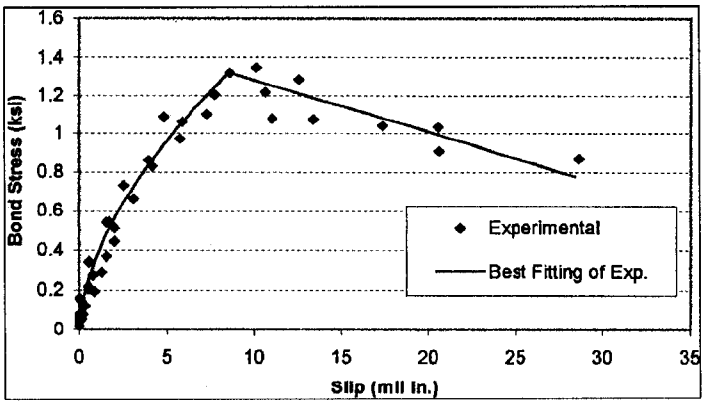

Fig. 2.9. Local bond slip along the CFRP bonded length, (De Lorenzis and Nanni 2002)

Cruz et al. (2004) investigated the bond behaviour of CFRP strip to concrete utilizing a pullout-beam test with specimens composed of two concrete specimens, specimen A and specimen B, as shown in Fig. 2.10. They used varying bonded length (40, 60 and 80 mm) and varying concrete compressive strength (35, 45, 70 MPa) with a fixed groove dimension, 15 mm depth and 3.3 mm width. Young's modulus of the CFRP strips was

158.3±2.6 GPa, 2,739.5±85.7 MPa tensile strength and the epoxy had a tensile strength of 25.8±2.1 MPa.

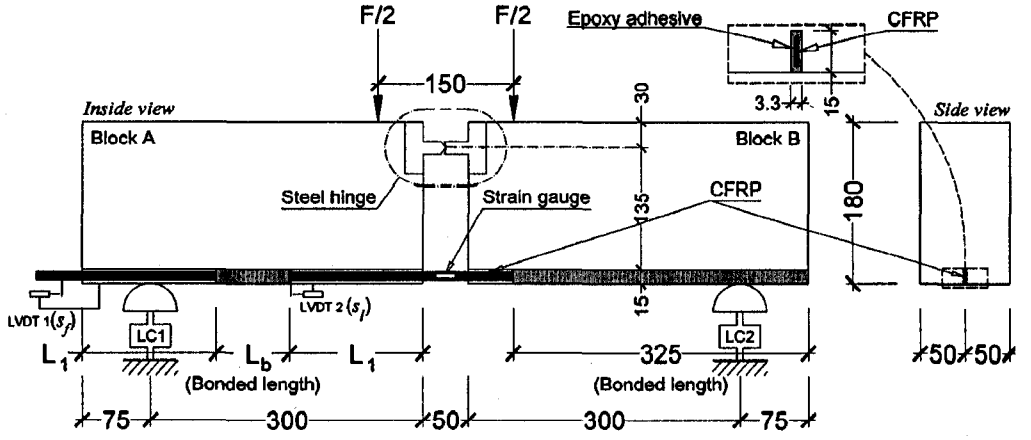

Fig. 2.10. Specimen of pullout-bending test, (Cruz et al. 2004)

The mode of failure for all the specimens was an interface failure or debonding failure between the epoxy and the concrete or between the CFRP strip and the epoxy. It was found from the experimental results that the pullout force was increased with the bond length, L_b as shown in Fig. 2.11. Also, the influence of the concrete compressive strength was marginal as the mode of failure was debonding failure and no cracks were observed in the concrete in this kind of test, as shown in Fig. 2.12. It was also found that the bond stress, τ_{max} decreases with bond length and is practically insensitive to concrete strength.

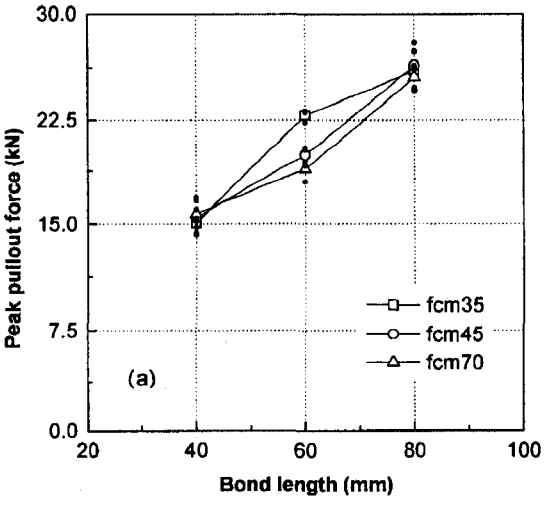

Fig. 2.11. Influence of bond length on the peak pullout force, (Cruz et al. 2004)

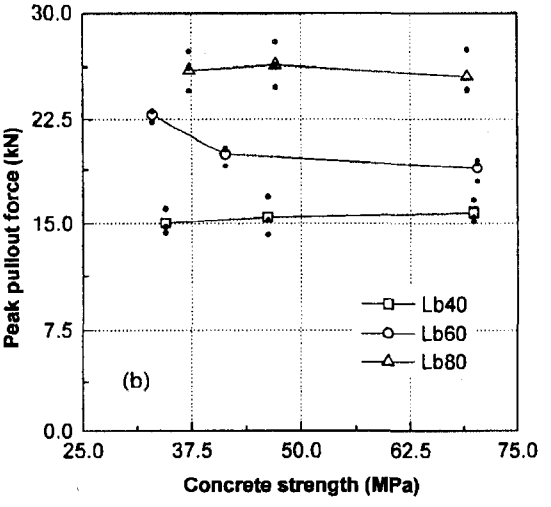

Fig. 2.12. Influence of concrete strength on the peak pullout force, (Cruz et al. 2004)

2.3.2. Flexural strengthening

One of the benefits of strengthening a structure is increasing its flexural strength. NSMR plays a great role in flexural strengthening. A lot of research was done on increasing the flexural capacity of concrete beams with FRP-NSMR. A large number of parameters can affect the flexural strengthening with FRP-NSMR.

Some research was done with bars and others with strips and a comparison was made between them. A summary of the exciting work will be summarized in the following section.

Hassan and Rizkalla (2003) conducted a flexural investigation on concrete beams strengthened with NSM CFRP strips using nine concrete T-section beams with a span of 2500 mm and a depth of 300 mm as shown in Fig. 2.13. Hassan and Rizkalla (2003) terminated the steel reinforcement in the middle to control the debonding failure and to locate it in the middle of the beam. One of their main objectives was to evaluate the minimum bonded length required to develop the ultimate force of the strip to provide sufficient increase in the flexural capacity. Eight different bonded lengths of 150, 250, 500, 750, 850, 950, 1050, and 1200 mm were used. The CFRP strips, which were produced by S&P Clever Reinforcement Company, Switzerland, have a width of 25 mm and a total thickness of 1.2 mm. The strips have a modulus of elasticity of 150 GPa and an ultimate tensile strength of 2,000 MPa as reported by the manufacturer. En-Force CFL epoxy adhesive was used for bonding the strips to the concrete.

It was clear from the results that using embedment lengths less than 250 mm provides insignificant improvement in strength as shown in Fig. 2.14. This is due to the early debonding of the CFRP strips. A small increase in strength (3.8%) was observed for embedment lengths greater than 250 mm. Specimens with embedment lengths of 500 and 750 mm provide an increase of about 15.4% and 42.3%, respectively; they failed due to debonding of the CFRP strips. Debonding was at both ends of the strips as well as at midspan. This was due to shear stress concentration at the cut-off points as well as at the flexural cracks at the midspan.

Beams with embedment lengths ranged from 850 to 1200 mm failed due to rupture of the CFRP strips. The measured failure loads for the four beams were almost identical as

shown in Fig. 2.15. They concluded that the minimum embedment length needed to rupture the near surface mounted CFRP strips, with the given dimensions used in this program is 850 mm. This means that for small embedment lengths less than 250 mm, debonding of the adhesive from the surrounding concrete occurred before yielding of the internal steel reinforcement.

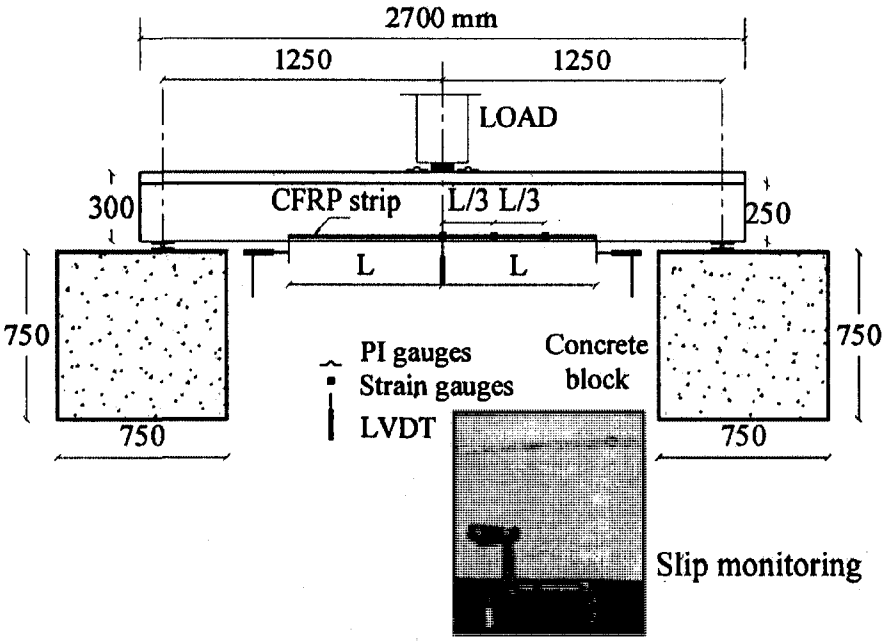

Fig. 2.13. Test Specimen, (Hassan and Rizkalla 2003)

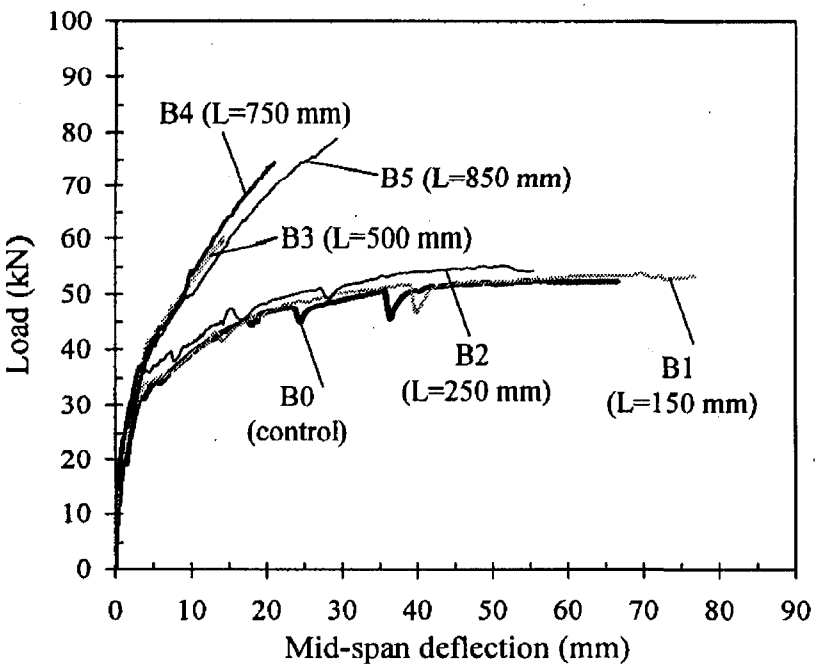

Fig. 2.14. Load-deflection behaviour of test specimens with embedded length (150-850 mm), (Hassan and Rizkalla 2003)

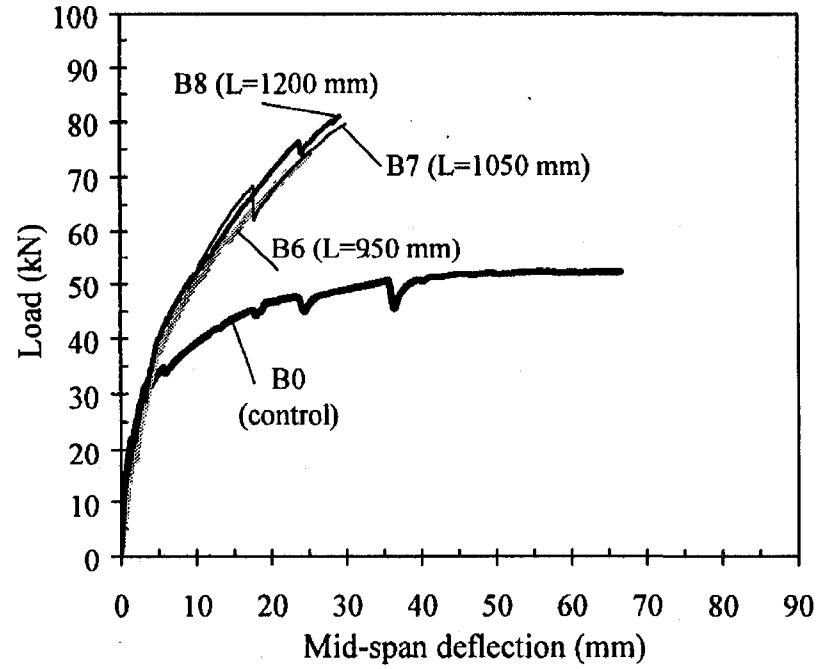

Fig. 2.15. Load-deflection behaviour of test specimens with embedded length (950-1200 mm), (Hassan and Rizkalla 2003)

Hassan and Rizkalla (2004) conducted another investigation using CFRP bars instead of the CFRP strips using the same dimensions and setup of the beams as in the previous investigation, (Fig. 2.13). The authors used two different kinds of epoxy adhesive with tensile strength and modulus of elasticity of 48 MPa and 1200 MPa, respectively, for the first adhesive. While the second type has a tensile strength and modulus of elasticity of 62 MPa and 3000 MPa, respectively to compare the effect of changing the adhesive tensile strength on the performance.

They used four different bonded lengths, 150, 550, 800 and 1200 mm. Beams with the smallest bonded length, 150 mm provided insignificant increase in the strength due to early debonding of the CFRP bar. Beams with 550, 800 and 1200 mm embedded length providing 19.6, 30.4 and 41.1 % increase in the ultimate capacity, respectively. Using two different kinds of adhesives had a negligible effect on the ultimate load as the mode of failure for all beams was debonding at midspan in the place where the internal steel reinforcement was terminated. The maximum measured tensile strain for the CFRP bars at failure was about 40% to 45% of the rupture strain of the bar.

El-Hacha and Rizkalla (2004) examined the structural performance of reinforced concrete beams strengthened in flexure with various NSM-FRP reinforcements compared to beams strengthened with externally-bonded FRP reinforcement. Eight simply supported concrete T-beams were constructed with a span of 2700 mm, a depth of 300 mm and a width of 150 mm. The beams were tested under a monotonically increasing concentrated load applied at mid-span. One beam was tested without strengthening as a control beam for comparison purposes, four beams were strengthened with different NSM-FRP systems, one CFRP bar, two types of CFRP strips, and a GFRP strip. Three beams were strengthened with externally bonded CFRP and GFRP strips as shown in Fig. 2.16. Table 2.3 summarises the test parameters for the tested beams.

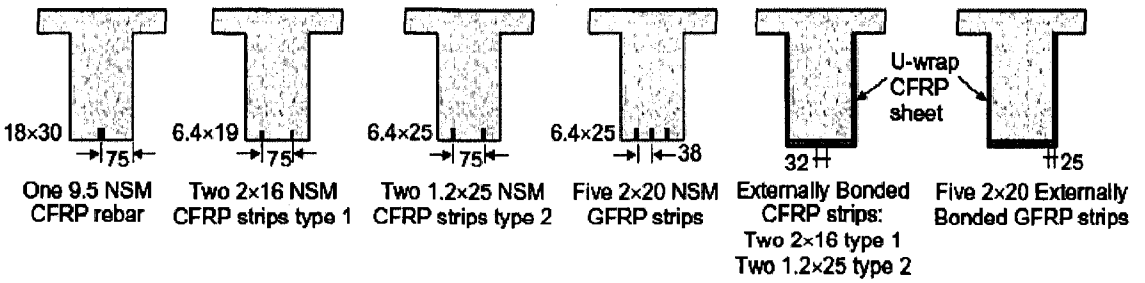

Fig. 2.16. FRP strengthening schemes, (El-Hacha and Rizkalla 2004)

Table 2.3. Test matrix for test specimens (El-Hacha and Rizkala 2004)

Beam No.	FRP Strengthening System
B0	No strengthening
B1	One 9.5 mm NSM CFRP bar (a)
B2	Two 2 mm×16 mm NSM CFRP strips type 1(a)
B3	Two 1.2mm×25 mm NSM CFRP strips type 2(b)
B4	Five 2 mm×20 mm NSM GFRP thermoplastic strips(c)
B2a	Two 2 mm×16 mm Externally Bonded CFRP strips type 1(a)
B3a	Two 2 mm×16 mm Externally Bonded CFRP strips type 2(b)
B4a	Five 2 mm×20 mm Externally Bonded GFRP Strips

(a) Hughes Brothers (b) Structural Composite (c) Dow Plastic Chemicals

The variable used in this investigation were the type of fibre (carbon or glass) and the shape of the FRP reinforcement (bars and strips), the effectiveness of the NSM-FRP bars and strips compared to the externally bonded FRP strips having the same axial stiffness. The embedded length of all the FRP-NSM bars and strips and the length of the externally bonded FRP strips were kept constant in all beams. Also the axial stiffness $(EA)_{FRP}$ for all FRP reinforcement was kept constant.

It was found that the flexural behaviour for all strengthened beams was similar to that of the unstrengthened beam before cracking and a nonlinear behaviour was observed up to failure as shown in Fig. 2.17. Using the same axial stiffness for the CFRP strips and bar, an increase in the ultimate strength of 69% for beam (B1) with FRP bar and 79 %, and 99

% increase for beams with two different types of strip respectively. Using NSM-FRP reinforcement resulted in a reduction in deflection and crack widths as well delayed the formation of new cracks in the strengthened beams.

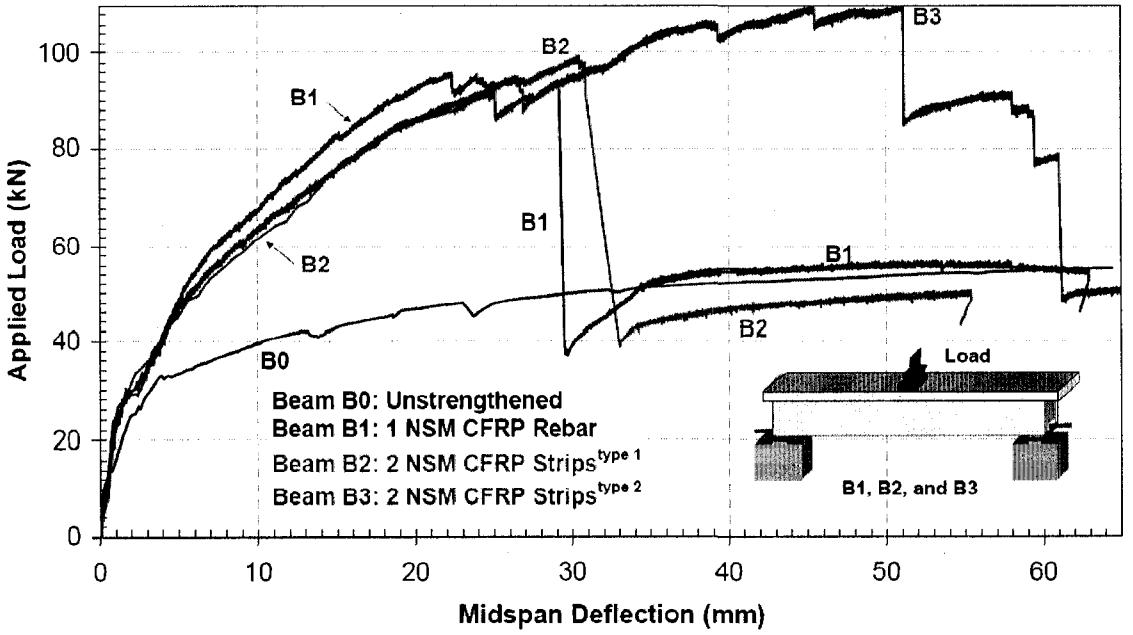

Fig. 2.17. Load-deflection curve for strengthened beams with NSM CFRP strips and rebar, (El-Hacha and Rizkalla 2004)

Using the same axial stiffness, $(EA)_{FRP}$, of the NSM-CFRP strips and the externally bonded CFRP strips, the externally bonded CFRP strips increased the strength by only 16.6 % and 25 % for the beams (B2a, B3a) compared to the unstrengthened beam due to debonding failure of the externally bonded strips from the concrete surface. However, the NSM CFRP strips increased the strength by 79 and 99 % for the beams (B2, B3) as shown in Fig. 2.18. The amount of strength increased using the same CFRP strips as NSM was about 4.8 and 4.0 times that obtained using externally bonded strips as shown in Fig. 2.18. Thus, the NSM strengthening technique using CFRP strips is more effective in comparison to externally bonded one.

The beam strengthened with GFRP strips as NSM reinforcement, exhibited significant enhancement in strength and stiffness in comparison to the unstrengthened beam. An increase in the ultimate strength of 85% was observed while the ultimate load carrying

capacity of the beam strengthened using externally bonded GFRP strips increased by 28 % as shown in Fig. 2.19.

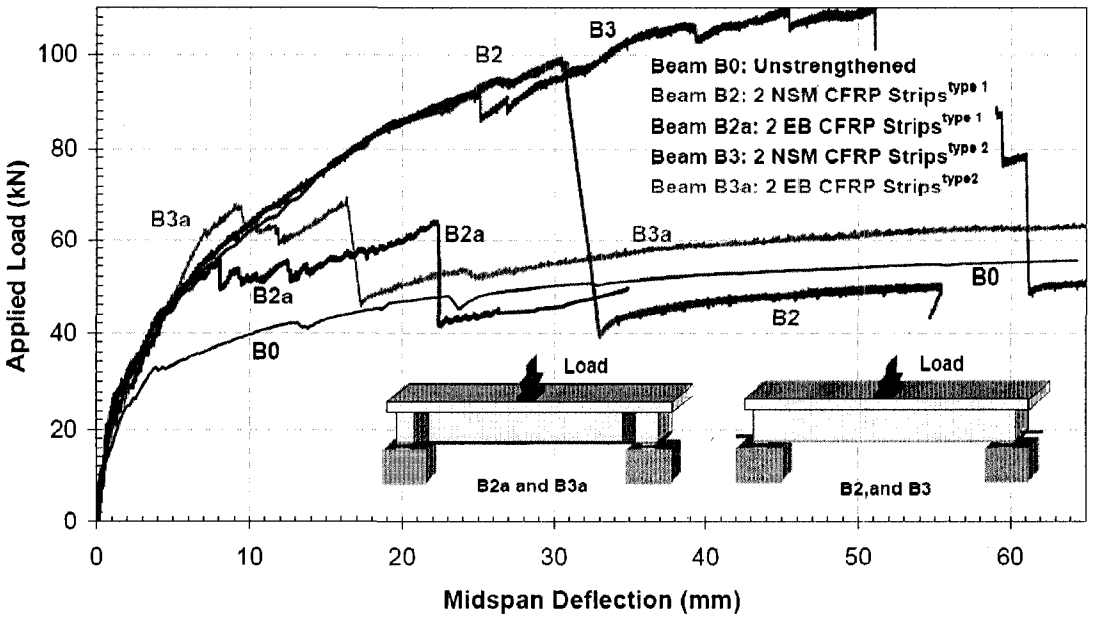

Fig. 2.18. Load-deflection curve for strengthened beams with NSM and externally bonded CFRP strips, (El-Hacha and Rizkalla 2004)

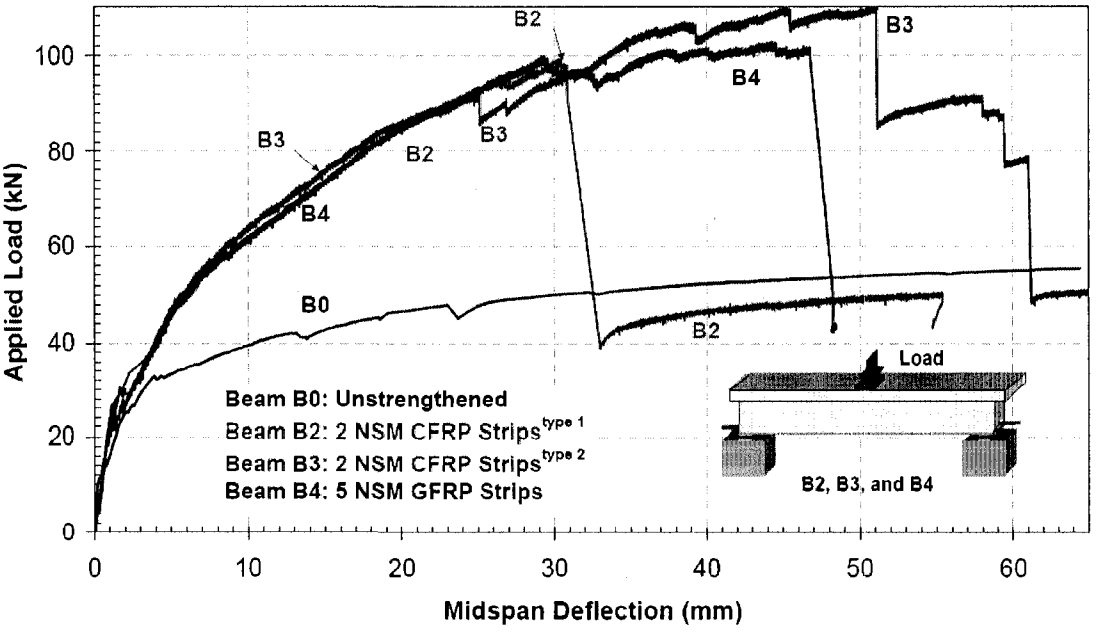

Fig. 2.19. Load-deflection curve for strengthened beams with NSM CFRP and GFRP strips, (El-Hacha and Rizkalla 2004)

Yost et al. (2007) investigated the flexure strengthening for rectangular-section beams with span using NSM CFRP strip. He tested 12 NSM strengthened beams and 3 unstrengthened control beams under four point bending with span 1292 mm. Various parameters including the amount of steel reinforcement ($\rho_s = A_s/bd$) and the amount of CFRP reinforcement ($\rho_f = A_f/bd$) were investigated. Specimens were designed to avoid concrete crushing or premature shear failure. It was concluded that flexural strengthening for steel reinforced concrete beams using NSM CFRP reinforcement is effective. Both the yield and ultimate strengths for the strengthened beams were increased by 30 % and 78 % respectively over those of the unstrengthened beams.

2.3.2.1. Modes of failure for flexural strengthening

The possible modes of failure for beams strengthened in flexural with NSM-FRP reinforcement are steel yielding followed by concrete crushing or bar rupture if a full composite action maintained between the RC beam and the FRP bar or strip. Failure can be premature debonding in the form of losing the composite action between the NSM-FRP reinforcement and the original structure. The debonding failure depends on many parameters for RC beams, steel or FRP reinforcement ratio, the shape and surface finishing of the FRP reinforcement, the roughness of the groove and the tensile strength of concrete and epoxy (De Lorenzis and Teng 2007).

The debonding failure can be found in many forms, concrete-epoxy debonding, FRP-epoxy debonding and concrete cover separation. Concrete cover separation is the common mode of failure for concrete beams strengthened in flexural with NSM reinforcement. (Kotynia 2006 and 2007; Teng et al. 2006). The concrete cover separation can start at the NSM-FRP reinforcement cut-off points (bar end) where the bar is terminated at a significant distance from the supports of the FRP reinforcement. The Bar end cover separation starts at the cutoff sections at the bottom of the beam at 45° to the beam axis and propagates inwards. These cracks propagate upwards on the two sides of the beam with the same inclination till it reaches the level of the tension steel (week plan), and then the concrete cover starts to split (Teng et al. 2006, Hassan and Rizkalla 2003). The concrete cover separation can starts also at the maximum moment zone by

intermediate crack (IC) debonding. Where debonding starts at a major flexural crack then propagate outwards to one of the supports (Kotynia 2006 and 2007).

2.3.2.2. Design equations for flexural strengthening

Taljsten et al. (2003) derived a theory for the ultimate bending capacity of concrete beams strengthened with NSMR using the following assumptions (Fig. 2.20).

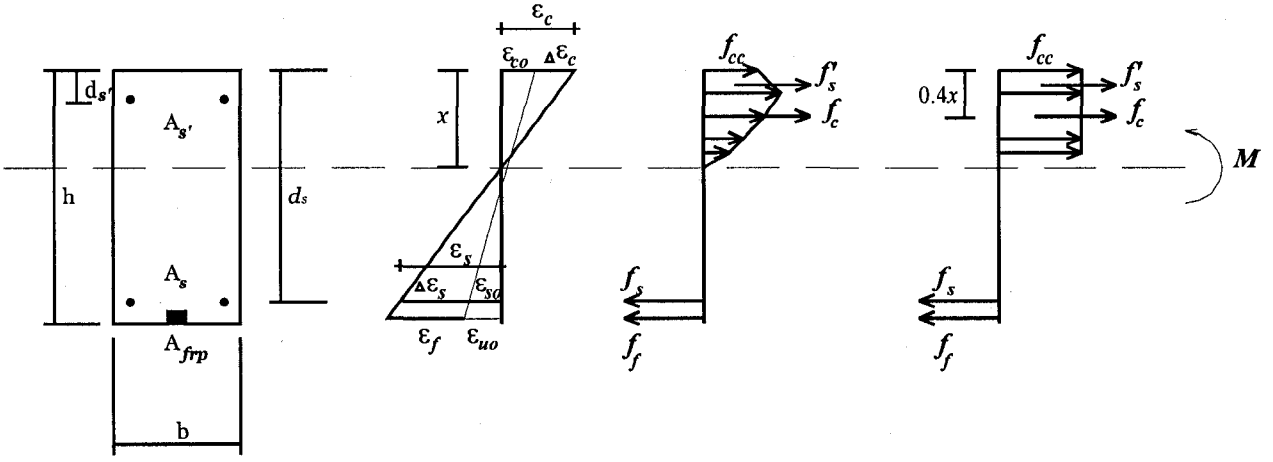

Fig. 2.20. Principles for strengthening in Bending, (Taljsten et al. 2003)

The strain across the cross section varies linearly as a function of the depth; this implies that linear strain in the concrete, steel reinforcement and the FRP that occurring in the same level is of the same amount. That means composite action applies between all the materials.

Concrete stresses are obtained from the material's characteristic curve. Concrete compressive strain is limited to failure strain ε_{cu}= 0.0035. For cracked sections, the concrete's tensile strength is ignored.

The FRP stress is obtained from the characteristic curve of the material and the total strain may not exceed the failure strain.

The FRP is assumed to be linearly elastic till failure.

$$M = \frac{x-d'_s}{h-x}(\varepsilon_{fu} + \varepsilon_{u0})A'_s E_s(0.4x - d'_s) + A_s f_s(d_s - 0.4x) + \varepsilon_{fu} E_f A_f(h - 0.4x) \qquad (2.5)$$

From horizontal equilibrium (Fig. 2.20)

$$0.8 f_{cc} bx + \frac{x - d'_s}{h - x}(\varepsilon_{fu} + \varepsilon_{u0}) A'_s E_s = A_s f_s + \varepsilon_{fu} E_f A_f \tag{2.6}$$

where x (distance of the N.A.) can be calculated by solving the following equation:

$$C_1 x^2 + C_2 x + C_3 = 0$$

$$C_1 = 0.8 f_{cc}\, b \tag{2.7}$$

$$C_2 = -0.8 f_{cc} bh - (\varepsilon_{fu} + \varepsilon_{u0}) A'_s E_s - A_s f_s - \varepsilon_{fu} E_f A_f \tag{2.8}$$

$$C_3 = (\varepsilon_{fu} + \varepsilon_{u0}) A'_s E_s d'_s + (A_s f_s + \varepsilon_{fu} E_f A_f) h \tag{2.9}$$

Taljsten et al. (2003) confirmed their equations with experimental work. they tested four rectangular cross section concrete beams with a span of 4000 mm, a depth of 300 mm and a width of 200 mm using static four point bending test. One served as a reference beam (RP), three beams were strengthened using NSM CFRP bars (Young's modulus E_f= 115 GPa and corresponding strain at failure 1.8 %). One was strengthened along the all length of the beam (4000 mm) with epoxy adhesive (E4), one beam was strengthened along 3400 mm of the length of the beam with epoxy adhesive (E3) and the last one was strengthened along 3400 mm of the length of the beam with cement adhesive (C3) as shown in Fig. 2.21.

It can be seen clearly from Fig. 2.22 that beam E4 had the best failure envelope where the failure was by rupture of the FRP bar. It was noticed from the result that the theory overestimates the failure load; this is due to some beams failed by anchorage failure and the theory didn't cover this point. In addition, the actual yield stress of steel was higher than the one given by the manufacturer.

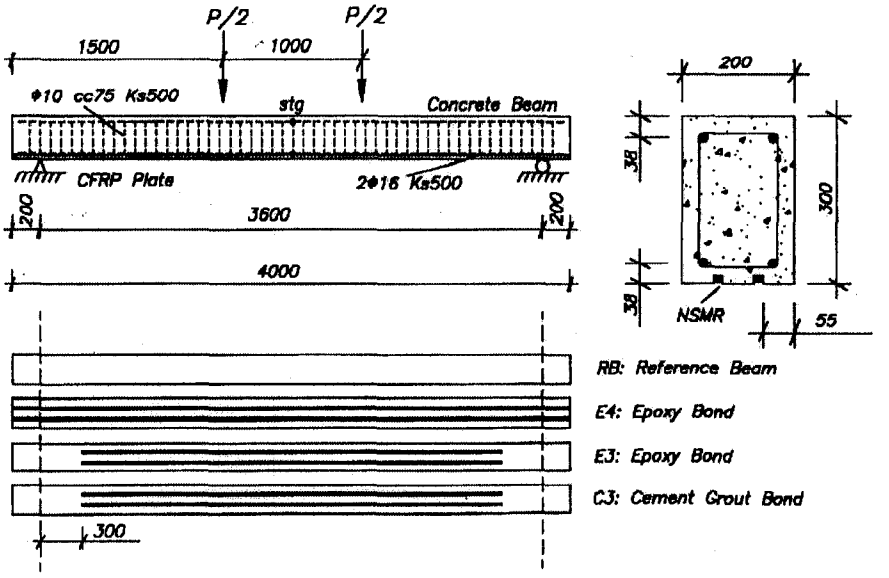

Fig. 2.21. Test set-up and dimensions of tested beams, (Taljsten et al. 2003)

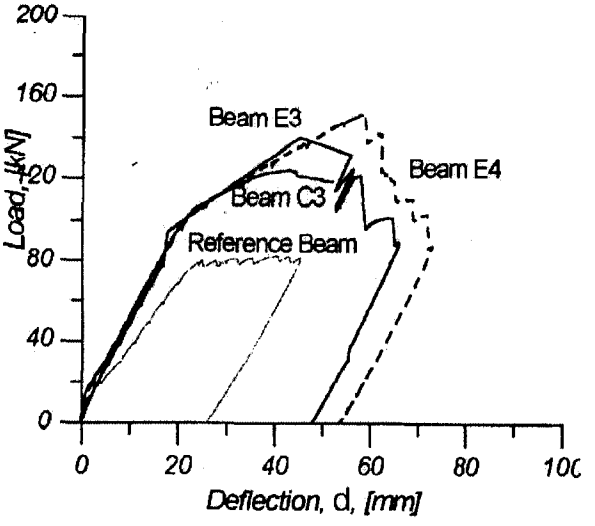

Fig. 2.22. Load deflection curve for the tested beams, (Taljsten et al. 2003)

The Canadian Highway Bridge Design Code, CHBDC, (CAN/CSA-S6-06 2006) have a provision for flexural strengthening using NSM if the concrete cover is equal to 20 mm or more.

For concrete member using NSMR, the anchorage length, l_d, beyond the point where no strengthening is required shall be calculated through the equation used to calculate the anchorage length for internal reinforcement through the following equation

$$l_d = 0.45 \frac{k_1 k_4}{\left(d_{cs} + K_{tr} \frac{E_{FRP}}{E_s} \right)} \left(\frac{f_{FRPu}}{f_{cr}} \right) A \tag{2.10}$$

where:

A : the area of cross-section of a strap or bar, mm^2

k_1 : a concrete strength factor.

k_4 : is a bar surface factor, being the ratio of the bond strength of the FRP bar to that of a steel deformed bar with the same cross-sectional area as the FRP bar, but not greater than 1.0.

K_{tr} : the transverse reinforcement index.

f_{cr} : the cracking strength of concrete, MPa

d_{cs} : the smaller of the distance from the closest concrete surface to the centre of the bar being developed, or two-thirds the centre-to-centre spacing of the bars being developed, mm

While for flexural strengthening using GFRP NSMR in timber beams the code gives the following provisions:

- The minimum fibre volume fraction for GFRP bars is 60%.
- There are at least two bars within the width of the beam.
- The total cross-sectional area for all bars on a beam is at least 0.002 times the cross-sectional area of the timber component.

As shown in Fig. 2.21, each bar is embedded in a groove, preferably with a rounded end. The depth of each groove is between 1.6 to 2.0 times d_b, the bar diameter; the width of each groove is not less than d_b+5 mm; the edge distance of the outer groove is not less than 25 mm, nor less than $2d_b$; and the clear spacing between grooves is not less than 25 mm, nor less than $3d_b$.

Before embedding the GFRP bars, the grooves in the beams were cleaned with pressurized air to remove any residue.

The adhesive used for bonding the GFRP bars to the timber beam is compatible with the preservative treatment used on the timber and chosen such that it is compatible with the expected volumetric changes of the timber.

In the longitudinal direction of the beam, the GFRP bar was extended as close to the beam support as possible.

Each GFRP bar was held in place as close to the tip of the groove as possible.

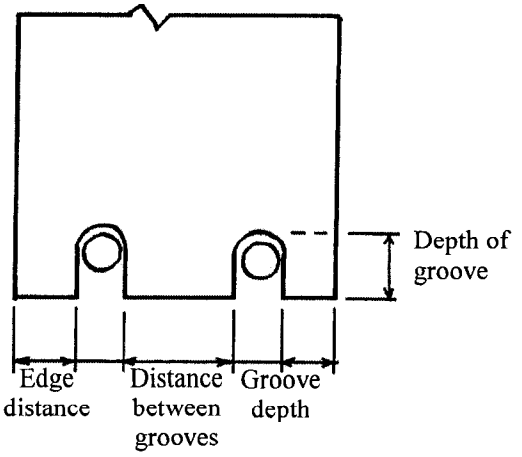

Fig. 2.23. Cross-section of a timber beam with GFRP NSMR, (CSA, 2006)

2.3.3. Flexural strengthening with prestressed NSM

Prestressing for strengthening purposes can increase the cracking load; minimize the crack width and better distribution between the cracks which in turn increase the durability as well as the stiffness of the structure. The greatest advantage of prestressing the strengthened materials is the increasing of the yielding load, which can be up to 25% in comparison to non prestressed strengthening materials (Wight et al. 1995, Nordin et al. 2001).

NSM bars or strips can be easily prestressed compared to externally-bonded laminates or sheets. Nordin and Taljsten (2006) tensioned NSM-FRP bar to 20% of its tensile strength as shown in Fig. 2.23; they released the prestressed force after curing the epoxy. As

expected the gain in the ultimate load and stiffness was achieved. The main problem for this technique was the access to the ends of the beam, which is not possible in reality.

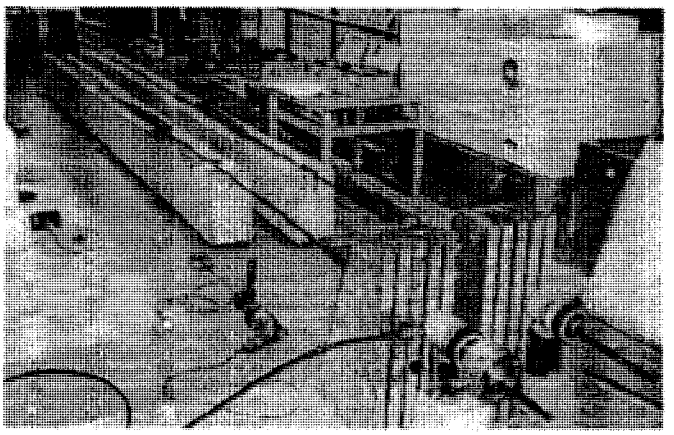

Fig. 2.24. Flexural strengthening with NSM prestressing, (Nordin and Taljsten 2006)

2.3.4. Shear strengthening

NSM-FRP reinforcement can also be used in increasing the shear capacity for RC beams. FRP bars or strips can be installed, whether vertical or inclined in slots or grooves cut on both sides of the RC beam. Very limited research was done on the shear strengthening using NSM FRP reinforcement and will be summarized bellow.

De Lorenzis and Nanni (2001c) tested eight full-scale RC beams with T-section having a span of 3-m long. Six beams were without steel stirrups and two contained steel stirrups less than that required by the ACI 318-02. The examined variables were the spacing between the NSM-FRP bars, inclination of bars whether vertical or inclined at 45° with the beam axis. NSM-FRP bars were anchored in the flange in two beams. It was found that using NSM as shear reinforcement can increase the capacity of the beam up to 106% with respect to the control beam without shear reinforcement and can also be significant in increasing the beam carrying capacity in the presence of internal steel stirrups.

Nanni et al. 2004 reported the test results of a single full scale PC girder taken from a bridge and strengthened in flexural with CFRP laminate and in shear with NSM-CFRP rectangular strips at 60° inclination with the beam axis (The increase in the shear capacity was of at least 53%). The beam failed in flexure at a shear force close to the shear

resistance predicted by De Lorenzis and Nanni (2001c), which will be discussed later in sec. 2.3.4.2.

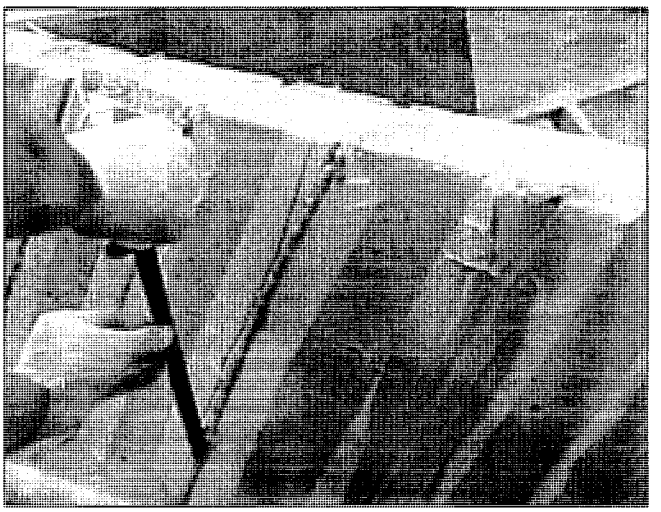

Fig. 2.25. Installation of CFRP for shear strengthening, (Nanni et al. 2004)

Dias and Barros (2005) tested 20 RC beams with different dimension and without steel stirrups. The beams were divided to four groups with different stirrups spacing. Each group consists of five beams, one without any steel stirrups, one with steel stirrups, one with externally bonded laminates and the last two with NSM strips inclined and vertical. The reported increase in strength was about 54 and 83% for the externally-bonded reinforcement and the NSM techniques, respectively.

2.3.4.1. Modes of failure for shear strengthening

The observed mode of failure for shear strengthening was debonding of one or more of the FRP bars due to splitting of the epoxy cover. But this was overcome by increasing the bonded length by inclination of the bar by 45° or by anchorage of the NSM bar in the beam flange, (De Lorenzis and Nanni 2001c). Once the debonding of the FRP bar is prevented the mode of failure changed to concrete cover splitting at the level of the longitudinal reinforcement. This can be explained as the difference in configuration between the internal stirrups and NSM reinforcement. As the NSM bars were not able to restrain the dowel force subjected on the longitudinal reinforcement. These forces, in conjunction with the wedging action of the deformed reinforcement, give rise to tensile

stresses in the surrounding concrete that may eventually lead to cover delemination and loss of anchorage.

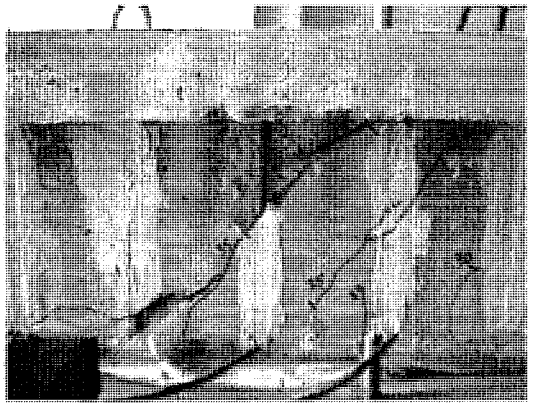

a) Splitting of epoxy cover

b) Splitting of concrete cover at the longitudinal reinforcement

Fig. 2.26. Modes of failure of shear strengthening, (De Lorenzis and Nanni 2001c)

2.3.4.2. Design equations for Shear strengthening

It is not yet possible to develop a comprehensive design approach for NSM shear strengthening including all the significant parameters. The nominal shear strength of a reinforced concrete beam may be computed by the basic design equation presented in ACI 318-05 (2005)

$$V_n = V_c + V_s \tag{2.11}$$

V_n is the nominal shear strength which is given by the sum of the shear strength of the concrete, V_c, and the shear strength provided by the steel shear reinforcement, V_s. In the case of beams externally strengthened with FRP, the nominal shear strength can be computed by adding a third term to account for the contribution of the FRP reinforcement

$$V_n = V_c + V_s + V_{FRP} \tag{2.12}$$

The design shear strength is obtained by applying a strength reduction factor, ϕ, to the nominal shear strength.

Several parameters influence the NSM-FRP bars contribution V_{FRP} to the shear capacity such as quality of bond, FRP bar type, groove dimensions and quality of substrate material.

Two design equations was given by Lorenzis and Nanni (2001c) to obtain V_{FRP} and suggests taking the lower of the two results as the contribution of NSM FRP bars to the shear capacity. The first equation V_{1FRP} computes the FRP shear strength contribution related to bond-controlled shear failure, the second equation V_{2FRP} calculates the shear resisted by NSM-FRP bars when the maximum strain in the bars is equal to 4,000με.

V_{1FRP} is computed using the following assumptions:

- The inclination angle of the shear cracks equals 45°.
- The bond stresses are uniformly distributed along the effective lengths of the FRP bars at ultimate.
- The ultimate bond stress is reached in all the bars intersected by the crack at ultimate.
- The shear force resisted by the FRP may be computed as the sum of the forces resisted by the FRP bars intersected by a shear crack. Each rod intersected by a crack may ideally be divided in two parts at the two sides of the crack. The force in each of these bars at the crack location can be calculated as the product of the average bond strength and the surface area of the effective length of the FRP rod.

$$V_{1FRP} = 2\pi . d_b . \tau_b . L_{totmin} \tag{2.13}$$

where

$$L_{totmin} = d_{net} - s \qquad \text{if } \frac{d_{net}}{3} < s < d_{net} \tag{2.14}$$

$$L_{totmin} = 2d_{net} - 4.s \qquad \text{if } \frac{d_{net}}{4} < s < \frac{d_{net}}{3} \tag{2.15}$$

$$d_{net} = d_r - 2.c$$

where d_r = length of the rods, c is concrete cover of the internal longitudinal reinforcement and s is the spacing of the NSM rods.

While in computing V_{2FRP} the same assumption that are used in computing V_{1FRP} are considered. The effective length of an FRP rod crossed by the crack corresponding to a strain of 4,000 με and the average bond strength τ_b is

$$\overline{L_i} = 0.001\frac{d_b.E_b}{\tau_b} \quad (2.16)$$

$\frac{d_{net}}{2} < s < d_{net}$ and if $\overline{L_i} > d_{net} - s$ so bond failure occurs before $\overline{L_i}$ the maximum strain reaches 4,000 με, therefore, V_{1FRP} controls but if $\overline{L_i} < d_{net} - s$ so V_{2FRP} with the value

$$V_{2FRP} = 2\pi.d_b.\tau_b.\overline{L_i} \quad (2.17)$$

$\frac{d_{net}}{3} < s < \frac{d_{net}}{2}$ V_{1FRP} controls if $\overline{L_i} > s$ but if $\overline{L_i} < s$ V_{2FRP} controls with the value

$$V_{2FRP} = 2\pi.d_b.\tau_b.(\overline{L_i} + d_{net} - 2s) \quad \text{if } d_{net} - 2s < \overline{L_i} < s \quad (2.18)$$

$$V_{2FRP} = 4\pi.d_b.\tau_b.\overline{L_i} \quad \text{if } \overline{L_i} < d_{net} - 2s \quad (2.19)$$

$\frac{d_{net}}{4} < s < \frac{d_{net}}{3}$ V_{1FRP} controls if $\overline{L_i} > d_{net} - 2s$ but if $\overline{L_i} < d_{net} - 2s$ V_{2FRP} controls with the value

$$V_{2FRP} = 2\pi.d_b.\tau_b.(\overline{L_i} + d_{net} - 2s) \quad \text{if } s < \overline{L_i} < d_{net} - 2s \quad (2.20)$$

$$V_{2FRP} = 2\pi.d_b.\tau_b.(2\overline{L_i} + dnet - 3s) \quad \text{if } d_{net} - 3s < \overline{L_i} < s \quad (2.21)$$

$$V_{2FRP} = 6\pi.d_b.\tau_b.\overline{L_i} \quad \text{if } \overline{L_i} < d_{net} - 3s \quad (2.22)$$

Lorenzis and Nanni (2001a) used the force resulting from the tensile stress in the FRP bars across the assumed crack to calculate the shear strength provided by the NSM reinforcement and it is expressed for rectangular bars by:

$$V_{FRP} = 4(a+b).\tau_b.L_{tot} \quad (2.23)$$

Where a and b represent the cross-sectional dimension of the rectangular FRP bars, τ_b represents the average bond stress of the bars crossed by the shear crack L_{tot} can be expressed as $\Sigma_i L_i$ where L_i represents the length of each single NSM bar intercepted by a shear crack and is expressed as:

$$L_i = \begin{cases} \dfrac{s}{\cos\alpha + \sin\alpha} i \le l_{0.004} \ldots\ldots i = 1 \ldots . \dfrac{n}{2} \\ l_{net} - \dfrac{s}{\cos\alpha + \sin\alpha} i \le l_{0.004} \ldots i = \dfrac{n}{2} + 1 \ldots n \end{cases} \tag{2.24}$$

where α represents the slope of the FRP bar with respect to the longitudinal axis of the beam, s is the horizontal FRP bar spacing, and l_{net} is defined as follows:

$$l_{net} = l_b - \frac{2c}{\sin\alpha} \tag{2.25}$$

where l_b is the actual length of the FRP bar, c is the clear concrete cover of the internal longitudinal reinforcement.

Where the first part of the equation takes into account bond as the controlling failure mechanics and represents the minimum effective length of a FRP bar intercepted by a shear crack as a function of the term n:

$$n = \frac{l_{eff}(1 + \cot\alpha)}{s} \tag{2.26}$$

where n is rounded off to the lowest integer and l_{eff} represents the vertical length of l_{net} and the second part of equation (2.24) takes into account the shear integrity of the concrete by limiting at 0.004 the maximum strain in the FRP reinforcement and $l_{0.004}$ can be determined as follows

$$l_{0.004} = 0.002 \frac{a.b}{a+b} \frac{E_f}{\tau_b} \tag{2.27}$$

The CHBDC (CAN/CSA-S6-06 2006) has also a provision for shear strengthening of timber bridges, which states that;

- The minimum volume fraction of GFRP bars is 60%.
- Horizontal splits in beams, if present, are closed by a mechanical device before the insertion of the GFRP bars.

As shown in Fig. 2.26, there are at least three GFRP bars at each end of the beam.

The diameter of the GFRP bar, db, is at least 15 mm, and the minimum diameter of hole containing a bar is db+3 mm.

The spacing of bars along the length of the beam is 25 mm ± h, the depth of the beam.

The adhesive used for bonding the GFRP bars to the timber beam is compatible with the preservative treatment used on the timber and chosen such that it is compatible with the expected volumetric changes of the timber.

As shown in Fig. 2.26, the GFRP bars are inclined to the beam axis at an angle of 45°±10° from the horizontal. The top ends of the inclined GFRP bars are within 10 to 25 mm from the top of the beam.

When there are daps present, the ingress of the drilled hole should be 100 mm ± 10 mm from the edge of the dap.

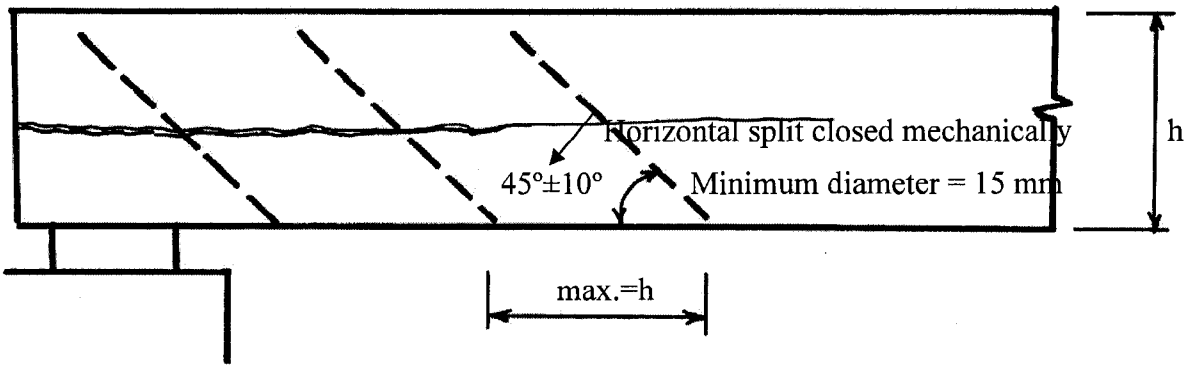

Fig. 2.27. Elevation of timber beam with GFRP bars for shear strengthening, (CSA, 2006)

Chapter 3 - Experimental Program

3.1. General

Extensive research programs are being conducted at the Université de Sherbrooke through the Natural Sciences and Engineering Research Council (NSERC) Industrial Research Chair in Innovative Fibre Reinforced Polymer (FRP) Composite Materials for Infrastructures. The use of FRP bars for strengthening of existing structure has not been yet investigated in our Research Chair. This research project focuses on the use of the newly developed FRP sand-coated bars for different strengthening techniques.

The main objectives of this experimental program are: 1) to develop/utilize a new NSM system composed of FRP V-ROD bars manufactured by Pultrall Inc. and adhesives manufactured by Hilti Inc., 2) to Investigate the bond performance of the proposed NSM system, 3) to investigate the effect of freeze/thaw cycles on the new proposed NSM system components, 4) to study the flexural behaviour of RC beams strengthened with NSM-FRP bars.

3.2. Experimental Program

The experimental program consisted of two phases. The first phase included the pullout testing of 76 C-shaped concrete specimens. The second phase included testing of 20 full-scale concrete beams strengthened in flexure using NSM-FRP system.

The first phase included the following parameters:

1. Type of FRP bar: two types were used: CFRP and GFRP
2. Diameter of FRP bar: two main diameters were used for CFRP reinforcement: No.10 (9.5 mm) and No.13 (12.7 mm) and one diameter for GFRP reinforcement, No.13 (12.7 mm).
3. Groove size: two different groove widths were used: namely 1.50 and 2.0 times the diameter of the FRP bar.
4. Bonded length: six different bonded lengths were used: namely 6, 12, 18, 24, 36 and 48 times the diameter of the FRP bar.

5. Type of adhesive: two types of adhesive were used: epoxy and cement-based.
6. Exposing 16 concrete specimens to 200 freeze/thaw cycles.

The main objectives of this phase are:

1) To investigate the different parameters affecting the bond performance of the NSM-FRP strengthening system.
2) To study the effect of severe environmental conditions such as moisture and freeze-thaw cycles on the bond performance of the NSM-FRP strengthening system.
3) To develop a bond–slip model for the NSM-FRP V-ROD bars.

The second phase included strengthening and testing of 20 full-scale RC beams.

This phase included the following parameters:

1. Steel reinforcement ratio: three steel reinforcement ratios were used: 1.60%, 0.80% and 0.40%.
2. Type of NSM-FRP reinforcement: two types were used: CFRP and GFRP.
3. Diameter of NSM-FRP bars: two diameters were used for each type of FRP reinforcement: No.10 (9.5 mm) and No.13 (12.7 mm).
4. Groove size: two different square groove sizes were used: namely 1.50 and 2.0 times the diameter of the FRP bar.
5. Bonded length: four different bonded lengths were used: 12, 18, 24, 48 and 60 times the diameter of the FRP bar.

The main objectives of this phase are:

1) To investigate the different parameters affecting the behaviour of reinforced concrete beam strengthened in flexure with NSM-FRP bars.
2) To establish design recommendations for the use of FRP bars in strengthening of RC beams using NSM system.

3.3. Phase I: Bond Behaviour of NSM-FRP Bars in Concrete

The NSM-FRP system depends mainly on bond stresses and its transfer from reinforced concrete element to FRP bars by a bonding agent to develop a composite action between concrete, steel reinforcement and FRP bars. This composite section acts together to increase the ultimate capacity of the concrete element such as flexural and shear capacity and to improve the serviceability aspects as cracking and flexural limitations. The bond stresses between concrete, bonding agent (epoxy or cement) and FRP bars are very important factors in the NSM system. To investigate and study the bond characteristics between the three materials and to analyze the influence of the most critical parameters, the pullout tests of NSM-FRP in concrete specimens were conducted.

This first phase of the experimental program represents the preliminary investigation for the bond behaviour of the used system.

3.3.1. Pullout test specimens

A total of 76 C–shaped concrete specimens were cast in this phase. The specimen configuration used in the pull out test is similar to the one developed by De Lorenzis et al. (2002) as shown in Fig. 3.1. The typical specimen consisted of a C–shaped concrete specimen with outside dimensions of 340 x 340 mm, inside dimensions of 170 x 170 mm, and a height of 500 mm. Four holes were located at the four corners of the specimen. This phase consists of two stages. The first stage included testing of 60 concrete specimens at normal room temperature. The second phase included testing of 16 concrete specimens after being subjected to 200 freeze/thaw cycles in a controlled environmental chamber.

3.3.1.1. Stage one: Bond characterization

Sixty C-shaped concrete specimens were prepared and tested at normal room temperature. Three specimens were tested for each parameter and an average was taken from the three results. Each specimen was given a designation in the format X/00.0-Y-0.00-00. The first character X represented the type of FRP bar, whether C for carbon or G for Glass. The first number represented the bar diameter whether 9.5 mm or 12.7 mm. The second character Y represented the type of adhesive, E for epoxy and C for cement,

the second number represented the groove depth in a multiple of the bar diameter whether 1.50 or 2.00. The third number represented the bonded length also in a multiple of the bar diameter whether 6, 12, 18, 24, 36 or 48. Table 3.1 summarizes the tested parameters for the pullout testing for the first stage of this phase. Each specimen was instrumented with two LVDTs with high accuracy (± 0.001 mm) to measure the free end and the loaded end slip of the FRP bar. Three electrical resistance strain gauges with gauge length of 6.0 mm were attached to the bar to capture the strain distribution along the bonded length. Reading from the load cell, LVDTs and the electrical strain gauges were collected using an automatic data acquisition system connected to a computer.

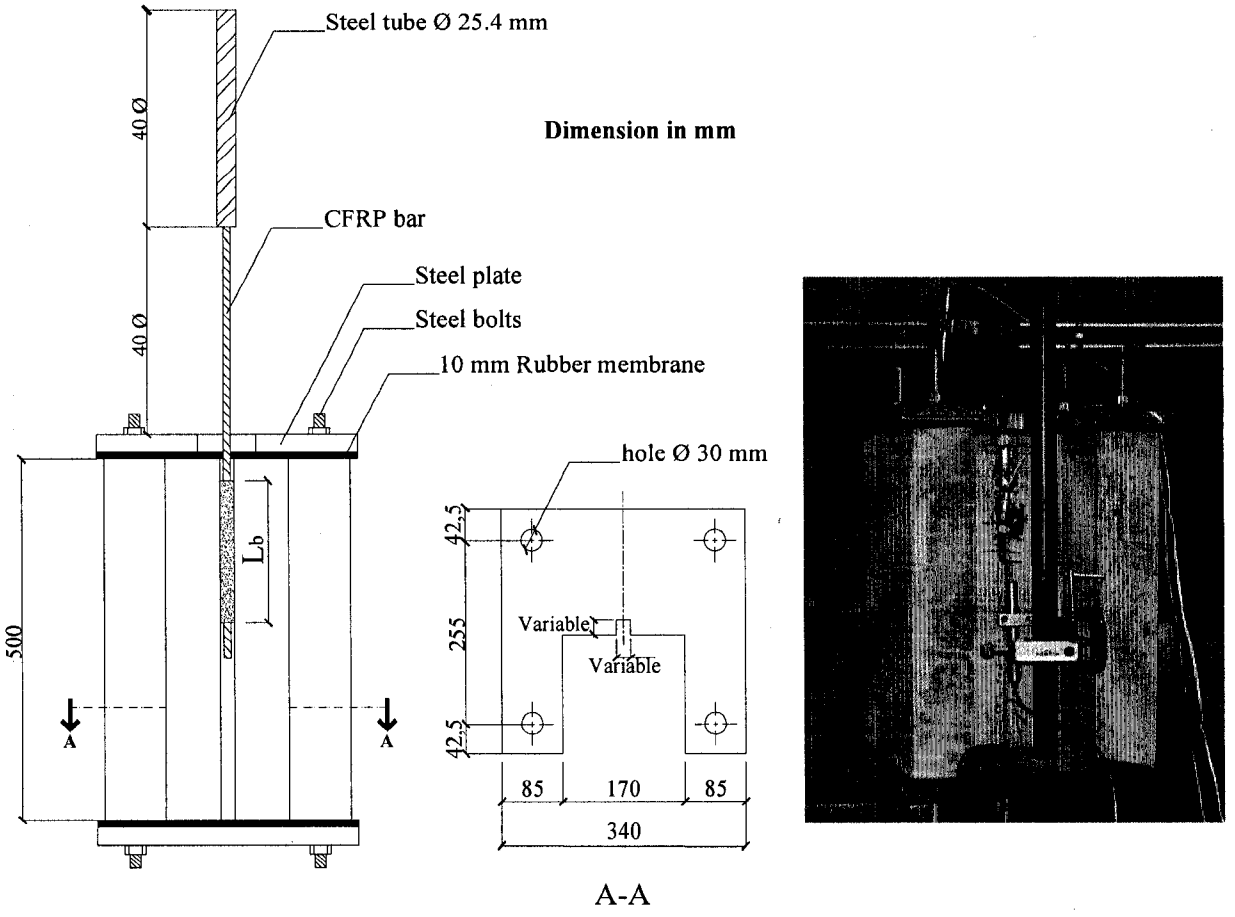

Fig. 3.1. Pullout test specimen

Table 3.1 Description of test specimens for bond characteristics

Specimen code	Type and diameter of FRP	Groove filling	Groove dimension	Bonded length
C/9.5-E-1.50-6	CFRP/9.5	Epoxy	1.50*d*	6*d*
C/9.5-E-1.50-12				12*d*
C/9.5-E-1.50-18				18*d*
C/9.5-E-1.50-24				24*d*
C/9.5-E-2.00-6	CFRP/9.5	Epoxy	2.00*d*	6*d*
C/9.5-E-2.00-12				12*d*
C/9.5-E-2.00-18				18*d*
C/9.5-E-2.00-24				24*d*
C/9.5-E-2.00-36				36*d*
C/9.5-E-2.00-48				48*d*
C/12.7-E-1.50-18	CFRP/12.7	Epoxy	1.50*d*	18*d*
C/12.7-E-2.00-18			2.00*d*	18*d*
G/12.7-E-2.00-12	GFRP/12.7	Epoxy	2.00*d*	12*d*
G/12.7-E-2.00-18				18*d*
G/12.7-E-2.00-24				24*d*
G/12.7-E-2.00-36				36*d*
C/9.5-C-1.50-12	CFRP/9.5	Cement	1.50*d*	12*d*
C/9.5-C-1.50-18				18*d*
C/9.5-C-1.50-24				24*d*
C/9.5-C-2.00-24	CFRP/9.5	Cement	2.00*d*	24*d*

3.3.1.2. Stage two: Effect of freeze/thaw cycles

The second stage, the freeze/thaw investigation, included testing of 16 concrete specimens with CFRP bars after being subjected to freeze/thaw cycles in a controlled environmental chamber. Before conditioning the specimens in the environmental chamber and to develop service cracks, each specimen was tensioned to the maximum allowable service load level according to the CAN/CSA-S6-06 (CSA, 2006). The specimens were tensioned to 30% of the failure load of the first stage.

Freeze/thaw cycles were performed in the walk-in controlled environmental chamber (3.70×2.60 m) in the department of civil engineering at the University of Sherbrooke as shown in Fig. 3.2. All specimens were subjected to 200 freeze/thaw cycles. During the freezing process, the lower bound was set to -20°C for 12 hours at 0% relative humidity. While during the thaw process, the temperature was raised to +25°C for 6 hours at 100% relative humidity as shown schematically in Fig. 3.3.

Each specimen was instrumented with one electrical strain gauge at the middle of the bonded length and one thermocouple as shown in Fig. 3.2. The thermocouples were placed outside the bonded length in two positions in the specimens; at the bar-epoxy interface and in the epoxy-concrete interface to capture the temperature at these interfaces. All the wires of the strain gauges and the thermocouples were collected together and extended outside the environmental chamber and connected to a data acquisition system for the first 20 cycles to capture the change in strain due to change in the temperature every minute. After the first 20 cycles, readings for the strains were taken manually by using a strain indicator box (P-3500) for the rest of the cycles. These readings were taken manually since it was not possible to assign an electrical data acquisition system for the long-term duration of the conditioning. Table 3.2 summarizes the tested parameters for the freeze- thaw investigation.

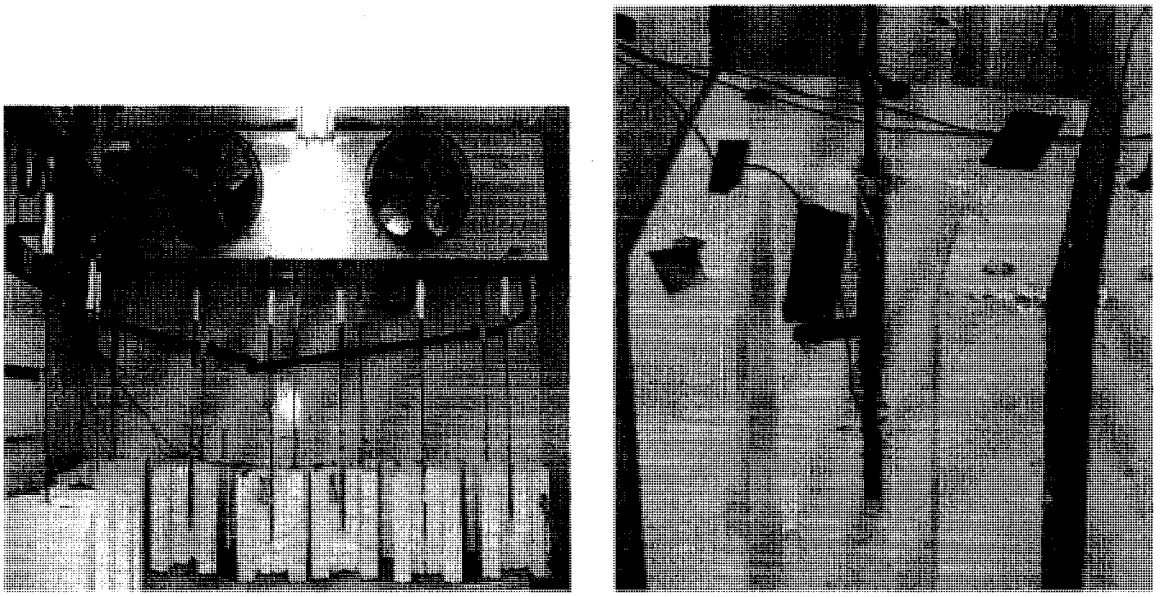

Fig. 3.2. Specimens in the environmental chamber and instrumentation

Table 3.2 Description of test specimens for the effect of freeze/thaw cycles

Specimen code	Groove filling	Groove dimension	Bonded length
D/E-1.50-12	Epoxy	1.50*d*	12*d*
D/E-1.50-18			18*d*
D/E-1.50-24			24*d*
D/E-2.00-12	Epoxy	2.00*d*	12*d*
D/E-2.00-18			18*d*
D/E-2.00-24			24*d*
D/C-1.50-12	Cement	1.50*d*	12*d*
D/C-1.50-18			18*d*
D/C-1.50-24			24*d*
D/C-2.00-12	Cement	2.00*d*	12*d*

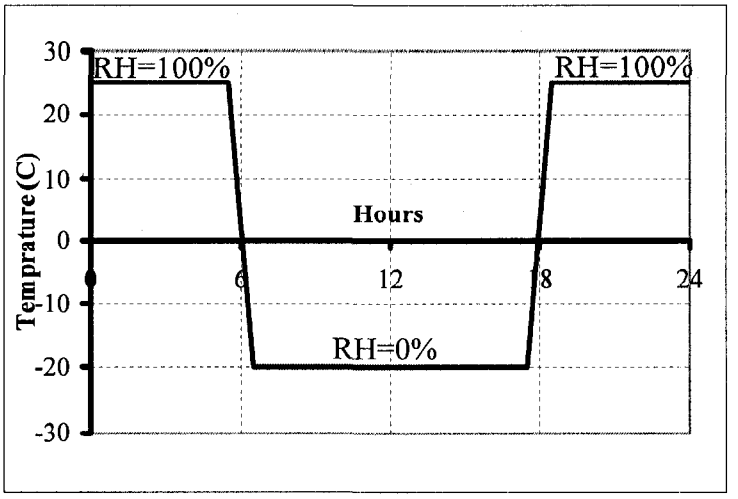

Fig. 3.3. Freeze/thaw cycles

3.3.2. Fabrication of pullout specimens

The pullout specimens were cast in two wooden formworks, which were designed so that six specimens to be cast for each formwork at each time as shown in Fig. 3.4. The formworks were made of 25 mm thick plywood having the same shape and the size of the specimens. Before each casting, the formworks were cleaned and lubricated to provide ease in the specimen removal. Plastic tubes were placed in the formwork in the place of the holes before casting and removed before the final setting of the concrete.

A normal weight ready mixed concrete was cast and compacted by using a mechanical vibrator. Test cylinders were cast at the same time of the specimens. Immediately after casting the specimens and the cylinders were covered with plastic sheets to avoid moisture loss. Twenty four hours after casting, the external sides of the formwork and the cylinders were stripped and the specimens and the cylinders were covered with wet burlap and plastic sheets to keep them wet. The burlap was kept wet all time during the curing period, which lasted 14 days. Then the formwork was stripped and the specimens were removed and stored in the laboratory to complete 28 days. After 28 days, three cylinders were tested in compression for each patch to ensure getting the designed compressive strength before making the groove in the specimens.

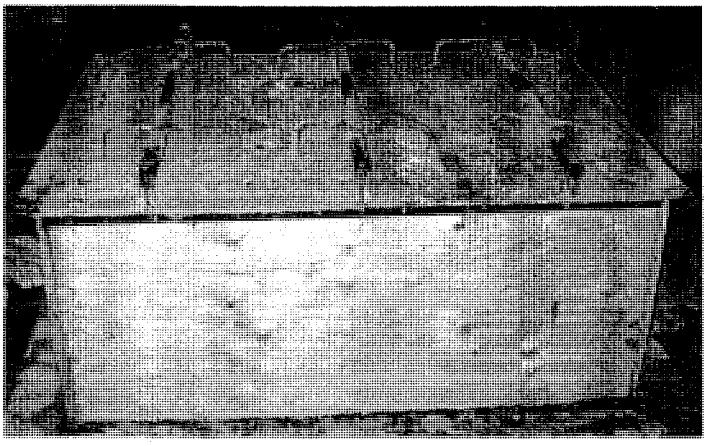

Fig. 3.4. Pullout specimens in the formwork

3.3.3. Cutting the grooves

After the 28-day curing period, a special concrete saw with a diamond blade was used to cut the groove in the middle of the C–shape with a variable depth and width. The groove was formed by making two cuts using the concrete saw and removing the concrete in between by a power hammer as shown in Fig. 3.5

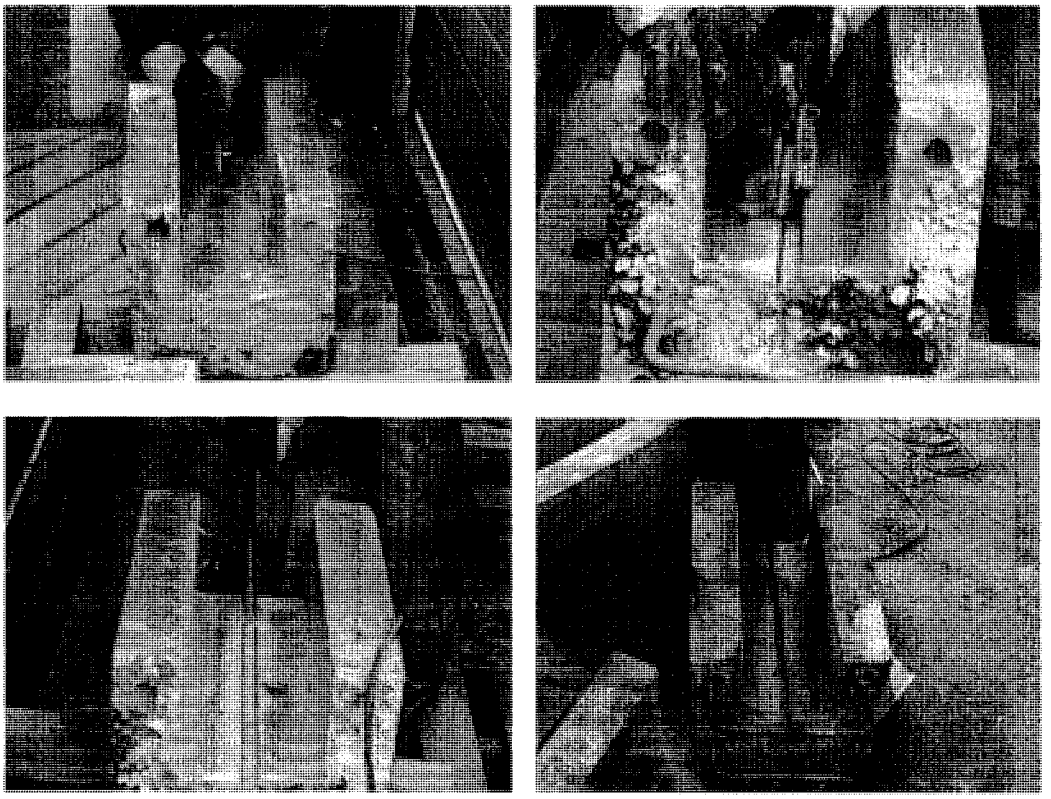

Fig. 3.5. Cutting the groove for the pullout test specimens

3.3.4. Installation of the NSM-FRP bar

A pressurized air was used to ensure that the groove is clean. The adhesive was injected into the groove to cover 2/3 of the groove depth. The bar was gently inserted into the groove over a foam support outside the bonded length to maintain the thickness of the adhesive and then gently pressed to displace the bonding agent. Extra adhesive was added to fill the groove. The excess adhesive was then removed as shown in Fig. 3.6.

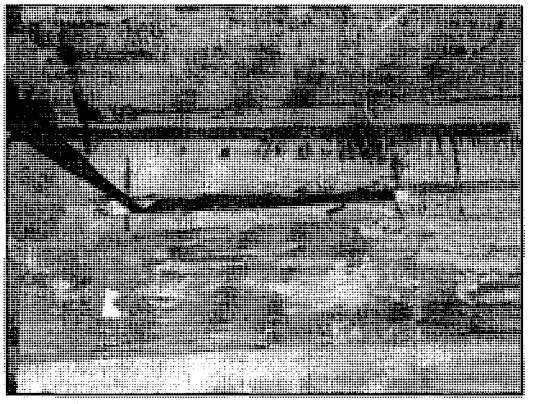

a) The adhesive injected into the groove to cover 2/3 of the groove depth

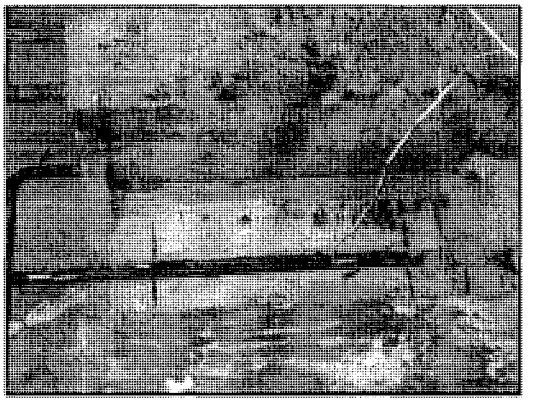

b) The bars were placed in the groove over foam support

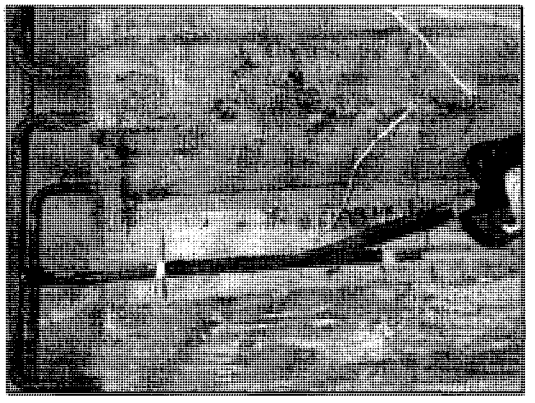

a) Extra adhesive was added to fill the groove.

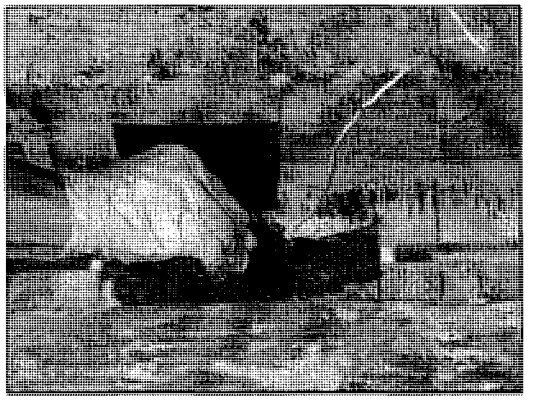

b) The excess adhesive was then removed

Fig. 3.6. Installation of NSM-FRP bar

3.3.5. Test setup

The concrete specimens were tested in a BALDWIN hydraulic machine as shown in Fig. 3.7. The applied load was reacted by means of four steel threaded bars inserted into holes (30-mm in diameter) near the corners of the specimen as shown in Fig. 3.1. The concrete specimens were encapsulated in between two steel plates (Fig. 3.8) to prevent any concentration of stresses at the threaded bar location.

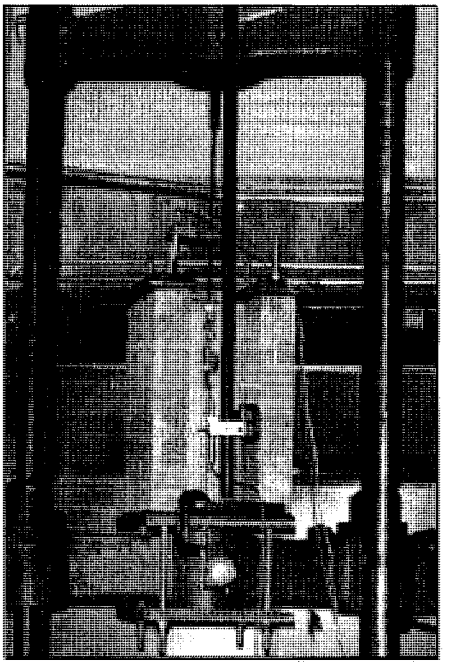

Fig. 3.7. Pullout test setup

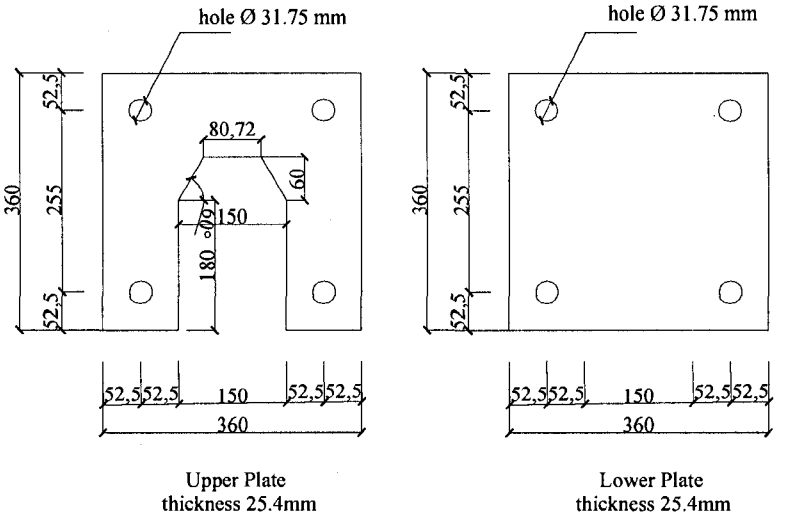

Fig. 3.8. Upper and lower steel plates

3.4. Phase II: Flexural Strengthening of RC Beams Using NSM-FRP Bars

This phase will describe the experimental program taken to evaluate the flexural performance of concrete beams strengthened in flexural with NSM-FRP (V-ROD) bars. The following section includes the tested specimens, fabrication process, instrumentation and testing setup for the strengthened RC beams.

3.4.1. Beam test specimens

A total of 20 reinforced concrete beams were constructed and tested to failure. The beam has dimensions of 3010 mm long, 200 mm wide and 300 mm deep. The beams are divided to three series according to their steel ratio, series A, B and C. All the beams were designed to be under flexure and having flexural failure. The first series, A has a steel ratio of 1.60% while the second series, B has a steel ratio of 0.80% and the third series, C has a steel ratio of 0.40%. Each series investigated different parameters. Two 10M steel bars were used as compression reinforcement for all the beams. Conventional 8-mm diameter steel stirrups were used in all beams with a spacing 100 mm over all the length of the beam to avoid shear failure and to ensure that the beam would fail in flexure. Fig. 3.9 shows the dimension and the reinforcement details for each series.

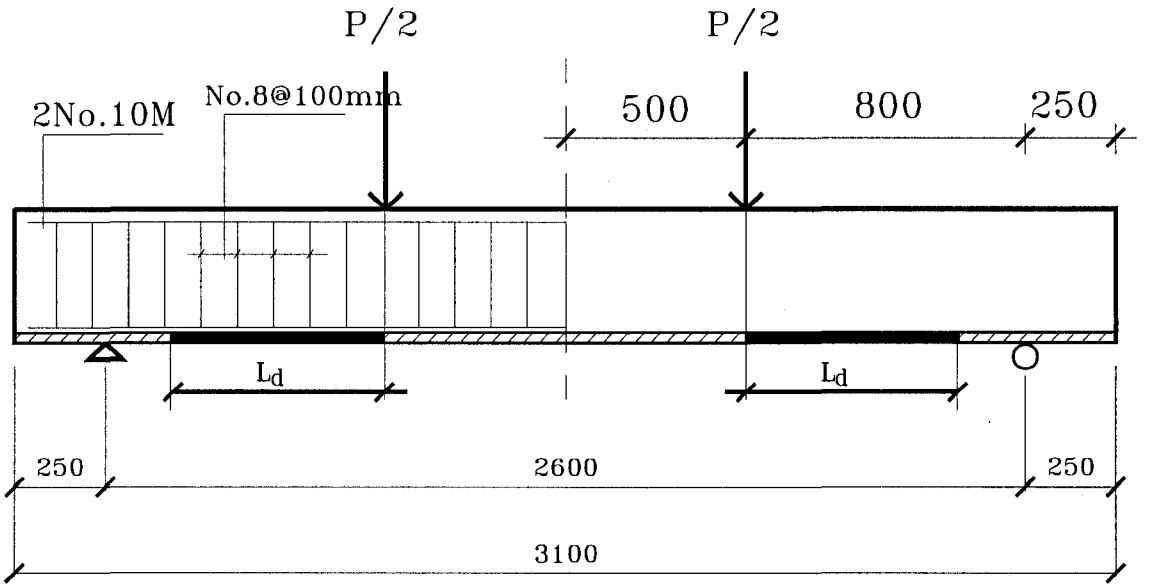

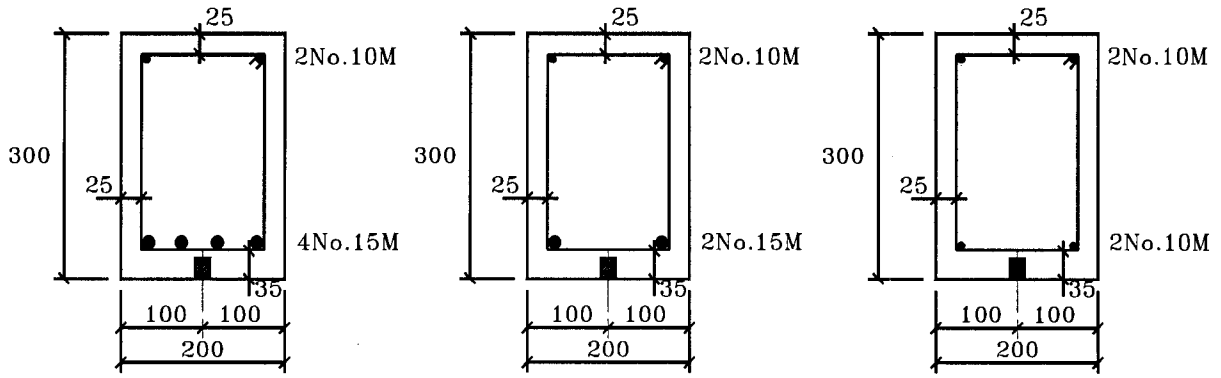

Fig. 3.9. Dimensions and reinforcement details of the beam test specimen

Series A:

A total of five beams were tested in series A. One beam was tested as a control specimen A0. While the other beams were strengthened with one 9.5 mm diameter CFRP bar. Beams A1, A2, A3 and A4 were strengthened with 12*d*, 18*d*, 24*d* and 48*d* bonded length respectively. The bottom steel reinforcement of this series was 4 No.15M corresponding to a reinforcement ratio of 1.60%. The objective of this series was to investigate the effectiveness of strengthening of beams reinforced with high steel ratio with different bonded length.

Series B:

A total of three beams were tested in series B. One beam was tested as a control specimen B0. While the other beams were strengthened with one 9.5 mm diameter CFRP bar. Beams A1 and A2 were strengthened with 24*d* and 48*d* bonded length respectively. The bottom steel reinforcement of this series was 2 No.15M corresponding to a reinforcement ratio of 0.80%. The objective of this series was to investigate the effect of decreasing the steel ratio from series A on the strengthening scheme.

Series C:

A total of twelve beams were tested in series C. One beam was tested as a control specimen C0. Beams C1, C2, C3 and C4 were strengthened with one 9.5 mm diameter CFRP bar with 12*d*, 24*d*, 48*d* and 60*d* bonded length having a square groove equal to 2.0 times the bar diameter. Beams C5, C6, C7 were strengthened with one 9.5 mm diameter CFRP bar with 24*d*, 48*d* and 60*d* bonded length having a square groove equal to 1.50 times the bar diameter. Beams C8 and C9 were strengthened with one 12.7 mm diameter

CFRP bar with 24*d* and 48*d* bonded length respectively having a square groove equal to 2.0 times the bar diameter. Beams C10 and C11 were strengthened with one 12.7 mm diameter GFRP bar with 24*d* and 48*d* bonded length respectively having a square groove equal to 2.0 times the bar diameter. The objective of this series is to investigate the effect of decreasing the groove size, the effect of increasing the FRP ratio and the feasibility of using GFRP bar in strengthening, respectively. The bottom steel reinforcement of this series was 2 No.10M corresponding to a reinforcement ratio of 0.40%. Table 3.3 summarizes the tested specimens

Table 3.3 Description of test specimens for the flexural strengthening:

Beam code	Type of FRP	Diameter of FRP	Groove dimension	Bonded length
Series A				
A0	Control			
A1	Carbon	9.5	2.00*d*	12*d*
A2				18*d*
A3				24*d*
A4				48d
Series B				
B0	Control			
B1	Carbon	9.5	2.00*d*	24*d*
B2				48*d*
Series C				
C0	Control			
C1	Carbon	9.5	2.00*d*	12*d*
C2				24*d*
C3				48*d*
C4				60*d*
C5	Carbon	9.5	1.50*d*	24*d*
C6				48*d*
C7				60*d*
C8	Carbon	12.7	2.00*d*	24*d*
C9				48*d*
C10	Glass	12.7	2.00*d*	24*d*
C11				48*d*

Note: *d* is the diameter of the NSM-FRP bar

3.4.2. Fabrication of beam specimens

The beams were cast in a wooden formwork which was designed so that four beams to be cast at each time. The formwork was made of 25-mm thick plywood having the same shape and the size of the specimens. The formwork was re-used 5 times for casting the 20 beams. Before each casting, the formwork was cleaned and lubricated to provide ease in the beam removal. The reinforcement cages were assembled, tied and placed in the formwork as shown in Fig. 3.10. Plastic chairs and spaces were used to maintain the cover requirements.

A normal weight ready mixed concrete was cast and compacted by using mechanical vibrator as shown in Fig. 3.11. Test cylinders were cast at the same time of the beams. Immediately after casting the beams and the cylinders were covered with plastic sheets to avoid moisture loss. Twenty four hours after casting, the external sides of the formwork and the cylinders, they were stripped and the beams and the cylinders were covered with wet burlap and plastic sheets to keep them wet. The burlap were kept wet all time during the curing period which lasted 14 days. Then the formworks were stripped and the beams were removed from it and stored in the laboratory to complete the 28 days. After 28 days, three cylinders were tested in compression from each patch to ensure getting the designed compressive strength before making the groove in them.

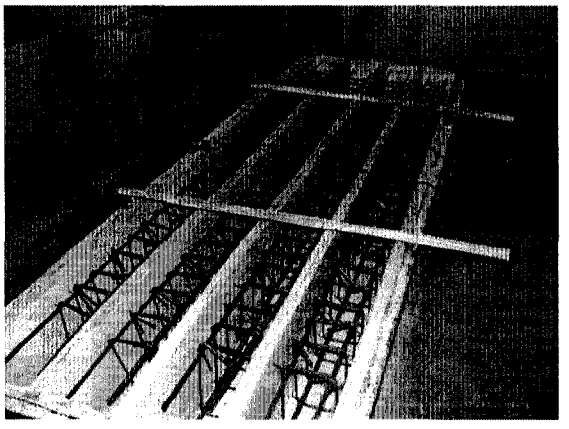

Fig. 3.10. Steel reinforcement cages in formwork

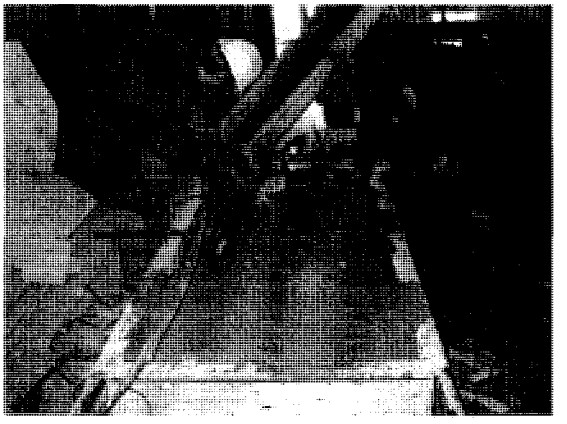

Fig. 3.11.Concrete casting

3.4.3. Strengthening procedures

Near surface mounted is one of the recent strengthening methods used for the rehabilitation of reinforced concrete structures using advanced composite materials. The structure is strengthened by bonding the FRP to concrete in a slit (groove).

3.4.3.1. Cutting the groove

After 28 days, all the beams were turned upside down to be prepared for making the grooves. The locations of the groove were first marked on the tension side of the beams. A special concrete saw with a diamond blade was used. The groove was formed in a similar way to the C-shaped specimens by making two cuts then chopping the concrete in between as shown in Fig. 3.12 and Fig. 3.13.

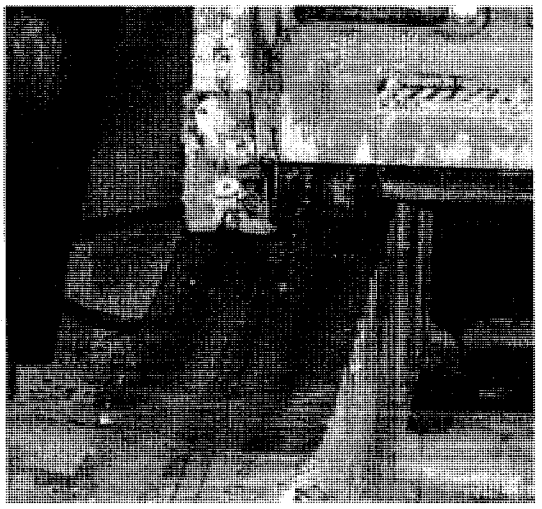

Fig. 3.12. Cutting the groove

Fig. 3.13. Chopping the concrete

3.4.3.2. Installation of the FRP bar

A silk brush was used to clean the groove and pressurized air and water was used to ensure that the groove is completely clean. The epoxy was injected into the groove to cover 2/3 of the groove depth. The bar was gently inserted into the groove over a plastic support outside the bonded length to maintain the thickness of the epoxy and to centre the bar in the middle of the groove. The bar was gently pressed to displace the bonding agent.

Extra adhesive was added to fill the groove. The excess epoxy was then removed as shown in Fig. 3.14. Quality control was achieved by continuous inspection and measurements during all the installation process.

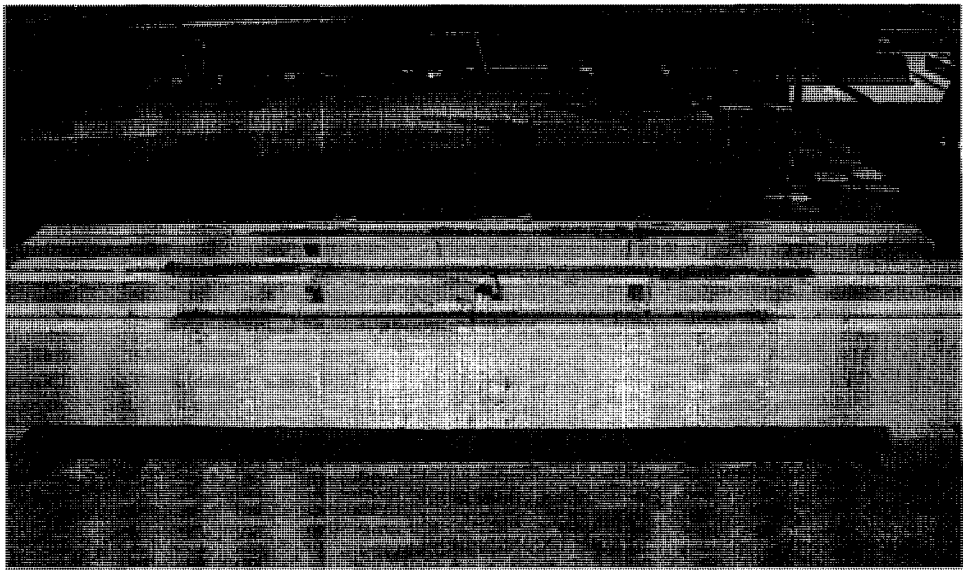

Fig. 3.14. NSM-FRP installation

3.4.4. Instrumentation

The instrumentation that was used to monitor the behaviour of the beams during testing consists of a combination of electrical strain gauges and linear variable differential transducers (LVDTs) with different stroke lengths as shown in Fig. 3.15.

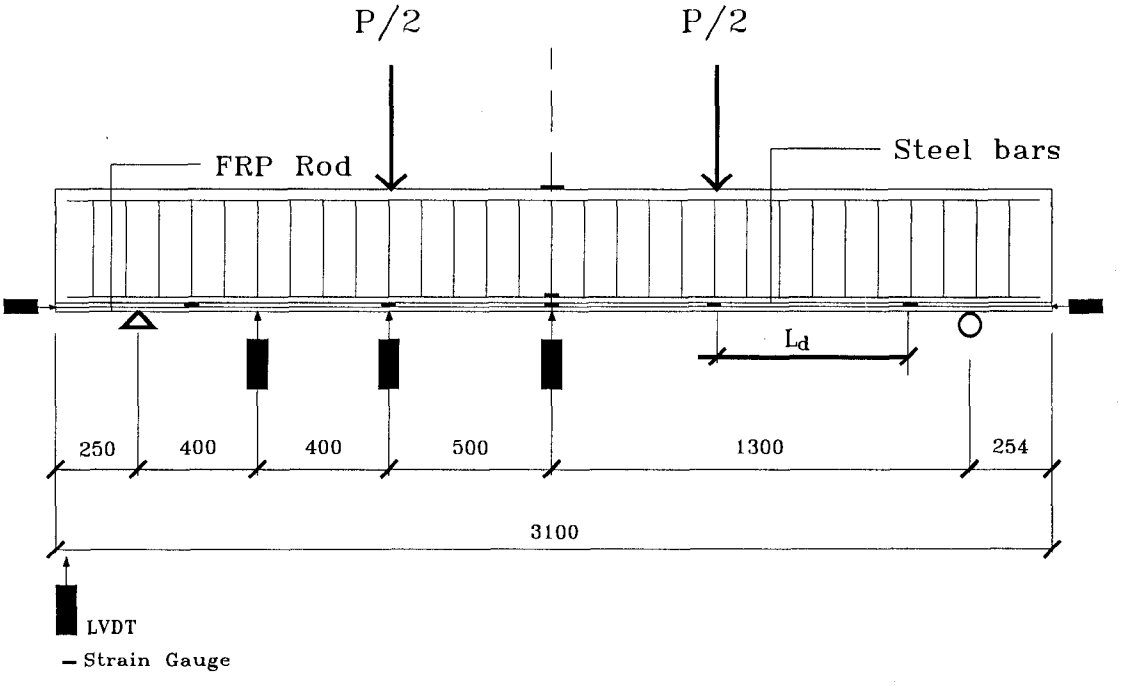

Fig. 3.15. Instrumentations layout

3.4.4.1. Strains monitoring

Different electrical strain gauges were used to capture the strains for the steel, concrete and FRP. All the electrical strain gauges used were produced by KYOWA ELECTRONIC INSTRUMENTS CO., LTD., Tokyo Japan with a resistance of 120Ω and a gauge factor of 2.11.

Two electrical strain gauges with a gauge length of 6 mm were installed on the mid-span of the steel tension reinforcement to measure the maximum tensile strain in the steel bars. The strain gauges were glued on the smoothened part of the steel bars by using M-bond then covered with water proof coating (M-Coat A and M-Coat B) as shown in Fig. 3.16. Then the strain gauges were covered with a 5-minute epoxy to protect the strain gauges from water and damage during casting.

Fig. 3.16. Strain gauges on steel bars

Other two electrical strain gauges with gauges length of 67 mm were installed on the mid-span of the top of the concrete to measure the maximum compressive strain in the concrete. The strain gauges were glued on the smoothened part of the concrete beam by using a 5-min epoxy.

Five electrical strain gauges with gauge length of 6mm were installed along the FRP embedded length. The strain gauges were glued on the smoothened part of the FRP bars by using M-bond then covered with water proof coating (M-Coat A only). Then the strain gauges were covered with 5 min epoxy to protect the strain gauges during installation.

3.4.4.2. Deflection monitoring

The deflection at mid span was monitored on both sides of the beam by using two LVDTs with stroke length of 100 mm. Other two LVDTs were placed at the load position and at the mid of the shear span to monitor the deflected shape of the beam as shown in Fig. 3.17.

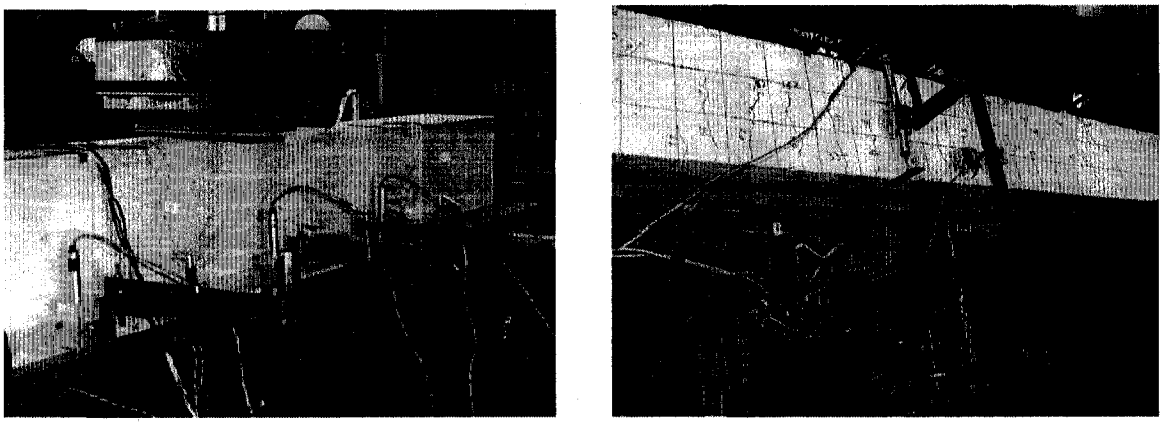

Fig. 3.17. Deflection monitoring

3.4.4.3. Slip monitoring

The slip at both free ends of the FRP bar was measured by using two high accuracy LVDT (± 0.001mm) with stroke length of 25 mm as shown in Fig. 3.18.

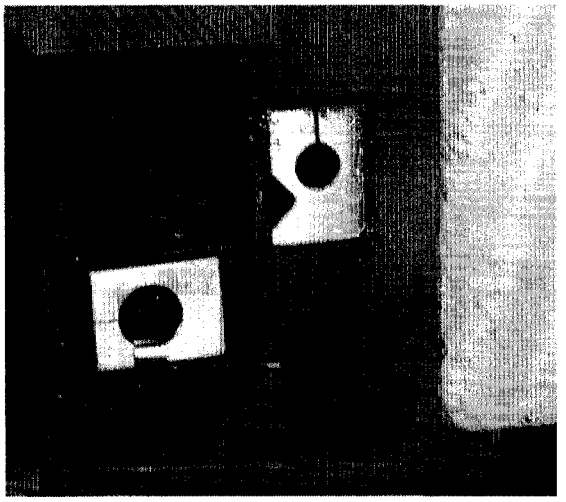

Fig. 3.18. NSM-FRP slip monitoring

3.4.4.4. Crack width monitoring

A microscope with magnification factor of 10X was used to measure the first crack width when it is initiated. A high accuracy LVDT (± 0.001 mm) was installed on the position of the first crack as shown in Fig. 3.19. During loading, the formation of the cracks were also marked and recorded at different load levels.

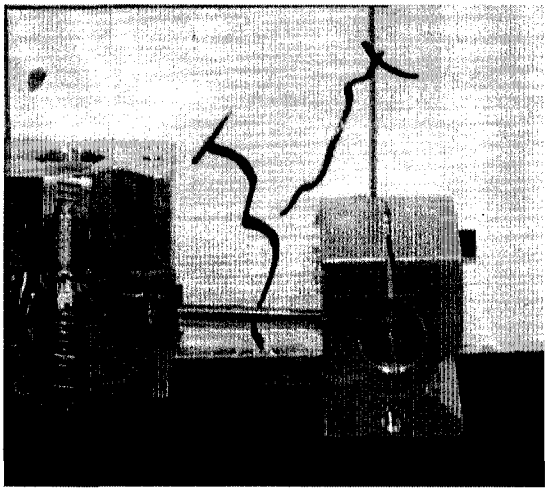

Fig. 3.19. Crack width monitoring

Readings from strain gauges and LVDTs were recorded during testing every second by using data acquisition system 6000 (manufactured by VISHAY), which was connected to a computer as shown in Fig. 3.20.

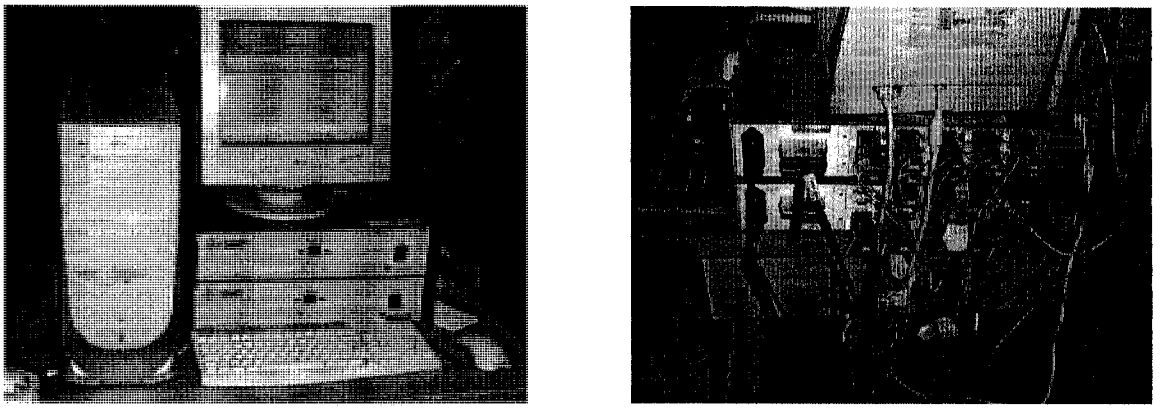

Fig. 3.20. Data acquisition system 6000

3.4.5. Test setup and procedure

The beams were tested in four-point bending over a simply- supported clear span of 2700 mm. A 500 kN closed-loop MTS actuator was used to apply the load. The actuator was supported by a steel frame and the load was transferred from the actuator to the tested beam through a steel spreader I-beam applied on the full width of the beam. A roller support was obtained by placing a steel cylinder between two steel flat plates. A pin support was obtained by using specially adapted steel I-beam. The upper plate of the I-

beam had a spherical end to house the plate and allow the rotation. At each end of the tested beam, the roller and pin support were tested on steel I-beam which was secured on the rigid floor of the lab. The different components of the test setup can be shown schematically in Fig. 3.21.

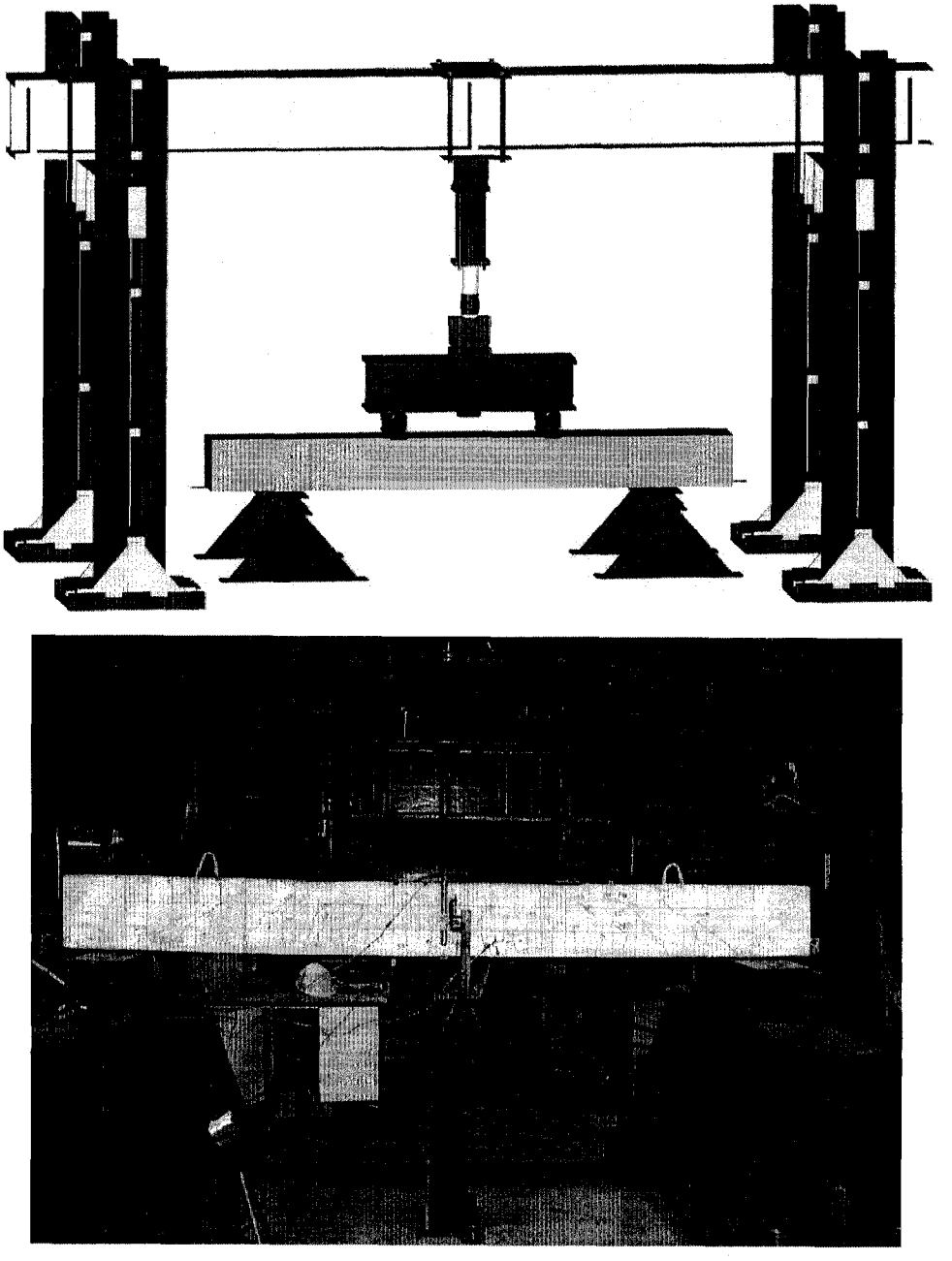

Fig. 3.21. Beam test setup

3.5. Material Properties

The materials used for the pullout specimens and the flexural beams are the same. There are four materials used in this study. These materials are concrete, steel and FRP reinforcing bars and adhesives.

3.5.1. Concrete

All the tested specimens for the pullout specimens and the flexural beams were constructed using a ready mix concrete in order to minimize the variations of all constituents. The targeted concrete compressive strength after 28 days was 35 MPa. As indicated before, after 28 days, three cylinders were tested in compression from each casting to ensure getting the designed compressive strength. The actual concrete compressive and tensile strength were determined based on the average values of three cylinder specimens (150x300 mm) for each tested specimen. The cylinders were tested at the same time of testing the specimen as shown in Fig. 3.22 and Fig. 3.23. The cylinders were cast from the same batch used for casting the specimens. These cylinders were cured under the same environmental conditions as those of the specimens. The cylinders and the specimens were tested on the same day of testing of the specimens. The average concrete compressive strength of the concrete cylinders ranged from 38 to 44 MPa. The average concrete tensile strength ranged from 2.9 to 3.8 MPa. The modulus of elasticity of concrete was calculated from the stress strain curve obtained as shown in Fig. 3.24. The concrete mix composition for one m^3 of fresh concrete is given in Table 3.4.

Table 3.4. Mix composition of the used concrete

Water-cement ratio	Water, kg/m3	Cement content, kg/m^3	Fine aggregate content, kg/m^3	Coarse aggregate content, kg/m^3	Air entrained, %	Slump, mm
0.39	169	430	672	1051	5	80

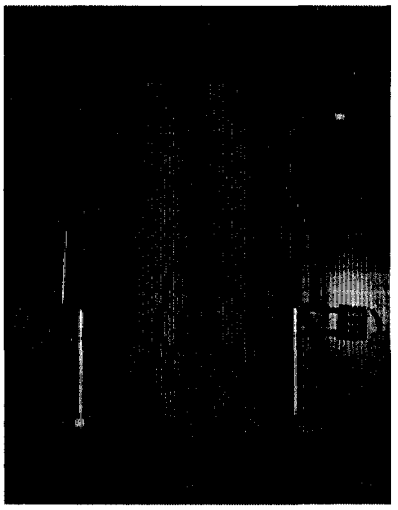

Fig. 3.22. Concrete compression test

Fig. 3.23. Concrete splitting test

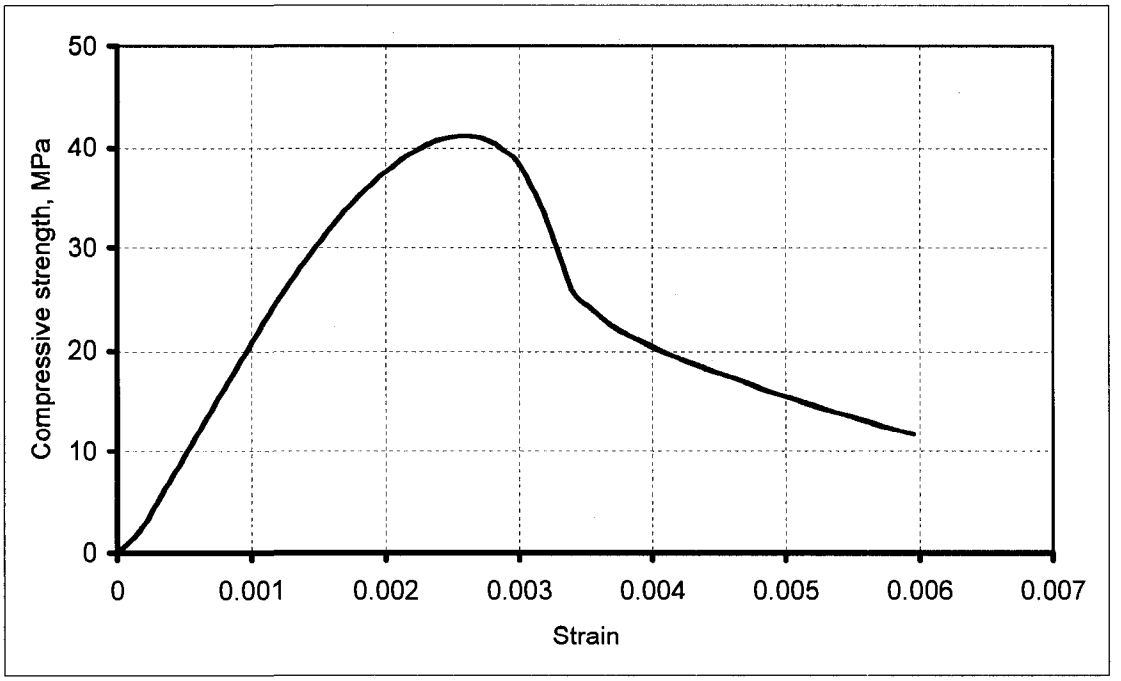

Fig. 3.24. Stress strain curve for the concrete cylinders

3.5.2. Steel bars

Deformed steel bars No.10M (11.3 mm in diameter) and No.15M (15.9 mm in diameter) were used in reinforcing the concrete beams. No steel bars were used for the specimens. The nominal steel yield stress and modulus of elasticity are 400 MPa and 200 GPa

respectively. The actual tensile properties were determined using standard tensile testes performed on six samples for each bar diameter. The actual average properties are given in Table 3.5.

Table 3.5. Mechanical properties of the reinforcing bars

Bar type	Bar diameter mm	Bar area mm^2	Modulus of elasticity, GPa	Tensile strength, MPa	Ultimate strain %
CFRP	9.5	71	124	1596	1.4
	12.7	127	134	1250	0.74
GFRP	12.7	127	45	756	1.8
Steel	11.3	100	200	f_y=454 f_u=571	0.23
	15.9	200	200	f_y=460 f_u=858	0.23

3.5.3.FRP bars

Two types of FRP bars were used in this study CFRP and GFRP, manufactured by Pultrall Inc. (2006). Two diameters were used for carbon 9.5 and 12.7 mm while only one diameter 12.7mm was used for glass. All specimens were tested for tensile strength and modulus of FRP bars according to the ACI 440.3R-04 (ACI 2004), part 2, B.2 (*Guide test methods for fibre reinforced polymers for reinforcing or strengthening concrete structures*). The total numbers of specimens were six specimens for each diameter. Each specimen was cut at a proper length and anchored at each end by an anchored method. The anchor consisted of a steel sleeve with length 50 times the nominal diameter of the bar and filled with high performance resign grout. The length of the tested section between the anchorage lengths was about 50 times the nominal diameter of the bar as shown in Fig. 3.25.

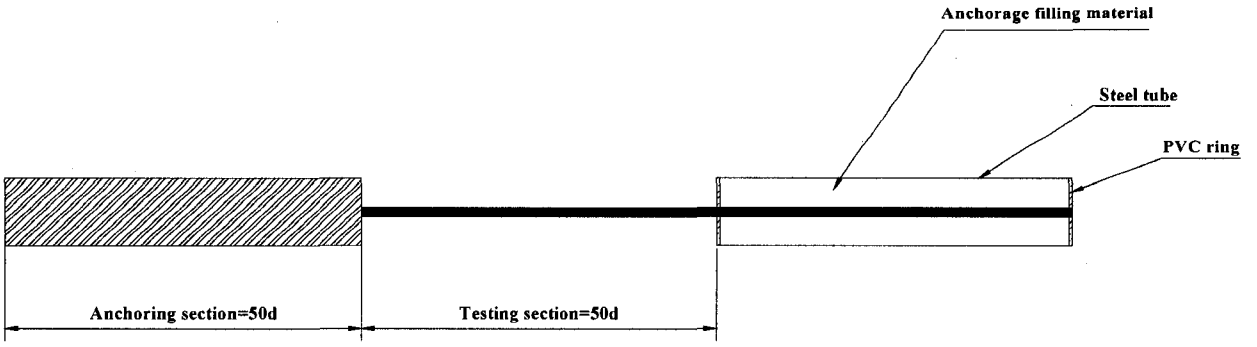

Fig. 3.25. Scheme of tensile test specimens for FRP bars

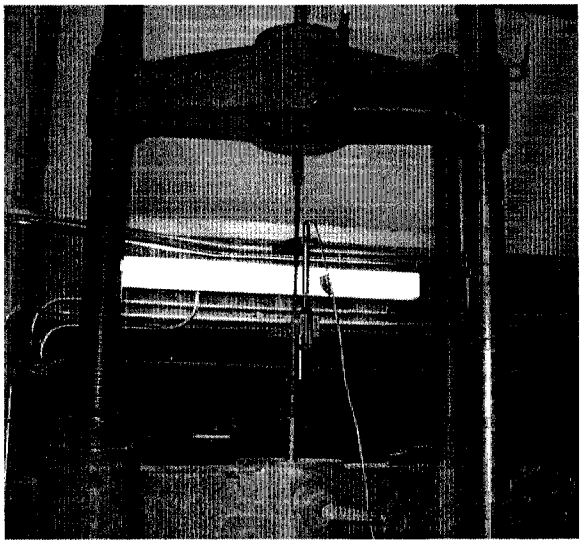

Fig. 3.26. Tensile test setup for FRP bars

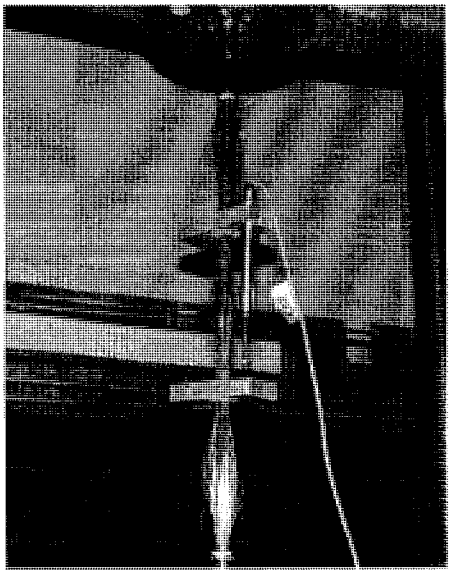

Fig. 3.27. Tensile failure for CFRP 9.5 mm-diameter

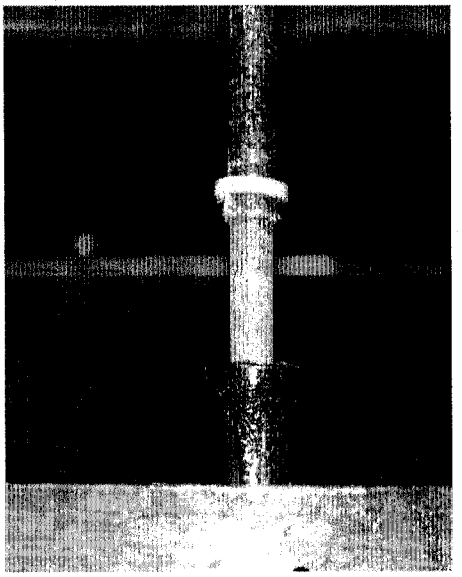

Fig. 3.28. Slippage failure for CFRP 12.7 mm-diameter

3.5.4. Adhesives

Two adhesive types produced by Hilti Inc. were used in this study. The first type, HIT RE 500 is a high strength two part epoxy based adhesive, resin and hardener as shown in Fig. 3.29. This type is specially designed for fastening into solid base materials in a wide range of material temperatures ranging from 49°C down to -5°C. It may be also used in underwater fastening for oversized holes up to twice the bar diameter but with a

maximum hole diameter of 76 mm. The HIT RE 500 can be used on wet or dry surfaces and is characterized by having excellent weathering resistance and high temperature resistance. The second type of adhesive, HIT HY 150, is a hybrid adhesive consisting of methaccrylate resin, hardener, cement and water. It is formulated for fast curing and installation in a wide range of material temperatures ranging from 40°C down to -5°C (Hilti Inc. 2006). The specifications of these adhesives are listed in Table 3.6.

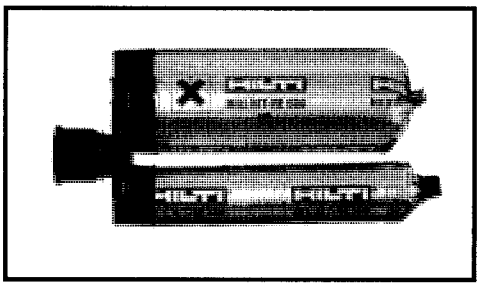

Fig. 3.29. The two-component adhesive package

Table 3.6. Material specifications of adhesives (Hilti 2006)

Adhesive	Compressive Strength, MPa	Tensile Strength, MPa	Modulus of Elasticity, MPa	CTE x10^6 $°C^{-1}$	Tg	Bond Strength, MPa
Epoxy, HIT RE 500	82.7	43.5	1493	42.5	81	12.4
Cement, HIT HY 150	71.8	15.9	7032	29.5	–	Not Specified

Chapter 4 - Bond Behaviour: Analysis and Discussion of Test Results

4.1. General

The NSM system depends mainly on bond stresses and their transfer from the concrete to FRP bars, through a bonding agent, to develop a composite action between the reinforced concrete element and the NSM-FRP bars. This composite section acts to increase the ultimate capacity of the concrete element, such as flexural and shear strength, and to improve the serviceability aspects such as cracking and deflection limitations. The bond stresses between the concrete, bonding agent (epoxy or cement) and FRP bars are very important factors in the NSM system. To investigate the bond characteristics between the three components and to analyze the influence of the most critical parameters that are known to affect such behaviour, a series of pullout tests of NSM-FRP bars in concrete specimens were carried out.

The pullout tests were carried out on 76 C-shaped concrete specimen specimens that were divided into two stages. The first stage, pull-out test, included 60 specimens tested in room temperature; while the second stage, durability investigation, included 16 specimens that were conditioned in freeze/thaw cycles before testing.

4.2. Stage One: Bond characterization

In this stage, 60 C-shaped concrete specimens were prepared and tested in normal room temperature. The specimens were divided according to the different parameters studied as given in Table 4.1 and explained in detail in chapter 3. The test results of these specimens were presented in terms of pullout load, average bond stress and mode of failure of the tested parameters as given in Table 4.1.

4.2.1. Modes of failure

4.2.1.1. Specimens with epoxy adhesive

The main mode of failure for most of the specimens using epoxy as an adhesive material was concrete shear tension failure (semi-cone failure) (Fig. 4.1a and b) accompanied with or without cracking in the epoxy, depending on the bonded length (Fig. 4.1c). This shear tension failure mode was due to tensile stresses along the inclined planes in the concrete surrounding the groove. Internal longitudinal cracks were observed in the epoxy in many specimens after failure. These cracks indicated the path of the tension force in the bar. This tensile force transferred to the epoxy. As a result of the fact that the tensile strength of the epoxy was much higher than that of concrete, most of the failure was in the concrete, while its tensile strength is very weak. These cracks usually start at the loaded end and propagated to the free end. Once a crack reached the free end, the epoxy cover suddenly split (Fig. 4.1d).

As the bonded length increases, the length of the path of the crack to the free end increases and the tensile stresses in the epoxy adhesive decreases. Increasing the tensile force in the bar increases its tensile stresses till it reached the FRP bar tensile strength. The FRP bar will rupture before the epoxy reaches its tensile strength as a result of increasing its bonded length. The bar rupture for specimens (C/9.5-E-1.50-24), (C/9.5-E-1.50-36), (C/9.5-E-1.50-48) and (G/12.7-E-2.00-36) are shown in Fig. 4.1e and Fig. 4.2d.

Specimens C/12.7-E-1.50-18 and C/12.7-E-2.00-18 failed by bar slip from the epoxy due to bond failure of the sand coated FRP bar as shown in Fig. 4.1f.

The modes of failure for specimens with a GFRP bar were similar to specimens with a CFRP bar. Specimen (G/12.7-E-2.00-12) with the smallest bonded length failed by bar slip at the bar epoxy interface (Fig. 4.2a). Specimens (G/12.7-E-2.00-18) and (G/12.7-E-2.00-24) failed by concrete cracking accompanied by splitting of the epoxy cover with a portion of concrete surrounding the groove, (Fig. 4.2b and c)

From the above given modes of failure, it can be concluded that the bond stresses between the concrete, adhesive material and FRP bar were a very important factor in the

adopted NSM system. In the following, the relation between the mode of failure and the average bond stress will be given for the different mode of failure.

When the failure was between the FRP bar and epoxy interface for slip or splitting of the epoxy cover, the average bond stress was calculated using the following equation (De Lorenzis and Nanni 2001)

$$\tau_{av} = \frac{P_u}{\pi.d.L_b} \tag{4.1}$$

Where τ_{av} is the average bond stress, P_u, pullout load at failure, d diameter of FRP bar and L_b bond length of FRP bar in the specimen.

Table 4.1. Test results for the Pullout Testing

Specimen code	Type and diameter of FRP	Groove filling	Groove width	Bonded length	Pullout Load at Failure, kN	Average bond stress, MPa	Mode of Failure
C/9.5-E-1.50-6	CFRP 9.5mm	Epoxy	1.50*d*	6*d*	28.68	16.02	C
C/9.5-E-1.50-12				12*d*	52.45	14.65	C
C/9.5-E-1.50-18				18*d*	74.85	13.93	C+Se
C/9.5-E-1.50-24				24*d*	84.77	—	R
C/9.5-E-2.00-6	CFRP 9.5mm	Epoxy	2.00*d*	6*d*	35.56	19.87	C
C/9.5-E-2.00-12				12*d*	59.35	16.58	C+Se
C/9.5-E-2.00-18				18*d*	64.57	12.10	C+Se
C/9.5-E-2.00-24				24*d*	75.62	10.56	C
C/9.5-E-2.00-36				36*d*	96.291	—	R
C/9.5-E-2.00-48				48*d*	96.23	—	R
C/12.7-E-1.50-18	CFRP 12.7mm	Epoxy	1.50*d*	18*d*	48.83	5.36	S
C/12.7-E-2.00-18			2.00*d*	18*d*	49.05	5.38	S
G/12.7-E-2.00-12	GFRP 12.7mm	Epoxy	2.00*d*	12*d*	52.19	10.90	S
G/12.7-E-2.00-18				18*d*	66.93	9.32	S
G/12.7-E-2.00-24				24*d*	77.74	8.12	C+E+S
G/12.7-E-2.00-36				36*d*	79.80	—	R
C/9.5-C-1.50-12	CFRP 9.5mm	Cement	1.50*d*	12*d*	31.73	4.81	Ic-c
C/9.5-C-1.50-18				18*d*	32.45	3.25	Ic-c
C/9.5-C-1.50-24				24*d*	44.68	3.38	Ic-c
C/9.5-C-2.00-24			2.00*d*	24*d*	35.24	2.45	Sc

C = Concrete tension failure, R = Rupture of bar, S = Slip of bar, Se = Splitting of epoxy, Sc = Splitting of Cement, Ic-c = failure at concrete–cement interface and E = epoxy cracking.

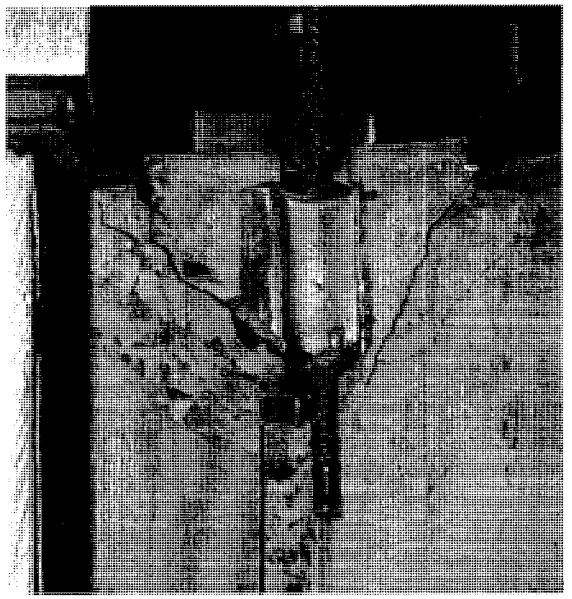

a) Concrete tension failure for C/9.5-E-2.00-6

b) Concrete tension failure for C/9.5-E-1.50-12

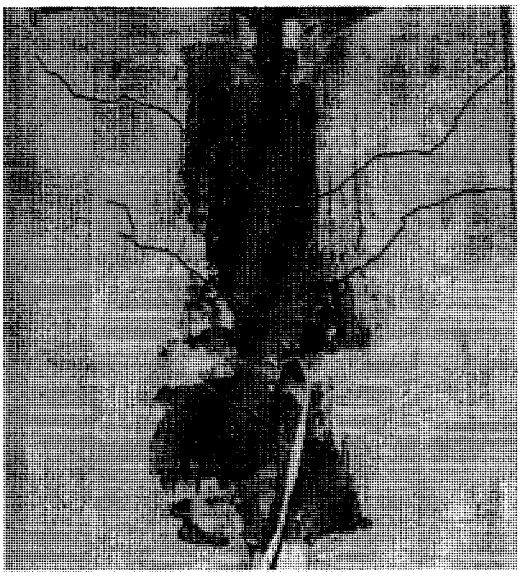

c) Concrete cracking with epoxy cracking for C/9.5-E-2.00-18

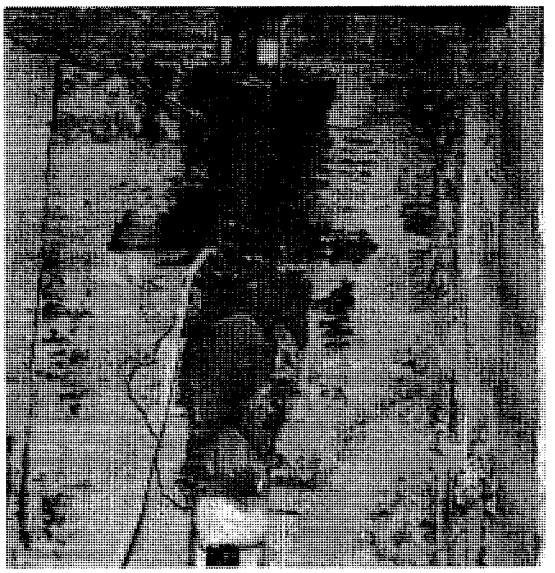

d) Concrete cracking with epoxy cover splitting for C/9.5-E-1.50-18

Fig.4.1. Mode of failure for specimens with NSM-CFRP bar and epoxy adhesive (cont. next page)

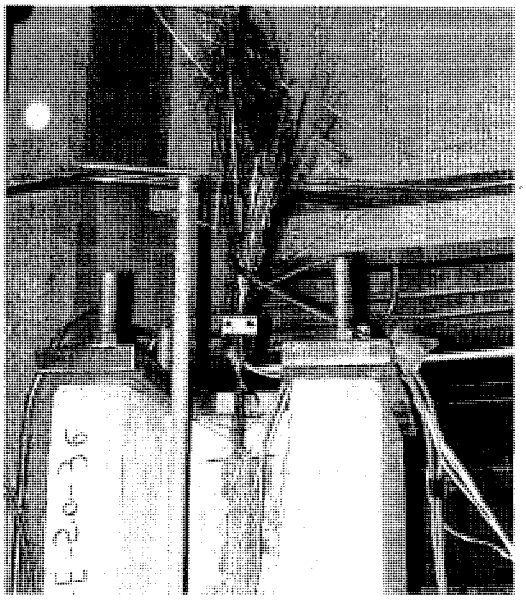

e) Bar rupture for C/9.5-E-2.00-36

f) bar slip for C/12.7-E-2.00-18

Fig. 4.1. Mode of failure for specimens with NSM-CFRP bar and epoxy adhesive.

a) Bar slip for G/12.7-E-2.00-12

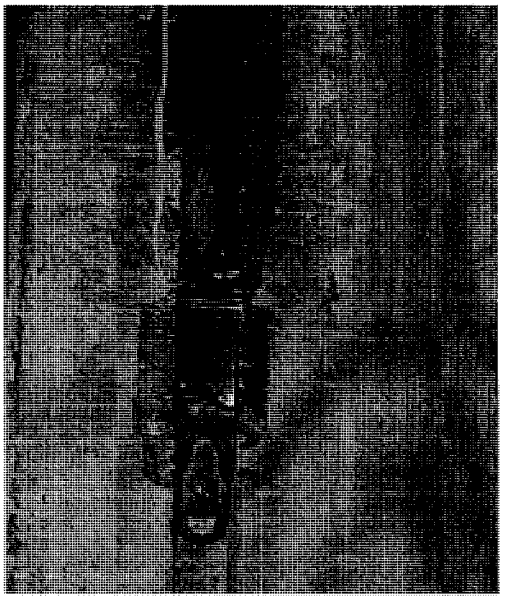

b) splitting of epoxy cover for G/12.7-E-2.00-18

Fig. 4.2. Mode of failure for specimens with NSM-GFRP bar and epoxy adhesive (cont. in next page)

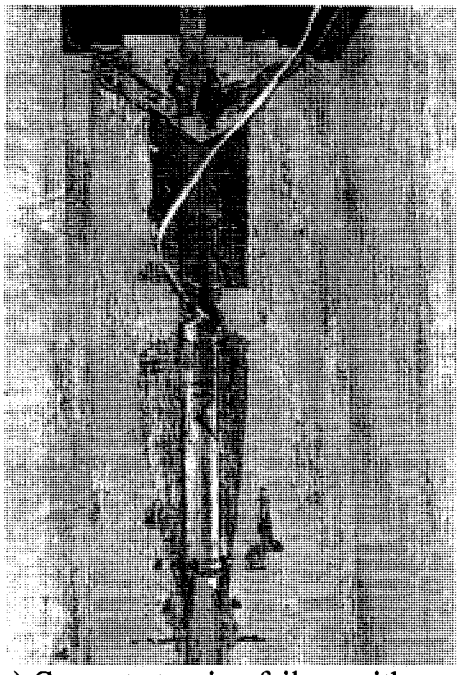

c) Concrete tension failure with epoxy cracking G/12.7-E-2.00-24

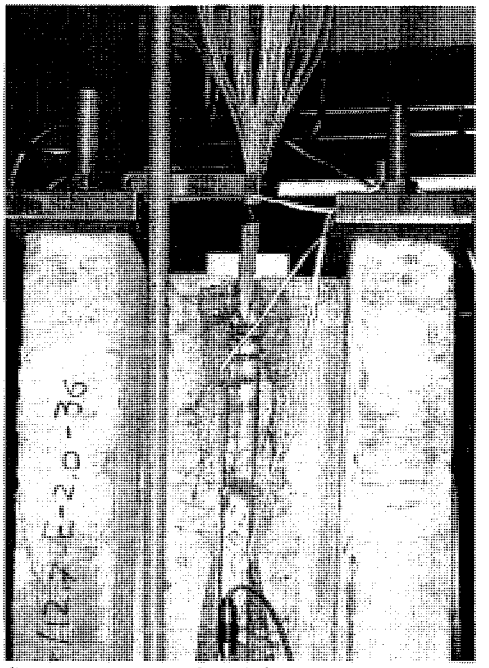

d) Bar rupture for G/12.7-E-2.00-36

Fig. 4.2. Mode of failure for specimens with NSM-GFRP bar and epoxy adhesive.

4.2.1.2. Specimens with cement adhesive

The main mode of failure was at the concrete-cement interface as shown in Fig. 4.3 and it occurred at low load levels compared to the epoxy adhesive as given in Table 4.1 and shown in Fig. 4.4. The ultimate loads for specimens with cement adhesive were 40 to 56% less than specimens with epoxy adhesive. This may be was due to the smooth surface of the sides of the groove.

Since the bond stress is calculated by dividing the pullout force by the failure contact area and the failure was at concrete-cement interface, the average bond stress was calculated by the following equation (De Lorenzis et al. 2002):

$$\tau_{av} = \frac{P_u}{(d_g + 2h)L_b} \tag{4.2}$$

where τ_{av} is the average bond stress, P_u, pullout load at failure, dg is the width of the groove, h is the height of the groove and L_b bond length of FRP bar.

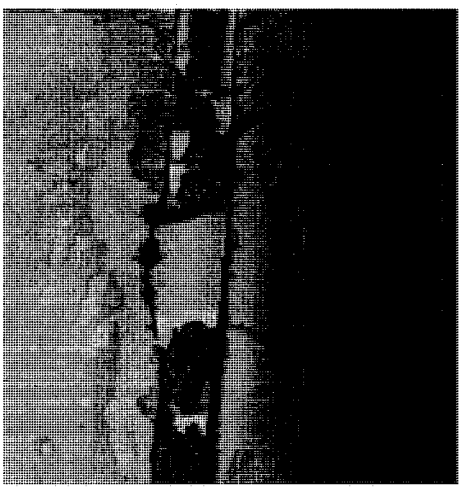

a) Failure at concrete-cement interface (C-1.50-24)

b) Splitting of cement cover for C/9.5-C-2.00-24

Fig. 4.3. Modes of failure for specimens with NSM-CFRP bar and cement adhesive.

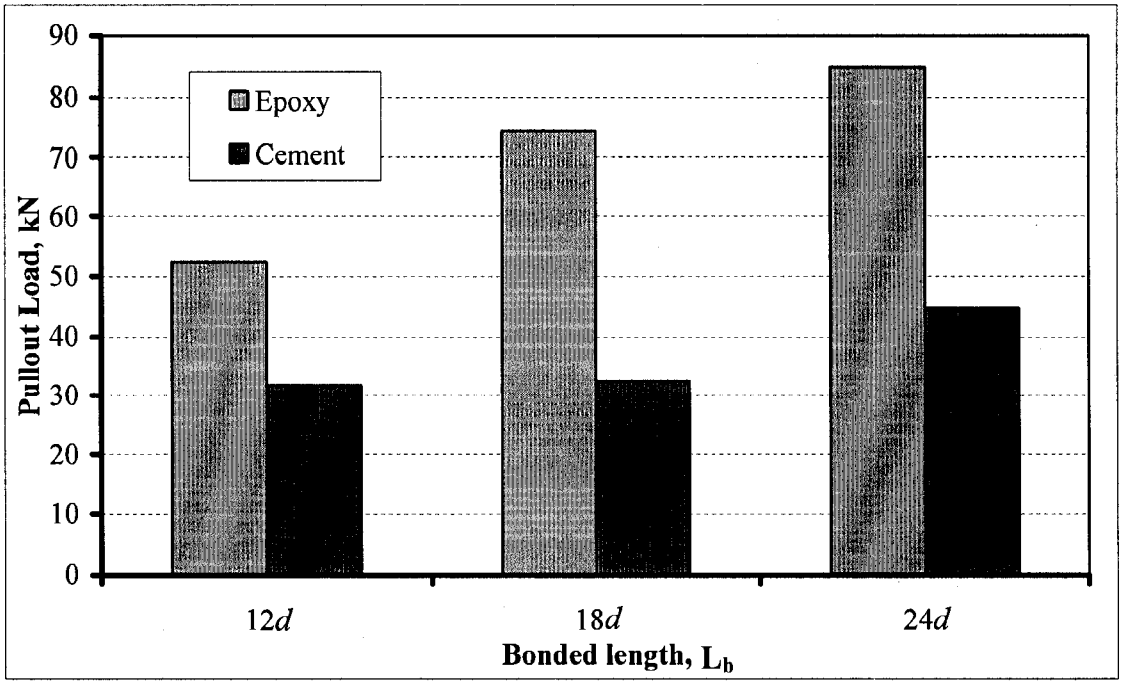

Fig. 4.4. Pullout load for epoxy and cement adhesive for groove size of 1.5 times the NSM bar diameter

4.2.2. Effects of different parameters on the bond characterization

4.2.2.1. Effect of bonded length

For a given groove size, as the bonded length was increased the ultimate load required to pullout the bar was increased as shown in Fig. 4.5. As well, the average bond stress was decreased due to the non-uniform distribution of the bond stresses along the bonded length.

4.2.2.2. Effect of groove size

For specimens with epoxy adhesive, increasing the groove size from 1.5*d* to 2.0*d* had insignificant effect on the pullout load at failure as shown in Fig. 4.5. This was due to the fact that failure was mostly controlled by the tensile strength of concrete not the splitting of the epoxy cover. Even when it occurred, in some specimens, it was following the formation of the inclined cracks in concrete.

For specimens with cement adhesive, the failure load for the specimens with a groove size equal to two times the bar diameter was lower than the specimens with groove size 1.5 times the bar diameter. This was due to the fact that shrinkage of the cement in a bigger groove size was greater than that of the smaller groove size, which accelerated the debonding of the cement from the concrete (Hilti Inc.2005).

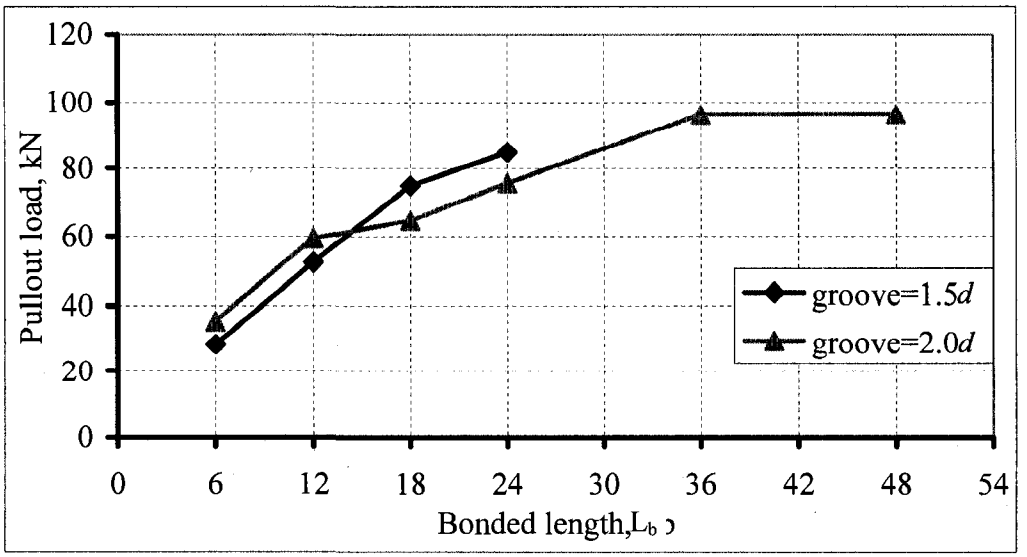

Fig. 4.5. Pullout load at failure versus bonded length for epoxy adhesive

4.3. Stage Two: Effect of Freeze/Thaw Cycles

In stage two, the freeze/thaw investigation included testing of 16 concrete specimens with CFRP bars after being subjected to freeze/thaw cycles in a controlled environmental chamber. Table 4.2 summarizes the test results for these conditioned specimens including failure load, bond strength, modes of failure and percent of change of failure load with respect to that of reference specimens.

4.3.1. Failure load

Figure 4.6 shows comparison between the failure load of the conditioned and reference specimens. For specimens with epoxy adhesive, the failure load for most of the specimens that were exposed to freeze/thaw cycling was slightly reduced. The percent of reduction for the conditioned specimens varied between 8 to 14 %. Two specimens only gained an increase in the failure load, D-E-1.50-12 and D-E-2.00-18. This increase was about 4.58% and 7.46% respectively. It is clear from Fig. 4.6 that the percent of reduction for specimens with groove width equal to 1.5 times the diameter of FRP bar was greater than specimens with groove width equal to 2.0 times the diameter of FRP bar and this was due splitting of epoxy, which will be explained in details in section 4.3.2. By increasing the groove width from 1.5 to 2.0d the resistance to splitting increases.

The failure load for the conditioned specimens with cement adhesive was about 30 to 45% less than that of reference specimens.

Table 4.2. Test results for the durability investigation

Specimen code	Groove filling	Groove dimension	Bonded length	Pullout load, kN	Bond strength, MPa	Failure mode	% of change
D-E-1.50-12	Epoxy	1.50*d*	12*d*	54.85	15.32	Se	4.58
D-E-1.50-18			18*d*	63.82	11.89	C+Se	-14.74
D-E-1.50-24			24*d*	74.21	10.37	C+Se	-12.46
D-E-2.00-12	Epoxy	2.00*d*	12*d*	52.24	14.59	Se	-11.98
D-E-2.00-18			18*d*	69.39	12.92	Se	7.46
D-E-2.00-24			24*d*	69.53	9.71	C+Se	-8.05
D-C-1.50-12	Cement	1.50*d*	12*d*	17.30	2.62	Ic-c	-45.48
D-C-1.50-18			18*d*	17.56	1.77	Ic-c	-45.89
D-C-1.50-24			24*d*	31.35	2.38	Ic-c	-29.83
D-C-2.00-24	Cement	2.00*d*	24*d*	35.27	2.45	Ic-c	0.09

C = Concrete tension failure, Se = Splitting of epoxy cover and Ic-c = concrete–cement interface failure.

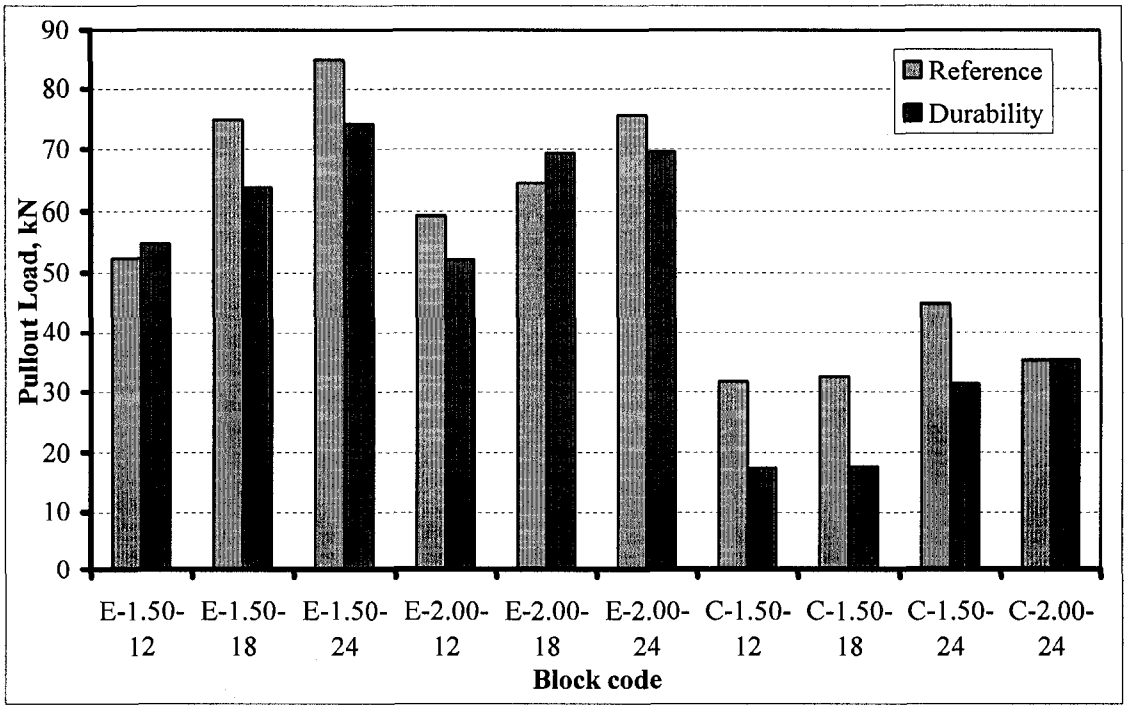

Fig. 4.6. Pullout load for the tested specimens

4.3.2. Modes of failure

Different modes of failure were obtained for the tested specimens; however, the concrete tension failure that was the common mode of failure for most of the reference specimens (section 4.2.1.1) was not the common mode of failure for the conditioned specimens. The mode of failure of each tested specimen is given in Table 4.2. The reference specimen C/9.5-E-1.50-12 failed by concrete tension failure (Fig. 4.1b), while its conditioned counterpart failed by epoxy splitting (Fig. 4.7a and Fig. 4.7b) showing higher slip (Fig. 4.9 and Fig. 4.10). Figures 4.9 shows a comparison between the average bond stress-slip for conditioned, D-E-1.5-12 and its reference specimen, C/9.5-E-1.50-12 which showed higher slip for the conditioned one than the reference one. For specimen D-E-1.5-18, two diagonal cracks were initially formed between the corner of the specimen and the groove at approximately 45 degrees (Fig. 4.7c). The width of these cracks got larger and further propagated with increasing the load till it reached the epoxy layer (Fig. 4.7d). When the tensile stress reached the tensile strength of the epoxy, cracks started to appear in the epoxy till the specimen failed. This mode of failure was the common mode of failure for most of the conditioned specimens with epoxy adhesive. Figure 4.10 shows comparison between the average bond stress-slip for conditioned, D-E-1.5-18 and reference specimen, C/9.5-E-1.50-18 which showed higher slip for the conditioned one with lower failure load.

The variation of the results between conditioned and unconditioned (reference) specimens, either in failure load or in failure mode, was due to the difference in values of thermal expansion coefficient between the adhesive material and the concrete. These changes in thermal expansion coefficient developed internal stresses and cracks. The difference in the results will decrease if the adhesive materials and the concrete specimens thermal expansion coefficient be closer to each other.

For the conditioned specimens with cement adhesive, the mode of failure was the same as the reference specimens. They failed by concrete-cement interface failure at lower load level compared to the reference specimens as described in section 4.2.1.2 of this thesis.

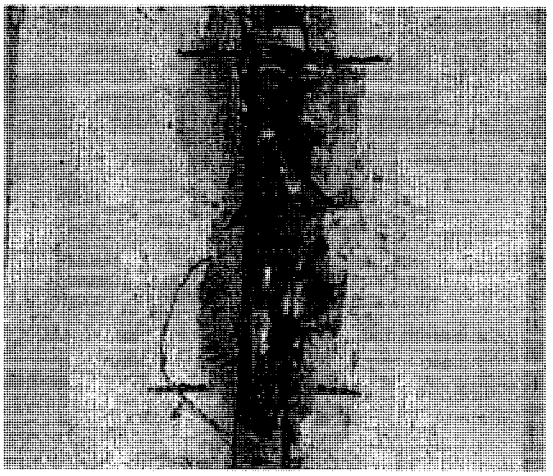

a) Splitting of epoxy covers (D-E-1.5-12)

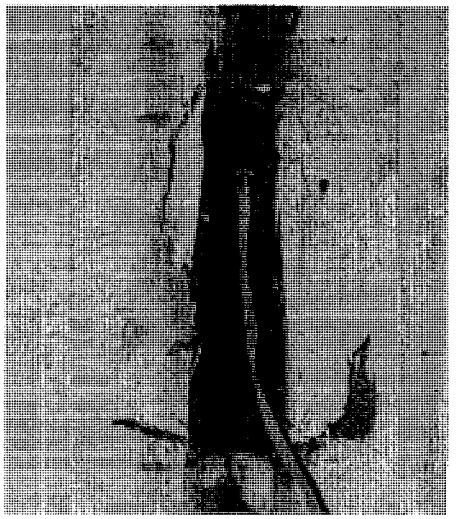

b) Splitting of epoxy covers (D-E-2.0-12)

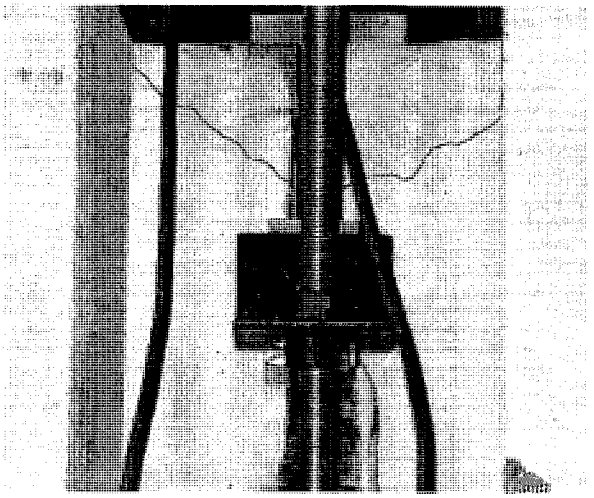

c) Diagonal crack start at the corner

d) concrete tension failure with longitudinal and transverse cracks in epoxy (D-E-1.5-18)

Fig.4.7. Modes of failure for the tested conditioned specimens with epoxy adhesive (cont. in the next page)

e) concrete tension failure with epoxy cover split (D-E-1.5-24)

f) concrete tension failure with longitudinal and transverse cracks in epoxy (D-E-2.0-24)

Fig. 4.7. Modes of failure for the tested conditioned specimens with epoxy adhesive

Concrete-cement interface failure (D-C-1.5-12)

Fig. 4.8. Mode of failure for the tested conditioned specimens with cement adhesive

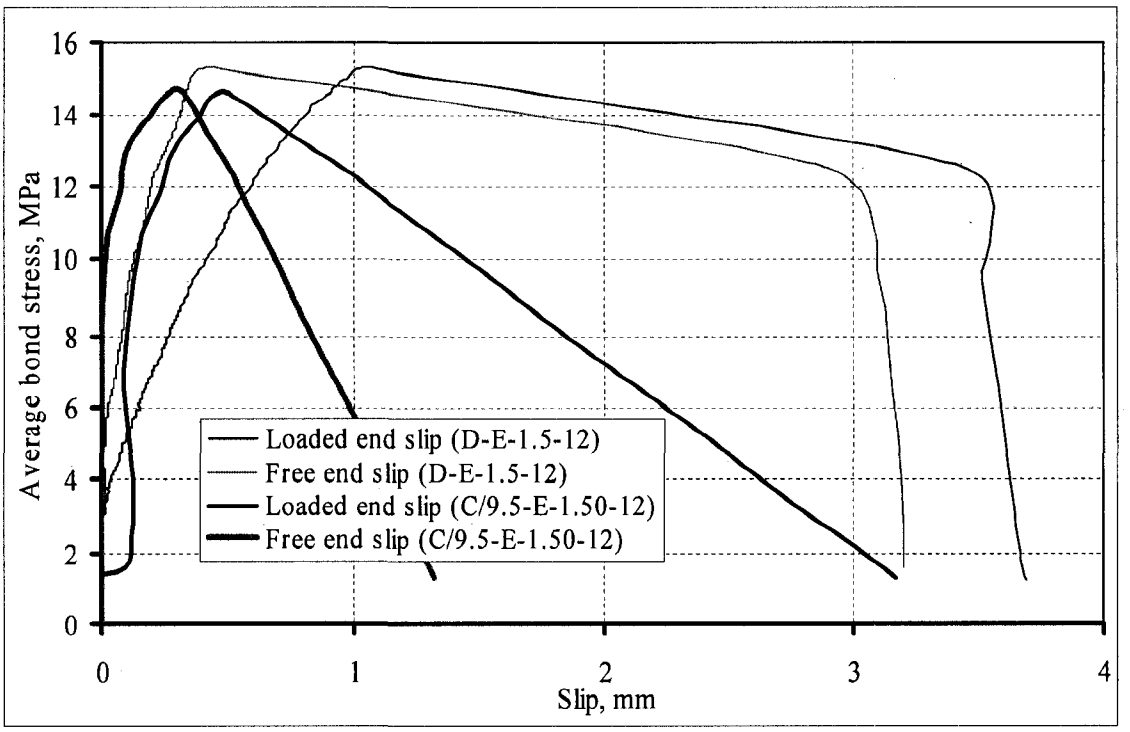

Fig. 4.9. Average bond stress-slip for C/9.5-E-1.50-12 and D-E-1.5-12

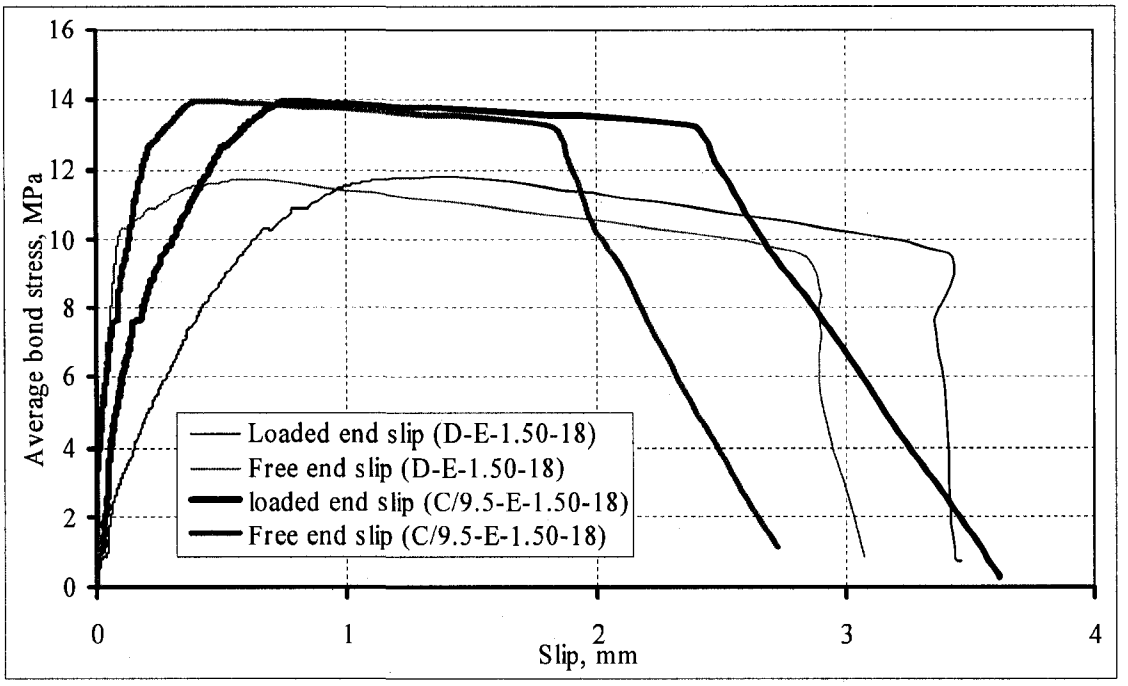

Fig. 4.10. Average bond stress-slip for C/9.5-E-1.50-18 and D-E-1.5-18

4.3.3. Strain distribution

As mentioned before in chapter 3, each specimen was instrumented with one electrical strain gauge at the middle of the bonded length. Strain readings were recorded every minute for the first 20 cycles as shown in Fig. 4.11. Differential thermal expansion which occurs between the FRP, adhesive and the concrete due to change of temperature creates residual stresses. As shown from Fig. 4.12, the strain increases with the increase of temperature from -20 ^{0}C to +25 ^{0}C during the thaw cycle then decreased again during the freeze cycle.

The strain distribution is divided to four stages. Stage I, (Fig. 4.13) started with the increase in temperature from -20 ^{0}C to +25 ^{0}C at the bar epoxy interface and this increase took around 2 to 3 hours. Then in stage II, the strain almost remained constant for the rest of the thaw cycle. At the end of the thaw cycle, the temperature started to decrease with a decrease in strain in stage III and this stage took around 4 to 6 hours to allow the temperature to reach -20 ^{0}C at the bar-epoxy and epoxy-concrete interfaces. The last 6 hours in the freeze cycle which represent stage IV, the temperature and the strain remains constant as shown in Fig. 4.14.

From the strain readings, the range of change in strain with the change of temperature was around 70 to 90 micro-strains in case of epoxy adhesive and around 120 to 170 micro-strains in case of cement adhesive. The change in strain increased with the increase in bonded length. Changing the groove width had no effect on the change of strain with temperature. The change in strain for specimens with cement adhesive was greater than specimens with epoxy adhesive.

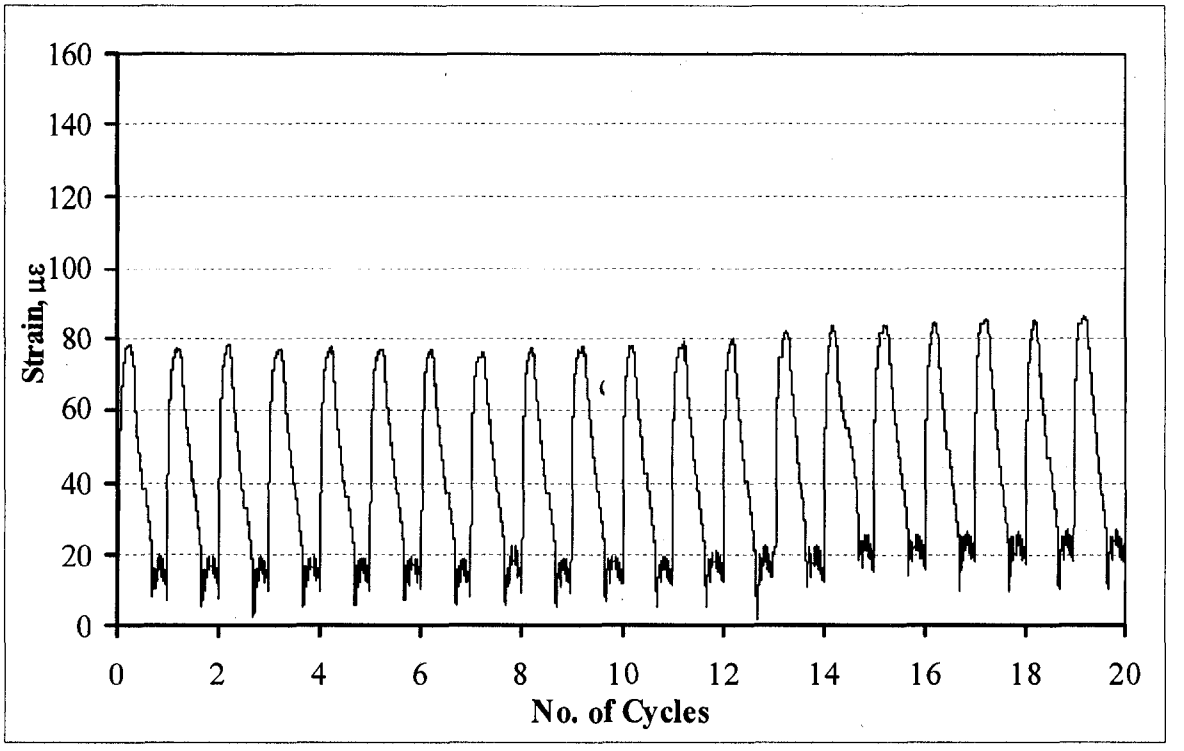

Fig. 4.11. Strain distribution in FRP bars during freeze/thaw cycling for D-E-1.5-12

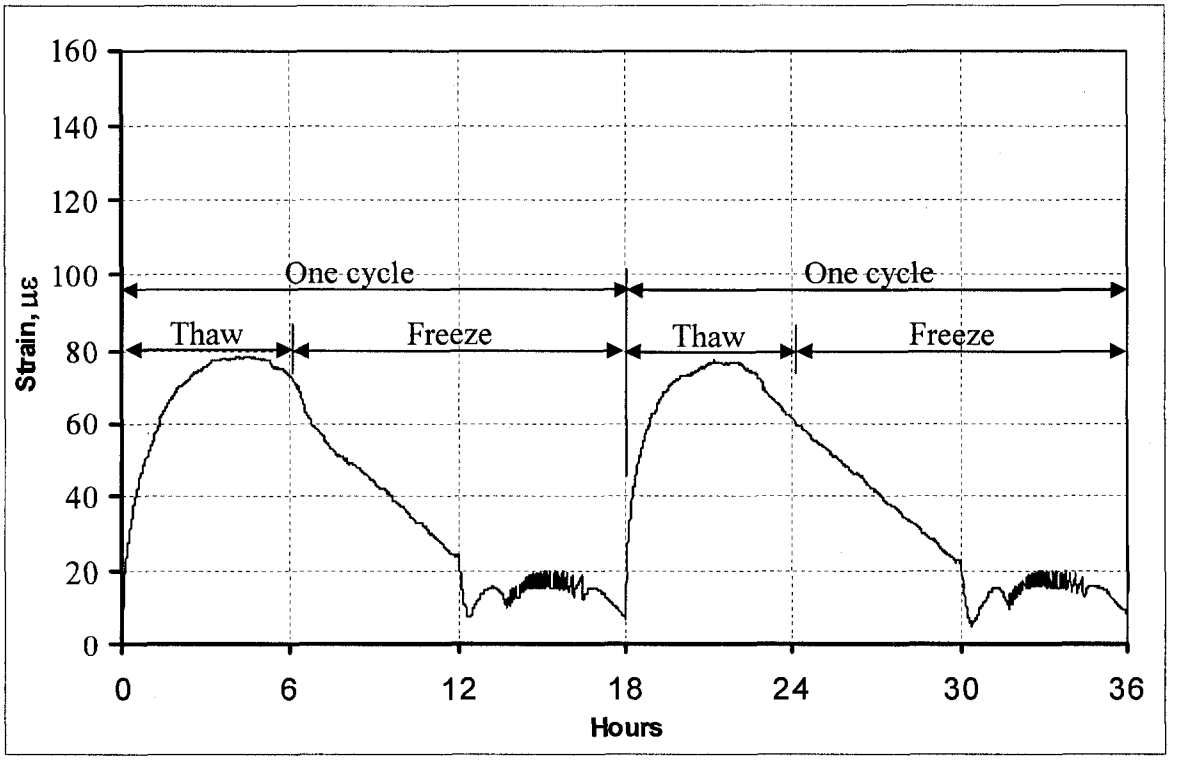

Fig. 4.12. Strain distribution in the FRP bars during freeze/thaw cycling for D-E-1.5-12

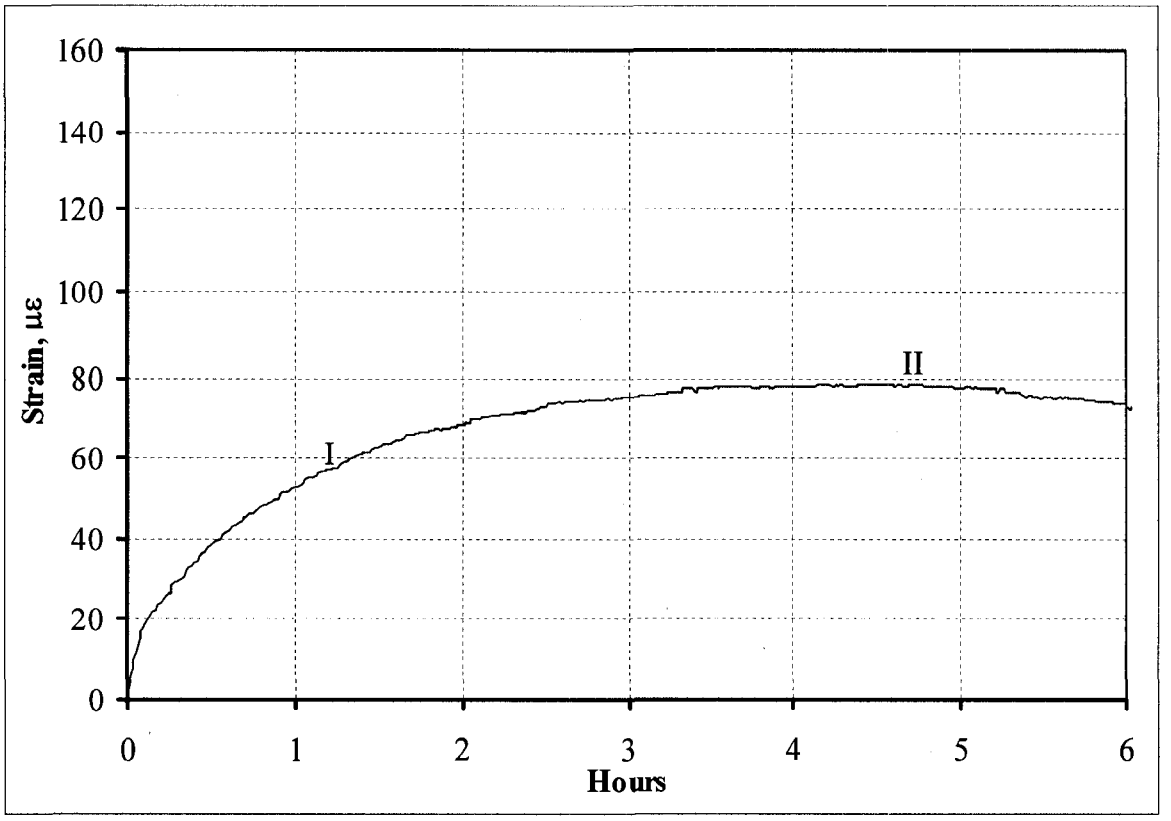

Fig. 4.13. Strain distribution in a thaw cycle for D-E-1.5-12

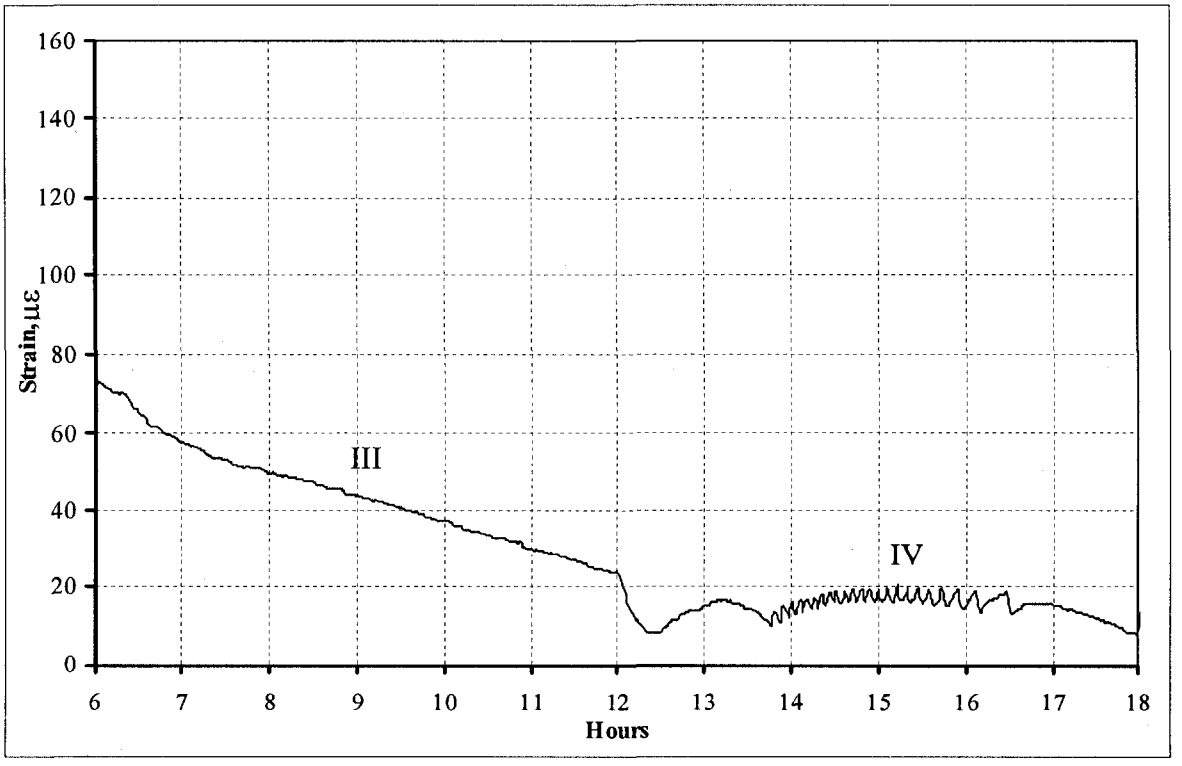

Fig. 4.14. Strain distribution in a freeze cycle for D-E-1.5-12

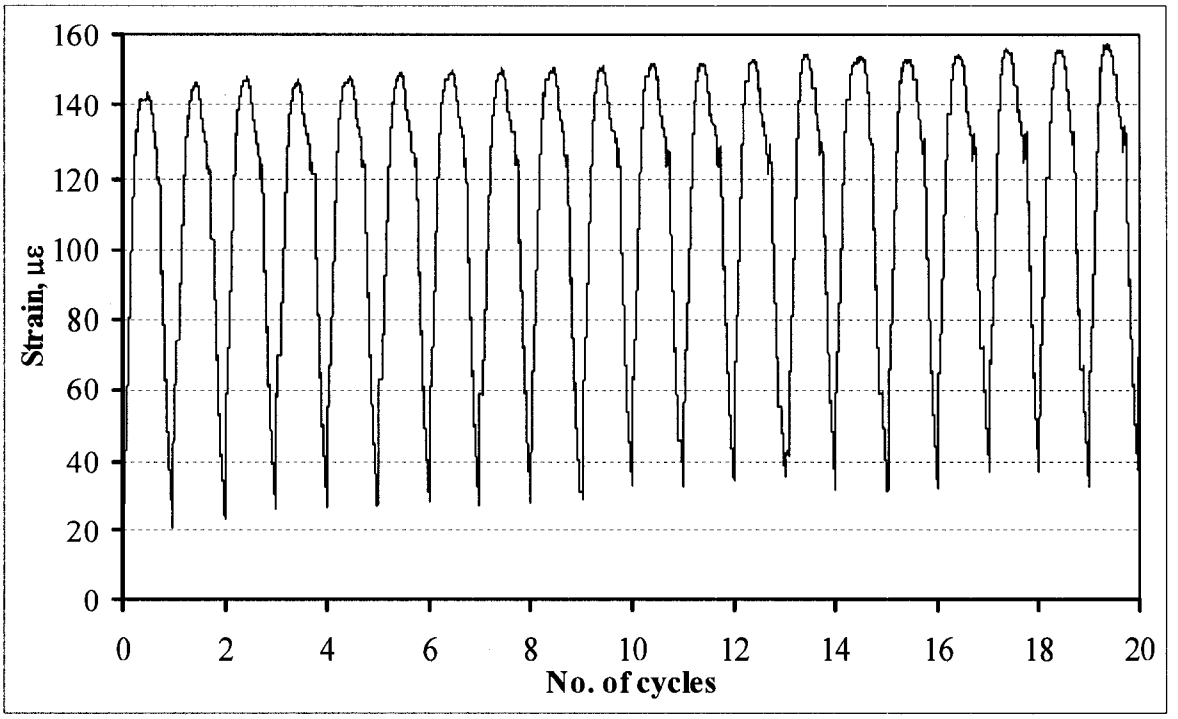

Fig. 4.15. Strain distribution during freeze/thaw cycling for D-C-1.5-12

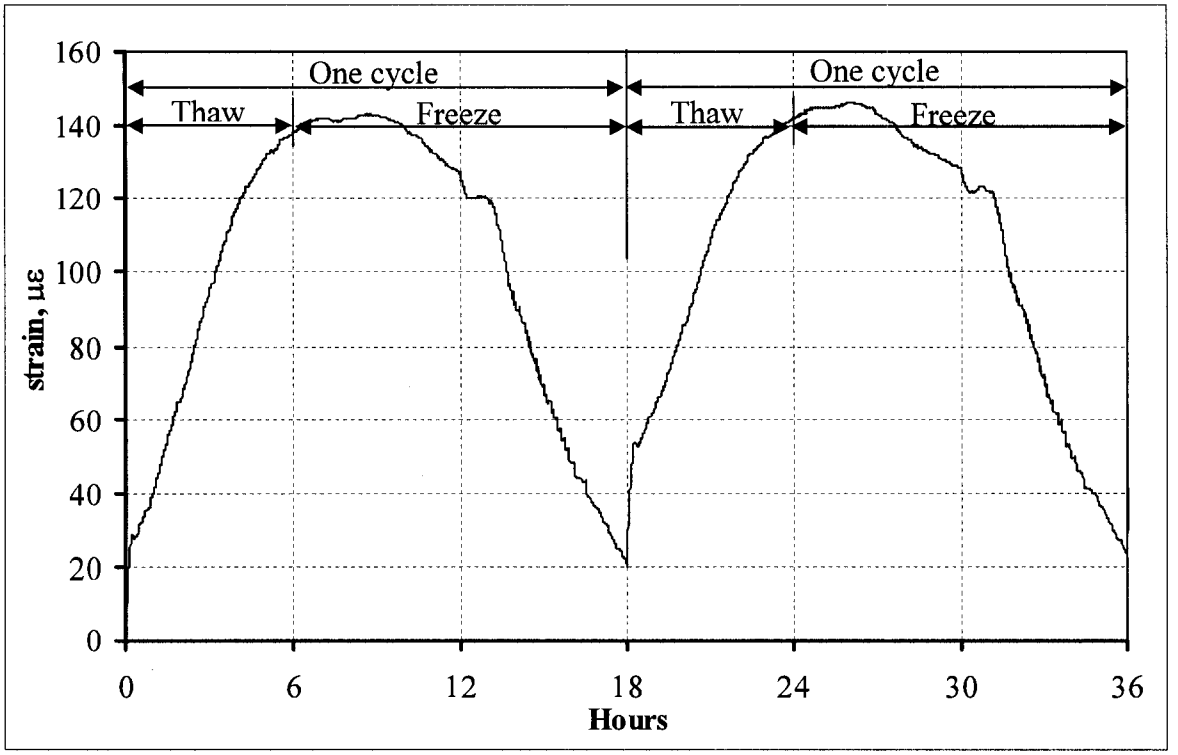

Fig. 4.16. Strain distribution during freeze/thaw cycling for D-C-1.5-12

4.4. Bond-Slip Analysis

4.4.1. Average bond stress-slip relationship

Figures 4.17 to 4.23 show the experimental average bond stress versus slip diagrams for the tested specimens. From the figures, we can observe that the free-end slip at the bottom has always a significant value independent on the bonded length. This value can be some what increased by increasing the bonded length which developed a bigger ultimate load. It can be stated that increasing the bonded length causes increase in the free end slip as a result of increasing the ultimate load. By using epoxy adhesive, the free end slip value ranged from 0.22 to 0.47 mm depending on the bonded length.

In case of cement adhesive specimens, the free-end slip value was very small. The slip ranged from almost zero to about 0.157 mm. In general it can be stated that using of cement adhesive produces a low free end slip at failure compared to using an epoxy adhesive as a result of reducing the failure load (Table 4.1) and also due to the elasticity difference between epoxy and cement as will be explained later.

The average bond stress-slip relationship can be divided into four categories. In the first category, the average bond stress increases linearly up to 50 to 60% of the ultimate bond stress. In this first category, no cracks were observed neither in the epoxy nor in the concrete where the bar and the adhesive material were in the elastic state. In the second category which is close to 50% of the ultimate bond stress, a crackling noise was heard which represents the starting of microcracks in the epoxy and concrete surrounding the groove. As the load increased, these cracks increased and became visible which represent the nonlinear part of the curve which leads to the ultimate bond stress. In this second category with the adhesive material was in the plastic stage, in which a relative slip between the bar, adhesive and concrete happened. At the third category, beyond the ultimate bond stress, a yielding plateau occurred for a noticeable slip distance followed by linear decrease in the last category. This yielding plateau was only measured due to using a high accuracy DAS which was able to take 10 readings per second. The difference in slip value shown in bond stress-slip diagrams between the loaded end slip and the free end slip at the ultimate bonded stress was due to the elongation developed in

the FRP bar bonded length and its adhesive during loading process, this elongation could be measured at the end of the elastic stage of the FRP bar and the adhesive.

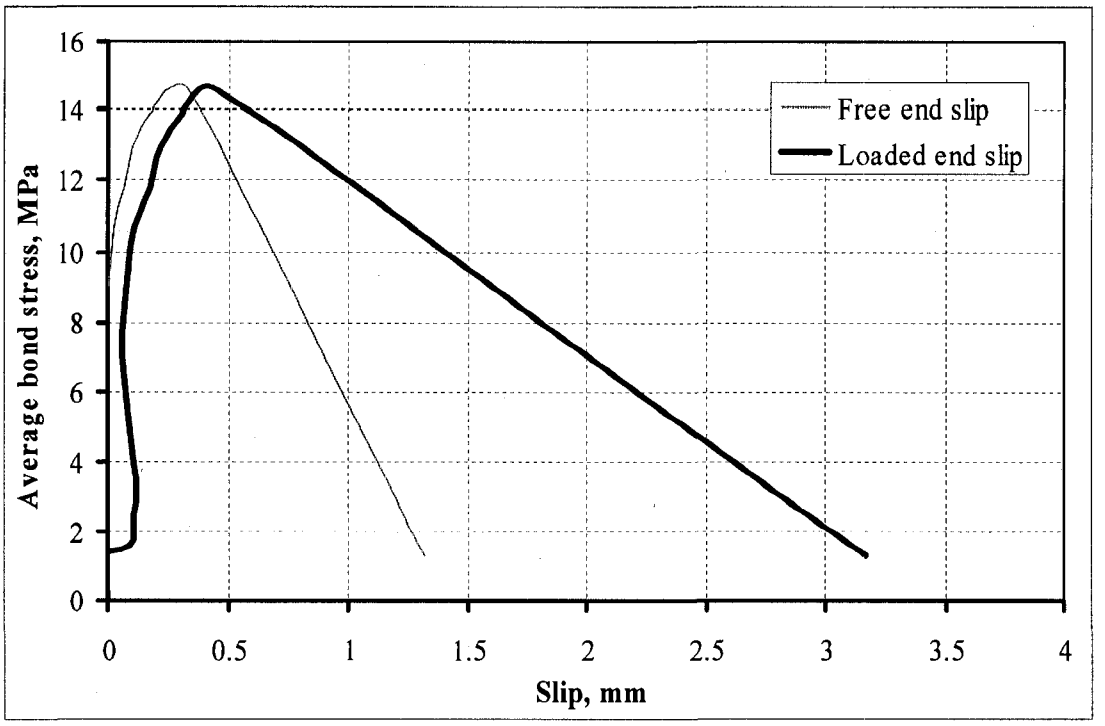

Fig. 4.17. Average bond stress-slip for C/9.5-E-1.50-12

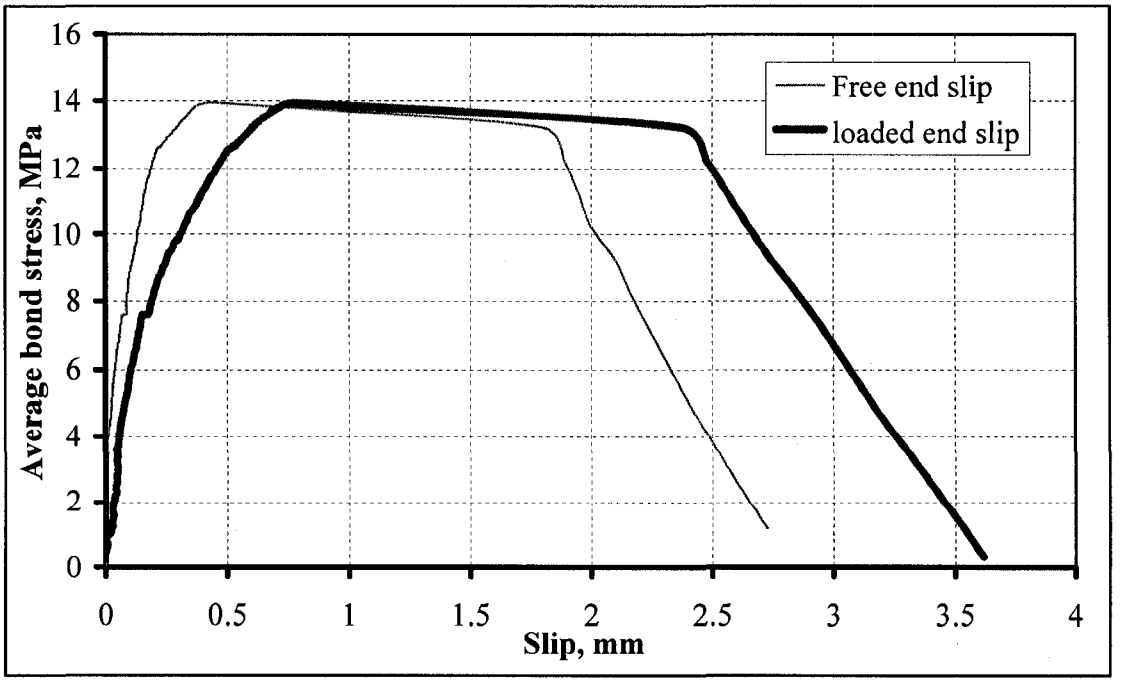

Fig. 4.18. Average bond stress-slip for C/9.5-E-1.50-18

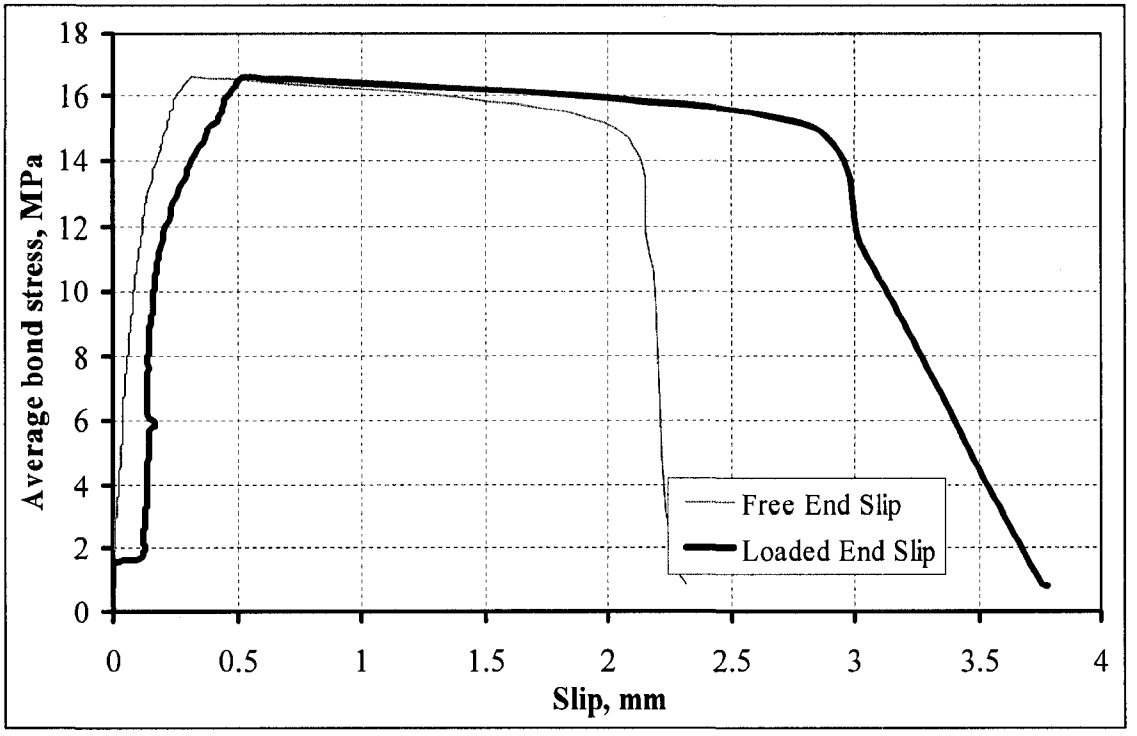

Fig. 4.19. Average bond stress-slip for C/9.5-E-2.00-12

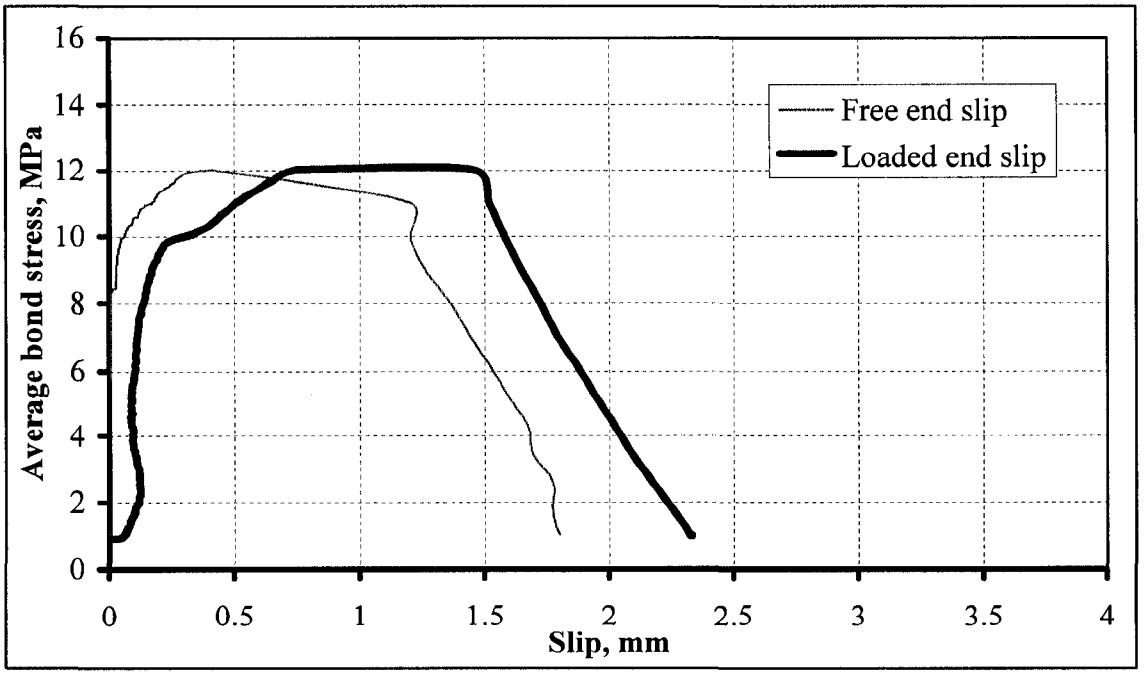

Fig. 4.20. Average bond stress-slip for C/9.5-E-2.00-18

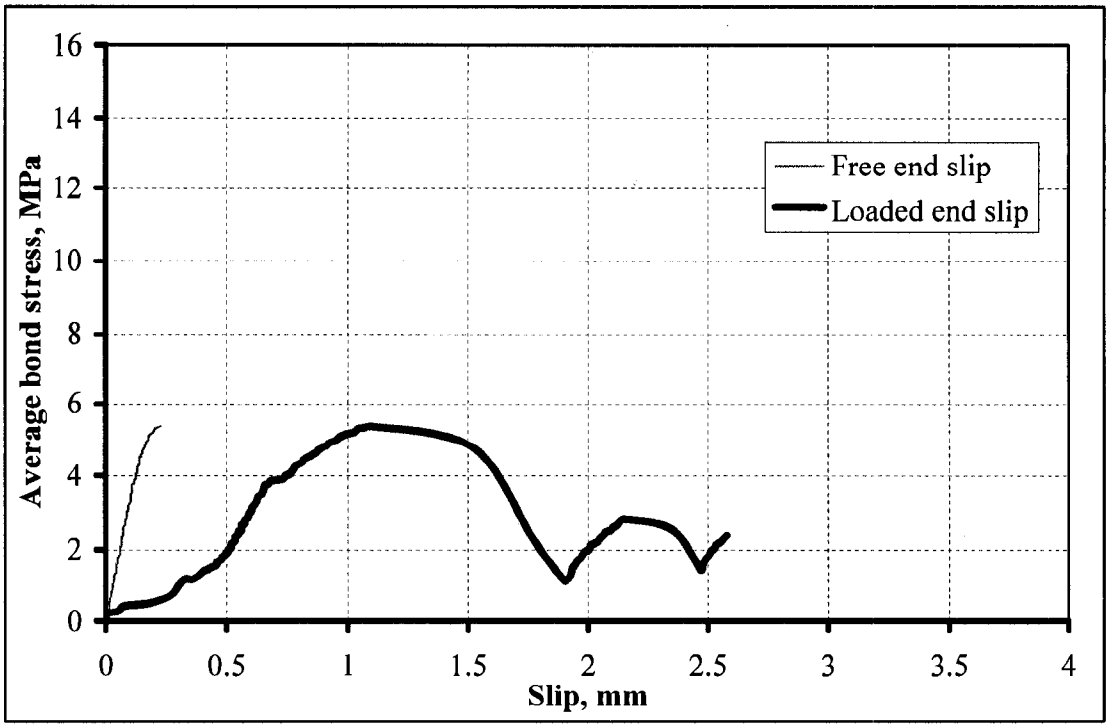

Fig. 4.21. Average bond stress-slip for C/12.7-E-2.00-18

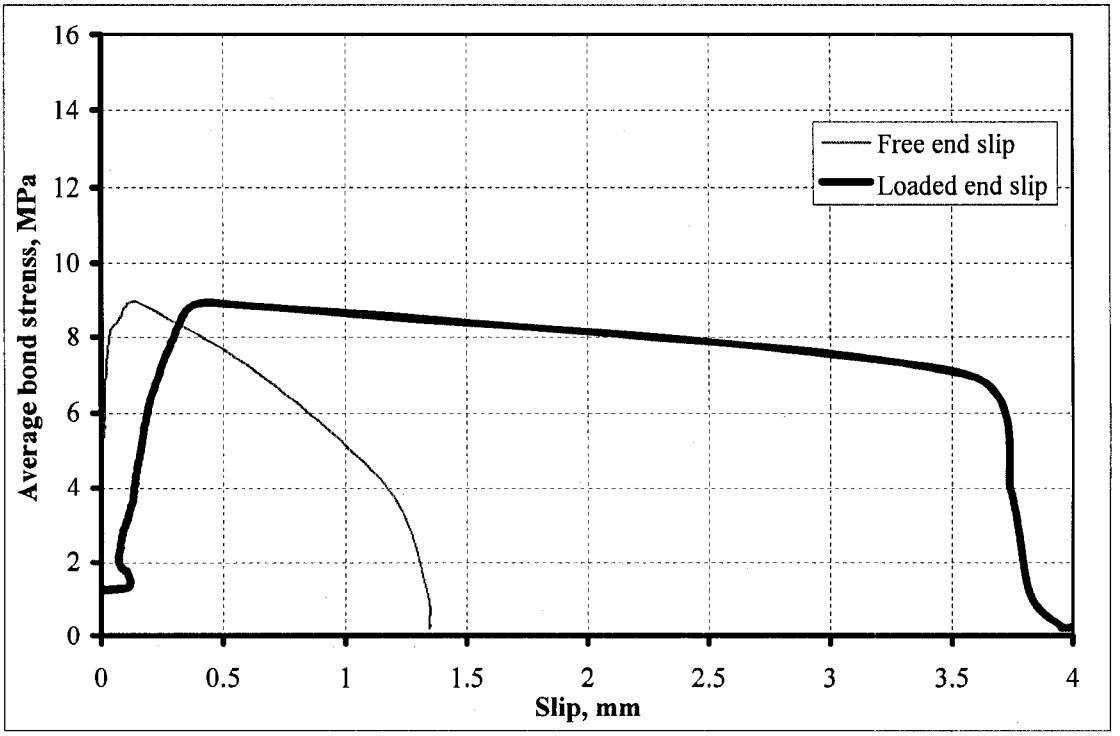

Fig. 4.22. Average bond stress-slip for C/9.50-C-1.50-12

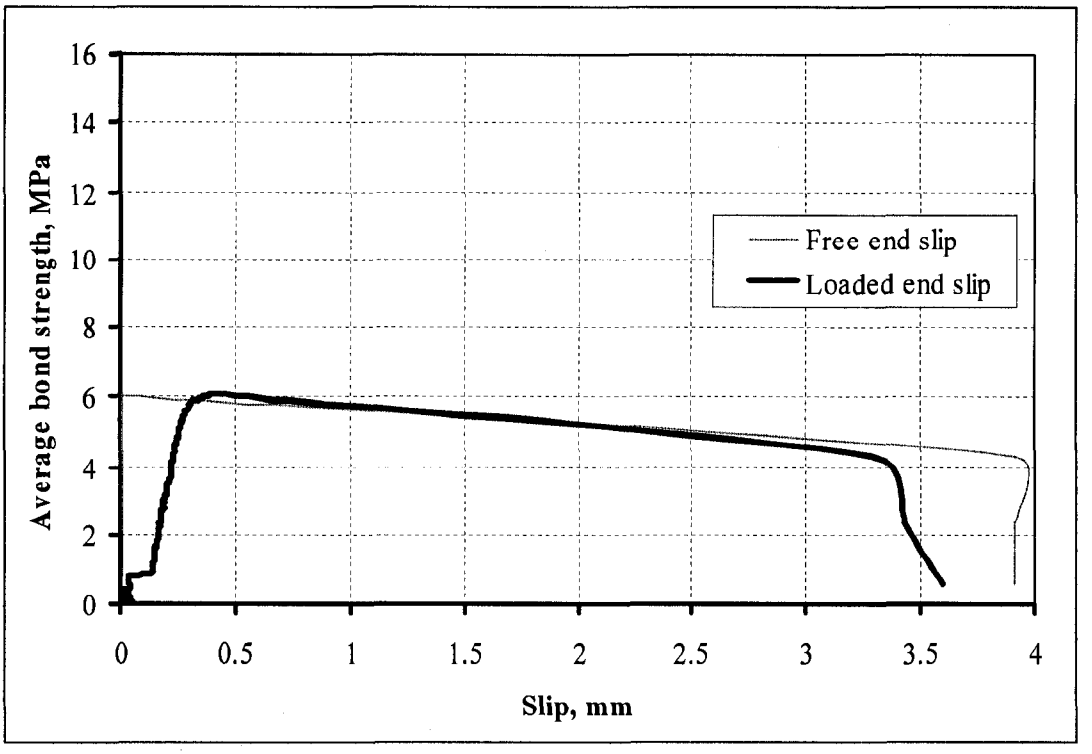

Fig. 4.23. Average bond stress-slip for C/9.50-C-1.50-18

FRP bar slip depends on the elasticity of the adhesive materials, its bonded length and groove size. In case of epoxy adhesive as an adhesive material, the slip is larger than using the cement as adhesive materials. Increasing the bonded length increases the slip and increasing the groove size increases the slip

The free slip gives the true indication for the elasticity of the adhesive materials but the loaded slip is equal to the free elasticity plus the elongation of the bonded length of the FRP bar and its cohesive. Figures 4.22 and 4.23 show the slip for concrete specimens with cement adhesive. In these two diagrams, where cement adhesive is used the slip curve for the free end is close to the vertical axes of the diagram, which means that the slip of the free end is small.

4.4.2. Local bond stress-slip relationship

The importance of finding the local bond stress relationship, as it defines the relationship between the applied stress and the corresponding slip value.

According to the literature, there are many ways that can be used to measure the local bond stress-slip relationship. Depending on the available experimental data, the local bond stress-slip can be identified by:

- the average bond stress-slip for small bonded length.

- reading from strain gauges placed along the FRP rod.

- by using numerical identification purposed by Focacci et al. (2000).

In this investigation the reading from the strain gauges will be used to obtain the local bond-slip relationship which in turn can express the behaviour of the bond between the FRP rod and the adhesive.

Equilibrium of a piece of rod of length dx is shown in Fig. 4.24. It is assumed that the behaviour is linearly elastic.

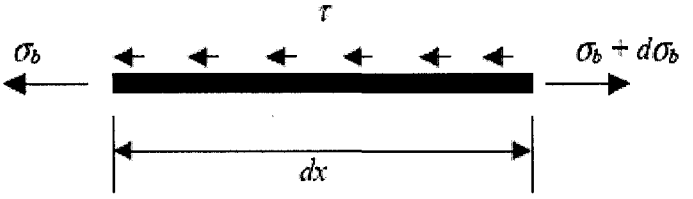

Fig. 4.24. Equilibrium forces for NSM bar

The bond stress applied on the FRP bar can by calculated by:

$$\tau = \frac{P_u}{\pi d\, d_x} \tag{4.3}$$

$$E_f = \frac{\frac{P_u}{\pi d^2/4}}{d\varepsilon_f(x)} \tag{4.4}$$

$$\tau = \frac{d}{4}.E_f.\frac{d\varepsilon_f(x)}{dx} \tag{4.5}$$

$$\tau_{(\frac{x_i+x_j}{2})} = \frac{d}{4}.E_f.\frac{\varepsilon_{fj}-\varepsilon_{fi}}{x_{fj}-x_{fi}} \tag{4.6}$$

Where x = coordinate along the longitudinal axis of the FRP bar within the bonded length, Therefore, the bond stress profile diagram at a given load level can be obtained from the first derivative of the strain profile at that load level multiplied by the elastic modulus, E_f and the diameter of the FRP bar, d.

And from the definition of slip:

$$S_l = u_f - u_e - u_c \tag{4.7}$$

Where u_f, u_e and u_c is the displacement of FRP bar, epoxy and concrete respectively, since

$$\varepsilon_f = \frac{du_f}{dx}, \varepsilon_e = \frac{du_e}{dx} \text{ and } \varepsilon_c = \frac{du_c}{dx} \tag{4.8}$$

and by assuming that the epoxy strain, ε_e and concrete, ε_c are very small and may be considered negligible when compared to that of the FRP, ε_f, which can be calculated as follows:

$$\varepsilon_f = \frac{dS_l}{dx} \tag{4.9}$$

$$S_l(x) = S_l(0) + \int_0^x \varepsilon_f(x)dx \tag{4.10}$$

$$S_l(x_i) = S_l(0) + \sum_{x=0}^{x=l_b} \varepsilon_f(x) \tag{4.11}$$

where $S_l(0)$ is the free-end slip of the FRP bar. Therefore, the slip profile for each given load level can be obtained by integrating the strain versus location curve and adding the free-end slip at that load level.

Figures 4.25 and 4.26 show the strain distribution along the bar bonded length for specimens C/9.5-E-1.50-48 and G/12.7-E-2.0-36. Each curve corresponded to a specific load represented as a percent of the ultimate load. The X-axis started from the free end to the loaded end along the bonded length of the bar. The strain distribution along the bond length, highly nonlinear at lower load levels, gradually approached an almost linear shape as the load increased. This means that, as the load increased, redistributions of the bond stress along the bond length occurred as a result of the changes in the state of the bond. Micro–cracking at the bar–epoxy interface and the consequent slip of the FRP tend to produce a more even distribution of the bond stress.

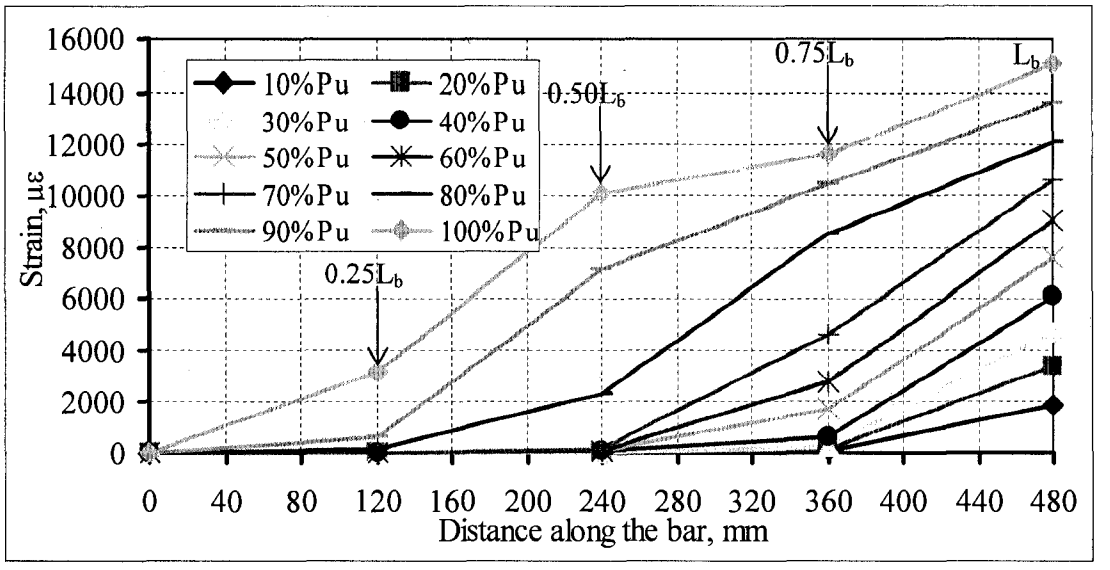

Fig. 4.25. Strain distribution along the bar bonded length for specimen C/9.5-E-1.50-48

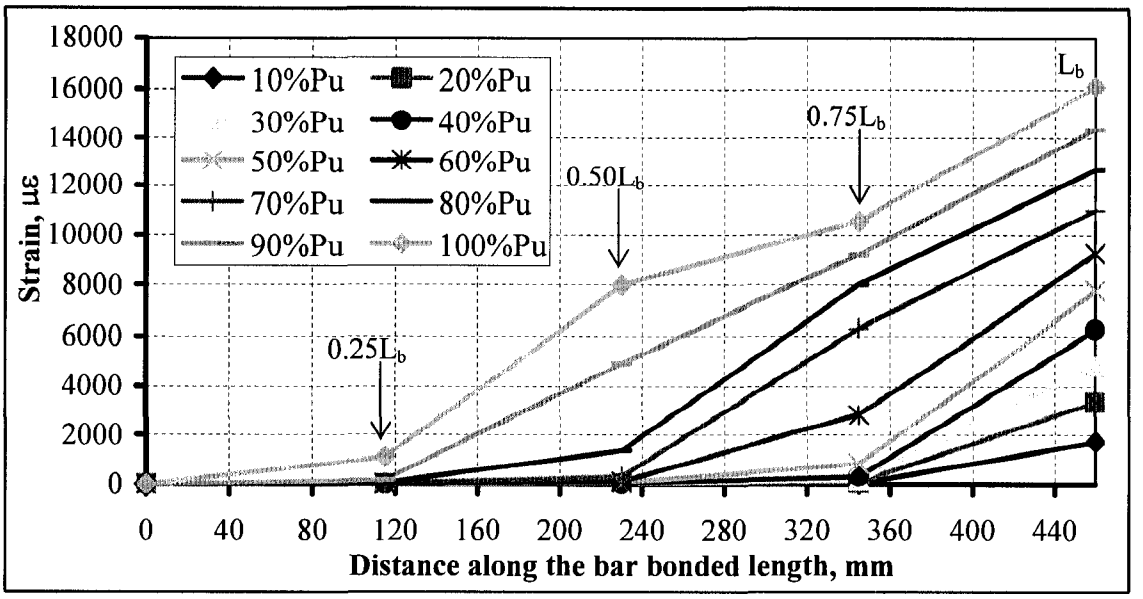

Fig. 4.26. Strain distribution along the bar bonded length for specimen G/12.7-E-2.0-36

Figures 4.27 and 4.28 show the bond stress distribution along the bar bonded length for specimens C/9.5-E-1.50-48 and G/12.7-E-2.0-36 corresponding to a specific load represented as a percent of the ultimate load. At low load levels, the bond stress at the bar free end was close to zero. As the load increases, the peak of the bond stress gradually shifts towards the free end. The presence of more than one peak in the bond stress distributions during the last loading stages is probably related to the presence of transverse concrete cracks which introduce local disturbances to the bond behaviour. As seen from the two figures, the bond stress for the specimens with CFRP are much higher with specimen with GFRP due to the great difference between the axial stiffness (EA) from the carbon bars and glass bars which has an effect on the bond strength of the bar.

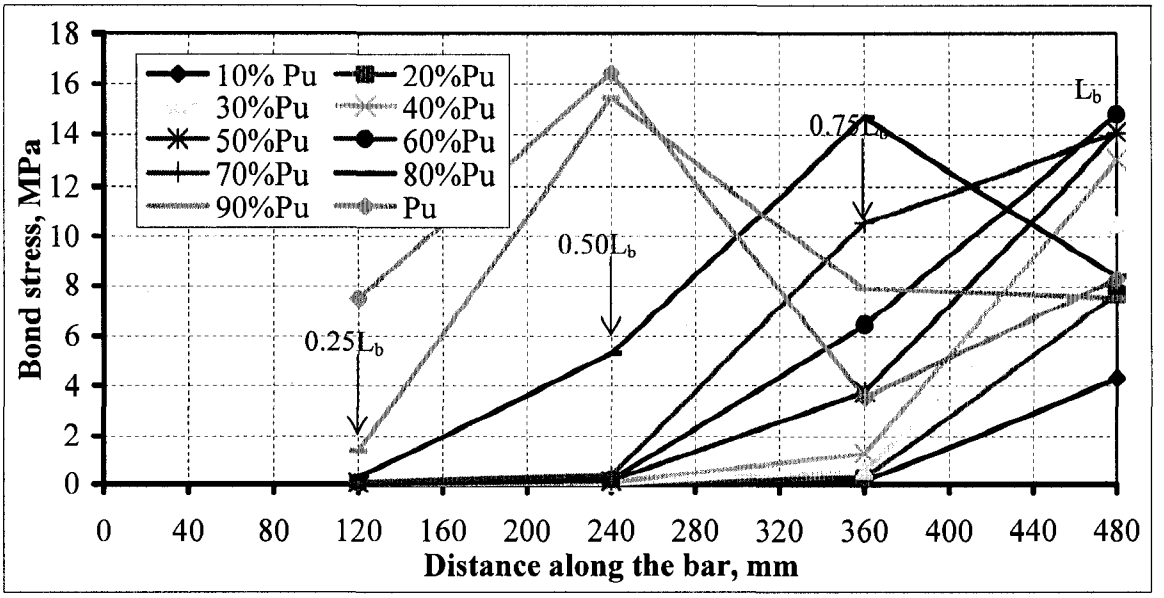

Fig. 4.27. Bond stress distributions along the bar bonded length for specimen C/9.5-E-1.50-48

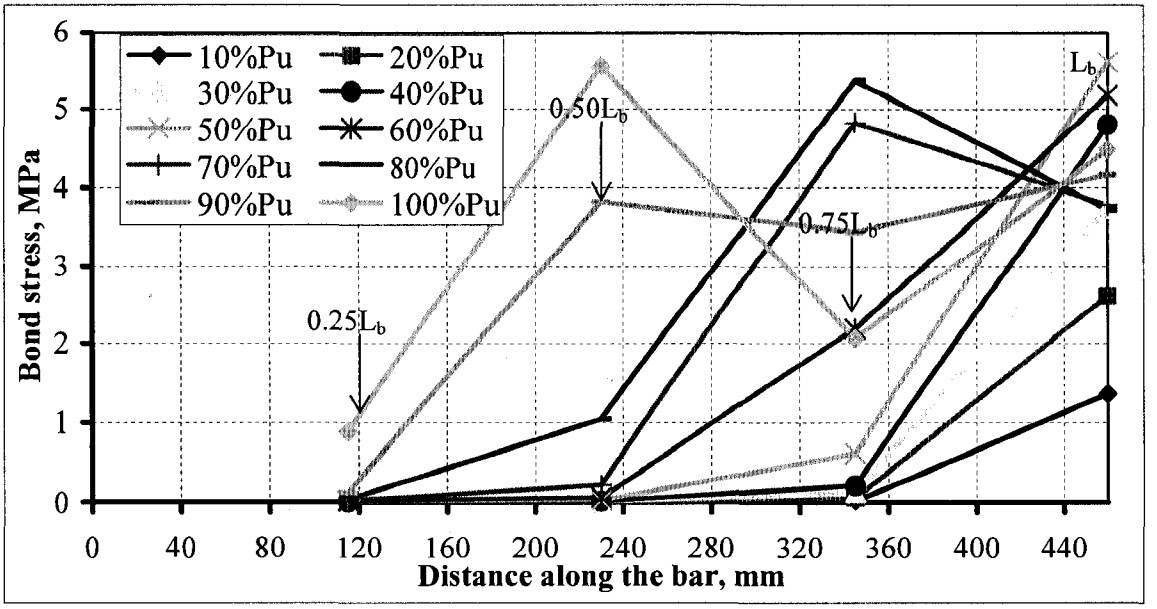

Fig. 4.28. Bond stress distributions along the bar bonded length for specimen G/9.5-E-2.0-36

Slips and bond stresses computed before from equations can be combined together to obtain the local bond-slip curves. The bond stress-slip data plotted at location of each strain gauge are shown in Fig. 4.29 and Fig. 4.30.

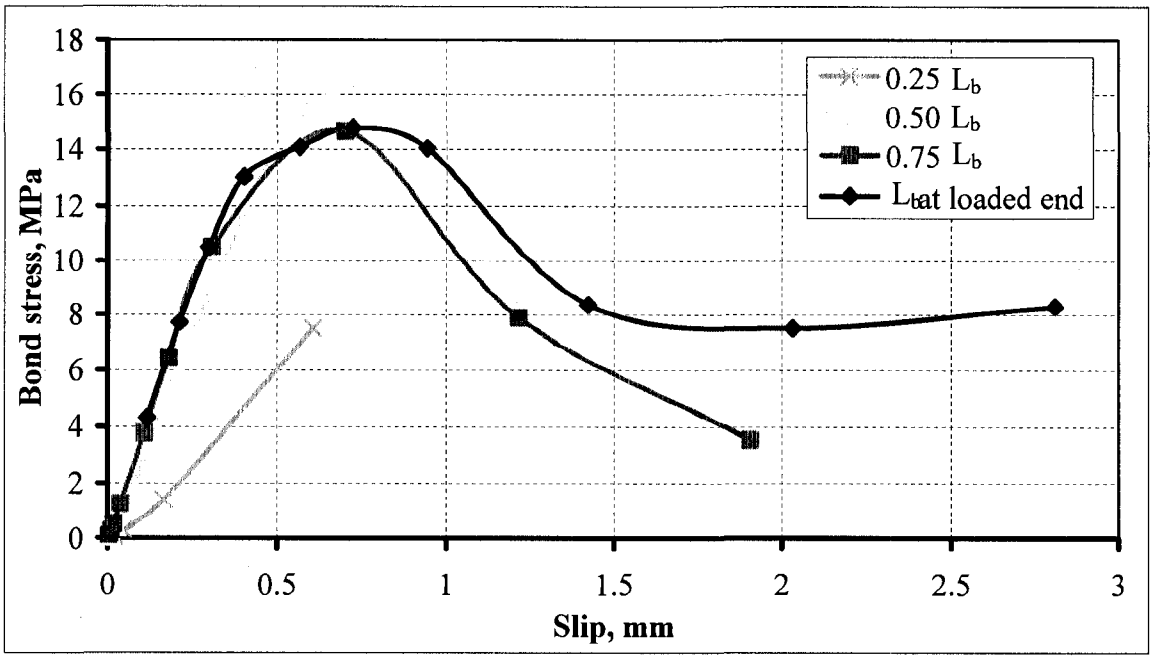

Fig. 4.29. Local bond stress-slip at different locations along the bar bonded length for specimen C/9.5-E-1.50-48

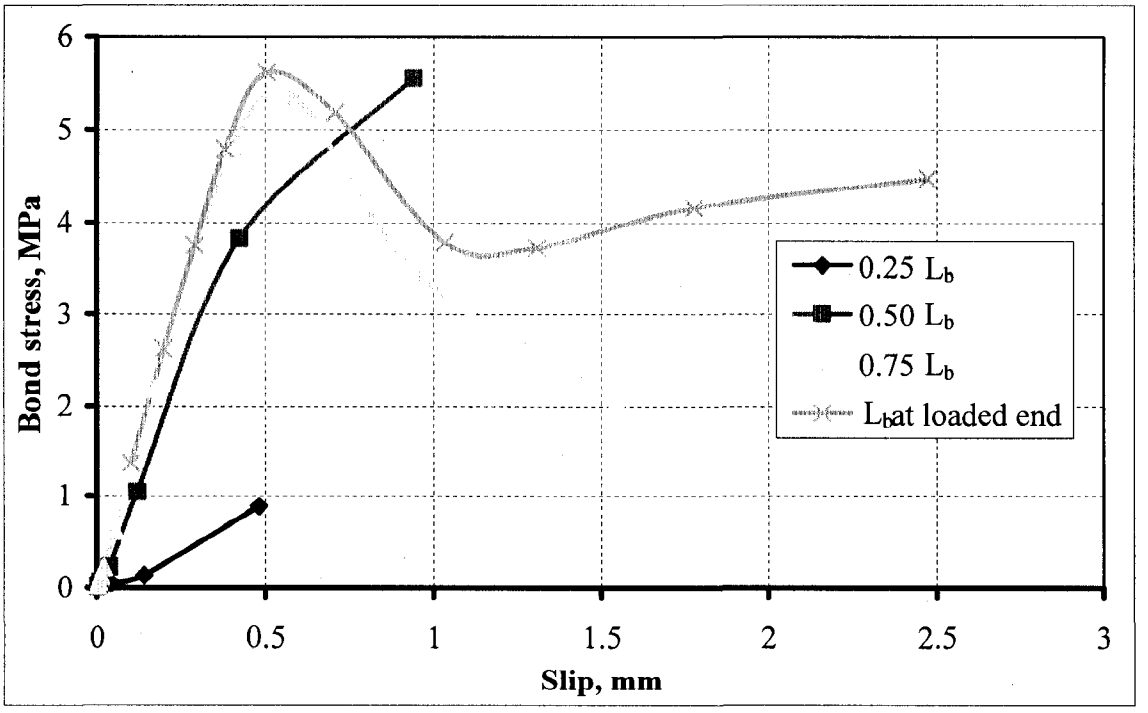

Fig. 4.30. Local bond stress-slip at different locations along the bar bonded length for specimen G/12.7-E-2.0-36

4.5. Nonlinear Regression Analysis

In this section, statistically based analysis is presented to predict the failure load for the pullout specimens with NSM-FRP bar.

A simple regression model or a mathematical equation can be used to set up a simplified model that best fits the experimental data in terms of failure load. One of the tools that can be used in developing such a model is the response surface methodology (RSM) and nonlinear statistical regression analysis. An application of this methodology on two way slabs has been presented by Ebead et al. (2002). A RSM is built up by simulating solutions at systematic points in a design space of various parameters and setting up a model to these points. We aim to use such models as design equations similar to those in the currently available specifications and guidelines.

The DataFit software, Version 8.1.69 is used for the calculations associated with the nonlinear regression analysis (DataFit, 2005). Generally, the goal of the nonlinear regression analysis is to determine the best-fit parameters for a model by minimizing the chosen test function. This function defines the difference between the actual and predicted responses and is given by:

$$x^2 = \sum_{i=1}^{i=N} \left[y_i - y(F_i) \right]^2 \tag{4.12}$$

Where N is the total number of random input data, *yi* is the actual response value (outputs of a particular RSM model) and $y(F_i)$ is the response value computed from the proposed nonlinear regression model.

Nonlinear regression analysis is essential when the response model exhibits a nonlinear dependence on the unknown variables (five variables in this study). Hence, the process of test function minimization is an iterative procedure. This iterative process begins with some initial estimates and incorporates algorithms to improve the estimates in an iterative manner. The new estimates then became a starting point for the next iteration. These iterations continued until the values of the test function converge (Oakdale-Engineering, 2005). Below, the nonlinear regression model (referred to as the proposed design equations) is presented.

In the following sections, the five variables used to perform the statistical analyses are elaborated upon. Then the RSM models for the five different responses are presented and considered in the RSM models. The design equation for the pullout load is predicted in term of axial stiffness of FRP bar, tensile strength and modulus of elasticity of adhesive, groove width and bonded length.

$$P_u = -1.25(EA)_{frp} + 1.7 f_{ta} + 0.0028 E_a - 1.52 dg + 0.137 * Lb \quad (4.13)$$

$R^2 = 0.85$

Where, P_u, is the pullout load at failure in kN, EA is the axial stiffness of the FRP bar in MN, f_{ta} is the tensile strength of the adhesive in MPa, E_a is the modulus of elasticity of adhesive in GPa, dg is the width of the groove in mm, and L_b is the bond length of FRP bar in mm.

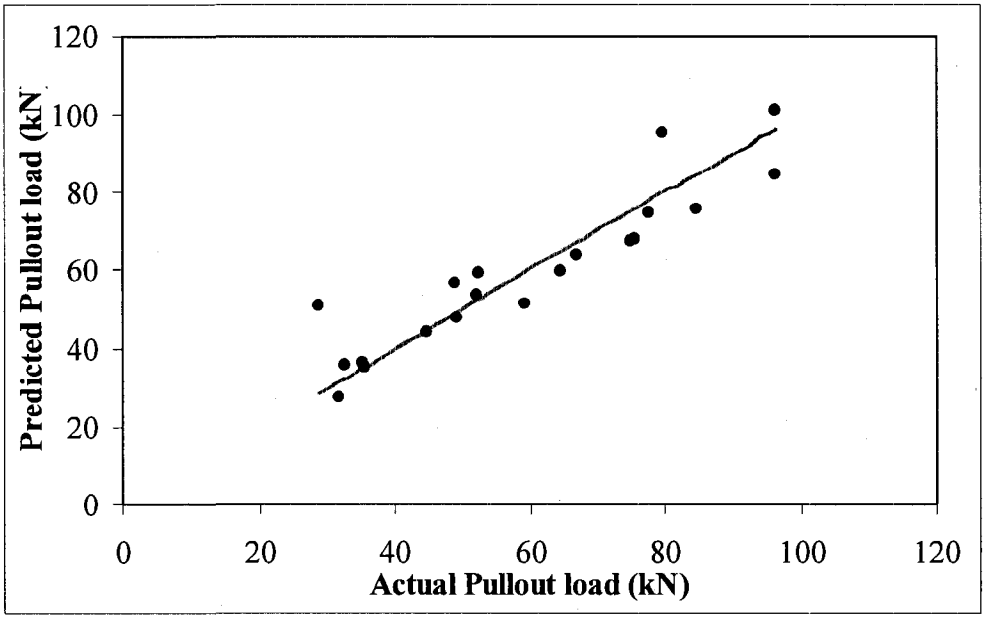

Fig. 4.31. Comparisons between load predictions from the regression models and the experimental results

Figure 4.31 shows the comparison between the predicted pullout load using the proposed model (equation 4.14) and that measured experimentally. In this figure, the R^2 value is 0.85 indicating good predicated capability of the proposed equation. Accordingly this equation can be employed to predict the ultimate capacity of pullout test specimens or in

other applications where the force transfer from the FRP to the concrete element through direct shear.

4.6. Summary

The following bullets summarieze phase one of the experimental program, which is the bond characteristics of NSM-FRP bars through pullout testing.

- The adopted system, FRP V-ROD bars and Hilti adhesives, seems to perform well in the NSM strengthening system.
- The adopted test methods seem to be efficient and produced consistent results.
- The main failure for most of the tested specimens with epoxy adhesive was concrete shear tension failure (semi-cone failure) accompanied with or without epoxy cracking (splitting). Specimens with longer bonded length failed by bar rapture.
- The main mode of failure for specimens with cement adhesive was at the concrete-cement interface.
- The failure load of specimens with cement adhesive was about 40 to 56% compared to the specimens with epoxy adhesive due to the smooth surface of the sides of the groove.
- Increasing the bonded length increased the pullout load and the bond stress was decreased due to longer length distribution.
- Increasing the groove size for specimens with epoxy adhesive did not have a significant influence on the pullout load. However, the factor that controlled failure was the tensile strength of concrete.
- Increasing the groove size for specimens with cement adhesive decreased the failure load, this was due to shrinkage of cement of bigger groove size. It is not recommended to use groove size equal to two times the bar diameter for cement adhesive.
- The percent of reduction for the conditioned specimens with epoxy adhesive varied between 8 to 14 % than the reference specimens.

- The failure load for the conditioned specimens with cement adhesive was about 30 to 45% less than that of reference specimens.
- Due to temperature change during freeze- thaw cycling, hair cracks developed in the adhesive materials. Therefore, these materials will govern the failure mode of the specimens as well as the slip performance.
- The change of strain due to freeze- thaw cycling was around 70 to 90 micro-strain in case of epoxy adhesive and around 120 to 170 micro-strains in case of cement adhesive.
- The change in strain increased with the increase in bonded length. Changing the groove width had no effect on the change of strain with temperature.
- The change in the results of the conditioned specimens compared to those of the reference ones were due to the difference in the coefficient of thermal expansion between the adhesive materials and the concrete.

Chapter 5 - Flexural Strengthening: Analysis and Discussion of Test Results

5.1. General

This chapter presents the experimental results for the flexural strengthening of 20 full-scale reinforced concrete beams. The beams were strengthened using V-ROD bars and Hilti epoxy. The dimensions of the beams are 3010 mm long, 200 mm wide and 300 mm deep. The 20 beams, strengthened using the NSM method, were divided into three series. Series A consisted of 5 beams, series B consisted of 3 beams and series C consisted of 12 beams. In each series, the behaviour of the strengthened beams will be discussed through the analysis of yield and failure loads, deflections, strains in concrete, steel and FRP, and modes of failure. In addition, the influence of different parameters such as bonded length, NSM-FRP diameter, NSM-FRP type, groove size and steel ratio on the flexural behaviour will be discussed.

5.2. Flexural Strengthening

During monotonic loading, the load deflection behaviour of a reinforced concrete beam consists of three stages: pre-cracking stage, pre-yielding and post-yielding till failure. These stages are identified by the cracking and yielding load. A beam strengthened with an FRP bar exhibits similar behaviour to the un-strengthened one but with higher cracking, yielding and ultimate loads. Figure 5.1 shows the effect of strengthening on load-deflection behaviour of reinforced concrete beams at different stages of loading.

The cracking load (P_{cr}) is defined as the load at which the tensile stress at the bottom of the beam is greater than the concrete tensile strength. This leads to the formation of the flexural cracks and reduction in the beam flexural stiffness. The yield load (P_y) is defined as the load at which the tensile steel yields. The ultimate load (P_u) is defined as the load at which the load drops due to beam failure whether it is concrete crushing, FRP rupture or slippage or concrete cover splitting at bottom reinforcement layer. The transition loads between these critical stages depends on many factors such as amount and grade of steel and FRP reinforcement, concrete strength and other parameters.

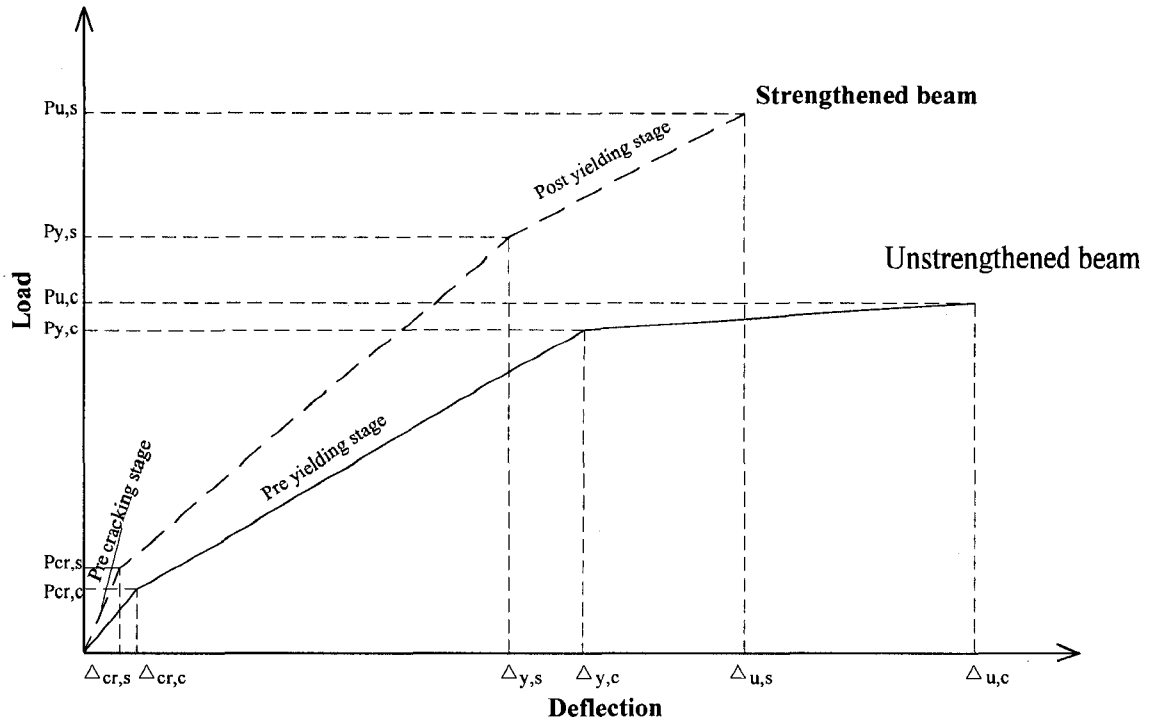

Fig. 5.1. Load-deflection behaviour for a strengthened and unstrengthened beam

Where:

$P_{cr,c}$: cracking load for a control beam.

$\Delta_{cr,c}$: deflection corresponding to the cracking load for a control beam.

$P_{cr,s}$: cracking load for a strengthened beam.

$\Delta_{cr,s}$: deflection corresponding to the cracking load for a strengthened beam.

$P_{y,c}$: yielding load for control beam.

$\Delta_{y,c}$: deflection corresponding to the yielding load for a control beam.

$P_{y,s}$: yielding load for a strengthened beam.

$\Delta_{y,s}$: deflection corresponding to the yielding load for a strengthened beam.

$P_{u,c}$: ultimate load for a control beam.

$\Delta_{u,c}$: deflection corresponding to the ultimate load for a control beam.

$P_{u,s}$: ultimate load for a strengthened beam.

$\Delta_{u,s}$: deflection corresponding to the ultimate load for a strengthened beam.

5.2.1. Series A

A total of five beams with a steel reinforcement ratio of 1.60% were tested in this series. One beam, A0, was tested as a control specimen. Four beams were strengthened using one 9.5 mm NSM-CFRP bar with bonded lengths of 12, 18, 24 and 48 times the bar diameter (d) in a square groove with a side length equal to 2.0d. Complete details of the tested specimens were given in (section 3.4.1). Table 5.1 summarizes the yield and ultimate loads, deflection, and percentage of increase in yield and ultimate loads. In addition, NSM-FRP debonding strains, ductility index and mode of failure for series A were also listed in the Table.

The control specimen, A0, was tested to obtain the capacity of the unstrengthened beam for series A. The load-deflection relationship for A0 is shown in Fig. 5.2. Beam A0 yielded at a load of 203.82 kN and failed at ultimate load of 232.72 kN. The mode of failure for A0 was steel yielding followed by concrete crushing (Fig. 5.5). Only 14.18% increase in the post yielding strength (the difference between ultimate and yielding load, $P_{u,c}$ - $P_{y,c}$) was observed.

Beams A1 to A4 failed by debonding in the form of concrete cover splitting starting at the cut-off points of the NSM-FRP bar as shown in Fig. 5.5. The maximum increase in the ultimate load was 9% for beam A4 with the maximum bonded length of 48d. However, there was no increase in ultimate load for the other beams with lesser bonded length. This indicated that the bonded length used was insufficient to develop the required strength for the beam. In addition to that, the percentage of steel reinforcement in this series was high (1.60%) and this led to increase in the yielding load. The difference between the yielding and the ultimate load was so small to allow the FRP to develop stresses more than those in the steel reinforcement which led to insignificant increase in the ultimate load for the strengthened beams over the unstrengthened one.

In spite of that there was no increase in the ultimate load; there was a decrease in the deflection at both yielding and failure. This indicated that strengthening a beam increases its stiffness even if there is no increase in its ultimate capacity.

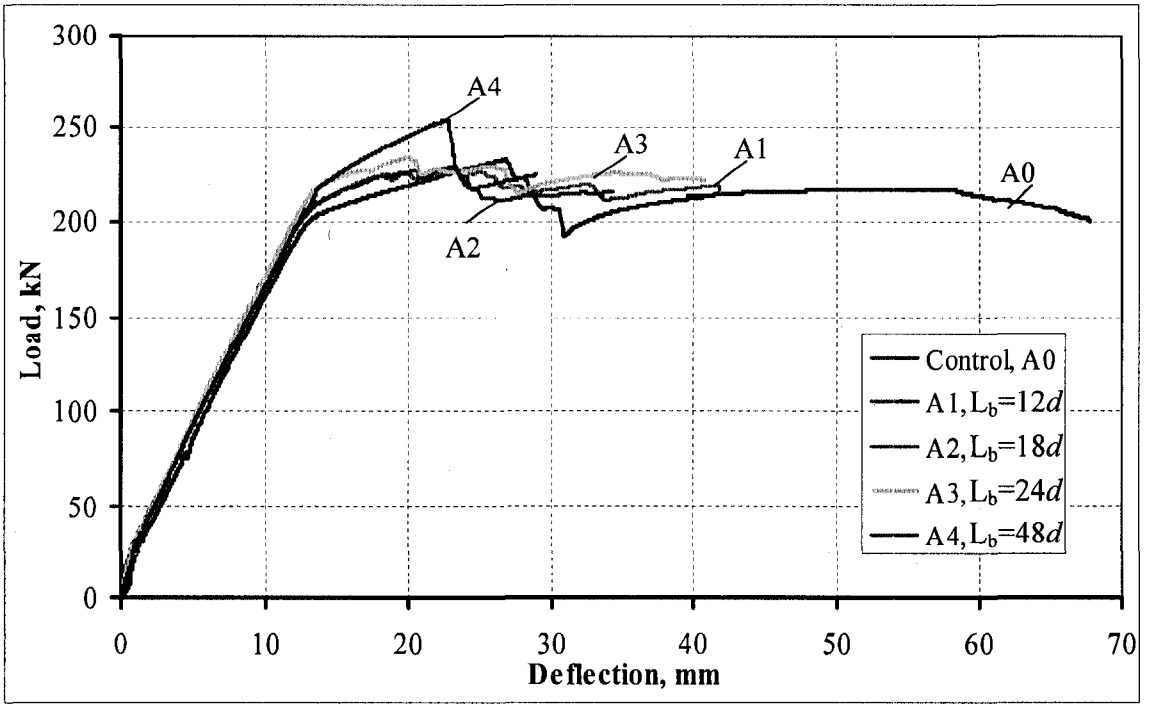

Fig. 5.2. Load-deflection curves for series A

Strain gauges are bonded at different locations on concrete, steel and NSM-FRP on each beam, as described earlier in section 3.3.5.

Figure 5.3 shows the load-strain relationship measured at the midspan of the beam for both concrete and reinforcing steel. Figure 5.4 shows the load-strain curve for the CFRP bar measured at midspan for the strengthened beams. This figure indicated that the beam strengthened with 48*d* showed the highest strain value, which corresponded to 45% of the FRP ultimate tensile strain. The drop in the strain for beams A1 and A2 with the smallest bonded length 12*d* and 18*d* was maybe due to cracks that occurred close to the strain gauges at late stages of loading.

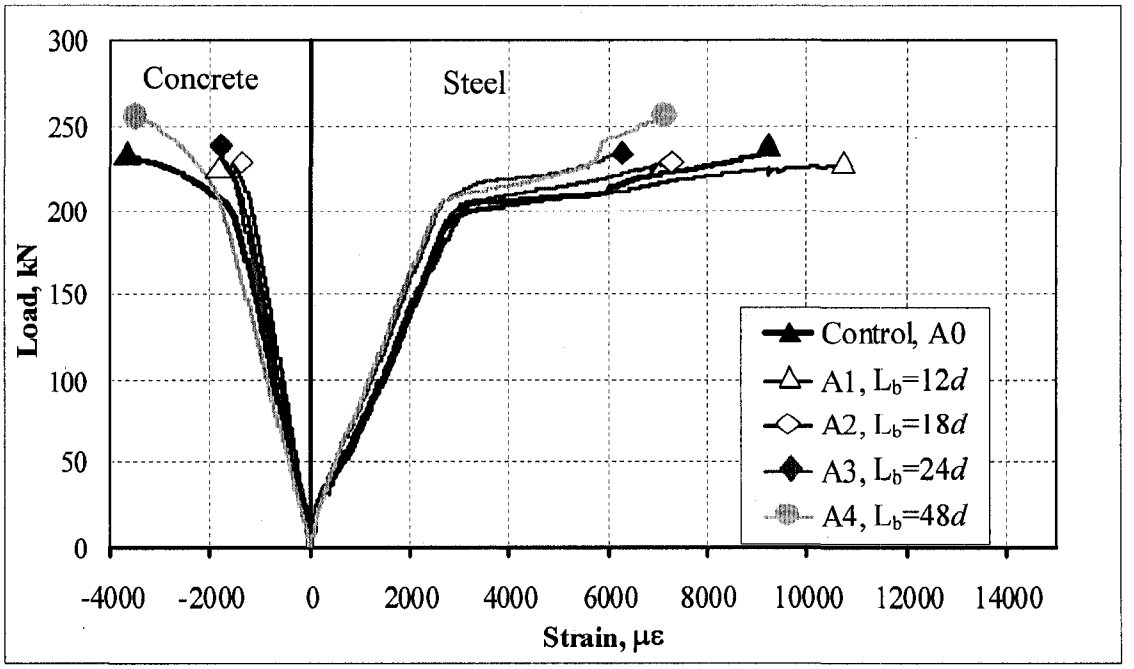

Fig. 5.3. Load-strain relationship for concrete and steel for beams of series A

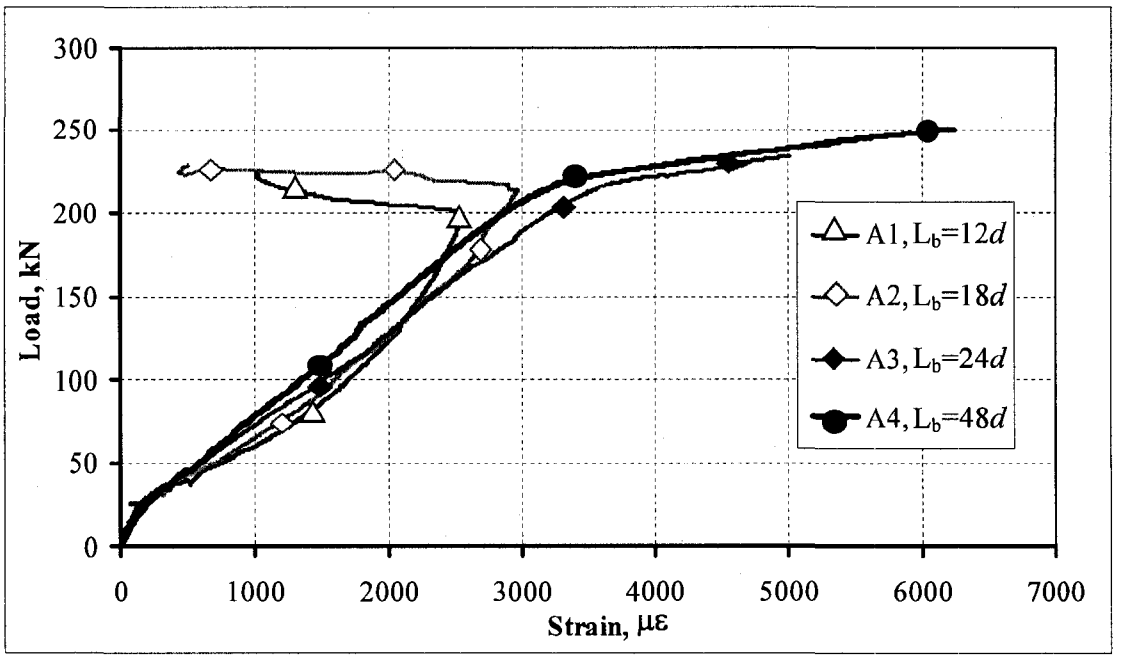

Fig. 5.4. Load-CFRP tensile strain at mid span for beams of series A

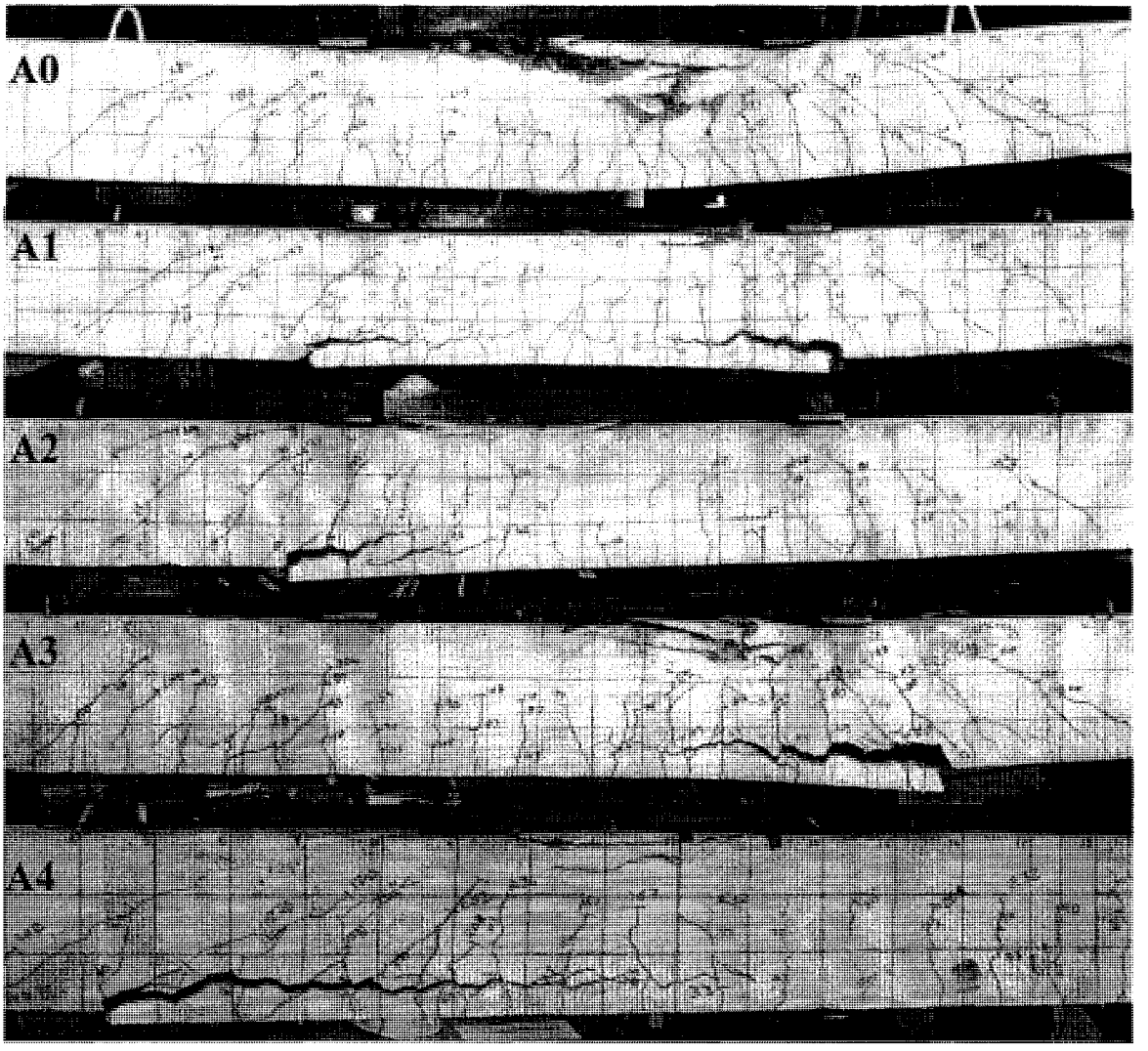

Fig. 5.5. Cracks pattern and modes of failure for beams of series A

Table 5.1 Test results for beams of series A

Specimens Name	Bonded length L_b	Yield load P_y, kN	Yield deflection, Δ_y, mm	Yield load increase %	Failure load P_u, kN	Ultimate deflection, Δ_u, mm	NSM-FRP debonding strain, με	Ductility Index	Failure mode	Ultimate capacity increase %
A0	—	204	13.71	—	233	26.75	—	1.95	C	—
A1	12*d*	206	12.90	1.23	227	23.96	2,534	1.86	Cs	-2.68
A2	18*d*	213	14.46	4.57	229	22.97	3,270	1.59	Cs	-1.83
A3	24*d*	222	14.38	8.70	234	19.95	5,065	1.39	Cs	0.4
A4	48*d*	220	14.1	7.70	254	22.63	6,244	1.6	Cs	9.02

Note: d is the diameter of the NSM-FRP bar, C is concrete crushing and Cs is concrete cover splitting

5.2.2. Series B

A total of three beams with steel reinforcement ratio of 0.80% were tested in this series. One beam, B0, was tested as a control beam. Two beams were strengthened using one 9.5 mm CFRP bar with bonded length 24 and 48 times the bar diameter (d) in a square groove with a side length equal to 2.0d. Complete details of the tested beams were given in section 3.4.1. Table 5.2 summarizes the yield and ultimate loads, deflection, and percentage of increase in yield and ultimate loads. In addition, NSM-FRP debonding strains, ductility index and mode of failure for series B were also listed in the Table.

The control specimen B0, was tested to obtain the capacity of the unstrengthened beam for series B. Beam B0 failed by steel yielding followed by concrete crushing at a load of 130.14 kN as shown in Fig. 5.9. Beams B1 and B2 failed by debonding in the form of concrete cover splitting as shown from Fig. 5.10 and Fig. 5.11 Beam B1 didn't give any increase in the ultimate load but it gave 15.60% increase in the yielding load. However, beam B2 with a bonded length of 48d gave 19 and 19% increase in the yield and ultimate load respectively. Beam B2 with a bonded length 48d gave the best results with respect to the ultimate load for this series. After debonding of the NSM-CFRP bar, the load dropped to act similar to the control beam B0.

The presence of the NSM-CFRP bar eliminated the flattening of the load deflection curve that was clear on the control specimen. Prior to yielding of the steel reinforcement the stiffness for all the strengthened beams was almost the same.

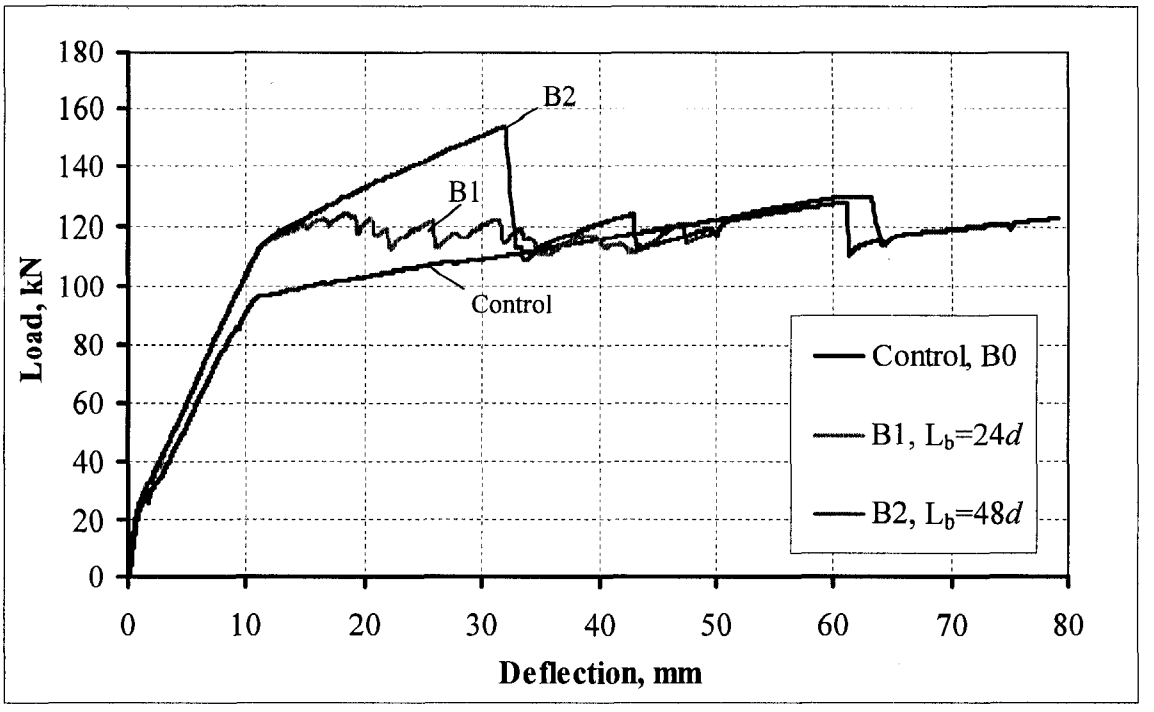

Fig. 5.6. Load deflection curve for series B

Figure 5.7 shows the load versus concrete and steel midspan strains relationship for beams of series B. It is clear from the figure that before yielding the behaviour was the same for the strengthened beams and the un-strengthened one. After yielding, beams B1 and B2 behaved identical till failure of B1 with the shorter bonded length at lower load and strain values than those of B2 of the longer bonded length.

As shown in Fig. 5.8, the measured NSM-CFRP strains at failure for beam B1 and B2 were about 45 and 85% of the rupture strains of the CFRP bar, respectively.

The ultimate strain measured for the CFRP bar of beam B2 was 94% more than that of B1. The reason for that decrease in CFRP strain of B1 is the insufficient bonded length which results to early debonding of CFRP reinforcement.

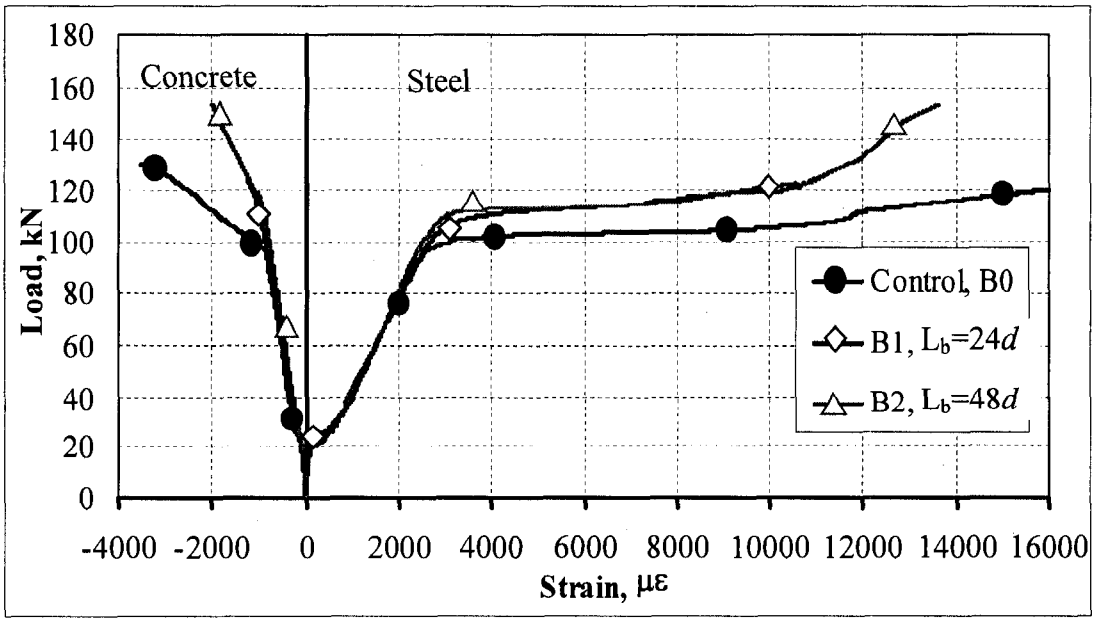

Fig. 5.7. Load-strain relationship for concrete and steel for beams of series B

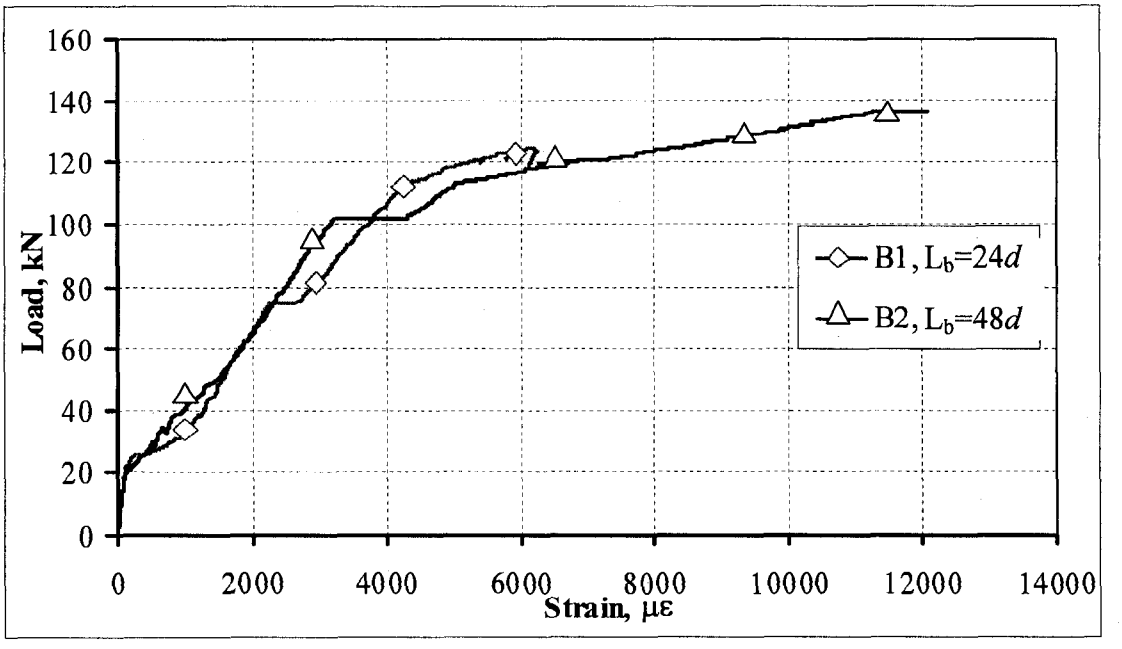

Fig. 5.8. Load-CFRP tensile strain at mid span for beams of series B

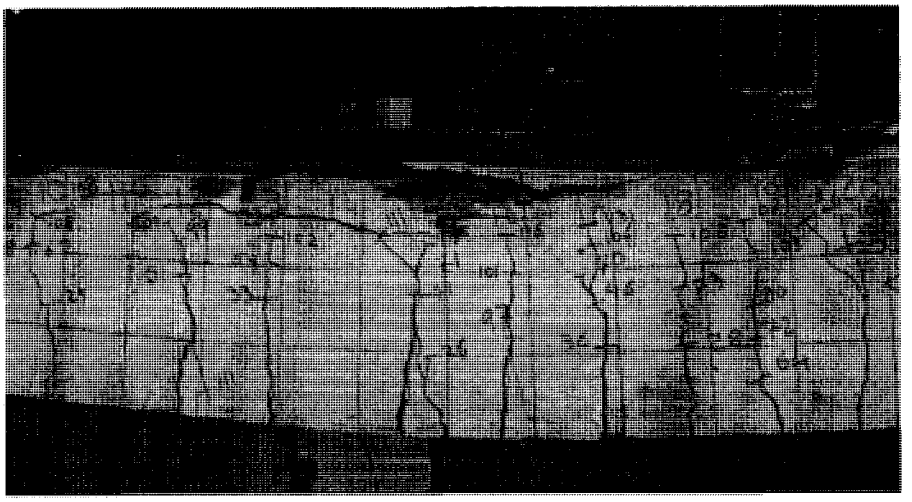

Fig. 5.9. Compression failure for B0

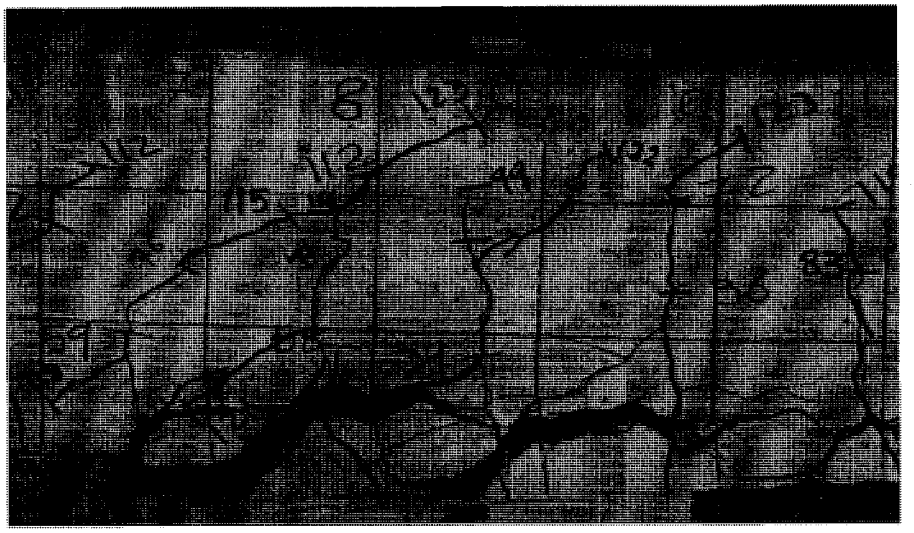

Fig. 5.10. Concrete cover split for B1

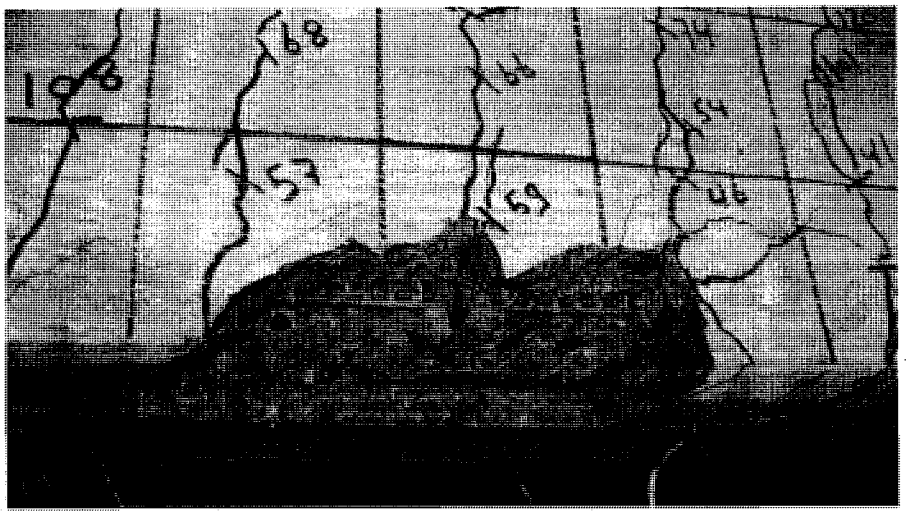

Fig. 5.11. Concrete cover split for B2

Table 5.2 Test results for series B

Specimens Name	Bonded length L_b	Yield load Py, kN	Yield deflection, Δ_y, mm	Yield load increase %	Failure load P_u, kN	Ultimate deflection, Δ_u, mm	NSM-FRP debonding strain, με	Ductility Index	Failure mode	Ultimate capacity increase %
B0	—	96	10.98	—	130	62.43	—	5.69	C	—
B1	24*d*	114	11.48	15.60	125	18.64	6,252	1.62	Cs	-4.37
B2	48*d*	115	11.52	19.02	154	31.34	12,104	2.78	Cs	18.17

Note: *d* is the diameter of the NSM-FRP bar, C is concrete crushing and Cs is concrete cover splitting

5.2.3. Series C

A total of twelve beams with steel reinforcement ratio of 0.40 % were tested in this series. One beam was tested as a control specimen C0. Beams C1, C2, C3 and C4 were strengthened with one 9.5 mm diameter NSM-CFRP bar with 12*d*, 24*d*, 48*d* and 60*d* bonded length respectively having a square groove with a side length of 2.0 times the bar diameter. Beams C5, C6 and C7 were strengthened with one 9.5 mm diameter CFRP bar with 24d, 48d and 60d bonded length having a square groove equal to 1.50 times the bar diameter. Beams C8 and C9 were strengthened with one 12.7 mm diameter CFRP bar with 24*d* and 48*d* bonded length respectively having a square groove equal to 2.0 times the bar diameter. Beams C10 and C11 were strengthened with one 12.7 mm diameter GFRP bar with 24*d* and 48*d* bonded length respectively having a square groove equal to 2.0 times the bar diameter. Complete details of the tested beams were given in section 3.4.1.

Table 5.3 summarizes the tested results for series C. Fig. 5.12 shows the load deflection behaviour for beams C1, C2, C3 and C4. The figure clearly indicated that the strength, stiffness and ductility of the strengthened beams were greatly improved due to the addition of the CFRP reinforcement.

Before cracking all the strengthened beams exhibited similar bending behaviour to the unstrengthened beams. This means that the NSM-FRP reinforcement had insignificant contribution to the increase of stiffness and strength in the elastic stage. However, after cracking, the bending stiffness and strength of the strengthened specimens were seen to increase significantly until failure compared to the unstrengthened one. It can be also stated that after cracking, a nonlinear behaviour was observed up to failure. The stiffness for the strengthened beams was higher due to the addition of the NSM-CFRP bar, as the CFRP bar provides constrains to the opening of the cracks and reduce the deflection (increasing the moment of inertia of the cracked section).

After debonding of the NSM-CFRP bar, the load dropped following the curve of the control beam C0.

The control beam C0 failed due to crushing of concrete at load of 54.95 kN. Beam C1 with the smallest bonded length, 12*d* failed at a load of 66.89 kN showing an increase of

21.73% in the ultimate load. Beams C2, C3 and C4 failed at loads of 72.64, 93.87 and 96.37 kN with an increase in the ultimate load of about 32, 71 and 75%, respectively.

Increasing the bonded length from 24*d* to 48*d* doubled the percentage of increase in the ultimate load from 32% to 71%. While increasing the bonded length from 48*d* to 60*d* gave only a 5% increase in the ultimate capacity.

It can be concluded that as the bonded length increases the ultimate load increases up to a certain limit beyond this limit any increase in the bonded length provide a small increase in the ultimate capacity. However, this statement can be changed depending on the internal steel reinforcement ratio and the diameter of NSM-FRP bar.

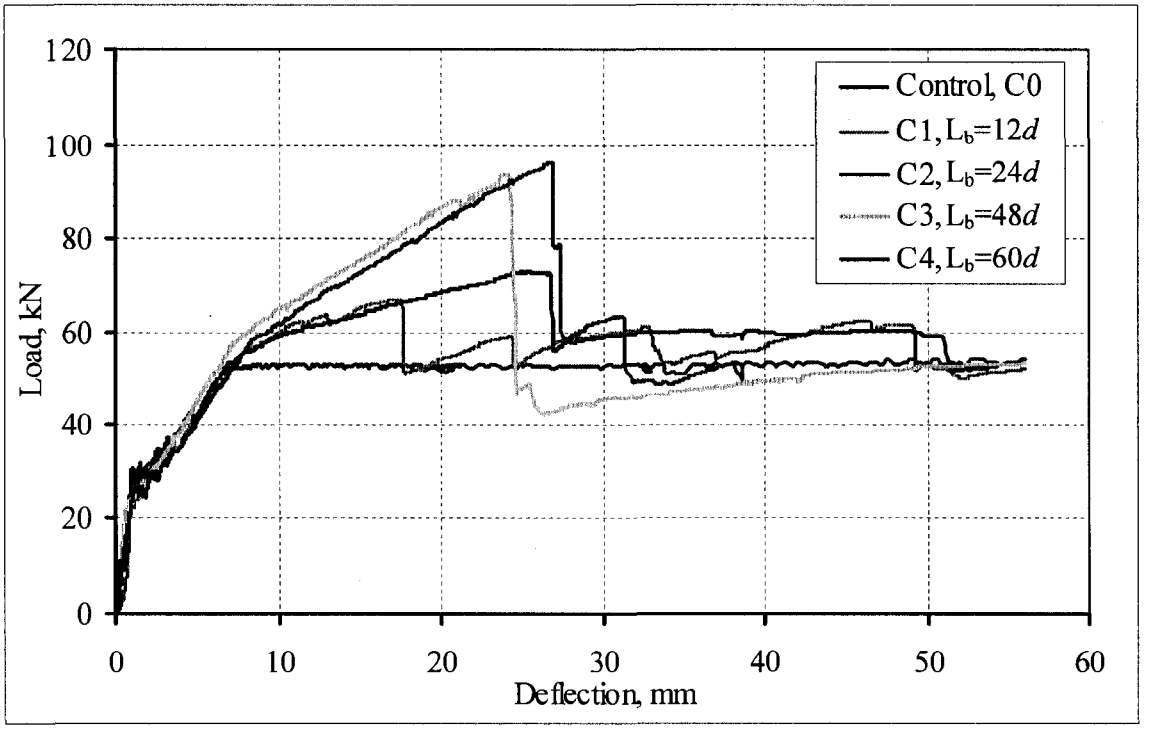

Fig. 5.12. Load-deflection curve for beams C1, C2, C3 and C4

The NSM-FRP strain distribution was monitored during testing using strain gauges located at different positions as described in chapter 3. The maximum NSM-CFRP tensile strains at midspan are shown in Fig. 5.13. Full composite action was achieved between the NSM-FRP and the concrete up to failure. This was proved by the increase in the FRP tensile strain with the increase in load up to failure. Identical tensile strains were observed for beams C3 and C4. The maximum measured CFRP strain was 8594 micro-

strains, which is 61% of the ultimate strain of the NSM-CFRP bar. The NSM-FRP strains for these beams ranged from 17.3 to 61.4% of the rupture strain.

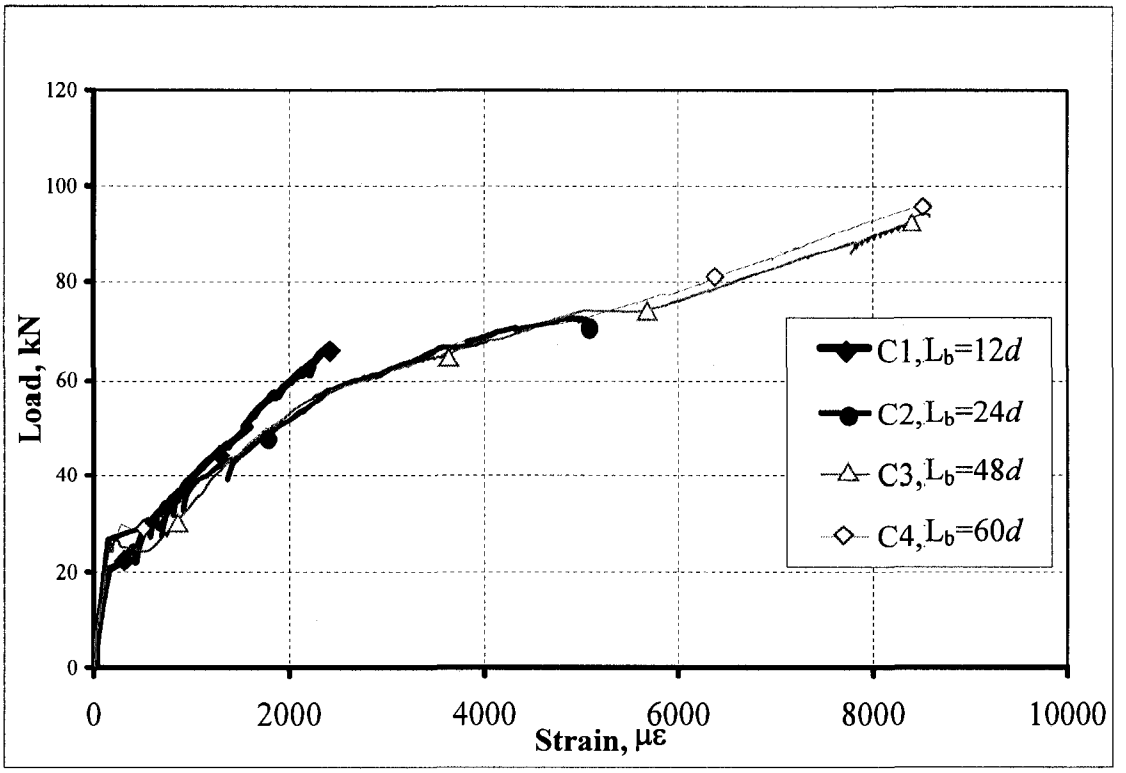

Fig. 5.13. Mid-span NSM-CFRP strains for beams C1, C2, C3 and C4

The groove dimension for beams C5, C6 and C7 was taken equal to 1.5*d* instead of groove dimension equal to 2.0*d* for all other beams of this series. The mode of failure for beams C5 and C7 was concrete cover splitting starting at the cut-off points of the CFRP bar. While for beams C6 with bonded length of 48*d* longitudinal splitting cracks started in the epoxy before concrete cover splitting. Beams C5, C6 and C7 failed at an ultimate load of 88, 90 and 102 kN, respectively.

Beam C5 with groove size 1.5*d* showed higher ultimate load with 21% more than that of beam C2 with groove size 2.0*d*; both have the same bonded length of 24*d*. Beam C7 with groove size 1.5*d* gave higher ultimate load with about 6% more than that of beam C4 with groove size 2.0*d*; both have the same bonded length of 60*d*. Beams C6 and C3 gave different results, the ultimate load for beam C6 decreased by about 4% compared to

Beam C3. This was due the failure of the epoxy layer before reaching the expected ultimate load as shown in Fig. 5.14. The failure of the epoxy layer could happen due to many reasons such as the presence of dust in a part of the groove during apply the epoxy layer or weakness of a part of the concrete layer adjacent to epoxy layer.

The stiffness of beams with bonded length $60d$ is greater for beams with groove size $2.0d$ than that of beams with groove size $1.5d$ as shown in Fig. 5.15. In general, if the bonded length is enough beams with groove size $2.0d$ can contain epoxy volume more than that of groove size $1.5d$. So its tensile strength is higher. This is only valid for longer bonded length ($48d$ or more).

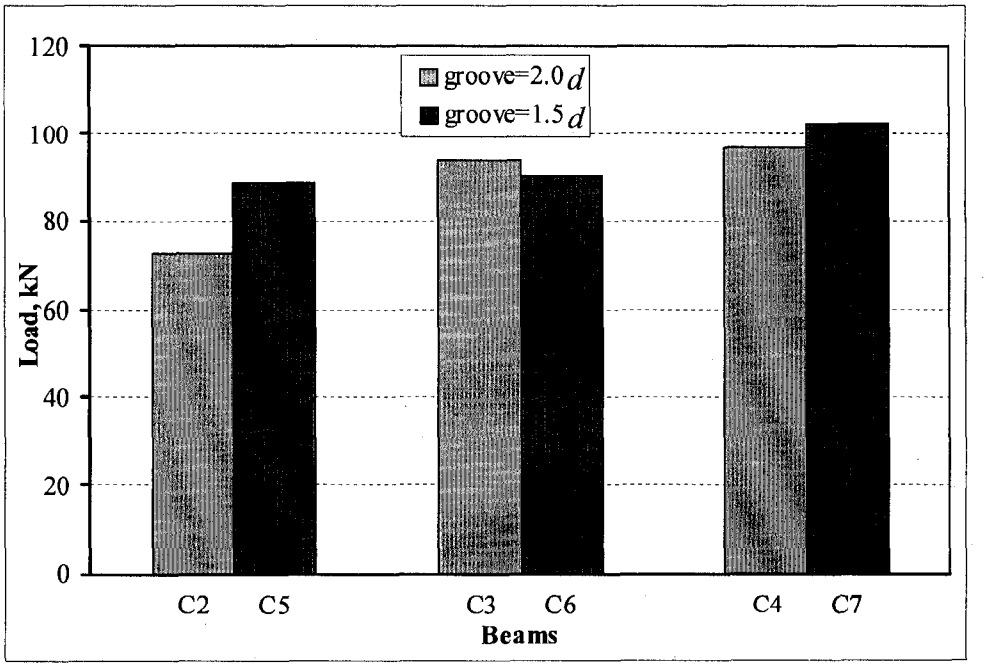

Fig. 5.14. Failure load for specimens with groove size $1.5d$ and $2.0d$

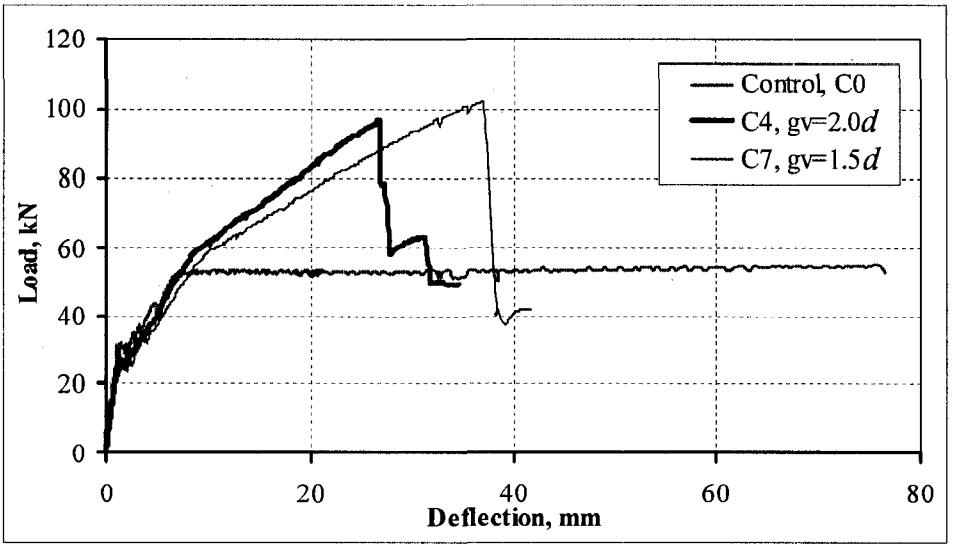

Fig. 5.15. Load-deflection curves for beams C4 and C7 with bonded length 60*d*

Two beams, C8 and C9 were tested with 12.7-mm diameter CFRP bars having bonded lengths of 24*d* and 48*d*, respectively. They failed at loads of 66.51 and 108.53 kN providing an increase in the ultimate capacity corresponding to 21 and 97 % over the unstrengthened beam, respectively. Beams C8 and C9 failed by debonding in the form of concrete cover splitting.

The NSM-FRP strains for beams C8 and C9 were very low compared to the other beams of series C.

Fig. 5.16Figures 5.16 and 5.17 show the NSM-CFRP strain distribution for beams C8 and C9. Beams C8 failed at very low strain values compared to C9 due to the insufficient bonded length, 24*d*, used for beam C8.

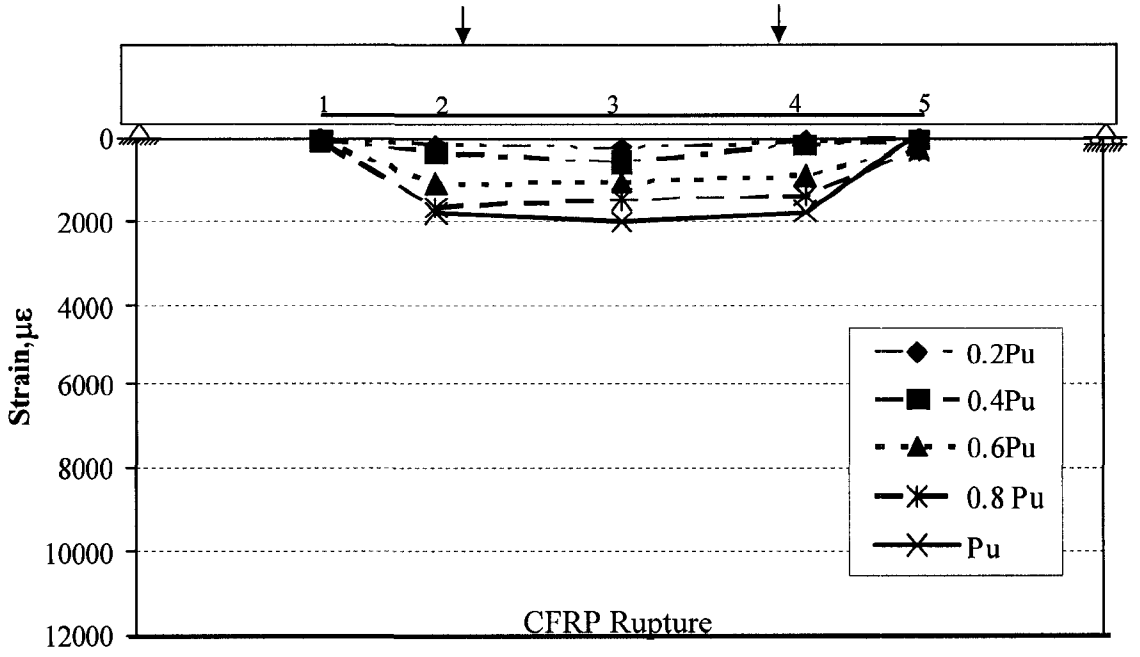

Fig. 5.16. NSM-FRP strain distribution for beam C8

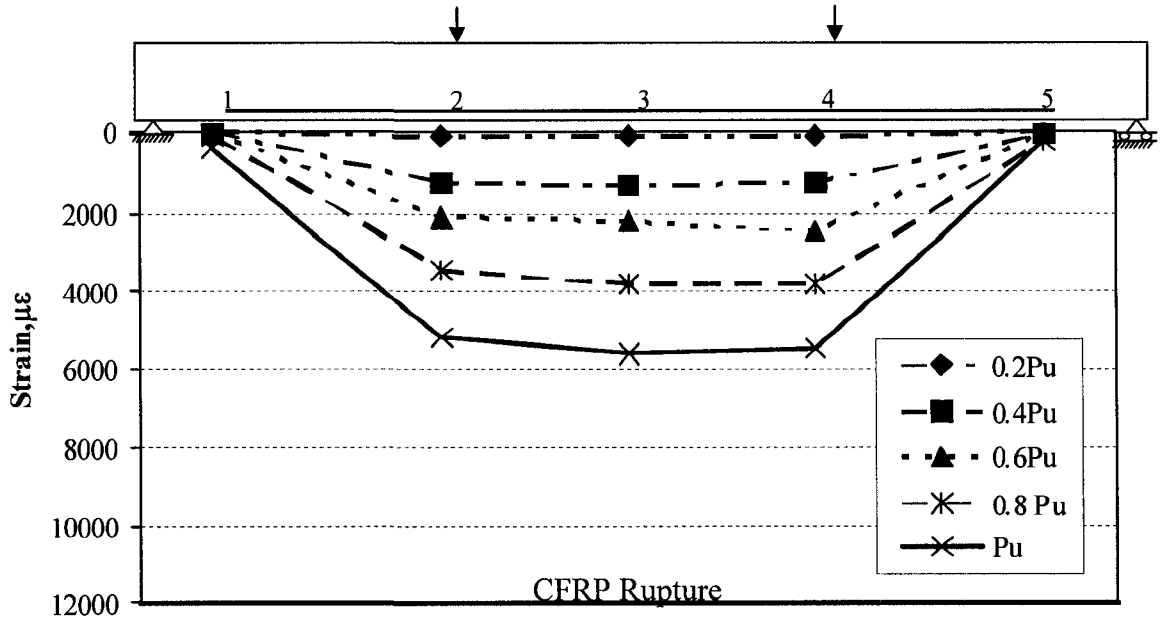

Fig. 5.17. NSM-FRP strain distribution for beam C9

Two beams, C10 and C11, were tested using 12.7-mm diameter GFRP bars having bonded lengths of 24*d* and 48*d*, respectively. The beams failed at loads of 71 and 112 kN, respectively, providing an increase in the ultimate load corresponding to 29 and 104 % over the unstrengthened beam, respectively. Figure 5.18 shows the load-deflection curves for beams C8 to C11. It is clear from the Figures that beams C10 and C11 carried higher loads to failure but showed lower stiffness than those of beams C8 and C9. This was due to the lower modulus of elasticity of GFRP bars.

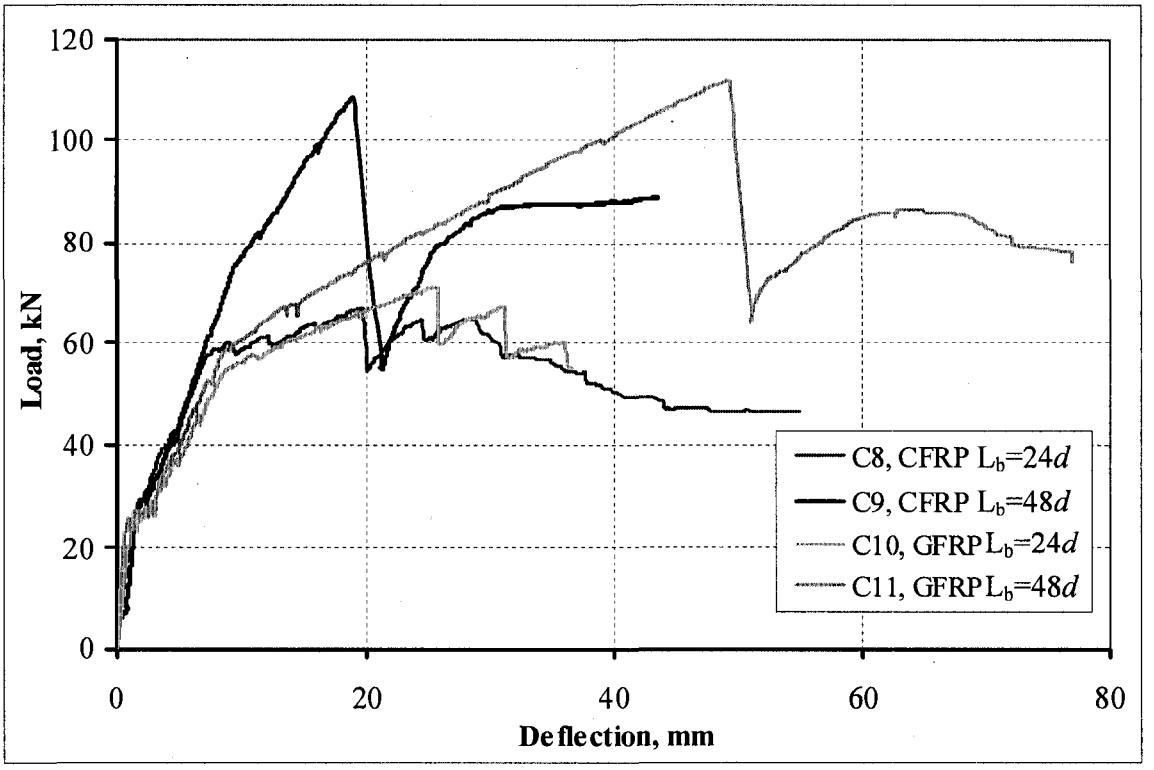

Fig. 5.18. Load-deflection curve for beams of series C

Similar to all beams, five strain gauges were placed on the GFRP bars to capture the strain distribution along the bonded length of the GFRP bar. The shape of strain distributions is proportional to the bending moment diagram. At low load levels the strain distribution are low for both beams and as the load increased the strain increased. Figures 5.19 and 5.20 show the strain distribution for beams, C10 and C11 strengthened with GFRP bar. The strain distributions are plotted at different load levels to illustrate the change in strain distribution with increasing loads.

Due to insufficient bonded length of beam C10 with bonded length 24*d*, the strain is lower than that of beam C11, with bonded length 48*d* at the same load levels, which decreases the utilization of the GFRP strengthened bar used.

The bonded length has a great influence on the strain developed in the FRP bar. However with strain nearly equal to rupture strain, maximum utilization of the FRP bar can be achieved. The codes cannot allow that and it needs two much bonded length. The use of enough and moderate bonded length can give better results. Table 5.3 for beams C10 with bonded length 24*d* gave maximum strain 50% lesser than C11 with bonded length 48*d*.

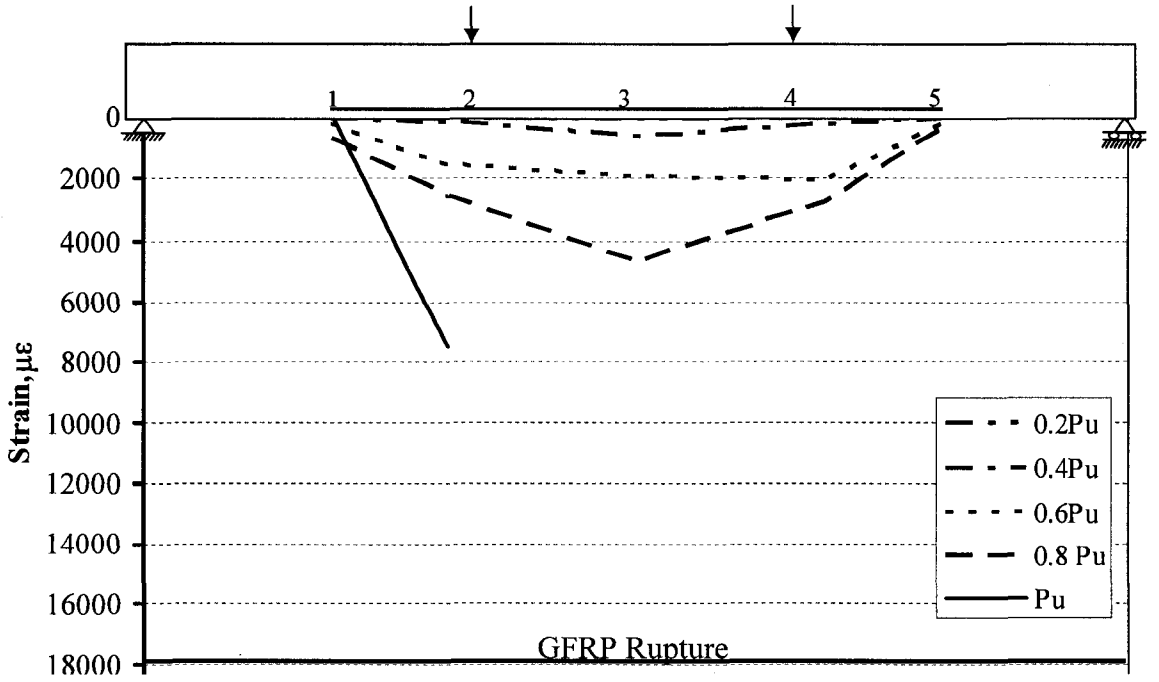

Fig. 5.19. NSM-FRP strain distribution for beamC10

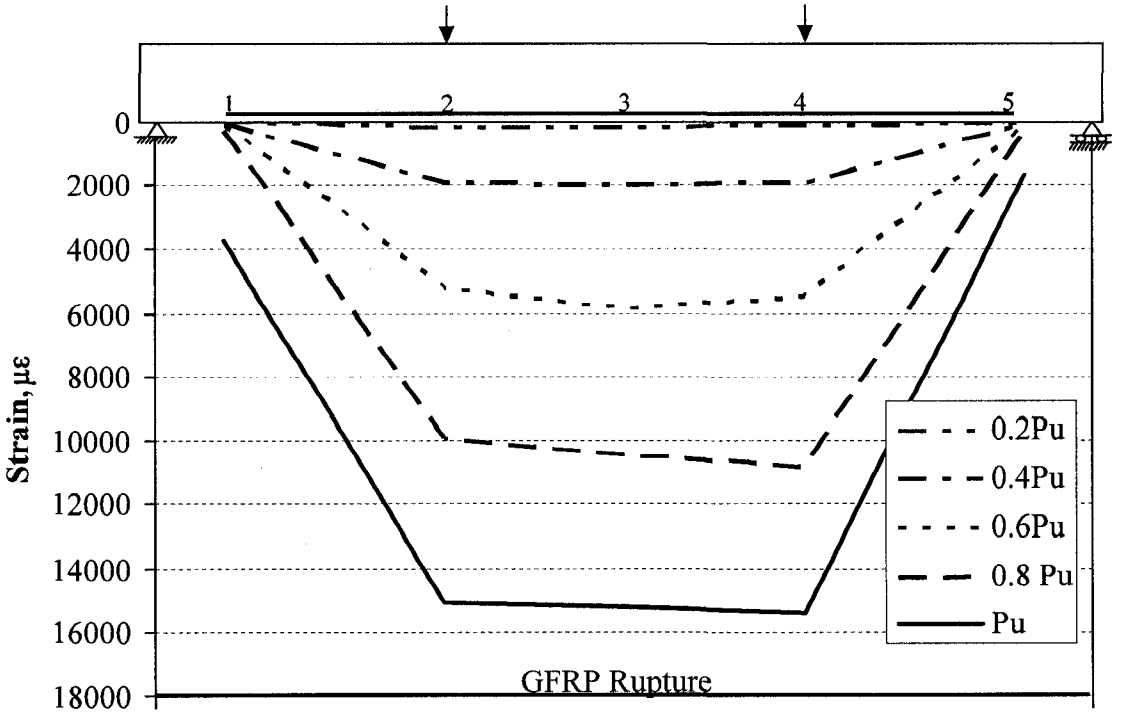

Fig. 5.20. NSM-GFRP strain distribution for beam C11

Table 5.3 Test results for series C

Specimens code	Bonded length Lb	Yield load Py, kN	Yield deflection, Δy, mm	Yield load increase %	Failure load Pu, kN	Ultimate deflection, Δu, mm	NSM-FRP debonding strain, με	Ductility Index	Failure mode	Ultimate capacity increase %
C0	—	52	6.77	—	55	75.89	—	11.21	C	—
C1	12*d*	58	8.43	10.58	67	17.20	2,423	2.04	Cs	21.73
C2	24*d*	54	7.08	3.77	73	25.38	5,058	3.58	Cs	32.19
C3	48*d*	58	7.38	11.55	94	23.97	8,583	3.25	Cs	70.83
C4	60*d*	60	9.06	15.07	96	26.80	8,595	2.96	Cs	75.38
C5	24*d*	65	10.59	26.08	88	31.42	6,464	2.97	Cs	60.66
C6	48*d*	72	12.28	39.05	90	24.60	9,012	2.00	Cs	63.91
C7	60*d*	61	11.28	18.21	102	37.01	12,400	3.28	Cs	85.79
C8	24*d*	59	7.70	13.51	67	19.71	2,026	2.56	Cs	21.04
C9	48*d*	76	9.92	47.62	109	18.97	5,650	1.91	Cs	97.51
C10	24*d*	54	8.52	3.73	71	25.54	7,515	3.00	Cs	29.17
C11	48*d*	59	8.88	14.16	112	49.36	15,333	5.56	Cs	103.89

Note: *d* is the diameter of the NSM-FRP bar, C is concrete crushing and Cs is concrete cover splitting

5.3. Effect of different parameters on the behaviour of the strengthened beams

5.3.1. Effect of internal steel reinforcement ratio

The ratio of internal steel reinforcement in rectangular section has a great effect on the efficiency of the NSM-FRP strengthening system. For the same bonded length of 48*d*, the use of steel reinforcement ratio of 1.60% gave 9% increase in ultimate capacity compared to the control beam. This increase in ultimate capacity reached 18% when a steel reinforcement ratio of 0.80% was used. Furthermore, the increase in ultimate capacity was 70% when a steel reinforcement ratio of 0.40% was used. It means that the use of NSM system is more effective for beams originally reinforced with small steel reinforcement ratios.

The NSM system is more effective with the increase of ρ_{tot}, where
$\rho_{tot} = A_s / (bd_s) + (A_f E_f / E_s)/(bd_f)$ is the equivalent reinforcement ratio, where b is the beam width and ds and df are the effective depth of the longitudinal steel bars and CFRP bar, respectively, A_f and E_f are the cross sectional area and the Young's Modulus of the CFRP bar, and A_s and E_s are the cross sectional area and the Young's Modulus of the longitudinal tensile steel bars. The effect of steel reinforcement has not been taken into account in any guidelines. If the $E_f < E_s$, this strengthening effectiveness is low. Hence, for beams originally reinforced with small steel reinforcement ratios this efficiency increases.

5.3.2. Effect of bonded length

The bonded lengths used were 12, 24, 48 and 60*d*. The ultimate load capacity increased with increasing the bonded length up to 48*d*. The percentage of increase in the ultimate load reached 225% when the bonded length increased from 12*d* (22% over the control beam) to 48*d* (71% over the control beam) for steel reinforcement ratio of 0.40 %. The increase in ultimate load due to the increase of bonded length from 48d to 60*d* was only 6% for the beams with the lowest steel reinforcement ratio of 0.40 %.

The ultimate deflection increased by 40% when the bonded length increased from 12*d* to 48*d* and 12% when the bonded length increased from 48*d* to 60*d* for same steel reinforcement ratio.

From the results of the experimental tests the effective bonded length which gives satisfactory results is 48*d*.

5.3.3. Effect of groove size

Decreasing the groove size from 2.0*d* to 1.5*d* increased the ultimate capacity of the tested beams but adversely affected their stiffness.

The groove size has a significant influence on the ultimate load and ultimate deflection. The decrease of groove size from 2.0*d* to 1.5*d* increases the ultimate load by about 11 % for bonded length 48*d* and steel reinforcement ratio of 0.40 %. It also resulted in decreasing the ultimate deflection by about 2.6 % for same bonded length and steel reinforcement ratio.

5.3.4. Effect of NSM-FRP axial stiffness (EA)

Three different axial stiffness were used in this phase of the experimental investigation, 5700, 8800 and 17000 kN. By increasing the axial stiffness the ultimate load increased and the ultimate deflection decreased.

5.3.5. Effect of NSM-FRP bar type

Two types of FRP bars were used for strengthening the beams, CFRP and GFRP bars. The ultimate load for beams strengthened with GFRP bars was greater by about 20% of that of beams strengthened with CFRP bars, having the same diameter (12.7 mm). The ultimate deflection of beams with GFRP bars was greater by about 95% of that of beams with CFRP bars. This was due to the lower value of modulus of elasticity of GFRP bars.

5.4. Summary

Based on the analysis of the results of phase two of the experimental program which is the flexural strengthening, the following summary can be drawn.

- The proposed NSM system, FRP bars and epoxy adhesive are effective to increase both the stiffness and flexural capacity of concrete beams. Using NSM-FRP bars, with bonded length 48d, increased the ultimate load of the tested beams by 9% for steel ratio 1.60%, 18% for steel ratio 0.80% and 71% for steel ratio 0.40% over the unstrengthened beam.
- The above given percentage can be increased with the decrease of the steel ratio of the beams.
- Increasing the bonded length increases the ultimate carrying capacity up to a certain limit beyond which the increase in the bonded length will not result in any increase in the capacity. This limit is in the range of 24 to 48 times the bar diameter.
- Using a small groove size increases the distance between the FRP-NSM bar and the original steel reinforcement which delays the concrete cover splitting and higher capacities can be achieved.
- Compared to carbon FRP bars, glass FRP bars as strengthening reinforcement provided nearly similar increase in the beam carrying capacity. However, due to the low modulus of elasticity of the GFRP bars, beams strengthened with GFRP bars showed more deflection at failure, and consequently higher deformability factors, than those utilizing CFRP bars. This result makes it very attractive to deeply investigate the use of glass FRP bars in this technique.
- The maximum measured NSM-FRP strains at failure was about 75 and 85% of the rupture strains of the FRP material for beams strengthened with CFRP and GFRP bars, respectively. This percentage depends on the bonded length of the FRP.
- The mode of failure for the strengthened beams was debonding in the form of concrete cover splitting at the level of the steel reinforcement.

Chapter 6 - Finite Element Modelling

6.1. General

A number of factors need to be considered when modelling the behaviour of reinforced concrete structures strengthened with FRP composites such as the nonlinearity of materials, the boundary conditions, and the interaction between the structure's constituents. Analytical methods are the traditional technique of modelling a structure's behaviour. Often, the influences from constituent materials and boundary conditions in composites structures are too complex to be simplified to a degree that a reasonable analytical expression can be derived. Therefore, a numerical approach must be selected to capture the behaviour of the structure. The most common numerical tool today is the finite element method. If a strengthened concrete structure is properly defined, a careful finite element analysis, linear-elastic or nonlinear, can give new insights and explanations to results from physical experiments. The analysis in this chapter is carried out using a finite element package Automatic Dynamic Incremental Nonlinear Analysis (ADINA) Version 8.4. The software is a one system program for comprehensive finite element analyses of structures including linear and nonlinear, dynamic and static, large strain and small strain analyses. The solution of the equilibrium equations is done in an incremental way using direct spare solution schemes as well as iterative. In this study, this well known finite element software, ADINA, is used to predict the flexural response of FRP NSM-strengthened reinforced concrete beams. All the materials constitutive laws and structural elements employed in this chapter are built in within this software.

6.2. Material Modelling

6.2.1. Concrete modelling

Concrete modelling through ADINA, can be employed with the 2-D solid and 3-D solid elements.

A compressive uni-axial nonlinear stress-strain relationship is used till the maximum concrete compressive strength, f'_c, is reached beyond which the behaviour softens with increasing compressive stresses till the crushing of concrete occurs as shown in Fig. 6.1. The ultimate uni-axial compressive strength is taken equals to $0.85f'_c$ and the ultimate uni-axial compressive strain is taken equals to 0.0035.

The concrete model can be used with the small displacement and large displacement formulations. The basic material characteristics are:

- A nonlinear stress-strain relation to allow for the weakening of the material under increasing compressive stresses; as shown in Fig. 6.1;
- Tensile failure at a maximum, relatively small principal tensile stress and compression crushing failure at high compression. The tensile and compression crushing failures are governed by tensile failure and compression crushing failure envelopes;
- A strategy to model the post-cracking and crushing behaviour of the material through the strain softening from compression crushing failure to an ultimate strain at which the material totally fails.

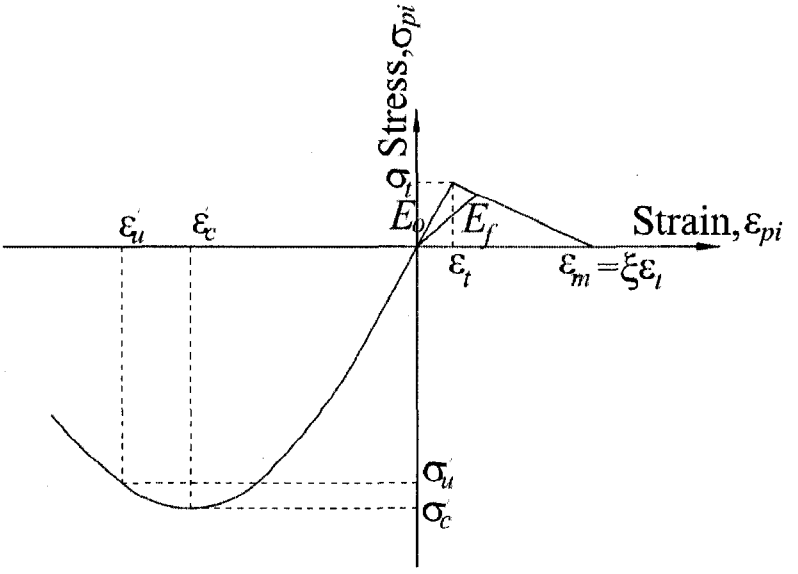

Fig. 6.1. Uni-axial stress-strain relationship used for the concrete model

Where:

σ_u, σ_c are the maximum and ultimate concrete compressive stress respectively. The maximum and ultimate strains are denoted as ε_u and ε_c respectively. In Fig. 6.1, E_o and E_f are the initial and the secant tangent Young's modulus. ξ is the tension stiffening factor.

Under multi-axial stress conditions, the stress-strain relations are evaluated differently depending on whether the material is being loaded or unloaded. Poisson's ratio is assumed to be constant and equal to 0.18. To characterize loading and unloading conditions, a loading scalar, t_g, is defined for each integration point,

$$t_g = t\sigma_e$$

Where $t\sigma_e$ is the effective stress at time t.

The material is considered as orthotropic with the directions of orthotropy being defined by the principal stress directions. Once cracking occurs in any direction, i, that direction is fixed from that point onward in calculating $t\sigma_{pi}$. The stress-strain matrix corresponding to these directions, for three-dimensional stress conditions, is

$$\mathbf{C} = \frac{1}{(1+\nu)(1+2\nu)} \times$$

$$\begin{bmatrix} (1-\nu)\,{}^{t}\tilde{E}_{p1} & \nu\,{}^{t}E_{12} & \nu\,{}^{t}E_{13} & 0 & 0 & 0 \\ & (1-\nu)\,{}^{t}\tilde{E}_{p2} & \nu\,{}^{t}E_{23} & 0 & 0 & 0 \\ & & (1-\nu)\,{}^{t}\tilde{E}_{p3} & 0 & 0 & 0 \\ & & & 0.5(1-2\nu)\,{}^{t}E_{12} & 0 & 0 \\ & \text{symmetric} & & & 0.5(1-2\nu)\,{}^{t}E_{13} & 0 \\ & & & & & 0.5(1-2\nu)\,{}^{t}E_{23} \end{bmatrix}$$

The failure envelopes are employed to establish the uni-axial stress-strain law accounting for multi-axial stress conditions, and to identify whether tensile or crushing failure of the material has occurred. Having established the principal stresses ${}^{t}\sigma_{pi}$ *with* ${}^{t}\sigma_{p1} \geq {}^{t}\sigma_{p2} \geq {}^{t}\sigma_{p3}$. The stresses ${}^{t}\sigma_{p1}$ *and* ${}^{t}\sigma_{p2}$ are held constant and the minimum stress that would have to be reached in the third principal direction to cause crushing of the material is calculated using the failure envelope.

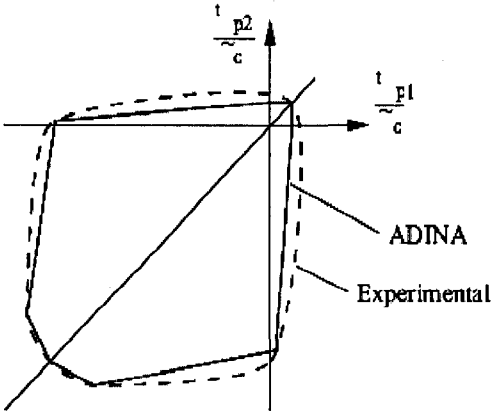

Fig. 6.2. Bi-axial concrete compressive failure envelope

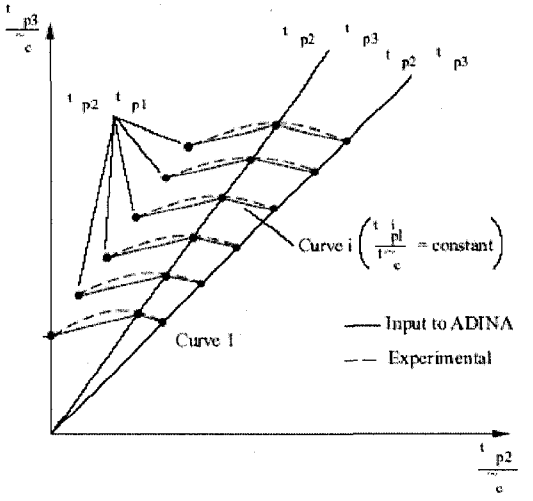

Fig. 6.3. Tri-axial concrete compressive failure envelope

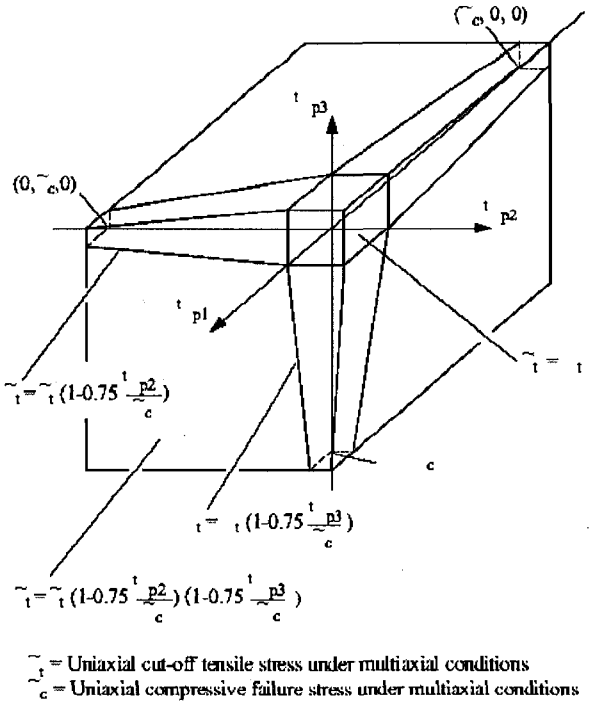

Fig. 6.4. Three-dimensional tensile failure envelope of concrete model

6.2.2. Steel reinforcement modelling

Bilinear elastic-plastic material with tangent modulus in the strain hardening taken equals to $E_s/100$ was used to model the steel bars in concrete as shown in Fig. 6.5. A full bond was assumed between the concrete and the steel reinforcement, both longitudinal and transverse. The material properties of steel bars used in the finite element modelling are given in Table 3.4.

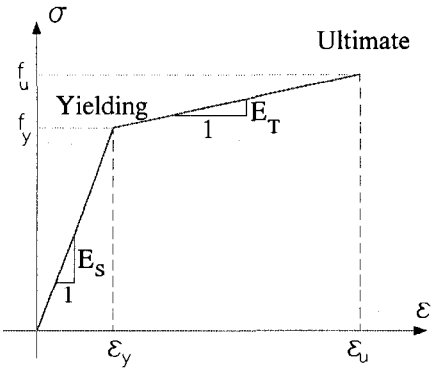

Fig. 6.5. Stress-strain relationship for steel

6.2.3. FRP reinforcement modelling

FRP material was modelled as linear-elastic up to failure as shown in Fig. 6.6. Different types of NSM-FRP reinforcement, (CFRP and GFRP) were used in this investigation. The tensile strength, modulus of elasticity and ultimate strain of the FRP bars are given in Table 3.4. A full bond was assumed between the epoxy and the FRP reinforcement.

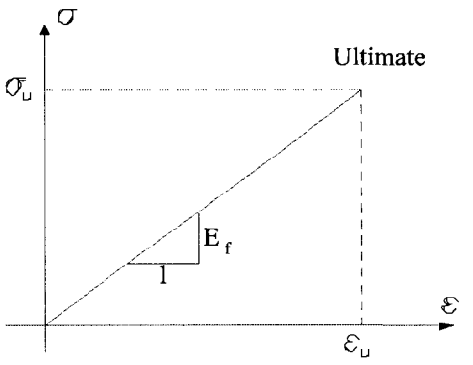

Fig. 6.6. Stress-strain relationship for FRP

6.2.4. Epoxy adhesive modelling

The epoxy adhesive was modelled as isotropic linear-elastic up to failure. The material properties of the epoxy adhesive used are given in Table 3.5.

6.2.5. Interface modelling

In this study, a special consideration was taken to account for the slip that occurs between the FRP bar and the concrete. The measured slip is usually very small and many investigations did not take it into consideration in the finite element modelling of NSM strengthening system (Hassan 2002 and Lundqvist 2007). However, in this study, a bond-slip model that was driven based on the pullout testing of concrete blocks with NSM-FRP bars (Chapter 4 in this thesis) is implemented in the finite element modelling introduced in the following sections.

Since the mode of failure for the tested beams was concrete cover separation, which is the common mode of failure for concrete beams strengthened in flexural with NSM reinforcement (Soliman et al. 2008b and 2008c, Kotynia 2006 and 2007 and Teng et al. 2006) as discussed in section 2.3.2.1, the slip at the interface between the concrete and

the epoxy was taken into consideration and a full bond was assumed between the FRP bar and the epoxy.

The bond–slip relationship correlates the local shear stress, τ , and the associated slip, s , between the FRP reinforcement and the concrete substrate. This bond–slip profile depends on the bonded length. For example, Fig. 6.7 shows the bond–slip relationship profile that was employed to constitute the interfacial behaviour between NSM system and the concrete layer

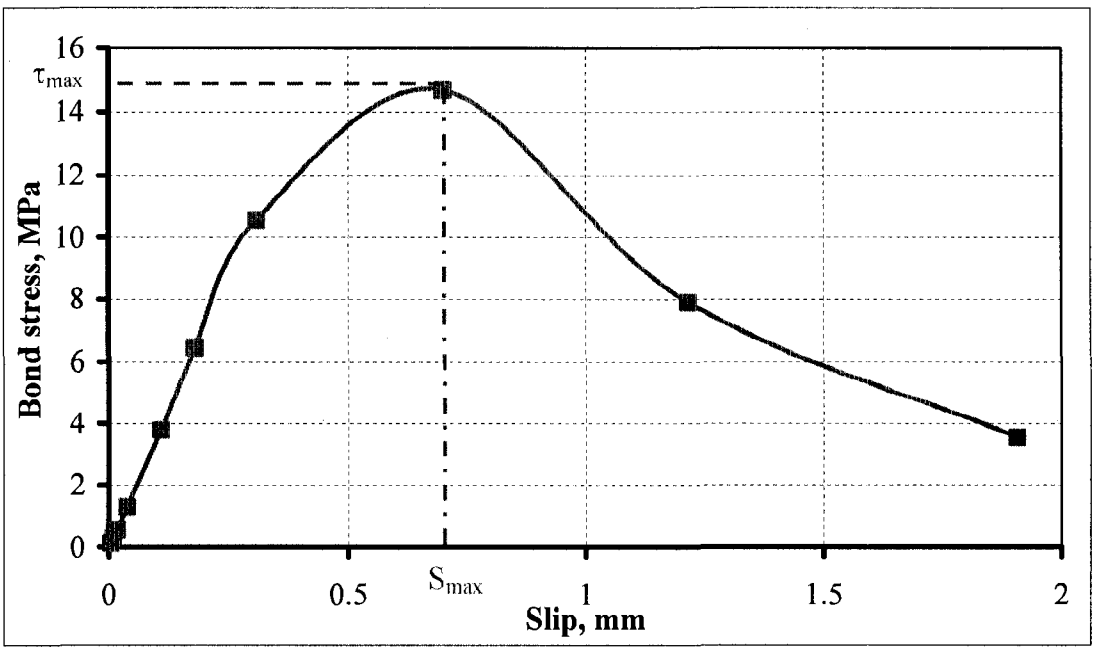

Fig. 6.7. Local bond stress-slip profile

6.3. Finite Element Modelling

The finite element analysis was carried out by using ADINA (**A**utomatic **D**ynamic **I**ncremental **N**onlinear **A**nalysis) version 8.4 software. Due to symmetry of the beam in the two directions, only a quarter of the beam is modeled.

A 20-node, 3-D solid element is used to represent the concrete, epoxy and FRP, as shown in Fig. 6.8.

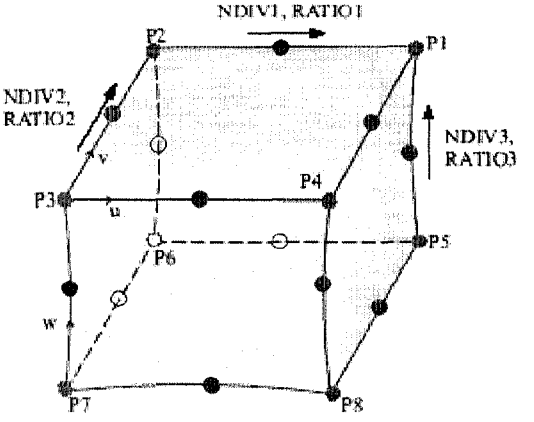

Fig. 6.8. A 20-node, 3-D solid element

The basic finite element assumptions for the coordinates are

$$X = \sum_{i=1}^{20} h_i x_i \qquad Y = \sum_{i=1}^{20} h_i y_i \qquad Z = \sum_{i=1}^{20} h_i z_i$$

and for the displacement

$$U = \sum_{i=1}^{20} h_i u_i \qquad Y = \sum_{i=1}^{20} h_i v_i \qquad W = \sum_{i=1}^{20} h_i w_i$$

where

h_i (r, s, t) = interpolation function corresponding to node i

r, s, t = isoparametric coordinates

x_i, y_i, z_i = nodal point coordinates

u_i, v_i, wi = nodal point displacements

A truss element is used to represent steel reinforcement as shown in Fig. 6.9. Using truss elements to represent steel is acceptable because the main force carried by steel is only axial force and there is no flexure response for the steel member due to its small dimensions and its negligible inertia compared to the concrete cross section. The number of nodes per element is automatically generated by the program.

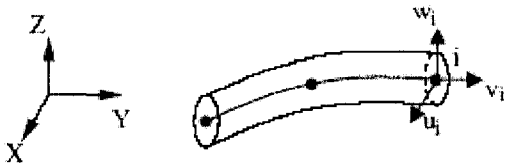

Fig. 6.9. Global displacement degrees of freedom (DOF)

The ADINA program has the capability to generate the truss elements and connect it to the 3-D solid elements at the intersection joints in which the truss elements lie. The ADIAN User Interface (AUI) does this during data file generation. For each reinforcing bar line, the ADINA finds the intersections of the rebar line and the faces of the 3-D elements. The ADINA then generates nodes at these intersections and generates truss elements that connect the successive nodes. The ADINA also defines constraint equations between the generated nodes and three corner nodes of the 3-D element faces as shown in Fig. 6.10. However, there are some restrictions on this capability. To make constraints between two different elements, both elements must have the same degree of freedom otherwise the ADINA will not generate constraint equations at the intersection points.

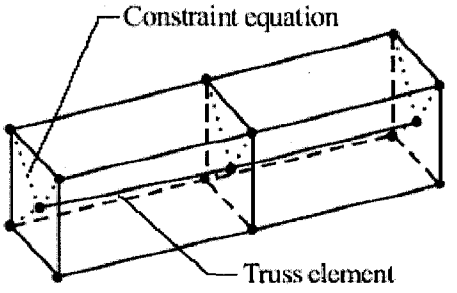

Fig. 6.10. A truss element generated into 3-D solid elements

The element size used in the analysis of the strengthened beams is 50x50x50 mm^3. A fine mesh is used with element size 25x25x25 mm^3 in the groove zone (close to the FRP and epoxy). To represent the concrete/FRP interface, 3-D two node truss elements are employed. These elements are employed in the direction of the slip of the bar. Suitable stress-strain relations are employed to suitable the response of these trusses in the horizontal direction. These relations are typically the bond-slip profile presented in Fig. 6.7.

Figure 6.11 shows the typical 3-D finite element mesh and the elements used for the different materials in the NSM strengthened beams.

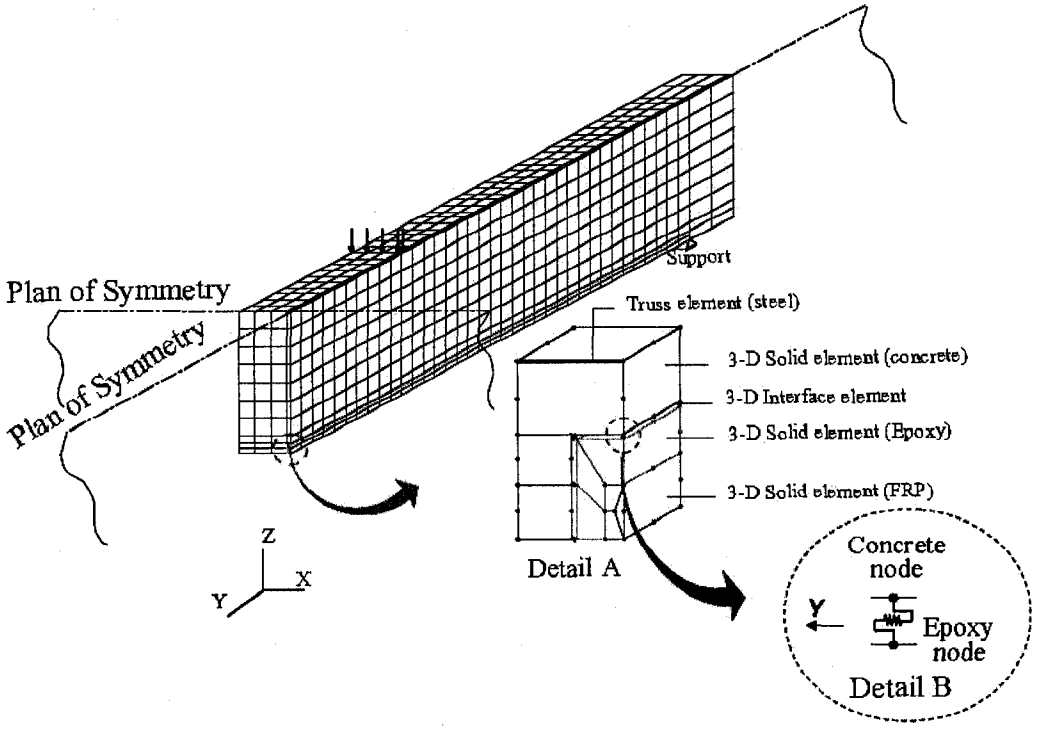

Fig. 6.11. Types of elements used for the strengthened beams

6.4. Finite Element Results and Discussion

In the following section, a validation for the proposed model is made by a comparison between the experimental and the numerical results for test series B and C. Following validation of the proposed model, a parametric study is conducted to study a wide variety of factors that known to affect the behaviour of the strengthened beams. In this numerical study different variables were considered in the parametric study. These are steel reinforcement ratio, concrete compressive strength, bonded length and axial stiffness of FRP bars (defined by the area times the young's modulus). The output responses of interest are the load deflection profile, ultimate load carrying capacity and debonding strain in NSM-FRP bars.

6.4.1. Validation of the proposed finite element model

A comparison is made between the experimental results for beams from series B and series C and the proposed model. Test results from the numerical analysis and the experimental results are given in Table 6.1. The comparison shows good agreement between the numerical and experimental results especially for beams with long bonded length. Figure 6.12 shows the load-deflection relationship for series B.

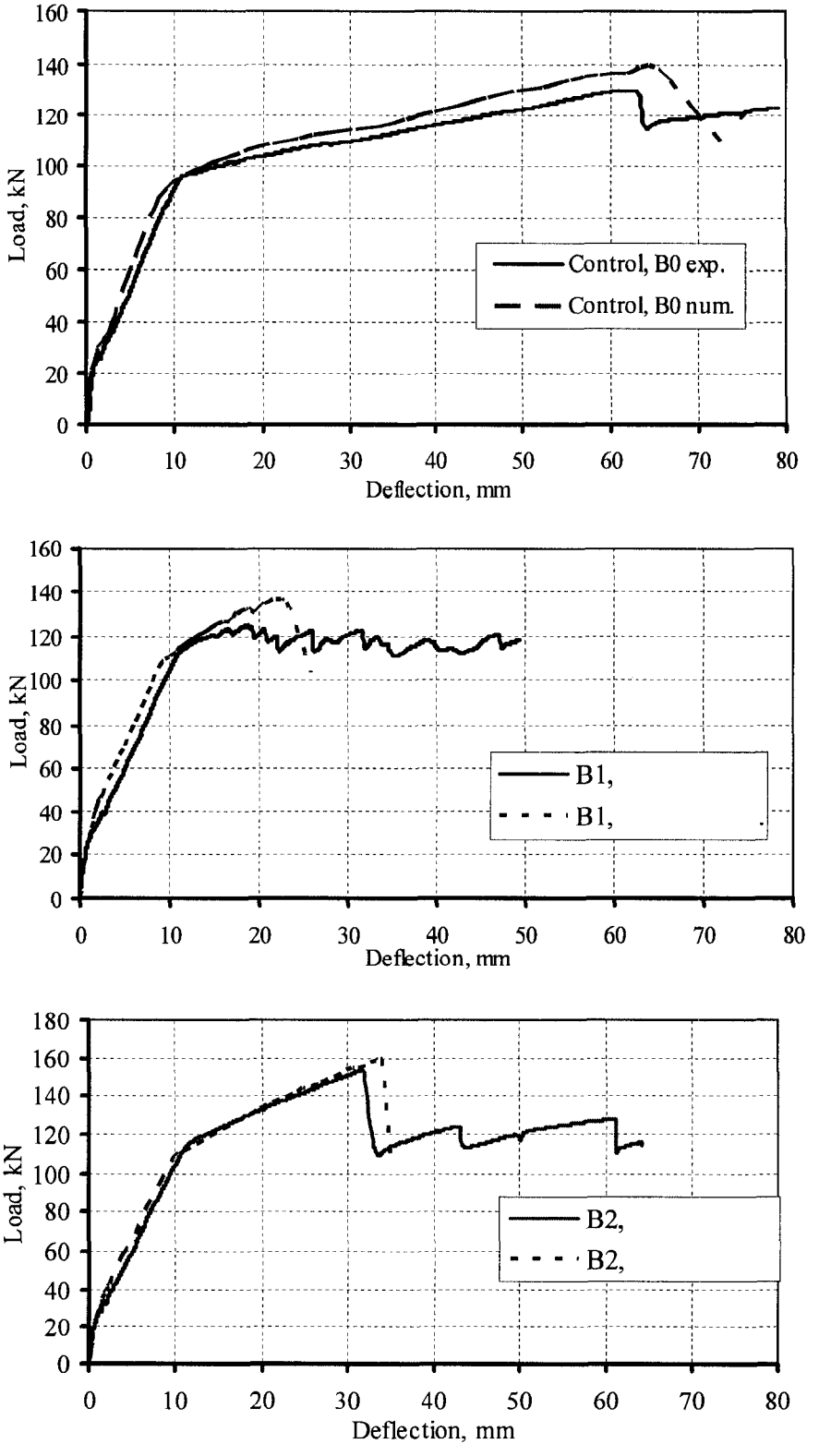

Fig. 6.12. Comparison between numerical and experimental load-deflection relationships for series B

Table 6.1 - Comparison of experimental and numerical results for series B and C

specimen	Experimental		Numerical		$P_{num.}/P_{exp.}$
	Failure load, P_{exp}, kN	Deflection, mm	Failure load, P_{num}, kN	Deflection, mm	
B0	130.14	62.43	138.45	65.41	1.06
B1	124.45	18.64	136.30	21.73	1.09
B2	153.77	31.34	160.09	34.05	1.04
C3	93.87	23.97	96.39	24.17	1.03
C4	96.37	26.80	102.63	26.67	1.06
				average	1.056
				Stand. dev.	0.023
				C.O.V.	2.17

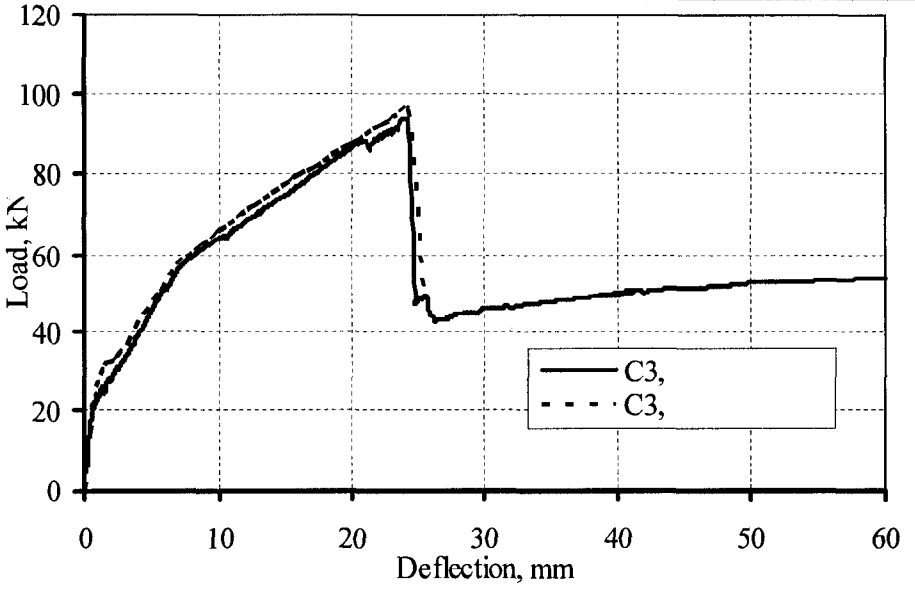

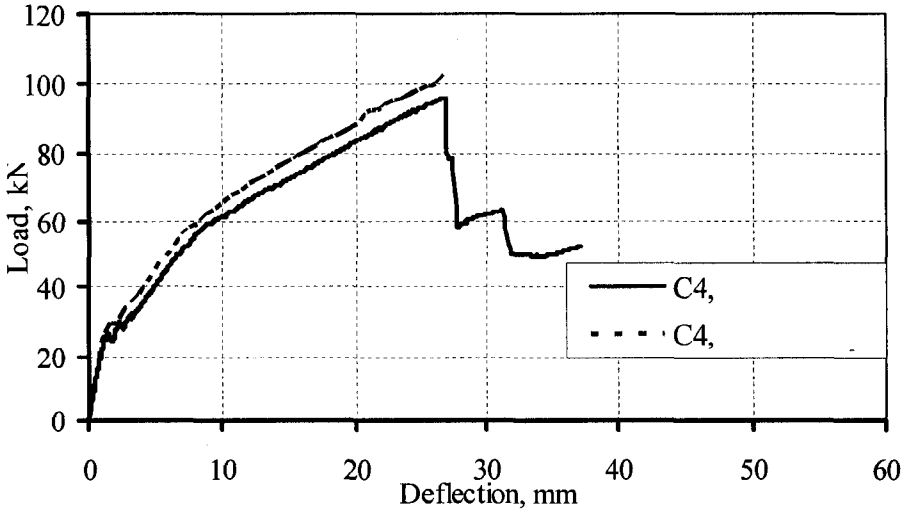

Fig. 6.13. Comparison between numerical and experimental load-deflection relationships for series C

Figure 6.14 shows the load-strain relationship for beam C3. It can be noticed from the curve that the debonding strain for the numerical analysis is lower than the experimental one. This may be due to the full bond assumption made between the epoxy and the FRP.

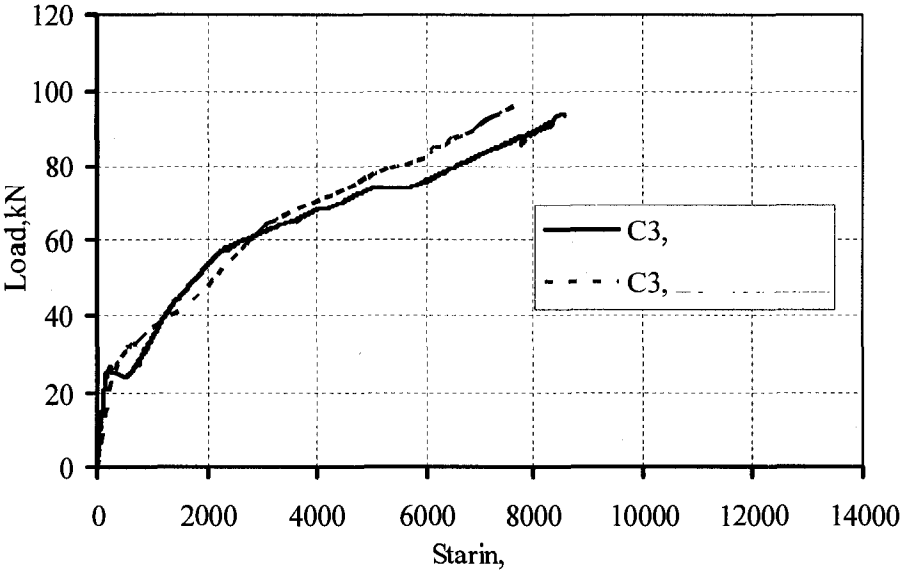

Fig. 6.14. NSM-FRP strains for beam C3

6.4.2. Parametric study

6.4.2.1. Effect of the steel reinforcement ratio

It has been demonstrated through the experimental program presented in chapter 5 that the steel reinforcement ratio is the main factor controlling the debonding load in NSM-FRP system. In this study, the effect of different levels of the steel reinforcement ratio on the predicted debonding load is investigated. The different steel ratio varied between ρ_s=0.2% which is less than the minimum steel ratio ($0.2\sqrt{f_c'}/f_y$) according to CSA A23.3-04 and $0.75\rho_{bal.}$. Fig. 6.15 shows the numerically predicted load-deflection relationships for six beams having different steel reinforcement ratio. Six ratios were considered in this study with values of 0.2, 0.32, 0.76, 1.0, 2.0 and 3.0%. These ratios are corresponding to 0.05, 0.08, 0.20, 0.25, 0.50 and $0.75\rho_{bal.}$, where $\rho_{bal.}$ is the balanced steel reinforced ratio. The beams have the same area of the CFRP bar, 71 mm^2 and the same bonded length of 48d. It is obvious that increasing the steel reinforcement ratio increases the ultimate capacity. The mode of failure for the four beams is debonding of FRP bars from the surrounding concrete. This is simulated numerically when an interface element reaches τ_{max} at a certain time step. In the subsequent time step, the slip value in this particular interface element tends to a huge value as a result of increasing the crack width passing through this element. Accordingly the debonding numerically occurs at this particular element. At reinforcement ratio of 3.0%, the failure initiates with concrete crushing at a load level of 378 kN before steel yielding, then the final failure occurs when the FRP bars debond off the concrete surface at a load level of 366 kN.

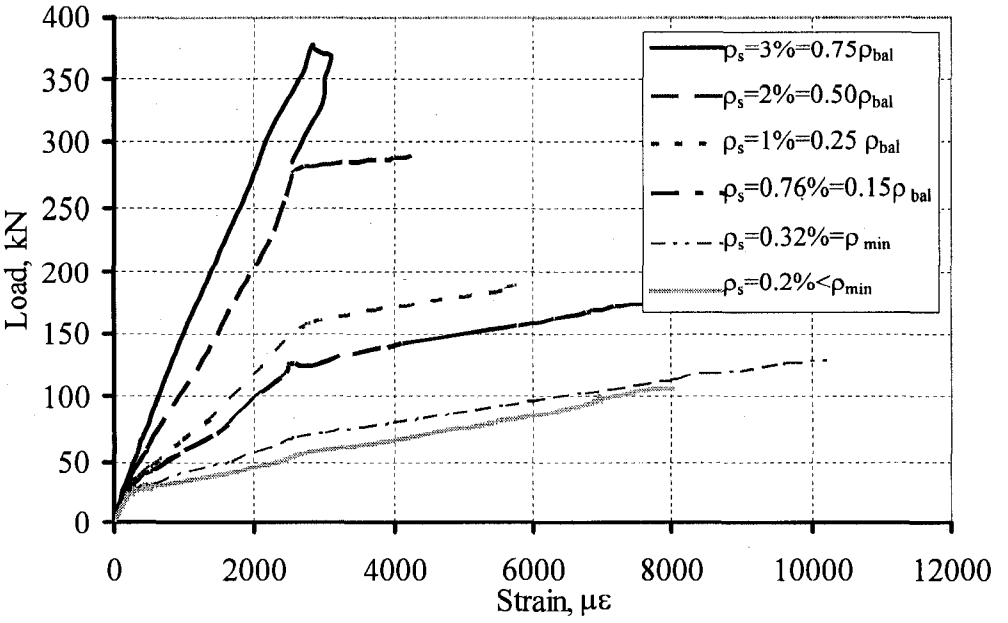

Fig. 6.15. Effect of the steel reinforcement ratio on load–strain relationships

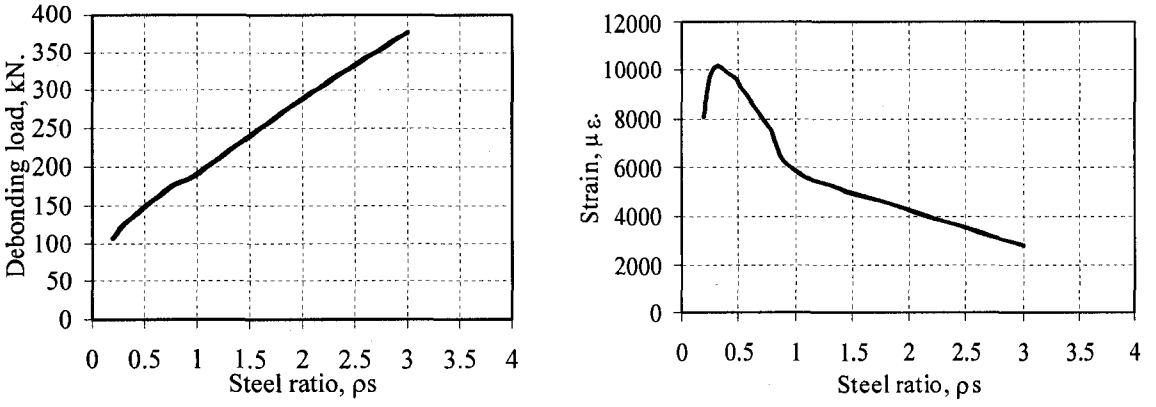

(a) (b)

Fig. 6.16. Effect of reinforcement ratio (ρ_s) on debonding load and strain

Figure 6.16a shows the effect of the steel reinforcement ratio on the predicted debonding load. Increasing the steel reinforcement area increases the ultimate capacity of the beam. However, as shown in Fig. 6.16b, the debonding strain level in NSM-FRP bars reduces with increasing the steel reinforcement. From this figure, it is concluded that the efficiency of the NSM-FRP system is higher for beams with low steel reinforcement ratios compared to those with higher ratios.

6.4.2.2. Effect of concrete compressive strength

Increasing the concrete compressive strength increases both the debonding load and debonding strain level in the NSM-FRP bars, as shown in Fig. 6.17 and Fig. 6.18, respectively. The higher the concrete compressive strength, the smaller the crack width as well as the smaller the associated slip values along the interface. In turn, the debonding strain increases. In Fig. 6.17, the load-deflection relationship is depicted for different concrete compressive strengths. With the increase in the concrete compressive strength, both the initial stiffness and cracking load increase as well yielding and debonding load levels. This indicated higher utilization for NSM-FRP bars associated with higher concrete compressive strength.

As shown in Fig. 6.18, the debonding strain increases in a second order function with the increase of the concrete compressive strength. This relationship is almost the same as the one adopted in the ACI-440.2R-08 (2008) design guidelines for the debonding strain in external strengthening

$$\varepsilon_{fd} = 0.41\sqrt{\frac{f_c'}{n.E_f.t_f}} \leq 0.9\varepsilon_{fu} \quad \text{(SI units)} \tag{6.1}$$

where n is the number of FRP layers, E_f is the modulus of elasticity of the FRP and t_f is the thickness of an FRP layer.

In the ACI-440.2R-08 (2008) design equation, the debonding strain increases with the square root of the concrete compressive strength. Similar equation (6.2) is employed in the *Fédération internationale du béton* (*fib*) (*fib*, 2001) code. The formula considers only the concrete tensile strength and the axial stiffness of the FRP as parameters affecting the debonding strain. This design equation is given by:

$$\varepsilon_{fd} = \alpha c_1 k_c k_b \sqrt{\frac{f_c'}{n.E_f.t_f}} \tag{6.2}$$

where α, k_c, and kb are factors accounting for the influence of cracks on the bond strength, the state of compacting of the concrete, and the width factor, respectively, and c_1 is a factor determined experimentally.

The relationship between the debonding strain and the concrete compressive strength in these design guidelines and code is approximately the same as presented in Fig. 6.18. However, unlike the ACI and *fib* equations, the relationship between the debonding strain and concrete compressive strength stays constant after a strength value of 40 MPa. Although the predicted debonding strain is constant after a concrete compressive strength of 40 MPa, the debonding load increases with the increase of the concrete compressive strength beyond this value (40 MPa) as observed in Fig. 6.19. This indicates that the increase in the ultimate capacity attributed to the increase in the concrete strength rather than the FRP strain.

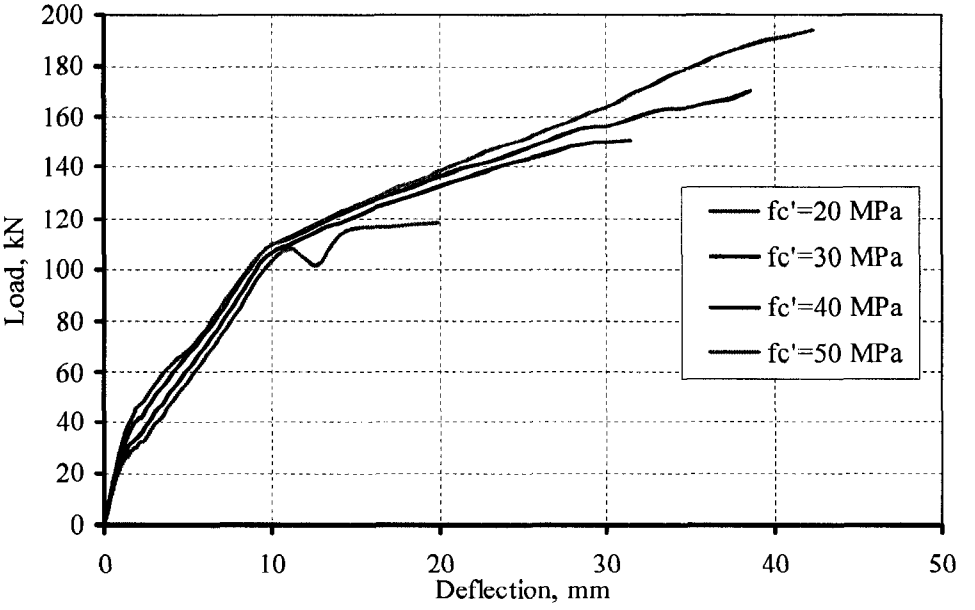

Fig. 6.17. Effect of concrete compressive strength on load deflection behaviour

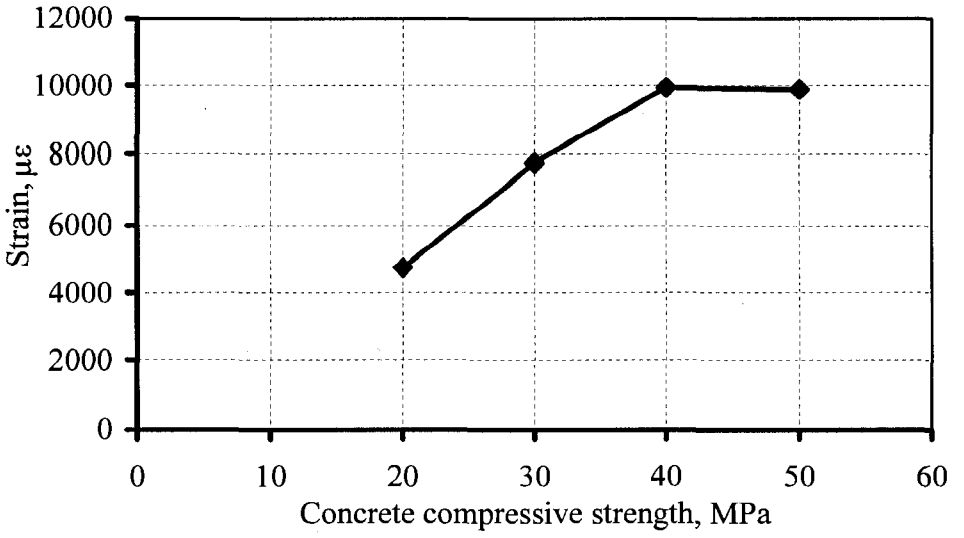

Fig. 6.18. Effect of concrete compressive strength on FRP debonding strain

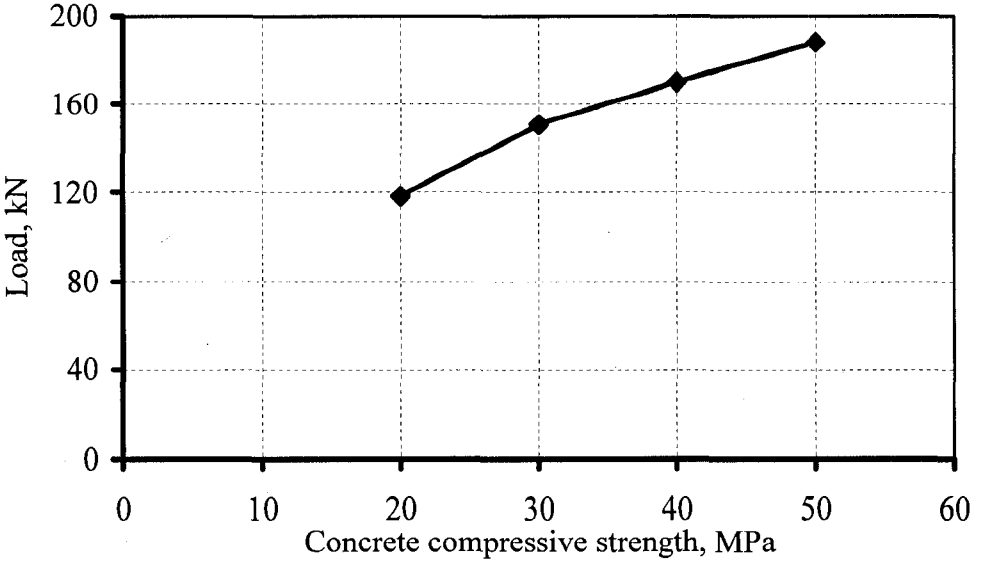

Fig. 6.19. Effect of concrete compressive strength on failure load

6.4.2.3. Effect of axial stiffness (EA) of NSM-FRP bars

The effect of the NSM-FRP axial stiffness on the debonding load and debonding strain levels is depicted in Fig. 6.20 and Fig. 6.21, respectively. As the axial stiffness of the FRP reinforcement increases the failure load increases and the debonding strain decreases. This was validated also by the ACI-440.2R-08 design equation (equation 6.1),

The debonding strain reduces with the square root of the NSM-FRP axial stiffness. The relationship between the concrete compressive strength has concave shape for the debonding load and convex shape for the debonding strain.

In terms of the load-deflection and load-strain relationships, the general trend of the profile is independent on the axial stiffness value; however the curve becomes stiffer after yielding point.

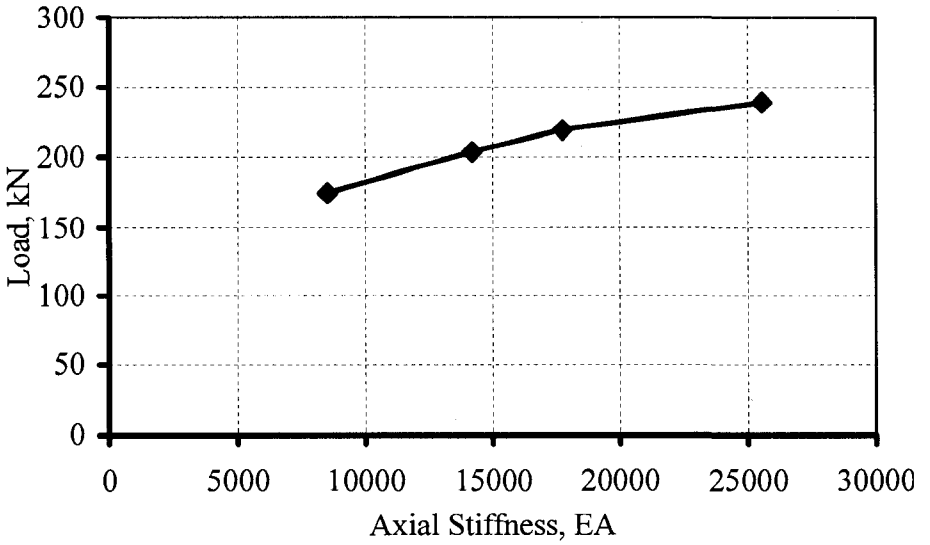

Fig. 6.20 Effect of axial stiffness on failure load

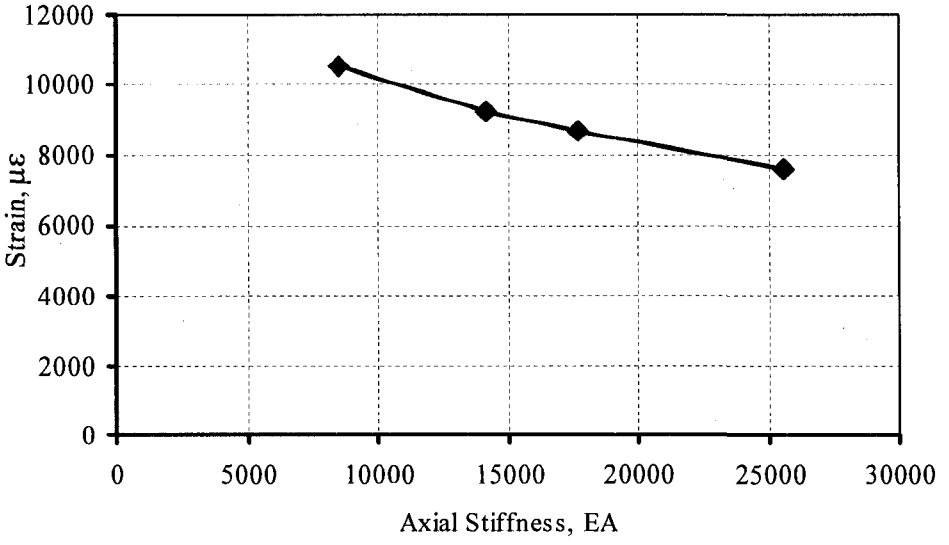

Fig. 6.21. Effect of axial stiffness on FRP debonding strain

6.4.2.4. Effect of bonded length.

The last parameter considered in this study is the bonded length of NSM-FRP bar on the characteristics of the load-deflection relationship. Four bonded lengths have been assumed as shown in Fig. 6.22; namely, 20d, 50d, 70d and 80d, where d is the diameter of the FRP bar. The area of FRP bar was kept constant for all beams and assumed as 71mm^2 and the reinforced steal ratio was taken 0.8%. It is obvious that with the increase of the bonded length the debonding strain increases and this mitigates the debonding failure. It is recommended according to this analysis and from the ACI440.2R-08 guide that the FRP bars extend all over the beam span or at least at a certain distance beyond the cracking point.

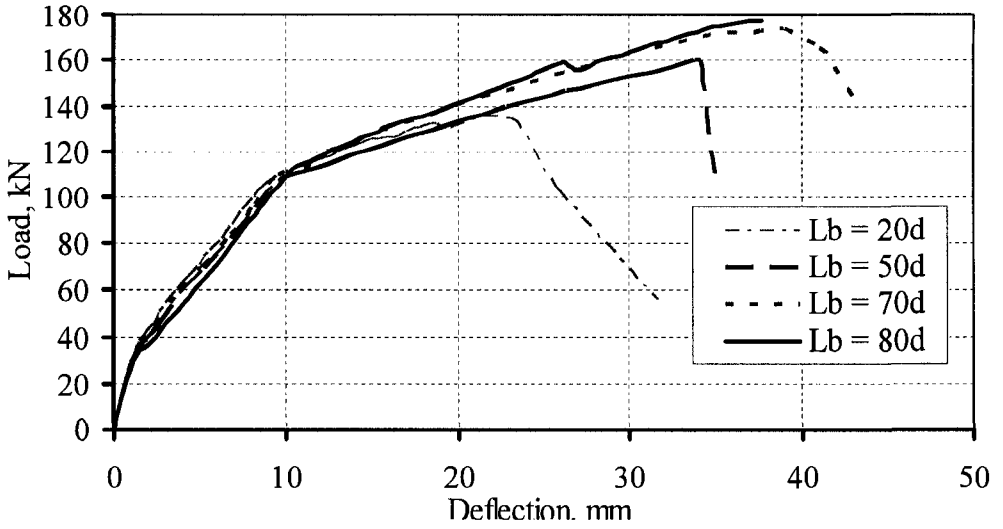

Fig. 6.22. Load-deflection behaviour for different bonded length used

Chapter 7 - Conclusions and Recommendations

7.1. General

The experimental and the analytical program reported in this thesis have provided an understanding of the behaviour of concrete beams strengthened with NSM-FRP bars. The main objective of this study was to study the behaviour of concrete beams strengthened with NSM-FRP bars and the factors affecting this strengthening technique. The following sections highlight the conclusions that can be drawn based on the results of this investigation. The experimental results are divided into pullout tests at different environments and flexural strengthening beam tests. In addition, conclusions from the analytical study are also reported.. The following sections include also recommendations for future work.

7.2. Experimental Results

7.2.1. Bond characteristics

- The adopted system, V-ROD FRP bars and Hilti adhesives, seems to perform well in the NSM-FRP strengthening system.
- The adopted test methods seem to be efficient and produced consistent results.
- The main failure for most of the tested specimens with epoxy adhesive was concrete shear-tension failure (semi-cone failure) accompanied with or without epoxy cracking (splitting). Specimens with longer bonded lengths failed by rupture of the FRP bar.
- The main mode of failure for specimens with cement adhesive was at the concrete-cement interface.
- The failure load of specimens with cement adhesive was about 40 to 56% compared to the specimens with epoxy adhesive due to the smooth surface of the sides of the groove.
- Increasing the bonded length increased the pullout load, while the bond stress was decreased due to longer length distribution.

- Increasing the groove size for specimens with the epoxy adhesive did not have a significant influence on the pullout load. However, the factor that controlled failure was the tensile strength of the concrete.
- Increasing the groove size for specimens with the cement adhesive decreased the failure load; this was due to shrinkage of a larger amount of cement grout inside the bigger groove size. It is not recommended to use a groove size equal to two times the bar diameter for the cement adhesive.
- The percentage of reduction in pullout load for the conditioned specimens with the epoxy adhesive varied between 8 to 14 % compared to the reference specimens.
- The failure load for the conditioned specimens with cement adhesive was about 30 to 45% less than that of reference specimens.
- Due to temperature changes during freeze/thaw cycles, hair cracks were developed in the adhesive materials. Therefore, the adhesive materials will govern the failure mode of the specimens and the slip performance.
- The measured change of strain due to freeze/thaw cycles was around 70 to 90 micro-strain in the case of epoxy adhesive and around 120 to 170 micro-strains in case of cement adhesive.
- The change in strain due to freeze/thaw cycles increased with the increase in bonded length. Changing the groove width had no effect on the change of strain due to freeze/thaw cycles.
- The conditioned specimens using freeze/thaw cycles are adversely affected due to the difference in the thermal expansion coefficient between the adhesive materials and the concrete.

7.2.2. Flexural strengthening: Beam tests

Based on the analysis of the results of phase two of the experimental program which is the flexural strengthening, the following conclusions can be drawn.

- The proposed NSM system, FRP bars and epoxy adhesive are effective to increase both stiffness and flexural capacity of concrete beams. Compared to the unstrengthened beam, using NSM-FRP bars, with a bonded length of 48*d*, increased the ultimate load of the tested beams by 9, 18, and 71% for beams with steel reinforcement ratios of 1.60, 0.80, and 0.40%, respectively. This means that the NSM-FRP system is more efficient when used with RC beams originally having low steel reinforcement ratio.
- Increasing the bonded length increases the ultimate carrying capacity up to a certain limit beyond which the increase in the bonded length will not result in any increase in the capacity. This limit is in the range of 48 times the bar diameter.
- Using a small groove size increases the distance between the FRP-NSM bar and the original steel reinforcement which delays the concrete cover splitting and higher capacities can be achieved.
- Compared to carbon FRP bars, GFRP bars as strengthening reinforcement provided nearly similar increases in the beam carrying capacity. However, due to the low modulus of elasticity of the GFRP bars, beams strengthened with GFRP bars showed more deflection at failure, and consequently higher deformability factors, than those utilizing CFRP bars. This result makes it very attractive to deeply investigate the use of glass FRP bars in this technique.
- The maximum measured NSM-FRP strains at failure was about 75 and 85% of the rupture strains of the FRP material for beams strengthened with CFRP and GFRP bars, respectively. This percentage depends on the bonded length of the FRP bar.
- The mode of failure for the strengthened beams was debonding in the form of concrete cover splitting at the level of the steel reinforcement.

7.3. FEA Results

Based on the analysis of the results of the analytical program the following conclusions can be drawn.

- All the investigation that was done before on strengthening with NSM was assuming full bond between concrete, epoxy adhesive and NSM-FRP reinforcement. Apparently this is the first analytical study on strengthening with NSM-FRP that takes in to account the slip behaviour between FRP and concrete.
- The proposed finite element model was capable of accurately predicting the load-deflection behaviour and mode of failure of the strengthened beams.
- The predicted axial strain in the NSM-FRP bar was lower than that observed experimentally. This maybe attributed to the full bond assumption made between the FRP and epoxy layers.
- The analysis was unable to predict the load-deflection behaviour for beams having a small bonded length. This was mainly due to the rapid premature failure of such beams.
- From the parametric study included in the investigation, it was observed that increasing the steel reinforcement ratio increases the ultimate capacity of the RC beam. However this is associated with reducing the debonding strain level in FRP bars. This implicity means that a high utilization ratio for FRP bars is obtained for a lower steel ratio beam.
- Increasing the concrete compressive strength increases both the debonding load and debonding strain level in the NSM-FRP bars.
- Increasing the axial stiffness for the NSM-FRP reinforcement increase the failure load and decrease the debonding the strain.
- Increasing the bonded increase the failure load up to a certain limit beyond no increase will be gained in the capacity.

7.4. Recommendations for Future Work

While the objectives of this study were achieved, more investigations are still needed to fully characterize the behaviour of concrete structures strengthened with NSM-FRP. Future work should concentrate on the following topics:

- The tolerance of the groove size needs to be deeply investigated especially in flexural strengthening and to study its effect on the mode of failure.
- All the experimental work that was done on prestressing with NSM-FRP bars can not be implemented in a real strengthening project as their procedure of tensioning and anchoring the bars requires access to the ends of the beam, which is generally not possible in reality. Therefore, easy and practical methods of pre-tensioning and anchoring are needed to be developed.
- More investigation needs to be done in the finite element modelling to take into account the bond-slip behaviour of the concrete/epoxy interface and epoxy/FRP interface.
- The effect of severe environmental conditions on strengthening with NSM techniques need to be widely investigated as very limited research was done in this area.
- The effect of sustained load on strengthening with NSM needs to be investigated.
- Fire resistance of the purposed strengthening technique and fire protection should be taken into consideration.
- Design guidelines are needed for strengthening with NSM-FRP taking into consideration the adequate reduction factors.

REFERENCES

ACI Committee 318, 2005. "Building Code Requirements for Structural Concrete and Commentary." *ACI 318-05/ ACI 318R-05*, American Concrete Institute, Farmington Hills Michigan, 430 p.

ACI Committee 440, 2002. "Guide for the Design and Construction of Externally Bonded FRP Systems for Strengthening Concrete Structures." *ACI 440.2R-02*, American Concrete Institute, Farmington Hills Michigan, 45 p.

ACI Committee 440, 2006. "Design Guide for the Design and Construction of Concrete Reinforced with FRP Bars." *ACI 440.1R-06* American Concrete Institute, Farmington Hills Michigan, 41 p.

ACI Committee 440, 2008. "Guide for the Design and Construction of Externally Bonded FRP Systems for Strengthening Concrete Structures." *ACI 440.2R-08*, American Concrete Institute, Farmington Hills Michigan, 109 p, (In press).

ACI Committee 440, 2004. "Guide Test Methods for Fiber-Reinforced Polymers (FRPs) for Reinforcing or Strengthening Concrete Structures." *ACI 440.3R-04*, American Concrete Institute, Farmington Hills, Mich., 40 p.

ADINA, 2004a. "Automatic Dynamic Incremental Nonlinear Analysis: Finite Element Software." Version 8.4. *ADINA R & D, Inc*, Watertown, MA, USA.

ADINA, 2004b. "Theory and Modeling Guide." Volume I. *ADINA R & D, Inc*, Watertown, MA, USA, Chapters 3 and 7.

Ashour, A. F., El-Refaie, S. A. and Garrity, S.W., 2004. "Flexural Strengthening of RC Continuous Beams Using CFRP laminates." *Journal of Cement and Concrete Composites*, Vol. 26, No. 7, October 2004, pp. 765-775.

Aly, R. S. and Benmokrane, B., 2004. "Flexural Behavior of Lap Splicing GFRP Bars in Concrete." *International Conference on Future Vision and Challenges for Urban Development*, 20-22 December, Cairo, Egypt, 8 p.

Asplund, S., 1949. "Strengthening Bridge Slabs with Grouted Reinforcement." *ACI Structural Journal*, American Concrete Institute, Vol.20, No.6, pp. 397-406.

Badawi, M. A. and Soudki, K., 2006. "Strengthening of RC Beams with Prestressed Near Surface Mounted CFRP Rods." *Third International Conference on FRP Composites in Civil Engineering (CICE 2006),* 13-15 December 2006, Miami, Florida, USA.

Badawi, M. A., 2007. "Monotonic and Fatigue Flexural Behaviour of RC Beams Strengthened with Prestressed NSM CFRP Rods." PhD thesis, University of Waterloo, Ontario, Canada.

Benmokrane, B., Chaallal, O. and Masmoudi, R., 1995. "Flexural Response of Concrete Beams Reinforced With FRP Reinforcing Bars." *ACI Materials Journal,* Vol. 91, No. 2, pp. 46-55.

Canadian Standard Association (CSA), 2004. "Design of Concrete Structure for Buildings." *CAN/CSA-A23.3 M-04, Canadian Standard Association*, Rexdale, Ontario, Canada, 220 p.

Canadian Standard Association (CSA), 2006. "Canadian High-Way Bridges Design Code." *CAN/CSA-S6-06, Canadian Standard Association*, Rexdale, Ontario, Canada.

CAN/CSA-S806-02, 2002. "Design and Construction of Building Components with Fibre Reinforced Polymers." *Canadian Standard Association*, Rexdale, Ontario, Canada, 192 p.

Carolin, A., 2003. "Carbon Fiber Reinforced Polymers for Strengthening of Structural Element." Doctoral Thesis, Luleå University of Technology, Sweden, 247 p.

Cruz, S., Barros, O., and Antonio, J., 2004a. "Modeling of Bond between Near-Surface Mounted CFRP Laminate Strips And Concrete." *Computers and Structures*, Vol.82, No.17, pp. 1513 -1523.

Cruz, S., Manuel, J., Barros, O., and Antonio J., 2004b. "Bond Between Near-Surface Mounted Carbon-Fiber-Reinforced Polymer Laminate Strips and Concrete." *ASCE, Journal of Composites for Construction*, Vol. 8, No. 6, pp. 519-527.

Cruz, S. and Barros J. 2006. "Bond Between Near Surface Mounted Carbon Fiber Reinforced Polymer Laminate Strips and Concrete." *ASCE, Journal of Composites for Construction*, Vol. 8, No. 6, pp. 519-527.

Cruz, S., Barros, J., Gettu, R. and Azevedo, A. 2006. "Bond Behavior of Near-Surface Mounted CFRP Laminate Strips Under Monotonic and Cyclic Loading." *Journal of Composites for Construction*, Vol. 10, No. 4, pp. 295-303.

DataFit. 2005. "Datafit Curve Fitting (Nonlinear Regression) and Data Plotting Software." *version 8.1.69*. Oakdale Engineering, Inc, Oakdale, PA, USA, 2005.

Design-Expert., 2000. "Design of Experiments (DOE) Software." *version 6.0.1*. Stat-Ease, Inc, Minneapolis, MN, USA, 2000.

Ebead, U., A., Marzouk, H. Lye, L., 2002. "Strengthening of Two-Way Slabs Using FRP Materials: A Simplified Analysis Based on Response Surface Methodology." *Second World Engineering Congress*. Sarawak, Malaysia, pp. 82-89.

El-Hacha, R. and Rizkalla, S., 2004. "Near Surface Mounted Fiber Reinforced Polymer Reinforcements for Flexural Strengthening of Concrete Structures." *ACI Structural Journal*, American Concrete Institute, Vol.101, No.5, pp. 717-716.

El-Gamal, S., El-Salakawy, E.F., and Benmokrane, B. 2007. "The Influence of Reinforcement on The Behaviour of Concrete Bridge Deck Slabs Reinforced With FRP Bars." *ASCE Journal of Composites for Construction*, Vol. 11, No. 5, pp. 449-458.

El Maaddawy, T. and Soudki, K., 2004. "Strengthening of Reinforced Concrete Slabs with Mechanically-Anchored Unbonded FRP System" *Journal of Construction and Building Materials*, Vol. 22, No. 4, pp. 444-455.

El-Ragaby, A., El-Salakawy, E.F., and Benmokrane, B. 2007. "Fatigue Performance of FRP Reinforced Concrete Bridge Deck Slabs." *ASCE Journal of Composites for Construction*, Vol. 11, No. 3, pp. 258-268.

El-Salakawy, E. and Benmokrane, B., 2003. "Design And Testing of A Highway Concrete Bridge Deck Reinforced with Glass and Carbon FRP Bars." *American Concrete Institute (ACI) Special Publication*, Field Applications of FRP Reinforcement: Case Studies, Farmington Hills, Michigan, SP-215-2: 37-54.

El-Salakawy, E. and Benmokrane, B., 2004. "Serviceability of Concrete Bridge Deck Slabs Reinforced with FRP Composite Bars." *ACI Structural Journal*, Vol. 101, No. 5, pp. 593-602.

El-Salakawy, E., Benmokrane, B., and Desgagné, G., 2003a. "FRP Composite Bars for The Concrete Deck Slab of Wotton Bridge." *Canadian Journal of Civil Engineering,* Vol. 30, No.5, pp. 861-870.

El-Salakawy, E. F., Benmokrane, B., Brière, F., Masmoudi, R., and Beaumier, E. 2003b. "Concrete Bridge Barriers Reinforced with GFRP Composite Bars." *ACI Structural Journal*, Vol. 100 No. 6, pp.815-824.

El-Sayed, A., El-Salakawy, E.F., and Benmokrane, B. 2006. "Shear Strength of FRP-Reinforced Concrete Beams without Transverse Reinforcement." *ACI Structural Journal,* Vol. 103, No.2, pp. 235-243.

Farmer, N., 2003b. "CAR PARKS-Near Surface Mounted Reinforcement Preserves Car Park for Merseyside Police." *Concrete Crowthorne*, Vol. 37, No. 9, pp. 36-38.

Farmer, N., 2003a, "REPAIR AND STRENGTHENING - Near-Surface-Mounted Carbon Fibre Reinforcement." *Concrete Crowthorne*, 2003, Vol. 37, No.1, pp. 20-22.

Grace, N., F., 2001. "Strengthening of Negative Moment Region of Reinforced Concrete Beams Using Carbon Pre-Reinforced Polymer Strips." *ACI Structural Journal*, Vol. 98 No. 3, pp.347-358.

Green, M., Bisby, L., Beaudoin, Y., and Labossiere, P., 2003. "Effect of Freeze-Thaw Cycles on the Bond Durability between Fibre Reinforced Polymer Plate Reinforcement and Concrete." *Canadian Journal of Civil Engineering*, Vol.27, No.5, pp. 949-959.

Hag-Elsafi, O.,Alampalli, S., and Kunin, J., 2001. "Application Of FRP Laminates for Strengthening a Reinforced-Concrete T-Beam Bridge Structure." *Journal of Composite Structures*, Vol.52, pp. 453–466.

Hassan, T. and Rizkalla, S., 2003. "Investigation of Bond in Concrete Structures Strengthened with Near Surface Mounted Carbon Fiber Reinforced Polymer Strips." *Journal of Composites for Construction*, Vol.7, No. 3, pp. 248-257.

Hassan, T. and Rizkalla, S., 2004. "Bond Mechanism of Near-Surface-Mounted Fiber-Reinforced Polymer Bars for Flexural Strengthening of Concrete Structures." *ACI Structural Journal*, American Concrete Institute, Vol. 101, No. 6, pp. 830-839.

Hilti Inc. 2006. Product Technical Guide, http://www.ca.hilti.com.

ISIS CANADA, 2007a. "Reinforcing Concrete Structures with Fibre Reinforced Polymers." *Design Manual No.3*, Winnipeg, Manitoba, Canada, 84 p.

ISIS CANADA, 2007b. "Strengthening Reinforced Concrete Structures with External Bonded Fibre Reinforced Polymers." *Design Manual No.4*, Winnipeg, Manitoba, Canada, 96 p.

Kotynia, R., 2005. "Strain Efficiency of Near Surface Mounted CFRP Strengthened Reinforced Concrete Beams.". In proceeding of CCC-05, Lyon, France.

Kotynia R., 2006. "Flexural Behaviour of Reinforced Concrete Beams Strengthened with Near Surface Mounted CFRP Strips." *Third International Conference on FRP Composites in Civil Engineering (CICE 2006)*. 13-15 December 2006, Miami, Florida, USA.

Kotynia R., 2007. "Analysis of the Flexural Response of NSM FRP Strengthened Concrete Beams." In proceeding of *FRPRCS-8*, Patras, Greece.

Laoubi, K., El-Salakawy, E. F., Pigeon, M., and Benmokrane, B., 2003. "Durability Of Concrete Beams Reinforced with GFRP Bars Under Different Environmental and Loading Conditions." Proceedings of the 6th International Symposium on Fibre Reinforced Polymer (FRP) Reinforcement for Concrete Structures (FRPRCS-6), Singapore, July, 10 p.

Lorenzis, L., 2004. "Anchorage Length of Near-Surface Mounted Fiber-Reinforced Polymer Rods for Concrete Strengthening, Analytical Modeling", *ACI Structural Journal*, American Concrete Institute, Vol.101, No.3, pp. 375.

Lundqvist, J., 2007. "Numerical Analysis of Concrete Elements Strengthened with Carbon Fiber Reinforced Polymers" Doctoral Thesis, Luleå University of Technology, Sweden 138 p.

Lorenzis, L. and Nanni, A., 2001a. "Shear Strengthening of Reinforced Concrete Beams with Near-Surface Mounted Fiber-Reinforced Polymer Rods." *ACI Structural Journal*, American Concrete Institute, Vol. 98, No.1, pp. 60-68.

Lorenzis, L. and Nanni, A., 2001b. "Technical Papers - Characterization of FRP Rods as Near-Surface Mounted Reinforcement." *Journal of Composites for Construction*, Vol. 5, No. 2, pp.114-122.

Lorenzis, L. and Nanni, A., 2001c. "Characterization of FRP Rods as Near-Surface Mounted Reinforcement." *Journal of Composites for Construction*, Vol.5, No.2, pp. 114-121.

Lorenzis, L. and Nanni, A., 2002. "Bond between Near-Surface Mounted Fiber-Reinforced Polymer Rods and Concrete in Structural Strengthening." *ACI Structural Journal*, American Concrete Institute, Vol. 99, No. 2, pp. 123-132.

Liu, I., Oehlers, D. and Seracino, R., 2006a. "Tests on the Ductility of Reinforced Concrete Beams Retrofitted with FRP and Steel Near-Surface Mounted Plates." *Journal of Composites for Construction*, Vol. 10, No. 2, pp. 106-114.

Liu, I., Oehlers, D. and Seracino, R., 2006a. "Moment Redistribution in FRP and Steel-Plated Reinforced Concrete Beams." *Journal of Composites for Construction*, Vol. 10, No. 2, pp. 115-124.

Lorenzis, L., Rizzo, A., La Tegola, A., 2002. "A Modified Pull-Out Test for Bond of Near-Surface Mounted FRP Rods in Concrete." *Composites Engineering Part B.*, Vol.33, No. 8, p. 589-604.

Lorenzis, L., Lundgren, K., Rizzo, A., 2004b. "Anchorage Length of Near-Surface Mounted Fiber-Reinforced Polymer Bars for Concrete Strengthening, Experimental Investigation and Numerical Modeling." *ACI Structural Journal*, American Concrete Institute, Vol.101, No. 2, pp. 269.

Mallic, P.K., 1988. "Fiber Reinforced Composites, Materials, Manufacturing and Design" Marcell Dekker, Inc., New York, 649 p.

Malek, A., Saadatmanesh, H., and Ehsani, M., 1998. "Prediction Of Failure Load Of R/C Beams Strengthened With FRP Plate Due To Stress Concentration At The Plate End." *ACI Structural Journal*, American Concrete Institute, Vol. 95, No. 1, pp.142-152.

Nanni, A., 1993. "Fibre-Reinforced-Plastic (FRP) Reinforcement for Concrete Structures." Properties and Application, Developments in Civil Engineering. 248p.

Nanni, A., 2000. "FRP Reinforcement for Bridge Structures. "Proceedings, Structural Engineering Conference, University of Kansas, Lawrence, Kansas, USA, No.16, pp. 1-5.

Nanni, A., Ludovico, M. and Parretti R., 2004. "Shear Strengthening of a PC Bridge Girder with NSM CFRP Rectangular Bars." *Advances in Structural Engineering,* Vol. 7, No. 4, pp. 97-109.

Nkurunziza, G., Cousin, P., Masmoudi, R., Benmokrane, B., 2003. "Effect of Sustained Tensile Stress and Alkaline on Durability of GFRP Bars." *International Journal of Materials and Product Technology*, 19(4&5), 1-13.

Nordin, H., 2003. "Fiber Reinforced Polymers in Civil Engineering." PhD. Thesis, Luleå University of Technology, Sweden, 57 p.

Nordin H and Taljsten B., 2006. "Concrete Beams Strengthened with Prestressed Near Surface Mounted CFRP." *ASCE, Journal of Composites for Construction*, Vol. 10, No. 1, pp. 60-68.

Novidis,D., Pantazopoulou, S.,J., and Tentolouris, E., 2007. "Experimental Study of Bond of NSM-FRP Reinforcement." Construction and Building Materials. V.21, pp.1760–1770.

Pultrall Inc. 2006. Product Technical Specifications, http://www.Pultrall.com.

Rostasy, F. S., 1993. "FRP Tensile Elements for Prestressed Concrete-State of the Art, Potentials and Limits." Fiber-reinforcement-Plastic reinforcement for concrete Structures, International Symposium, ACI-SP-138, pp.347-366.

Sika Canada Inc., 2004, Technical specification, http://www.Sika.ca.

Smith S. and Teng J., 2002a. "FRP-Strengthened RC Beams. I: Review of Debonding Strength Models. " Engineering Structure Vol. 24, No. 4, pp. 385–95.

Smith S. and Teng J., 2002b. "FRP-Strengthened RC Beams. II: Assessment of Debonding Strength Models. " Engineering Structure, Vol. 24, No. 4 pp. 397–417.

Smith, S. and Teng, J., 2003. "Shear-Bending Interaction in Debonding Failures of FRP-Plated RC Beams." Advances in Structural Engineering, Vol. 6 No. 3, pp.183–200

Soliman, S., M., El-Salakawy, E., and Benmokrane, B., 2007. "Bond Properties of Near Surface Mounted (NSM) Carbon FRP Bars in Concrete." *Annual General Meeting &*

Conference Canadian Society of Civil engineering, June 6-9, Yellowknife, Northwest Territories, Canada, 10 p.

Soliman, S., M., El-Salakawy, E., and Benmokrane, B., 2008a. "Effect of Freeze-thaw Cycles on Bond Behaviour of Near Surface Mounted CFRP Bars." *The Fifth Middle East Symposium on Structural Composites For Infrastructure Applications (MESC5)*, 23-25 May, Hurghada, Egypt, 10 p.

Soliman, S., M., El-Salakawy E. and Benmokrane B. 2008b. "Effectiveness of Using NSM CFRP Bars in Flexural Strengthening of Reinforced Concrete Beams." *Annual General Meeting & Conference Canadian Society of Civil engineering*, June 10-13, Quebec city, Quebec, Canada, 9 p.

Soliman, S., M., El-Salakawy, E., and Benmokrane, B., 2008c. "Flexural Behaviour of Concrete Beams Strengthened with Near Surface Mounted FRP Bars." Fourth International Conference on FRP Composites in Civil Engineering (CICE2008), 22-24 July, Zurich, Switzerland, 8 p.

Stone, D., Tumialan, G., Nanni, A., Parretti, R., 2002. "Reinforcement and Accessories, Near Surface Mounted FRP Reinforcement: Application of an Emerging Technology." *Concrete Crowthorne*, Vol. 36, No. 5, pp. 42-44.

Taljsten, B. and Carolin, A., 2007. "CFRP Strengthening of Concrete Beams– Testing in Sub-Zero Temperature." *International Journal of Materials and Product Technology* (IJMPT), Vol. 28, No. 1/2, pp. 29-45.

Taljsten, B., Carolin, A., Nordin, H., 2003. "Concrete Structures Strengthened with Near Surface Mounted Reinforcement of CFRP." *Advances in Structural Engineering*, Vol.6, No.3, pp. 201-214.

Tegola, L. A. and Micelli, F., 2003. "Environmental Effect on RC Beams with Near Surface Mounted FRP Rods." *Sixth International Symposium on FRP Reinforcement for Concrete Structures* (FRPRCS-6), 8-10 July, Singapore, 10 p.

Teng, J.G., De Lorenzis, L., Wang, B., Li, R., Wong, T.N., and Lam, L., 2006. "Debonding Failures of RC Beams Strengthened with Near Surface Mounted CFRP Strips." *Journal of Composites for Construction*, Vol. 10, No. 2, pp. 92-105.

Wang, P., Masmoudi, R., and Benmokrane, B., 2002. "Durability of GFRP Composite Bars for Concrete Structures: Assessment and Improvement." *Proceedings of the Second Int. Conf. on Durability of FRP composites for Construction, CDCC'2002,* Montreal, Quebec, pp.153-164.

Wenwei, W. and Guo, L., 2006. "Experimental Study and Analysis of RC Beams Strengthened with CFRP Laminates Under Sustaining Load." *International Journal of Solids and Structures,* Vol.43, pp.1372–1387.

Yost, J., R., Gross, S., P., 2004. "Near Surface Mounted CFRP Reinforcement for the Structural Retrofit of Concrete Flexural Members." *Advanced Composite Materials in Bridges and Structures*, Calgary, Alberta, July 20-23, 2004, 8 p.

Yost, J., R., Gross, S., P, Dinehart, D., W. and Mildenberg J., 2007. "Flexural Behavior of Concrete Beams Strengthened with Near-Surface-Mounted CFRP Strips." *ACI Structural Journal*, V. 104, No. 4, pp. 688-697.

APPENDIX

SPECIMENS DESIGN

Design of series A:

Design of control beam (A0):

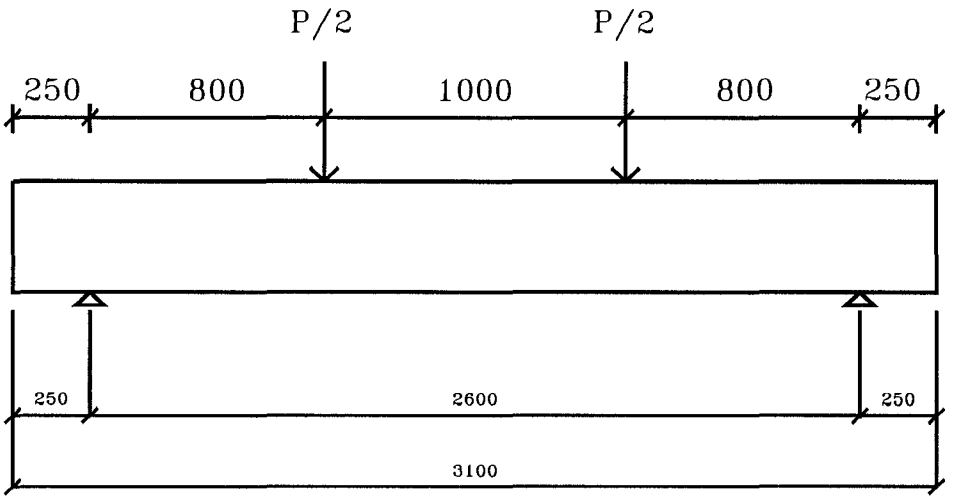

Data:

$f'_c = 40\ MPa$ $\varepsilon_{cu} = 0.0035$

$f_y = 460\ MPa$ $E_s = 200\ GPa$

using 4 No.15M:

using CSA A23.3-94

$E_c = 4500\sqrt{f'_c}$ *Equation 8.2*

$E_c = 4500\sqrt{40} = 28.46\ GPa$

$A_s = 800\ mm^2$ $\rho_s = 1.61\%$

Calculating the balanced Area of steel:

$$\frac{c}{d-c} = \frac{\varepsilon_c}{\varepsilon_s}$$

$$\frac{c}{249-c} = \frac{0.0035}{0.002}$$

$c_b = 164.21mm$

Use $\Phi_c = 1.00$ $\Phi_s = 1.00$

$$C = T$$

$$\alpha_1.\phi_c.F'_c.a.b = \phi_s.A_s.f_y$$

$$0.8x1.0x40x0.87x200x164.21 = 1.0xA_s x460$$

$$\underline{A_s=1987.65\ mm^2}$$

$$\underline{\rho_b=3.99\ \%}$$

$\alpha_1 = 0.85 - 0.0015 f_c'$ *Equation 10.1*

$\beta_1 = 0.97 - 0.0025 f_c'$ *Equation 10.2*

$\alpha_1 = 0.85 - 0.0015x40$ $\alpha_1 = 0.80$

$\beta_1 = 0.97 - 0.0025x40$ $\beta_1 = 0.87$

$d = 300 - 35 - 8 - 16/2$ $\underline{d = 249\ mm}$

$\underline{A_s = 800\ mm^2}$ $\rho_s=1.61\%$

Balanced condition:

Use $\Phi_c = 1.00$ $\Phi_s = 1.00$

$$C = T$$

$$\alpha_1.\phi_c.F_c'.a.b = \phi_s.A_s.f_y$$

$$0.8x1.0x28460x\varepsilon_c x0.87x200xC = 1.0x800x460$$

$$\varepsilon_c C = 0.092 \ldots\ldots\ldots\ldots\ldots\ldots 1$$

$$\frac{C}{d} = \frac{\varepsilon_c}{\varepsilon_c + \varepsilon_s}$$

$$\frac{C}{249} = \frac{\varepsilon_c}{\varepsilon_c + 0.002} \ldots\ldots\ldots\ldots\ldots\ldots 2$$

from 1& 2

$0.002c^2 + 0.092c - 22.9 = 0$ **c = 86.45 mm**

$$M_r = \phi_s.F_y.A_s.\left(d - \frac{a}{2}\right)$$

$$M_r = 1.0x460x800x(249 - \frac{0.87x86.45}{2})$$

$M_r = 77.79\ KN.m$

$P/2x0.8=M_r$ ***P=194.5KN***

Check of shear:

$V_r = V_c + V_s$ *Equation 11.4*

V_c :

$V_c = 0.2.\phi_c.\sqrt{f_c'}.b.d$ *Equation 11.5*

$V_c = 0.2x1.0x1.0x\sqrt{40}x200x249$ ***V_c = 62.99 KN***

V_s :

For stirrups 8M Φ = 8 mm Area = 52.27 mm^2

$V_s = \frac{\phi_s.F_y.A_v.d}{S}$ $V_s = \frac{1.0x400x2x52.27x249}{100}$ ***V_s = 104.12 KN***

$V_r = 62.99+104.12=167.11KN$

P=334 KN

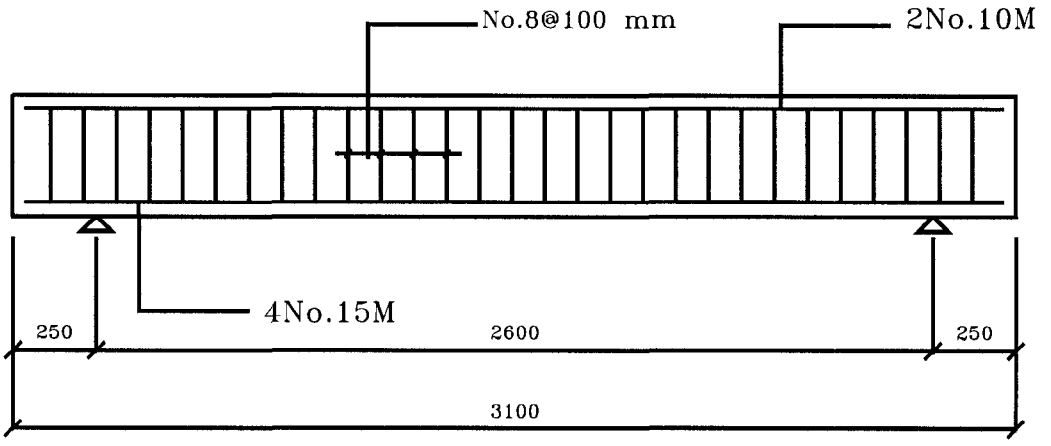

Strengthening scheme I

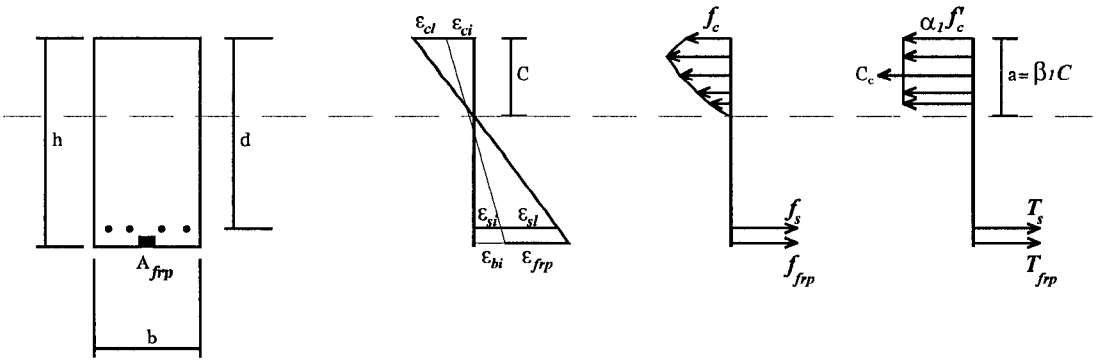

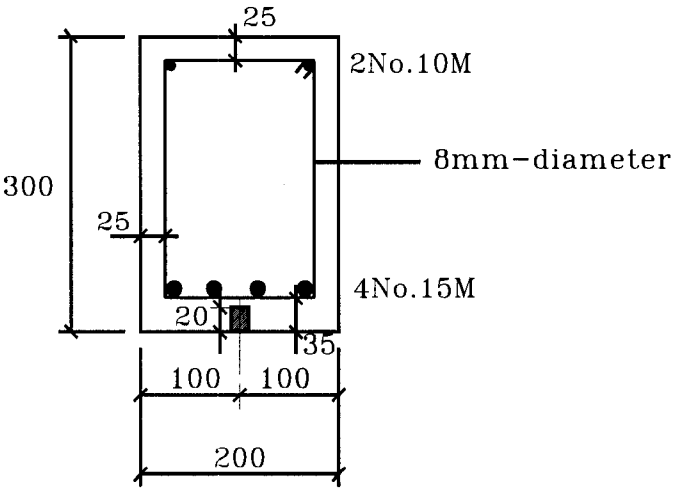

I-(using one CFRP No. 10), A_f=71 mm^2:

Data :

$f'_c = 40\ MPa$ $\quad\quad$ $\varepsilon_{cu} = 0.0035$

$f_y = 460\ MPa$ $\quad\quad$ $E_s = 200\ GPa$

$f_{fu} = 1551\ MPa$ $\quad\quad$ $E_f = 120\ GPa$

$A_s = 4\ No.\ 15M$ $\quad\quad$ $\varepsilon_y = 0.002$

By using ISIS CANADA Design Manuel No.4

Assume failure mode is crushing of concrete with yielding of steel reinforcement

$$C = T_s + T_f$$

$$\alpha_1.\phi_c.f'_c.\beta_1.b.c^2 + \left(\phi_{frp}.E_{frp}.A_{frp}.(\varepsilon_{cu}+\varepsilon_{bi}) - \phi_s.f_s.A_s\right)c - \phi_{frp}.E_{frp}.A_{frp}.\varepsilon_{cu}.h = 0$$

Equation 4-25

$\alpha_1 = 0.85 - 0.0015 f'_c$ *Equation 4-6a*

$\beta_1 = 0.97 - 0.0025 f'_c$ *Equation 4-6b*

$\alpha_1 = 0.85 - 0.0015x40$ $\quad\quad$ $\alpha_1 = 0.80$

$\beta_1 = 0.97 - 0.0025x40$ $\quad\quad$ $\beta_1 = 0.87$

Use $\Phi_c = 1.00$ $\quad\quad$ $\Phi_s = 1.00$ $\quad\quad$ $\Phi_f = 1.00$

$A_s = 800\ mm^2$ $\quad\quad$ $A_f = 71\ mm^2$

d = 300 – 35 – 8 – 16/2 $\underline{d = 249\ mm}$

$$0.8x1.0x40x0.87x200xc^2 + (1.0x120000x71x(0.0035+0) - 1.0x460x800)xc - (1.0x120000x71x0.0035x300) = 0$$

$$5568c^2 - 338180c - 8946000 = 0$$ **C = 80.66 mm**

Check for failure mode:

$$\varepsilon_s = \varepsilon_{cu}.\frac{d-c}{c} \qquad \varepsilon_s = 0.0035x\frac{249-80.66}{80.66} \qquad \varepsilon_s = 0.0073$$

$\varepsilon_y = 0.002$ $\varepsilon_s \succ \varepsilon_y$ steel yield **OK**

$$\varepsilon_f = \varepsilon_{cu}.\frac{h-c}{c} - \varepsilon_{pi} \qquad \varepsilon_f = 0.0035x\frac{300-80.66}{80.66} - 0 \qquad \varepsilon_f = 0.0095$$

$\varepsilon_{fu} = 0.014$ $\varepsilon_f \prec \varepsilon_{fu}$ no rupture of FRP **OK**

$$M_r = \phi_s.F_y.A_s.\left(d - \frac{a}{2}\right) + \phi_f.A_f.E_f.\varepsilon_f.\left(h - \frac{a}{2}\right)$$

$$M_r = 1.0x460x800x\left(249 - \frac{0.87x80.66}{2}\right) + 1.0x71x120000x0.0095\left(300 - \frac{0.87x80.66}{2}\right)$$

$M_r = 100.16\ KN.m$

$P/2x0.8 = M_r$ ***P=250KN***

II-(using 1 CFRP No. 13), A_f=127 mm^2:

$f'_c = 40\ MPa$ $\varepsilon_{cu} = 0.0035$

$f_y = 460\ MPa$ $E_s = 200\ GPa$

$f_{fu} = 986\ MPa$ $E_f = 134\ GPa$

$A_s = 4\ No.\ 15M$ $\varepsilon_y = 0.002$

By using ISIS CANADA Design Manuel No.4

Assume failure mode is crushing of concrete with yielding of steel reinforcement

$$C = T_s + T_f$$

$$\alpha_1.\phi_c.f'_c.\beta_1.b.c^2 + \left(\phi_{frp}.E_{frp}.A_{frp}.(\varepsilon_{cu} + \varepsilon_{bi}) - \phi_s.f_s.A_s\right)c - \phi_{frp}.E_{frp}.A_{frp}.\varepsilon_{cu}.h = 0$$

Equation 4-25

$\alpha_1 = 0.85 - 0.0015 f'_c$ *Equation 4-6a*

$\beta_1 = 0.97 - 0.0025 f'_c$ *Equation 4-6b*

$\alpha_1 = 0.85 - 0.0015x40$ $\alpha_1 = 0.80$

$\beta_1 = 0.97 - 0.0025x40$ $\beta_1 = 0.87$

Use $\Phi_c = 1.00$ $\Phi_s = 1.00$ $\Phi_f = 1.00$

$A_s = 800\ mm^2$ $A_f = 127\ mm^2$

d = 300 – 35 – 8 – 16/2 $d = 249\ mm$

$$0.8x1.0x40x0.87x200xc^2 + \left(1.0x134000x127x(0.0035+0) - 1.0x460x800\right)xc$$
$$-\left(1.0x134000x127x0.0035x300\right) = 0$$

$5568c^2 - 308437c - 17868900 = 0$ **C = 92.76 mm**

Check for failure mode:

$\varepsilon_s = \varepsilon_{cu}.\dfrac{d-c}{c}$ $\varepsilon_s = 0.0035x\dfrac{249-92.76}{92.76}$ $\varepsilon_s = 0.0061$

$\varepsilon_y = 0.002$ $\varepsilon_s \succ \varepsilon_y$ steel yield **OK**

$\varepsilon_f = \varepsilon_{cu}.\dfrac{h-c}{c} - \varepsilon_{pi}$ $\varepsilon_f = 0.0035x\dfrac{300-90.76}{90.76} - 0$ $\varepsilon_f = 0.0072$

$\varepsilon_{fu} = 0.0074$ $\varepsilon_f \prec \varepsilon_{fu}$ no rupture of FRP **OK**

$$M_r = \phi_s . F_y . A_s . \left(d - \frac{a}{2} \right) + \phi_f . A_f . E_f . \varepsilon_f . \left(h - \frac{a}{2} \right)$$

$$M_r = 1.0x460x800x \left(249 - \frac{0.87x92.76}{2} \right) + 1.0x127x134000x0.007 \left(300 - \frac{0.87x92.76}{2} \right)$$

$M_r = 107.71\ KN.m$

$P/2x0.8 = M_r$ ***P=270KN***

III-(using 1 GFRP No. 13), A_f=129 mm^2:

$f'_c = 40\ MPa$ $\varepsilon_{cu} = 0.0035$

$f_y = 460\ MPa$ $E_s = 200\ GPa$

$f_{fu} = 617\ MPa$ $E_f = 42\ GPa$

$A_s = 4\ No.\ 15M$ $\varepsilon_y = 0.002$

By using ISIS CANADA Design Manuel No.4

Assume failure mode is crushing of concrete with yielding of steel reinforcement

$$C = T_s + T_f$$

$$\alpha_1.\phi_c.f'_c.\beta_1.b.c^2 + \left(\phi_{frp}.E_{frp}.A_{frp}.(\varepsilon_{cu} + \varepsilon_{bi}) - \phi_s.f_s.A_s\right)c - \phi_{frp}.E_{frp}.A_{frp}.\varepsilon_{cu}.h = 0$$

Equation 4-25

$\alpha_1 = 0.85 - 0.0015 f'_c$ *Equation 4-6a*

$\beta_1 = 0.97 - 0.0025 f'_c$ *Equation 4-6b*

$\alpha_1 = 0.85 - 0.0015x40$ $\alpha_1 = 0.80$

$\beta_1 = 0.97 - 0.0025x40$ $\beta_1 = 0.87$

Use $\Phi_c = 1.00$ $\Phi_s = 1.00$ $\Phi_f = 1.00$

$A_s = 800\ mm^2$ $A_f = 129\ mm^2$

d = 300 – 35 – 8 – 16/2 $d = 249\ mm$

$$0.8x1.0x40x0.87x200xc^2 + \left(1.0x42000x129x(0.0035+0) - 1.0x460x800\right)xc$$
$$-\left(1.0x42000x129x0.0035x300\right) = 0$$

$5568c^2 - 349037c - 5688900 = 0$ **C = 76.11 mm**

Check for failure mode:

$\varepsilon_s = \varepsilon_{cu}.\dfrac{d-c}{c}$ $\varepsilon_s = 0.0035x\dfrac{249-76.11}{76.11}$ $\varepsilon_s = 0.008$

$\varepsilon_y = 0.002$ $\varepsilon_s \succ \varepsilon_y$ steel yield **OK**

$\varepsilon_f = \varepsilon_{cu}.\dfrac{h-c}{c} - \varepsilon_{pi}$ $\varepsilon_f = 0.0035x\dfrac{300-76.11}{76.11} - 0$ $\varepsilon_f = 0.010$

$\varepsilon_{fu} = 0.018$ $\varepsilon_f \prec \varepsilon_{fu}$ no rupture of FRP **OK**

$$M_r = \phi_s . F_y . A_s . \left(d - \frac{a}{2} \right) + \phi_f . A_f . E_f . \varepsilon_f . \left(h - \frac{a}{2} \right)$$

$$M_r = 1.0x460x800x \left(249 - \frac{0.87x76.11}{2} \right) + 1.0x129x42000x0.018 \left(300 - \frac{0.87x76.11}{2} \right)$$

$M_r = 82.1\ KN.m$

$P/2x0.8 = M_r$ ***P=205KN***

II-in case of using 2CFRP No. 10, A_f=142 mm^2:

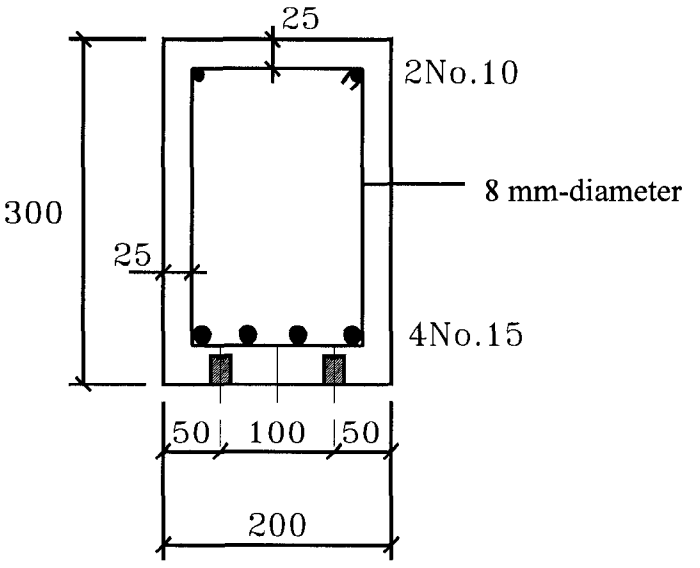

By using ISIS CANADA Design Manuel No.4

Assume failure mode is crushing of concrete with yielding of steel reinforcement

$$C = T_s + T_f$$

$$\alpha_1.\phi_c.f_c'.\beta_1.b.c^2 + \left(\phi_{frp}.E_{frp}.A_{frp}.(\varepsilon_{cu} + \varepsilon_{bi}) - \phi_s.f_s.A_s\right)c - \phi_{frp}.E_{frp}.A_{frp}.\varepsilon_{cu}.h = 0$$

Equation 4-25

$\alpha_1 = 0.80$

$\beta_1 = 0.87$

Use $\Phi_c = 1.00$ $\Phi_s = 1.00$ $\Phi_f = 1.00$

$A_s = 800\ mm^2$ $A_f = 142\ mm^2$

d = 300 – 35 – 8 – 16/2 $d = 249\ mm$

$$0.8x1.0x40x0.87x200xc^2 + \left(1.0x120000x142x(0.0035+0) - 1.0x460x800\right)xc$$
$$-\left(1.0x120000x142x0.0035x300\right) = 0$$

$5568c^2 - 308360c - 17640000 = 0$ **C = 90.78 mm**

Check for failure mode:

$$\varepsilon_s = \varepsilon_{cu}.\frac{d-c}{c} \qquad \varepsilon_s = 0.0035x\frac{249-90.78}{90.78} \qquad \varepsilon_s = 0.0061$$

$\varepsilon_y = 0.002$ $\varepsilon_s \succ \varepsilon_y$ steel yield **OK**

$$\varepsilon_f = \varepsilon_{cu}.\frac{h-c}{c} - \varepsilon_{pi} \qquad \varepsilon_f = 0.0035x\frac{300-90.87}{90.78} - 0 \qquad \varepsilon_f = 0.0081$$

$\varepsilon_{fu} = 0.014$ $\varepsilon_f \prec \varepsilon_{fu}$ no rupture of FRP **OK**

$$M_r = \phi_s.f_y.A_s.\left(d-\frac{a}{2}\right)+\phi_f.A_f.E_f.\varepsilon_f.\left(h-\frac{a}{2}\right)$$

$$M_r = 1.0x460x800x\left(249-\frac{0.87x90.78}{2}\right)+1.0x142x120000x0.0071\left(300-\frac{0.87x90.78}{2}\right)$$

$M_r = 113.1\ KN.m$

$P/2x0.8=M_r$ ***P=282.64 KN***

III- in case of using 3 No. 10, A_f=213 mm^2:

By using ISIS Design Manuel No.4

Assume failure mode is crushing of concrete with yielding of steel reinforcement

$$C = T_s + T_f$$

$$\alpha_1.\phi_c.f_c'.\beta_1.b.c^2 + \left(\phi_{frp}.E_{frp}.A_{frp}.(\varepsilon_{cu} + \varepsilon_{bi}) - \phi_s.f_s.A_s\right)c - \phi_{frp}.E_{frp}.A_{frp}.\varepsilon_{cu}.h = 0$$

Equation 4-25

$\alpha_1 = 0.80$

$\beta_1 = 0.87$

Use $\Phi_c = 1.00$ $\Phi_s = 1.00$ $\Phi_f = 1.00$

$A_s = 800\ mm^2$ $A_f = 213\ mm^2$

d = 300 – 35 – 8 – 16/2 $d = 247\ mm$

$$0.8x1.0x40x0.87x200xc^2 + \left(1.0x120000x213x(0.0035+0) - 1.0x460x800\right)xc - \left(1.0x120000x213x0.0035x300\right) = 0$$

$$5568c^2 - 278540c - 26838000 = 0 \qquad \mathbf{C = 98.81mm}$$

Check for failure mode:

$$\varepsilon_s = \varepsilon_{cu}.\frac{d-c}{c} \qquad \varepsilon_s = 0.0035x\frac{249-98.81}{98.81} \qquad \varepsilon_s = 0.0053$$

$\varepsilon_y = 0.002$ $\varepsilon_s \succ \varepsilon_y$ steel yield **OK**

$$\varepsilon_f = \varepsilon_{cu}.\frac{h-c}{c} - \varepsilon_{pi} \qquad \varepsilon_f = 0.0035x\frac{300-98.81}{98.81} - 0 \qquad \varepsilon_f = 0.0071$$

$\varepsilon_{fu} = 0.014$ $\varepsilon_f \prec \varepsilon_{fu}$ no rupture of FRP **OK**

$$M_r = \phi_s.f_y.A_s.\left(d - \frac{a}{2}\right) + \phi_f.A_f.E_f.\varepsilon_f.\left(h - \frac{a}{2}\right)$$

$$M_r = 1.0x460x800x\left(249 - \frac{0.87x98.81}{2}\right) + 1.0x213x120000x0.0071\left(300 - \frac{0.87x98.81}{2}\right)$$

$M_r = 122.46\ KN.m$

$P/2x0.8 = M_r$ ***P=306 KN***

But it is very difficult to use three bars in 200mm width

Design of series C

Design of control beam (C0):

using 2No.10M:

using CSA A23.3-94

$E_c = 4500\sqrt{f'_c}$ *Equation 8.2*

$E_c = 4500\sqrt{40} = 28.46\ GPa$

$A_s = 200\ mm^2$ $\rho_s = 0.38\%$

$\alpha_1 = 0.85 - 0.0015 f'_c$ *Equation 10.1*

$\beta_1 = 0.97 - 0.0025 f'_c$ *Equation 10.2*

$\alpha_1 = 0.85 - 0.0015x40$ $\alpha_1 = 0.80$

$\beta_1 = 0.97 - 0.0025x40$ $\beta_1 = 0.87$

$d = 300 - 25 - 8 - 11.3/2$ $d = 261.35\ mm$

Use $\Phi_c = 1.00$ $\Phi_s = 1.00$

Concrete:

$C_c = \alpha_1.\phi_c.F_c.a.b$

$F_c = E_c.\varepsilon_c\left[1 - \frac{\varepsilon_c}{\varepsilon_o}\right]$

$E_c = 4500\sqrt{40} = 28.46\ GPa$

$\frac{\varepsilon_c}{\varepsilon_s + \varepsilon_c} = \frac{c}{d}$

$261.35.\varepsilon_c = (0.0023 + \varepsilon_c)a / 0.87$

$227.07.\varepsilon_c = (0.0023 + \varepsilon_c)a$

$$\varepsilon_c = \frac{0.0023a}{227.07 - a}$$

$$C_c = 0.8x1.0x0.87x200x28460\left[\frac{0.0023a}{227.07-a}\right]\left[1-\frac{0.0023a}{227.07-a}\right]a$$

$$C_c = 9111.75\left[\frac{a^2}{227.07-a}\right]\left[\frac{227.07-2.15a}{227.07-a}\right] \quad 1$$

Compression reinforcement:

$$C_s = \phi_s.E_s\varepsilon'_s A'_s$$

$$C_s = 1.0x200000x800x\varepsilon'_s$$

$$\frac{\varepsilon'_s + \varepsilon_s}{\varepsilon'_s} = \frac{d-d'}{c-d'}$$

$$\frac{\varepsilon'_s + 0.0023}{\varepsilon'_s} = \frac{261.35-35}{c-35}$$

$$226.35\varepsilon'_s = \left(\frac{a}{0.87} - 35\right)\left(\varepsilon'_s + 0.0023\right)$$

$$\left(226.35 + 35 - \frac{a}{0.87}\right)\varepsilon'_s = \left(\frac{a}{0.87} - 35\right)x0.0023$$

$$\varepsilon'_s = 0.0023\left(\frac{a-30.45}{227.07-a}\right)$$

$$C_s = 36.8x10^4\left(\frac{a-30.45}{227.07-a}\right) \quad 2$$

Tension reinforcement:

$$T_s = \phi_s.f_y.A_s$$

$$T_s = 1.0x460x200 = 92000 \quad 3$$

$$\boldsymbol{C_c + C_s = T_s}$$

$$92000 = 9111.75\left[\frac{a^2}{227.07-a}\right]\left[\frac{227.07-2.15a}{227.07-a}\right] + 36.8x10^4\left(\frac{a-30.45}{227.07-a}\right)$$

$$92000\left(a^2-454.14a+51560.78\right)=$$

$$36.8x10^4\left(-a^2+257.52a-6914.28\right)+9111.75\left(227.07a^2-227.07a^3\right)$$

By solving the third degree equation we got

a=114.62 a=42.99 a=-75.4

Check:

a=114.62	a=42.99
$\varepsilon'_s = 0.0017$	$\varepsilon'_s = 0.000156$
$\varepsilon_c = 0.0023 > \varepsilon_o$ Not acceptable	$\varepsilon_c = 0.00053$ OK

C=$\frac{a}{0.87}$ =49.41 mm

$$M_r = C_c.\left(d-\frac{a}{2}\right)+C_s.\left(d-d'\right)$$

$$M_r = 66911.75(261.35-\frac{42.99}{2})+25069.1(261.35-35)$$

$M_r = 22.57\ KN.m$

$P/2x0.8=M_r$ ***P=56.42KN***

Check of shear:

$V_r = V_c + V_s$ *Equation 11.4*

V_c :

$V_c = 0.2.\phi_c.\sqrt{f'_c}.b.d$ *Equation 11.5*

$V_c = 0.2x1.0x1.0x\sqrt{40}x200x249$ ***V_c = 62.99 KN***

V_s :

For stirrups 8M Φ = 8 mm Area = 52.27 mm^2

$V_s = \frac{\phi_s.F_y.A_v.d}{S}$ $V_s = \frac{1.0x400x2x52.27x249}{100}$ ***V_s = 104.12 KN***

$V_r = 62.99+104.12=167.11KN$

P=334 KN

Strengtheninsg scheme I

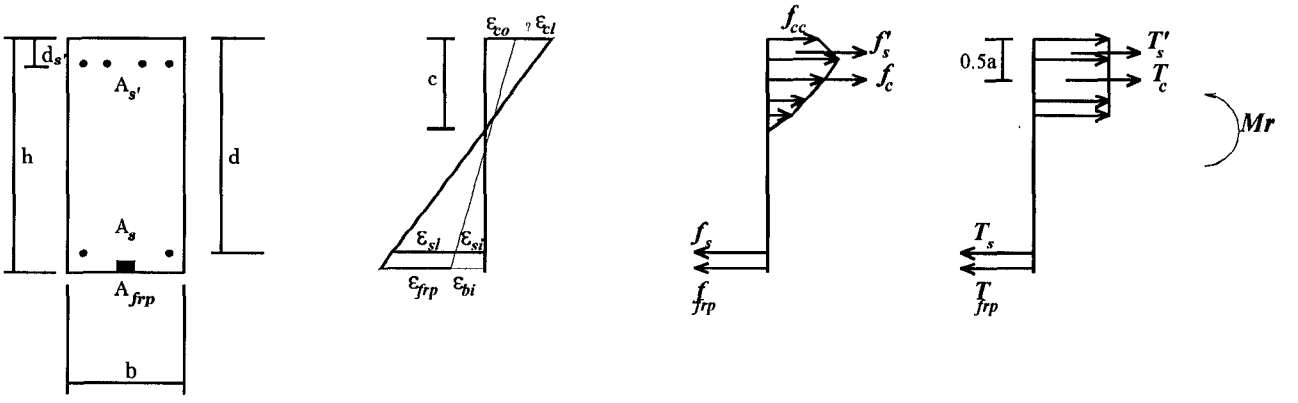

I-(using one CFRP No. 10), A_f=71 mm^2:

Data :

$f'_c = 40\ MPa$ $\varepsilon_{cu} = 0.0035$

$f_y = 460\ MPa$ $E_s = 200\ GPa$

$f_{fu} = 1551\ MPa$ $E_f = 120\ GPa$

$A_s = 2\ No.\ 10M$ $\varepsilon_y = 0.0023$

Assume rupture of FRP bar and yielding of steel reinforcement

$$C_c + C_s = T_s + T_f$$

$T_f = \phi_{frp}.E_{frp}.A_{frp}.\varepsilon_{cu}.h$

$T_f = 1.0x120000x0.014x71 = 119280$

$$119280+92000 = 9111.75\left[\frac{a^2}{227.07-a}\right]\left[\frac{227.07-2.15a}{227.07-a}\right]+36.8x10^4\left(\frac{a-30.45}{227.07-a}\right)$$

$211280x51560.78+211280a^2-211280x454.14a+36.8x10^4a^2-36.8x10^4x257.52a+36.8x10^4$
$x6914.28-9111.75x227.07a^2+9111.75x2.15a^3=0$

By solving the third degree equation we got

a= 107.16 a= 65.95 a= –97.06

Check:

a=107.16

$\varepsilon'_s = 0.00147$

$\varepsilon_c = 0.0021 > \varepsilon_o$ Not acceptable

a=65.95

$\varepsilon'_s = 0.00051$

$\varepsilon_c = 0.00094$ OK

$C=\frac{a}{0.87}$ =75.08 mm

$$M_r = C_c.\left(d-\frac{a}{2}\right)+C_s.\left(d-d'\right)$$

$$M_r = 130186.8(261.35-\frac{65.95}{2})+81082.42(261.35-35)$$

$M_r = 48.08\ KN.m$

$P/2x0.8=M_r$ **<u>P=120KN</u>**